



UNIVERSITÀ DEGLI STUDI DI MILANO
FACOLTÀ DI SCIENZE DEL FARMACO
Department of Pharmaceutical Sciences
PhD Course in Pharmaceutical Sciences
-XXIX Cycle-

**Design, synthesis and biological evaluation of novel
antiproliferative compounds as potential anticancer agents**

Tutor: Prof. Alessandro Pedretti

Coordinator: Prof. Marco De Amici

Federica Porta

R10459

Academic year 2015/2016

***It is not the most intellectual or the strongest species that survives,
but the species that survives is the one that is able to adapt to or
adjust best to the changing environment in which it finds itself.***

Attributed to Charles Darwin

Abstract

Selectivity for cancer cells is one of the most important characteristics of anticancer agents. The transition from cytotoxic chemotherapy to molecularly targeted cancer drug discovery and development resulted in an increasing number of successful therapies that impacted the lives of a large number of cancer patients.

The extreme toxicity and the development of resistance have made it essential to keep searching for new potential targeted anticancer agents, endowed with higher efficacy and minor toxicity.

In order to achieve this goal, I followed different approaches:

- starting from antiproliferative compounds, I sought their molecular target;
- developing STAT3 inhibitors, I obtained dual-target compounds with enhanced cytotoxicity;
- employing computationally driven drug design, I investigated new chemical scaffolds, able to disrupt STAT3 dimerization and characterized by suitable drug-like properties.

1,2,5-Oxadiazoles have received considerable attention in recent years from Prof. Barlocco's research group because of the interesting results as potential antitumor agents. Among all, MD77 displayed a very interesting antiproliferative profile. Therefore, I focused my research efforts in the identification of its molecular target employing a combined synthetic-computational approach. I synthesized a wide pool of MD77 derivatives which were evaluated for their antiproliferative activity by the MTT-assay on human colon cancer cells by Dr. N. Ferri (University of Padua, Italy) and underwent a structure-activity relationship analysis using Activity Miner module of Cresset Forge, in collaboration with Prof. S. Guccione's research group (University of Catania, Italy). The obtained disparity matrix will be used as query in search of a potential target.

Platinum based anticancer drugs are still among the most effective drugs used for the treatment of solid cancers. Their strong side effects and the increasing resistance are limitations to their use. Even if DNA was established to be the primary target of platinum drugs, an extensive investigation into their biochemistry highlighted the evidence that also non-DNA targets, such as STAT3, are involved in determining cytotoxic effects. The second part of my PhD project, carried out in collaboration with Dr. I. Rimoldi's research group (University of Milan) and Dr. N. Ferri (University of Padua), aimed at the identification of Pt(II) complexes endowed with antiproliferative activity due to a dual mechanism of action: interference with DNA replication and inhibition of STAT3 signaling pathway. Among the synthesized derivatives, Pt-15b and Pt-16a were selected for *in vivo* studies thanks to the collaboration with Prof. C. Marzano and Prof. V. Gandin (University of Padua), showing that the chemotherapy with these compounds reduced the tumor mass similarly to cisplatin and, despite the higher dose, they seemed to be better tolerated than the reference compound.

A dual targeting approach was also pursued, in collaboration with Prof. A. Sparatore's research group, by investigating a new series of sulfurated compounds as STAT3 and NF- κ B inhibitors. Dithiolethiones (DTTs) and methanethiosulfonates (MTTSs) were synthesized in light of their recently reported chemopreventive and anticancer activities.

Fragment-based drug design (FBDD) has emerged as promising methodology to generate lead molecules against therapeutic targets in the past decade. Compared with high-throughput screening hits, the advantage is that the identified small molecules are expected to be efficiently optimized into a drug candidate which maintains low molecular weight and possesses both binding affinity and favorable pharmacokinetic profile. The aim of this branch of my PhD project was the identification of new chemical scaffolds able to disrupt

STAT3 protein-protein interactions and characterized by an increased activity and appropriate drug-like properties, employing a FBDD approach. The computational protocol was firstly validated and then applied on a larger base set of fragments leading to nine drug candidates. The synthesized compounds and the commercial ones were evaluation by an *in vitro* binding assay to determine their affinity for the target.

This project was partially supported by PRIN Research Project, grant no. 20105YY2H_007.

TABLE OF CONTENTS

| | |
|--|-----------|
| Chapter 1: Introduction | 1 |
| 1.1 Cancer | 2 |
| 1.1.1 Chemotherapy and targeted therapy..... | 3 |
| 1.2 STAT3..... | 5 |
| 1.2.1 STAT3 signaling pathway | 6 |
| 1.2.2 STAT3 inhibitors..... | 7 |
| 1.3 Platinum based anticancer drugs..... | 8 |
| 1.3.1 How platinum-based chemotherapeutics work | 8 |
| 1.3.2 Structure-activity relationships | 10 |
| 1.3.3 Platinum compounds and STAT3..... | 11 |
| 1.4 Topoisomerases | 12 |
| 1.4.1 DNA Topoisomerases inhibitors | 13 |
| 1.5 Hit finding..... | 15 |
| 1.5.1 Scaffold hopping..... | 15 |
| 1.5.2 Fragment-based drug design..... | 15 |
| Chapter 2: MD77 derivatives | 17 |
| 2.1 Research project | 18 |
| 2.2 Synthetic chemistry..... | 20 |
| 2.3 Results and discussion..... | 25 |
| 2.3.1 Antiproliferative activity | 26 |
| 2.3.2 AlphaScreen-based assay | 28 |
| 2.3.3 Cresset Forge | 28 |
| 2.3.3.1 Computational methodologies | 31 |
| 2.3.4 Crystallographic studies..... | 32 |
| 2.4 Conclusions | 33 |
| Chapter 3: Platinum (II) Complexes | 35 |
| 3.1 Research project | 36 |
| 3.1.1 3-aminomethyl-1,2,5-oxadiazole derivatives as ligands in Pt(II) complexes..... | 36 |
| 3.1.2 3-hydroxylaminomethyl-1,2,5-oxadiazole derivatives as ligands in Pt(II) complexes..... | 36 |
| 3.2 Synthetic chemistry..... | 38 |
| 3.3 Results and discussion..... | 40 |
| 3.3.1 3-aminomethyl-4-methyl-1,2,5-oxadiazoles | 40 |
| 3.3.1.1 Analysis of the coordination environment of Pt(II) core | 41 |
| 3.3.1.2 Aqueous stability and lipophilicity | 42 |
| 3.3.1.3 pH dependent enolization of ligands 15a-c | 42 |
| 3.3.1.4 <i>In vitro</i> biological evaluation..... | 43 |
| 3.3.1.5 DNA binding study | 44 |
| 3.3.1.6 Intracellular and nuclear accumulation of Pt-15b and induction of p53..... | 45 |
| 3.3.1.7 Effect of Pt-15b on STAT3 expression and phosphorylation | 46 |
| 3.3.1.8 Glutathione binding study | 46 |
| 3.3.1.9 Cytotoxic effect of Pt-15b and 15b on cell lines poorly sensitive to cisplatin | 47 |
| 3.3.2 3-hydroxylaminomethyl-4-methyl-1,2,5-oxadiazoles | 48 |
| 3.3.2.1 Enolization of ligand 16a..... | 48 |
| 3.3.3 <i>In vivo</i> tumor growth inhibition..... | 49 |
| 3.4 Conclusions and perspectives | 50 |

| | |
|--|-----------|
| Chapter 4: DTT and MTTs derivatives | 51 |
| 4.1 Research project | 52 |
| 4.2 Synthetic chemistry..... | 53 |
| 4.3 Conclusions | 54 |
| Chapter 5: Computationally Driven Drug Design..... | 55 |
| 5.1 Research project | 56 |
| 5.2 STAT3 structure..... | 57 |
| 5.3 Computational methods | 59 |
| 5.3.1 Conformational analysis and molecular mechanics | 59 |
| 5.3.2 Molecular docking | 59 |
| 5.3.2.1 PLANTS software..... | 60 |
| 5.3.3 Preparation of the STAT-SH2 domain structure..... | 61 |
| 5.3.4 Preparation of the dataset of fragments and compounds..... | 61 |
| 5.4 Results and discussion..... | 62 |
| 5.4.1 Virtual screening..... | 62 |
| 5.4.2 Synthetic chemistry | 66 |
| 5.4.3 AlphaScreen-based assay | 69 |
| 5.5 Conclusions and perspectives | 70 |
| Chapter 6: Outcomes | 71 |
| Chapter 7: Experimental Part: Chemistry | 73 |
| Materials and Methods..... | 74 |
| Physical Measurements | 74 |
| Crystallization, data collection and structural determination | 74 |
| Stability test | 75 |
| Log P_{ow} determination | 75 |
| General procedures for the synthesis of 4-phenyl-1,2,5-oxadiazol-3-amines (105a-d,g-j,l,r)..... | 76 |
| 4-phenyl-1,2,5-oxadiazol-3-amine (105a)..... | 77 |
| 4-(2-chlorophenyl)-1,2,5-oxadiazol-3-amine (105b)..... | 77 |
| 4-(3-chlorophenyl)-1,2,5-oxadiazol-3-amine (105c)..... | 77 |
| 4-(4-chlorophenyl)-1,2,5-oxadiazol-3-amine (105d)..... | 77 |
| 4-(4-trifluoromethyl)-1,2,5-oxadiazol-3-amine (105g) | 77 |
| 4-(4-bromophenyl)-1,2,5-oxadiazol-3-amine (105h)..... | 78 |
| 4-(4-methylphenyl)-1,2,5-oxadiazol-3-amine (105i)..... | 78 |
| 4-(1,1'-biphenyl]-4-yl)-1,2,5-oxadiazol-3-amine (105j)..... | 78 |
| 4-(4-benzyloxyphenyl)-1,2,5-oxadiazol-3-amine (105l)..... | 78 |
| 4-(4-nitrophenyl)-1,2,5-oxadiazol-3-amine (105r)..... | 78 |
| Procedures for the synthesis of 4-(4-chlorophenyl)-3-aminoisoxazole (109) | 79 |
| Synthesis of ethyl 4-(4-chlorophenyl)isoxazole-3-carboxylate (106) | 79 |
| Synthesis of 4-(4-chlorophenyl)-3-hydrazinecarboxylisoxazole (107) | 79 |
| Synthesis of 4-(4-chlorophenyl)-3-acylazideisoxazole (108)..... | 80 |
| Synthesis of 4-(4-chlorophenyl)-3-aminoisoxazole (109) | 80 |
| Procedures for the synthesis of 3-(4-chlorophenyl)-4-aminoisoxazole (114) | 81 |
| Synthesis of 4-chlorobenzoylchloride oxime (102d)..... | 81 |
| Synthesis of ethyl (<i>E</i>)-3-pyrrolidin-1-yl acrylate (110) | 81 |
| Synthesis of ethyl 3-(4-chlorophenyl)isoxazole-4-carboxylate (111) | 81 |
| Synthesis of 3-(4-chlorophenyl)isoxazole-4-carboxylic acid (112)..... | 82 |

| | |
|--|----|
| Synthesis of [3-(4-chlorophenyl)isoxazol-4-yl]-carbamic acid <i>tert</i> -butyl ester (113) | 82 |
| Synthesis of 3-(4-chlorophenyl)-4-aminoisoxazole (114) | 83 |
| Procedures for the synthesis of 5-(4-chlorophenyl)-1-methyl-4-amino-imidazole (116) | 84 |
| Synthesis of 5-(4-chlorophenyl)-1-methyl-4-nitro-imidazole (115) | 84 |
| Synthesis of 5-(4-chlorophenyl)-1-methyl-4-amino-imidazole (116) | 84 |
| Procedures for the synthesis of ethyl 3-amino-4-(4-chlorophenyl)furan-2-carboxylate (118) ... | 85 |
| Synthesis of 4-chlorophenyl-acrylonitrile sodium salt (117) | 85 |
| Synthesis of ethyl 3-amino-4-(4-chlorophenyl)furan-2-carboxylate (118) | 85 |
| Synthesis of 4'-chloro-[1,1-biphenyl]-2-amine (121) | 86 |
| General procedures for the synthesis of <i>N</i>-aryl amides (1-5, 7-12) | 87 |
| <i>N</i> -(4-(4-chlorophenyl)-1,2,5-oxadiazol-3-yl)-4-(trifluoromethyl)benzamide (MD77) | 89 |
| <i>N</i> -(4-phenyl-1,2,5-oxadiazol-3-yl)benzamide (1aa) | 89 |
| 4-(chloro)- <i>N</i> -(4-phenyl-1,2,5-oxadiazol-3-yl)benzamide (1ad) | 89 |
| 4-(trifluoromethyl)- <i>N</i> -(4-phenyl-1,2,5-oxadiazol-3-yl)benzamide (1ag) | 89 |
| <i>N</i> -(4-(2-chlorophenyl)-1,2,5-oxadiazol-3-yl)benzamide (1ba) | 90 |
| 4-(trifluoromethyl)- <i>N</i> -(4-(2-chlorophenyl)-1,2,5-oxadiazol-3-yl)benzamide (1bg) | 90 |
| <i>N</i> -(4-(3-chlorophenyl)-1,2,5-oxadiazol-3-yl)benzamide (1ca) | 90 |
| 4-(trifluoromethyl)- <i>N</i> -(4-(3-chlorophenyl)-1,2,5-oxadiazol-3-yl)benzamide (1cg) | 90 |
| <i>N</i> -(4-(4-chlorophenyl)-1,2,5-oxadiazol-3-yl)benzamide (1da) | 91 |
| 4-chloro- <i>N</i> -(4-(4-chlorophenyl)-1,2,5-oxadiazol-3-yl)benzamide (1dd) | 91 |
| 2-(trifluoromethyl)- <i>N</i> -(4-(4-chlorophenyl)-1,2,5-oxadiazol-3-yl)benzamide (1de) | 91 |
| 3-(trifluoromethyl)- <i>N</i> -(4-(4-chlorophenyl)-1,2,5-oxadiazol-3-yl)benzamide (1df) | 91 |
| 4-bromo- <i>N</i> -(4-(4-chlorophenyl)-1,2,5-oxadiazol-3-yl)benzamide (1dh) | 92 |
| 4-methyl- <i>N</i> -(4-(4-chlorophenyl)-1,2,5-oxadiazol-3-yl)benzamide (1di) | 92 |
| 4-methoxy- <i>N</i> -(4-(4-chlorophenyl)-1,2,5-oxadiazol-3-yl)benzamide (1dk) | 92 |
| 4-nitro- <i>N</i> -(4-(4-chlorophenyl)-1,2,5-oxadiazol-3-yl)benzamide (1dr) | 92 |
| 4-cyano- <i>N</i> -(4-(4-chlorophenyl)-1,2,5-oxadiazol-3-yl)benzamide (1dt) | 93 |
| 4-trifluoromethyl- <i>N</i> -(4-(4-bromophenyl)-1,2,5-oxadiazol-3-yl)benzamide (1hg) | 93 |
| 4-trifluoromethyl- <i>N</i> -(4-(4-trifluoromethylphenyl)-1,2,5-oxadiazol-3-yl)benzamide (1gg) | 93 |
| 4-chloro- <i>N</i> -(4-(4-trifluoromethylphenyl)-1,2,5-oxadiazol-3-yl)benzamide (1gd) | 93 |
| 4-trifluoromethyl- <i>N</i> -(4-(<i>p</i> -tolyl)-1,2,5-oxadiazol-3-yl)benzamide (1ig) | 94 |
| <i>N</i> -(4-([1,1'-biphenyl]-4-yl)-1,2,5-oxadiazol-3-yl)benzamide (1ja) | 94 |
| 4-(trifluoromethyl)- <i>N</i> -(4-([1,1'-biphenyl]-4-yl)-1,2,5-oxadiazol-3-yl) benzamide (1jg) | 94 |
| 4-trifluoromethyl- <i>N</i> -(4-(4-benzyloxyphenyl)-1,2,5-oxadiazol-3-yl)benzamide (1lg) | 95 |
| 4-trifluoromethyl- <i>N</i> -(4-(4-nitrophenyl)-1,2,5-oxadiazol-3-yl)benzamide (1rg) | 95 |
| <i>N</i> -(4-(4-chlorophenyl)-1,2,5-oxadiazol-3-yl)cyclohexanecarboxamide (2) | 95 |
| <i>N</i> -(4-(4-chlorophenyl)-1,2,5-oxadiazol-3-yl)heptanamide (3) | 95 |
| <i>N</i> -(4-(4-chlorophenyl)-1,2,5-oxadiazol-3-yl)butyramide (4) | 96 |
| <i>N</i> -(4-(4-chlorophenyl)-1,2,5-oxadiazol-3-yl)acetamide (5) | 96 |
| <i>N</i> -(5-(4-chlorophenyl)-1,3,4-oxadiazol-2-yl)benzamide (7da) | 96 |
| 4-trifluoromethyl- <i>N</i> -(5-(4-chlorophenyl)-1,3,4-oxadiazol-2-yl)benzamide (7dg) | 96 |
| <i>N</i> -(4-(4-chlorophenyl)-isoxazol-3-yl)benzamide (8da) | 97 |
| 4-trifluoromethyl- <i>N</i> -(4-(4-chlorophenyl)-isoxazol-3-yl)benzamide (8dg) | 97 |
| <i>N</i> -(3-(4-chlorophenyl)-isoxazol-4-yl)benzamide (9da) | 97 |
| 4-trifluoromethyl- <i>N</i> -(3-(4-chlorophenyl)-isoxazol-4-yl)benzamide (9dg) | 97 |
| <i>N</i> -(5-(4-chlorophenyl)-1-methyl-1 <i>H</i> -imidazol-4-yl)benzamide hydrochloride (10da · HCl) | 98 |

| | |
|--|-----|
| 4-trifluoromethyl- <i>N</i> -(5-(4-chlorophenyl)-1-methyl-1H-imidazol-4-yl)benzamide hydrochloride (10dg · HCl) | 98 |
| ethyl 3- <i>N</i> -benzamido-4-(4-chlorophenyl)furan-2-carboxylate (119da)..... | 98 |
| ethyl 3- <i>N</i> -(4-trifluoromethylbenzamide)-4-(4-chlorophenyl)furan-2-carboxylate (119dg) | 98 |
| <i>N</i> -(4-chloro-[1,1-biphenyl]-2-yl)benzamide (12da) | 99 |
| 4-trifluoromethyl- <i>N</i> -(4-chloro-[1,1-biphenyl]-2-yl)benzamide (12dg) | 99 |
| Synthesis of <i>N</i>-benzyl-4-(4-chlorophenyl)-1,2,5-oxadiazol-3-amine (6) | 100 |
| Synthesis of 4-hydroxy-<i>N</i>-(4-(4-chlorophenyl)-1,2,5-oxadiazol-3-yl) benzamide (1dm) | 101 |
| Synthesis of <i>N</i>-((4-(4-hydroxyphenyl)-1,2,5-oxadiazol-3-yl)-4-trifluoromethylbenzamide (1mg) | 102 |
| Synthesis of dibenzyl phenylphosphates (1dn,ng) | 103 |
| dibenzyl (4-((4-(4-chlorophenyl)-1,2,5-oxadiazol-3-yl)carbamoyl)phenyl) phosphate (1dn)... | 103 |
| dibenzyl (4-(4-(4-(trifluoromethyl)benzamido)-1,2,5-oxadiazol-3-yl)phenyl) phosphate (1ng)103 | 103 |
| Synthesis of phenyl dihydrogenphosphates (1do,og) | 104 |
| 4-((4-(4-chlorophenyl)-1,2,5-oxadiazol-3-yl)carbamoyl)phenyl dihydrogen phosphate (1do) 104 | 104 |
| 4-(4-(4-(trifluoromethyl)benzamido)-1,2,5-oxadiazol-3-yl)phenyl dihydrogen phosphate (1og).. | 104 |
| Synthesis of ethyl 2-(4-(4-(4-(trifluoromethyl)benzamido)-1,2,5-oxadiazol-3-yl)phenoxy)acetate (1pg) | 105 |
| Synthesis of 4-aminophenyl derivatives (1ds,sg) | 106 |
| 4-amino- <i>N</i> -(4-(4-chlorophenyl)-1,2,5-oxadiazol-3-yl)benzamide (1ds)..... | 106 |
| 4-trifluoromethyl- <i>N</i> -(4-(4-aminophenyl)-1,2,5-oxadiazol-3-yl)benzamide (1sg) | 106 |
| General procedures for the nitrile or ester hydrolysis under basic conditions (1du,qg, 120da,dg) | 107 |
| 4-(<i>N</i> -(4-(4-chlorophenyl)-1,2,5-oxadiazol-3-yl)carbamoyl)benzoic acid (1du) | 107 |
| 2-(4-(4-(4-(trifluoromethyl)benzamido)-1,2,5-oxadiazol-3-yl)phenoxy)acetic acid (1qg) | 108 |
| 3-benzamido-4-(4-chlorophenyl)furan-2-carboxylic acid (120da)..... | 108 |
| 4-(4-chlorophenyl)-3-(4-(trifluoromethyl)benzamido)furan-2-carboxylic acid (120dg)..... | 108 |
| Synthesis of ethyl 4-((4-(4-chlorophenyl)-1,2,5-oxadiazol-3-yl) carbamoyl)benzoate (1dv) | 109 |
| Synthesis of <i>N</i>-(4-(4-chlorophenyl)-furan-3-yl)benzamides (11da,dg) | 110 |
| <i>N</i> -(4-(4-chlorophenyl)furan-3-yl)benzamide (11da) | 110 |
| 4-trifluoromethyl- <i>N</i> -(4-(4-chlorophenyl)furan-3-yl)benzamide (11dg)..... | 110 |
| Procedure for the synthesis of 1-(4-(4-chlorophenyl)-1,2,5-oxadiazol-3-yl)methanamine hydrochloride (14 · HCl) | 111 |
| Synthesis of ethyl 4-chlorocinnamate (122) | 111 |
| Synthesis of 4-chlorocinnamyl alcohol (123) | 111 |
| Synthesis of 4-(4-chlorophenyl)-3-(hydroxymethyl)-1,2,5-oxadiazole 2-oxide (124)..... | 112 |
| Synthesis of 4-(4-chlorophenyl)-3-(hydroxymethyl)-1,2,5-oxadiazole (125)..... | 112 |
| Synthesis of 4-(4-chlorophenyl)-3-(azidomethyl)-1,2,5-oxadiazole (126) | 113 |
| Synthesis of 1-(4-(4-chlorophenyl)-1,2,5-oxadiazol-3-yl)-methanamine hydrochloride (14 · HCl). | 113 |
| Procedure for the synthesis of 2-amino-2-(4-(4-chlorophenyl)-1,2,5-oxadiazol-3-yl)-1-phenylethan-1-one hydrochlorides (15a-c · HCl) | 114 |
| Synthesis of 1-(4-chlorophenyl)-2-(hydroxyimino)propan-1-one (127) | 114 |
| Synthesis of 1-(4-chlorophenyl)propane-1,2-dione dioxime (128) | 114 |
| Synthesis of 3-(4-chlorophenyl)-4-methyl-1,2,5-oxadiazole (129) | 115 |

| | |
|--|------------|
| General procedure for the synthesis of 2-(4-(4-chlorophenyl)-1,2,5-oxadiazol-3-yl)-1-phenylethan-1-ones (130a-c)..... | 115 |
| 2-(4-(4-chlorophenyl)-1,2,5-oxadiazol-3-yl)-1-(4-trifluoromethyl)phenylethan-1-one (130a) .. | 116 |
| 2-(4-(4-chlorophenyl)-1,2,5-oxadiazol-3-yl)-1-phenylethan-1-one (130b)..... | 116 |
| 2-(4-(4-chlorophenyl)-1,2,5-oxadiazol-3-yl)-1-(4-methoxy)phenylethan-1-one (130c) | 116 |
| Synthesis of 2-(4-(4-chlorophenyl)-1,2,5-oxadiazol-3-yl)-2-(hydroxyimino)-1-phenylethan-1-ones (131a-c)..... | 117 |
| 2-(4-(4-chlorophenyl)-1,2,5-oxadiazol-3-yl)-2-(hydroxyimino)-1-(4-trifluoromethyl)phenylethan-1-one (131a) | 117 |
| 2-(4-(4-chlorophenyl)-1,2,5-oxadiazol-3-yl)-2-(hydroxyimino)-1-phenylethan-1-one (131b).... | 117 |
| 2-(4-(4-chlorophenyl)-1,2,5-oxadiazol-3-yl)-2-(hydroxyimino)-1-(4-trifluoromethyl)phenylethan-1-one (131c) | 118 |
| Synthesis of 2-amino-2-(4-(4-chlorophenyl)-1,2,5-oxadiazol-3-yl)-1-phenylethan-1-one hydrochlorides (15a-c · HCl)..... | 118 |
| 2-amino-2-(4-(4-chlorophenyl)-1,2,5-oxadiazol-3-yl)-1-(4-trifluoromethyl)phenylethan-1-one hydrochloride (15a · HCl) | 118 |
| 2-amino-2-(4-(4-chlorophenyl)-1,2,5-oxadiazol-3-yl)-1-phenylethan-1-one hydrochloride (15b · HCl)..... | 119 |
| 2-amino-2-(4-(4-chlorophenyl)-1,2,5-oxadiazol-3-yl)-1-(4-methoxy)phenylethan-1-one hydrochloride (15c · HCl)..... | 119 |
| Synthesis of 2-(4-(4-chlorophenyl)-1,2,5-oxadiazol-3-yl)-2-(hydroxyamino)-1-phenylethan-1-ones (16a-c) | 120 |
| 2-(4-(4-chlorophenyl)-1,2,5-oxadiazol-3-yl)-2-(hydroxyamino)-1-(4-(trifluoromethyl)phenyl)ethan-1-one (16a)..... | 120 |
| 2-(4-(4-chlorophenyl)-1,2,5-oxadiazol-3-yl)-2-(hydroxyamino)-1-phenylethan-1-one (16b)..... | 120 |
| 2-(4-(4-chlorophenyl)-1,2,5-oxadiazol-3-yl)-2-(hydroxyamino)-1-(4-methoxyphenyl)ethan-1-one (16c) | 121 |
| General procedure for the synthesis of platinum complexes | 122 |
| Pt-13 | 122 |
| Pt-14 | 122 |
| Pt-15b | 122 |
| Pt-15c | 123 |
| Pt-16a | 123 |
| Pt-16b | 123 |
| Pt-16c | 123 |
| Procedures for the synthesis of methyl 1-(2-(1H-indol-3-yl)ethyl)-5-(1-hydroxyethyl)-1,4,5,6-tetrahydropyridine-3-carboxylates (19,20) | 124 |
| Synthesis of methyl 2-cyano-2-hexenoate (134) | 124 |
| Synthesis of methyl 2-chloro-5-ethylnicotinate (135) | 124 |
| Synthesis of methyl 5-ethylnicotinate (136) | 125 |
| Synthesis of methyl 5-(1'-bromoethyl)nicotinate (137) | 125 |
| Synthesis of methyl 5-(1'-hydroxyethyl)nicotinate (138) | 125 |
| Synthesis of 1-(2-(1H-indol-3-yl)ethyl)-3-(1-hydroxyethyl)-5-(methoxycarbonyl)pyridin-1-ium bromide (139) | 126 |

| | |
|--|------------|
| Synthesis of methyl 1-(2-(1H-indol-3-yl)ethyl)-5-(1-hydroxyethyl)-1,4,5,6-tetrahydropyridine-3-carboxylates (19,20)..... | 126 |
| General procedures for the synthesis of 21-23 | 128 |
| Synthesis of <i>O,O'</i> -diacetyl-D-pantothenic acid (140)..... | 128 |
| Synthesis of <i>O,O'</i> -diacetyl-D-pantothenamides (141,144) | 128 |
| methyl <i>O,O'</i> -diacetyl-D-pantothenamide (141)..... | 129 |
| tert-butyl <i>N</i> -(<i>O,O'</i> -diacetyl-D-pantothenoyl)- γ - aminobutanoate (144)..... | 129 |
| Synthesis of <i>N</i> -(<i>O,O'</i> -diacetyl-D-pantothenoyl)- γ -aminobutyric acid (145)..... | 129 |
| Synthesis of Meldrum's acid derivatives (142,146) | 130 |
| (R)-4-((3-(2,2-dimethyl-4,6-dioxo-1,3-dioxan-5-ylidene)-3-hydroxypropyl)amino)-2,2-dimethyl-4-oxobutane-1,3-diyl diacetate (142) | 130 |
| <i>N</i> -[4-(2,2-dimethyl-4,6,-dioxo-1,3-dioxan-5-ylidene)-4-hydroxybutyl]- <i>O,O'</i> -diacetyl-D-pantothenamide (146)..... | 130 |
| Synthesis of methyl β -ketoesters (143,147) | 131 |
| (R)-4-((5-methoxy-3,5-dioxopentyl)amino)-2,2-dimethyl-4-oxobutane-1,3-diyl diacetate (143) | 131 |
| <i>O,O'</i> -diacetylmalonylcarba(dethia)pantetheine methylester (147) | 131 |
| Deprotection of <i>O,O'</i> -diacetyl groups (21-23) | 132 |
| (R)-2,4-dihydroxy-3,3-dimethyl- <i>N</i> -(3-(methylamino)-3-oxopropyl)butanamide (21) | 132 |
| methyl (R)-5-(2,4-dihydroxy-3,3-dimethylbutanamido)-3-oxopentanoate (22) | 132 |
| malonyl carba(dethia)-pantetheine methylester (23) | 132 |
| Procedures for the synthesis of 2-amino-4-(1H-indol-3-yl) pyrimidine-5-carbonitrile (24) | 133 |
| Synthesis of 3-(1H-Indol-3-yl)-3-oxo-propionitrile (148) | 133 |
| Synthesis of (2 <i>Z</i>)-3-(dimethylamino)-2-(1H-indole-3-carbonyl)acrylonitrile (149)..... | 133 |
| Synthesis of 2-amino-4-(1H-indol-3-yl)pyrimidine-5-carbonitrile (24) | 134 |
| Chapter 8: Experimental Part: Biology | 135 |
| 8.1 Materials and Methods..... | 136 |
| 8.1.1 MTT-assay..... | 136 |
| 8.1.2 AlphaScreen-based assay | 136 |
| 8.1.3 <i>In vivo</i> antitumor activity in Lewis Lung Carcinoma | 136 |
| 8.1.4 Determination of intracellular and DNA-bound Pt concentrations | 136 |
| 8.1.5 Binding study with 9-ethylguanine and GSH | 137 |
| 8.1.6 Western blot analysis | 137 |
| 8.1.7 RNA Preparation and Quantitative Real Time PCR..... | 137 |
| Abbreviations | 139 |
| References | 143 |

Chapter 1

Introduction

1.1 Cancer

Cancer affects all of humankind. The incidence of cancer has increased from 12.7 million in 2008 to 14.1 million in 2012. This trend is expected to continue, bringing the number of cancer cases close to 25 million over the next two decades.^[1]

The most common sites of cancer diagnosed in 2012 include:

- lung (16.7% of the total), prostate (15.0%), colorectum (10.0%), stomach (8.5%), and liver (7.5%), among men;
- breast (25.2% of the total), colorectum (9.2%), lung (8.7%), cervix (7.9%), and stomach (4.8%), among women.

However, there is a marked variability across local, national, and regional boundaries. Worldwide, differences in cancer incidence can be related to different causes and, by inference, different opportunities for prevention. Indeed, each tumor type may be characterized with reference to epidemiology, etiology, pathology, genetics, and prevention. Nevertheless, it is clear that cancer is not a single disease but a multiplicity of different diseases, therefore, understanding cancer biology is critical to develop rationally designed therapy and offer preventive options.

The survival of organisms depends on the accurate transmission of genetic information from one cell to its daughters. Such faithful transmission requires not only extreme accuracy in replication of DNA and precision in chromosome distribution, but also the ability to survive spontaneous and induced DNA damage while minimizing the number of heritable mutations.

Hence, the identification of the differences between tumor cells and normal ones is crucial: cumulative genetic and epigenetic changes may mediate, amongst other effects, altered metabolism or modified intracellular signaling in response to growth-altering stimuli. Cancer cells provide their own growth signals, ignoring inhibitory ones, avoiding cell death, replicating without limit, sustaining angiogenesis, and invading tissues through basement membranes and capillary walls.

Thus, the roles of cancer stem cells (a subpopulation of tumor cells with aberrant unlimited proliferative potential and the capacity to confer tumor heterogeneity and to migrate) and the tumor microenvironment have to be considered in the search of novel approaches to cancer therapy. The tumor microenvironment encompasses the biochemical and cellular composition of the tissue. Bidirectional signaling between cancer and stromal cells has effects on cancer cell division, immune cell function, and resistance to therapeutic intervention, resulting in poor clinical outcome. For these reasons, a combined therapy that targets cancer cells and modifies the tumor microenvironment (i.e. anti-angiogenic therapy) could have synergic benefits.

Curative or palliative treatments^[2] require a wide strategy and, at the moment, the fundamental therapeutic approaches include:

- Surgery, often the first approach used against the disease, it is effective if the tumor mass is sufficiently small to allow its safe removal. It is usually combined with radiotherapeutic and chemotherapeutic treatments in order to increase chances of healing and survival.
- Radiotherapy (ionizing radiations, X-ray or γ -ray) which targets the tumor DNA leading to the death of cancer cells as a consequence of their inadequate capacity to repair their own genomic damages. It can be used alone or in association with chemotherapy to treat self-contained cancers and to control primary metastatic cancers.
- Immunotherapy, using the patient immune system to eradicate neoplasms. Actually, this therapy requires the administration of α -interferon and interleukin-2 in order to increase T and B lymphocyte levels.

- Chemotherapy, fundamental against both primary cancer and metastasis. It is characterized by administration of cytotoxic drugs, which enter into the bloodstream, thus reaching any part of the body.

Surgery and radiation therapy are preferred for restricted cancers while immunotherapy and chemotherapy are recommended for metastatic cancers.

1.1.1 Chemotherapy and targeted therapy

Antitumor agents^[2] are most effective at killing cells that are rapidly dividing due to the higher vulnerability to their cytotoxic action. Indeed, slow-growing cancers, such as non-small cell lung cancer (NSCLC) characterized by a high percentage of cells in G₀ phase, are comparatively less sensitive to standard chemotherapy. Some chemotherapeutic agents are cell cycle non-specific (e.g. alkylating agents), some others attack cells at very specific phases in the cell cycle (for instance antimetabolites mainly act on cells in S phase while mitotic-spindle inhibitors kill cells in M phase). It is very important to fight cancer as soon as possible in order to increase the chances of therapeutic success.

The selectivity for cancer cells is one of the most important characteristics of anticancer agents. This feature is only an ideal because all anticancer drugs have side effects on healthy tissues. These effects refer specifically to rapidly proliferating tissues: bone marrow (leukopenia, thrombocytopenia, anemia, immunosuppression and infection), gastrointestinal mucosa (stomatitis, enteritis, muco-membranous colitis, diarrhea), cutaneous annexes (alopecia) and gonads (amenorrhea and azoospermia).

Beyond side effects, another problem associated with chemotherapy is the rising of resistance which can compromise therapy. This phenomenon has many causes: it can arise naturally, regardless of the contact between drug and cell, or it can be acquired if a continuous treatment with the same drugs produce modifications in the cell.

The transition from cytotoxic chemotherapy to molecularly targeted cancer drug discovery and development resulted in an increasing number of successful therapies that impacted the lives of a large number of cancer patients.^[3] Also targeted therapy drugs, like any drug used to treat cancer, can technically be considered “chemotherapy.” But while standard chemotherapies act on all rapidly dividing cells, both normal and cancerous, targeted cancer therapy drugs block the growth and spread of cancer by interfering with specific molecules that are involved in these processes.

Considering their different mechanism, targeted therapies are often cytostatic (blocking tumor cell proliferation), whereas standard chemotherapy agents are cytotoxic (killing tumor cells). Moreover, they are often able to selectively attack cancer cells since they are more dependent on the targets than normal cells, doing less damage to these latter having different (and often less severe) side effects than standard chemotherapy drugs. Resistance can also occur as a consequence of modifications of the target itself and/or the development of a new pathway capable of bypassing it.

For this reason, even if the first approach consists in mono-chemotherapy, the combination of targeted therapies or a targeted therapy with one or more traditional chemotherapy drugs could be more effective^[4] fighting tumor cells through various mechanisms and overcoming resistance problems. Moreover, in order to limit side effects (such as immunosuppression), these drugs are administrated according to treatment cycles. In this way the organism can recover from side effects and new cancer cells can enter in replication phase.

Most targeted therapies use either small molecules or monoclonal antibodies, developed for targets that are located inside the cell or on its surface, respectively.

Since signaling pathways regulate a plethora of biological processes mediating cell survival, proliferation, response to growth factors, and related biological processes, transcription factors are important meeting

points for controlling these homeostasis processes through modulation of gene expression. Therefore, considering their dysregulation in many cancer cell lines, targeting transcription factors, such as STAT3 (see **Section 1.2**), as well as the DNA itself (see **Section 1.3**), may increase the efficiency of anticancer therapy. Moreover, although cancer chemotherapy plays a very important role in the reduction of mortality, the extreme toxicity of anticancer drugs and the development of resistance to their action have made it essential to continue researching with the aim to identify new compounds endowed with higher efficacy and minor toxicity.

1.2 STAT3

STATs (Signal Transducer and Activator of Transcription) are latent cytosolic transcription factors that directly relate signals from the plasma membrane to the nucleus and, depending on their main function, the seven isoforms^[5] can be categorized into two groups:

- STAT2, STAT4 and STAT6 are activated by a reduced number of cytokines, which are involved in development of T-cells and interferon- γ (IFN- γ) pathway;
- STAT1, STAT3 and STAT5 are concerned respectively with IFN signaling, development of mammary glands and response to growth hormone and embryogenesis. They are also involved in cell cycle control and apoptosis.

According to their physiological role, in pathological conditions STAT3 and STAT5 are the isoforms more related to human cancer.^[6] In particular STAT3 was found to participate in cell signaling events, leading to oncogenic transformation, and to be constitutively activated in more than half of breast and lung cancers, hepatocellular carcinomas, multiple myelomas, and in more than 95% of head and neck cancers.^[7,8] Constitutive STAT3 dimer induces nuclear translocation, DNA-binding, transactivation of target genes, oncogenic transformation, and tumorigenesis. Furthermore, numerous reports have shown that blocking constitutively activated STAT3 signaling leads to tumor cell apoptosis, with minimal effect on normal cells.^[9] This selective inhibition might reflect an irreversible dependence of tumor cells on high levels of activated STAT3 for growth and survival, whereas normal cells could withstand lower levels of STAT3 activity or use alternative pathways.^[8]

STAT proteins are characterized by seven structurally and functionally conserved domains (see **Section 5.2**) and among them, the Src homology 2 (SH2) is the one primarily involved in its activation, triggered by cytokines and growth factors, as well as by oncogenic proteins, such as Src and Ras. Upon phosphorylation of the tyrosine residue at position 705, STAT3 dimerizes through specific reciprocal SH2-phosphotyrosine interaction (**Figure 1**).^[8]

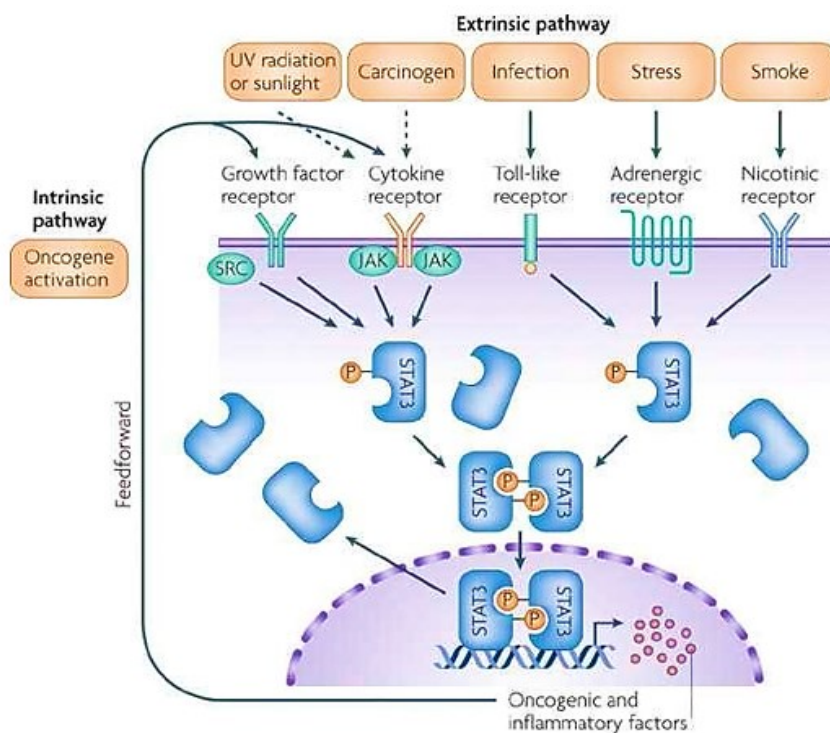


Figure 1. STAT3 connects inflammation and cancer.^[10]

The dimer translocates into the nucleus, binds to specific DNA-binding elements and activate the transcription of target genes involved in cell proliferation, differentiation, apoptosis and inflammation.^[6]

In detail, STAT3 promotes the activation of cell inflammatory pathway, including the pro-inflammatory transcription factor NF- κ B pathway, playing an important role in inflammation acute-phase. Neoplasm and inflammation are connected by extrinsic/environmental (chemical carcinogens, infection, ultraviolet radiation, stress and cigarette smoke) and intrinsic/genetic pathways. Since it promotes the malignant properties correlated with chronic inflammation, STAT3 is crucial for both of these mechanisms. Moreover, STAT3 seems to facilitate tumor evasion of the immune system, positively regulating the transcription of different cytokines that suppress the immune response.^[10]

Another heavily impaired process in cancer is apoptosis. Genes coding for apoptosis inhibitors (such as Bcl-2 family) are STAT3 targets and, for this reason, are overexpressed in cancerous cell. Besides suppressing apoptosis, STAT3 also enhances proliferation by controlling the expression of proteins that lead the cell cycle throughout each phase (such as cyclin D1 protein).^[7]

Also angiogenesis is essential for tumor growth at the primary site and for its progression to the metastatic site in order to satisfy the high demand of oxygen and energy required for growth and metabolism. This process is regulated by the balance of pro-angiogenic (e.g., basic fibroblast growth factor and VEGF-A) and anti-angiogenic (e.g., endostatin and angiostatin) factors in the tumor microenvironment. STAT3 modulates angiogenesis up-regulating various pro-angiogenic factors,^[6] and participates in metastatic progression through different molecular mechanisms, such as inducing the expression of matrix metalloproteinases.^[11]

1.2.1 STAT3 signaling pathway

Growth factors, cytokines and other polypeptide ligands, unable to cross the cytoplasmic membrane, have to interact with membrane receptors and the message has to be internalized and transferred to the nucleus where it determines the expression of the ligand-dependent genetic program. STAT3 recruitment, activation, nuclear translocation and deactivation has a main role in the general above mentioned signaling pathway.

In regard to STAT3 activation, there are several pathways among which the most significant is the JAK/STAT canonical pathway, where STAT3 is activated by phosphorylation and dimer formation. Otherwise, the non-canonical one is characterized by dimer formation without tyrosine phosphorylation.

In detail, STAT3 is located in the cytoplasm or on the cytosolic side of the cellular membrane in a latent hypophosphorylated form. Many membrane receptors have intrinsic tyrosine-kinase activity (such as growth factors receptors including EGFR and HER2) but some others, lacking this property (such as IL-6 or interferon receptors), have to recruit cytoplasmic tyrosine kinases (TKs), for instance JAK (Janus Kinase) proteins, to operate as mediators for STAT activation. Therefore, in the JAK/STAT3 canonical pathway, after ligand-receptor association and activation, its phosphorylated portion acts as a docking site for the SH2 domain of the STAT3 monomer. STAT3 itself is phosphorylated at the C-terminus tyrosine residue (Tyr 705 in STAT3) leading to dimer formation, through a reciprocal pTyr - SH2 domain interaction. This complex translocates into the nucleus, binds specific DNA-response elements and modulates gene transcription.^[12]

Recent studies demonstrate that not only phosphorylated STAT3 but also unphosphorylated STAT3 can form the dimer, translocate into the nucleus, and bind to the STAT3 binding sites. Therefore, even if the mechanism of unphosphorylated STAT3 binding to the promoter remains unclear, its significant role in oncogenesis has been validated.^[13]

The importation exploits the active transport through the nuclear pore complexes (NPC), since the dimensions (about 180 kDa) of the dimeric structure are excessive for passive diffusion. Importins are karyopherin involved in STAT nuclear translocation. They are constituted of two subunits, respectively importin- α and importin- β . After the binding with STAT dimer, importin α interacts with importin- β and

mediates the movement of the complex into the nucleus.^[14] The isoforms usually implicated in the canonical STAT3 activation pathway are importin- α_5 and $-\alpha_7$, while the unphosphorylated STAT3 dimer move to the nucleus thanks to the participation of importin- α_3 . This mechanism suggests that in addition to phosphorylated STAT3, also the non-canonical pathway (unphosphorylated STAT3) permits the transcription of STAT3 target genes, playing an important role in oncogenesis.^[13] If in the JAK/STAT activation pathway the *tyrosine activation domain* plays a crucial role for dimerization, in the non-canonical pathway this role seems to be performed by the *N-terminal domain* probably interacting with another domain (maybe the SH2 domain) instead of forming homotopic interactions. Indeed, while the *N-terminal domain* is essential for unphosphorylated STAT3 dimerization, deletion of the same domain allows the complexation of canonical pTyr-STAT3.^[15]

Like the nuclear import, nuclear export requires the presence of carriers called exportins, which mediate the translocation of STAT3 dimer, that has already interacted with DNA target sequences, from the nucleus to the cytoplasm.^[15]

Recent studies have shown that STAT3 activation can be negatively modulated by different mechanisms, including direct dephosphorylation of JAKs and STATs, proteolytic disruption through ubiquitin-proteasome pathway and participation of specific inhibiting protein families, such as PIAS (proteins that inhibit activated STAT proteins family) and SOCS (suppressors of cytokine signaling family).^[12]

1.2.2 STAT3 inhibitors

The association between constitutive STAT3 activation and malignant transformation was originally discovered more than 20 years ago.^[16] Since then, substantial efforts have been made towards the identification of novel STAT3 inhibitors. Despite the potential involvement of uSTAT3 in oncogenesis and signaling in cancer cells, to date, the research has focused on the inhibition of the phosphorylated form.^[17] Two general approaches have been explored in the inhibition of STAT3 signaling^[12,18]: indirect, involving the inhibition of factors that lead to STAT3 activation, and direct, based on the interaction of small molecules with the protein. However, since all known STAT3 inhibitors are still at the experimental stage and not in a suitable form for clinical utility, the challenge is the discovery of new drug candidates, with high potency and *in vivo* activity. In order to achieve this goal, a direct inhibitory approach is preferred, as the nonspecific nature of the indirect strategy could cause important adverse effects. Regarding the direct approach, considerable attention has been directed at disrupting the STAT3 dimerization, a fundamental step in the activation process. The slow progress in obtaining suitable STAT3 inhibitors for clinical development could be attributed to the challenge of targeting protein-protein interactions (PPIs), given the large surface area of the target and the chemistry of these interactions.^[19]

Based on their structural characteristics, the direct inhibitors can be divided into five groups: peptides, peptidomimetics, natural compounds, synthetic compounds and oligonucleotides.^[12]

The purpose of part this PhD project is the identification of novel synthetic compounds able to directly inhibit STAT3 activity through binding to its SH2 domain. In the literature, there are several promising small molecules candidates identified through computational studies and screening of chemical libraries, which are able to inhibit STAT3 activity^[12]. They include:

- 3,4- disubstituted-1,2,5 oxadiazoles (see **Section 2.1**);
- platinum-based compounds (see **Section 1.3.3**);
- compounds containing pTyr-mimetic fragments, such as 4-phosphonodifluoromethyl-cinnamate^[20,21], arylsulfonamide^[22], 4-amino and 4- hydroxyl salicylic acid^[23], catechol structure^[24] or purine scaffold^[25].

1.3 Platinum based anticancer drugs

Although metal-based compounds were exploited for years for the treatment of several diseases, the discovery of cisplatin^[26] (cis-[PtCl₂(NH₃)₂]) in the 1960s meaningfully enhanced the attention to the field of chemotherapy based on metalorganic entities^[27]. Over the last fifty years, a huge amount of analogues was prepared with the aim to enlarge the spectrum of activity, overcome the resistance issue and reduce the toxicity of both the first (cisplatin) and the second (carboplatin^[28]) generation of platinum compounds (**Figure 2**).

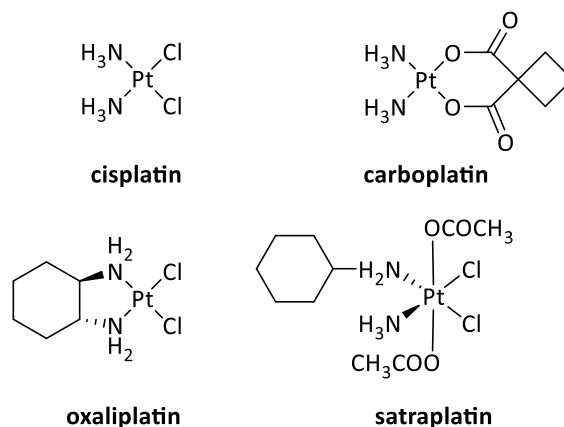


Figure 2. Main platinum drugs in clinics.

Among all, oxaliplatin^[29] achieved anticancer activity in cell lines intrinsically resistant to cisplatin and carboplatin as well as in those that had developed acquired resistance, while satraplatin was the first orally administered platinum drug with a promising profile in the treatment of prostate cancer. Up to now, the Food and Drug Administration (FDA)-approved platinum based anticancer drugs cisplatin, carboplatin and oxaliplatin are still among the most effective drugs used for the treatment of solid cancers, but the strong side effects and the increasing resistance are limitations to their use, thus highlighting the need for new platinum-based chemotherapeutics.^[30]

Since DNA was established to be the primary target of platinum drugs, an extensive investigation was carried out in order to characterize the mechanism of cellular accumulation and the types of adducts formed with the DNA.

1.3.1 How platinum-based chemotherapeutics work

The metals' property to become positively charged ions in aqueous solution makes them able to interact with negatively charged biological molecules. In aqueous solution, cisplatin (as well as platinum complexes in general) undergoes a series of aquation and hydrolysis reactions due to the displacement of the chloro ligands by water molecules (**Figure 3**).^[31]

Upon administration to the bloodstream through an intravenous injection, cisplatin is relatively stable (68% of the complex remains in its original form / 24% as chloridohydroxido species) due to the high concentration of chloride ions. All these species are suitable for passive diffusion across the cell membrane and the lower concentration of chloride ions inside the cell facilitates aquation reactions to form the cationic aqua species unable to diffuse back out of the cell before interacting with intracellular targets.^[27]

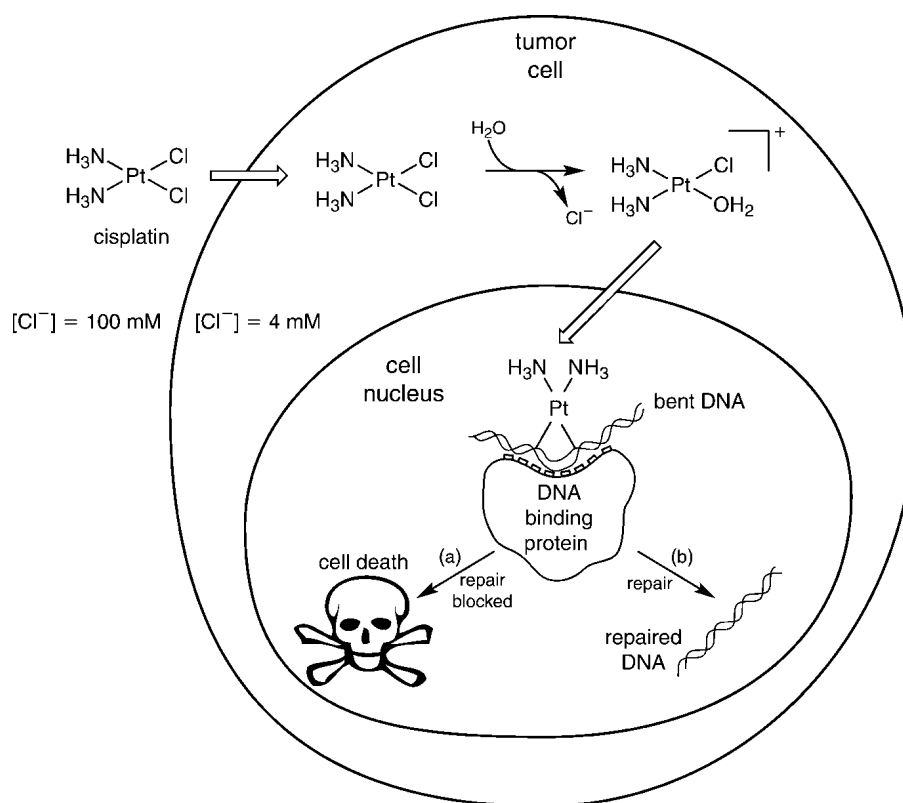


Figure 3. Cytotoxic pathway for cisplatin: after entering the cell, cisplatin is aquated, then binds to cellular DNA. If the DNA lesion is not repaired by the cell (path a), cell death (apoptosis) can occur. ^[31]

Even if passive diffusion is the major mechanism of transport for entering into the cells, active transport in cisplatin uptake was also observed. These active or facilitated pathways also have a role in resistance issue which, for instance, appeared to be increased in cells transfected with copper-transporting P-type ATPase (ATP7B, an efflux transporter) or lacking copper transporter 1 (Ctr-1, an influx transporter). ^[32,33] Besides, different organic cation transporters (OCTs) were related to specific tumor activities of various platinum complexes: OCT1 and OCT2 increased accumulation and cytotoxicity of oxaliplatin but not those of cisplatin and carboplatin. These results also strongly suggest that the expression of OCTs could be a marker for selecting specific platinum-based therapies in individual patients. ^[34]

Once inside the cell, the hydrolysis reactions which replaced one or both of the chloro ligands by water molecules lead to the formation of different activated species endowed with a higher reactivity towards nucleophiles considering that water is a much better leaving group than chloride. The formation of the monoaqua species $\text{cis-}[\text{Pt}(\text{NH}_3)_2\text{Cl}(\text{H}_2\text{O})]^+$ is the rate-limiting step in DNA coordination. This activated species binds guanine-N7 (or adenine-N7) releasing the water molecule and leading to monofunctional adducts, which is considered to be unable to display cytotoxic effects. Indeed, the release of a second chloride is necessary to produce intrastrand and interstrand cross-links, responsible for platinum drug ability to block DNA replication and/or transcription. ^[31]

Compared to cisplatin, oxaliplatin displayed a lower reactivity with DNA probably due to a slower dissociation rate of the oxalate ligand under physiological conditions. Moreover, oxaliplatin uptake was proved to be independent from Ctr-1 transporter at higher concentrations. Therefore, differences in spectrum of activity could be a consequence of its different uptake mechanism but could also be related to the formation of Pt-adducts able to flee from being identify by DNA recognition and repair systems. ^[29]

A deeper analysis of platinum complex biochemistry highlighted the evidence that non-DNA targets (such as STAT3) are involved in determining cytotoxic effects, too; therefore:

- inside the nucleus, platinum drug reacts preferentially with DNA, due to the high nucleotide concentration;^[35]
- in the cytosol, it targets thiol-containing proteins leading to cytotoxic effects or being deactivated, due to the interaction with thiol-rich metallothioneins (MT) or conjugation to glutathione (GSH).^[36]

However, some studies hypothesized that the binding to GSH may also represent a valid mechanism for the drug storage inside the cell, thus modulating the kinetics of DNA platination.^[37]

The equilibrium between these aspects is different for each platinum drug. For instance, only 5-10% of cisplatin covalently bound to cells is detectable in DNA fraction while 75-85% of the drug resulted bound to proteins.^[38]

The insurgence of resistance is a common drawback in platinum-based chemotherapy and the molecular mechanisms can be divided into two main groups:^[38]

- mechanisms that prevent the drug from reaching its cellular targets, due to a diminished influx/increased efflux process or drug inactivation;
- mechanisms responsible for inhibiting the possible cell-death pathways (necrosis or apoptosis), once platinum-DNA adducts are formed thanks to enhanced DNA repair processes (such as nucleotide excision repair (NER) involved in the removal of platinum 1,2-lesions from DNA).

1.3.2 Structure–activity relationships

Early studies on cisplatin allowed to determine the structural features that a platinum compound requires for displaying antitumor properties (**Figure 4a**):^[31]

- the compound should have two amines coordinated with a *cis*-geometry, as the *trans* ones were proved inactive or at least less active;
- although it does not appear sufficient for exhibiting activity, the complex has to possess two groups that can be more easily lost, the so-called “leaving groups”, once again arranged in *cis* configuration;
- the leaving groups, which the toxic profile of the compound relies on, should be moderately bound to the metal center as the ones with too labile groups result excessively toxic whereas those carrying functions too tightly bound are inactive;
- the neutrality of the compound is necessary;
- the fewer are the alkyl groups on the amine ligands, the greater is the activity. At least one hydrogen atom should be carried by each amine ligand for a significant activity to be observed.

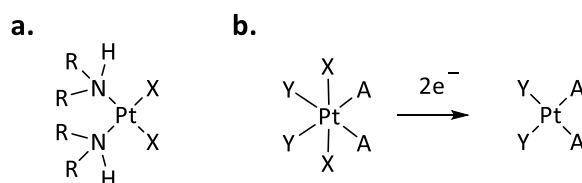


Figure 4. a. The general structure of platinum(II) complexes where X = leaving groups (e.g. two chloro groups or a bidentate malonate), ligand R = H or an alkyl substituent. **b.** The general structure of a platinum(IV) complex and its reduction to more reactive platinum(II) analogue, where: A = *cis* amine, Y = leaving groups in equatorial plane, and X = axial ligands.

The majority of the research efforts focused on platinum(II) compounds resulted in a plethora of new platinum complexes which proved to possess anticancer properties without adhering to the SAR rules

mentioned above.^[39] One of the approaches to overcome the toxicity consists in the use of prodrugs that are selectively activated in tumors and the use of carrier groups capable of selectively targeting tumors. Platinum(IV) compounds^[40], such as satraplatin, showed high activity, low toxicity and an increased stability so that they might be orally administered. Considering the inert oxidation state, they behave as prodrugs that have to be reduced to their active platinum(II) analogues with the loss of the axial ligands^[41] (**Figure 4b**). These latter play a pivotal role in modulating pharmacokinetic parameters such as the rate of reduction, the lipophilicity and the molecular targeting.^[27] In addition, the axial ligands themselves could confer additional cytotoxicity upon their release.

1.3.3 Platinum compounds and STAT3

The connection between these chemotherapeutic agents, which typically form bifunctional DNA cross-links, and STAT3 activity is supported by literature (**Figure 5**). Indeed, kinetically labile platinum(IV) complexes, reported by Turkson and co-workers to induce tumor regression in a mouse model of colon cancer, were established to inhibit STAT3 activity in living cells through an irreversible interaction with the STAT3-DNA-binding domains.^[42,43] Besides, the involvement of STAT3-activated cellular responses in cisplatin resistant tumors was highlighted by the ability of Stattic, an effective STAT3 inhibitor targeting the SH2 domain, to restore the sensitivity to platinum-based drugs both *in vitro* and *in vivo*.^[44,45]

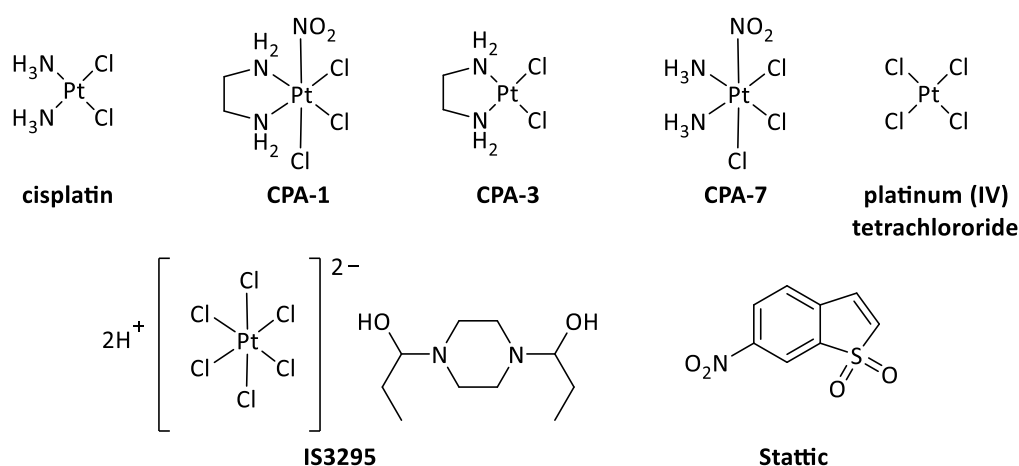


Figure 5. Structures of platinum complexes developed as STAT3 inhibitors.

Compound IS3295 was found to display selective inhibition of constitutive STAT3 over STAT1 (STAT3, $IC_{50} = 1.4 \mu\text{M}$ vs STAT1, $IC_{50} = 4.1 \mu\text{M}$), inducing cell cycle arrest and apoptosis, by directly binding STAT3, both as monomer and dimer. Its inhibitory activity occurred through non-competitive kinetics and by irreversibly binding STAT3 through a cysteine residue of the protein. Preliminary evaluations of the potential activity of IS3295 complex on human and mouse cancer cells demonstrated its ability to induce cell cycle arrest and apoptosis, making the development of platinum compounds as STAT3 inhibitors very promising.^[42]

Moreover, cells readily become resistant to anticancer drugs that target a single protein, utilizing alternative metabolic pathways.^[46]

1.4 Topoisomerases

DNA topoisomerases are nuclear enzymes which play an essential role in the management of the topological state of DNA in cells. DNA is rolled up on itself to form a double helix, which has to be temporarily (transcription or recombination) or permanently (replication) separated in order to access the information stored herein.

There are two classes of topoisomerases, type I and type II, and they have a key role in regulating the degree of DNA supercoils, causing a break into the DNA, followed by the formation of a phosphodiester bond between a tyrosine residue of the enzyme and one at the ends of the broken strand. [47]

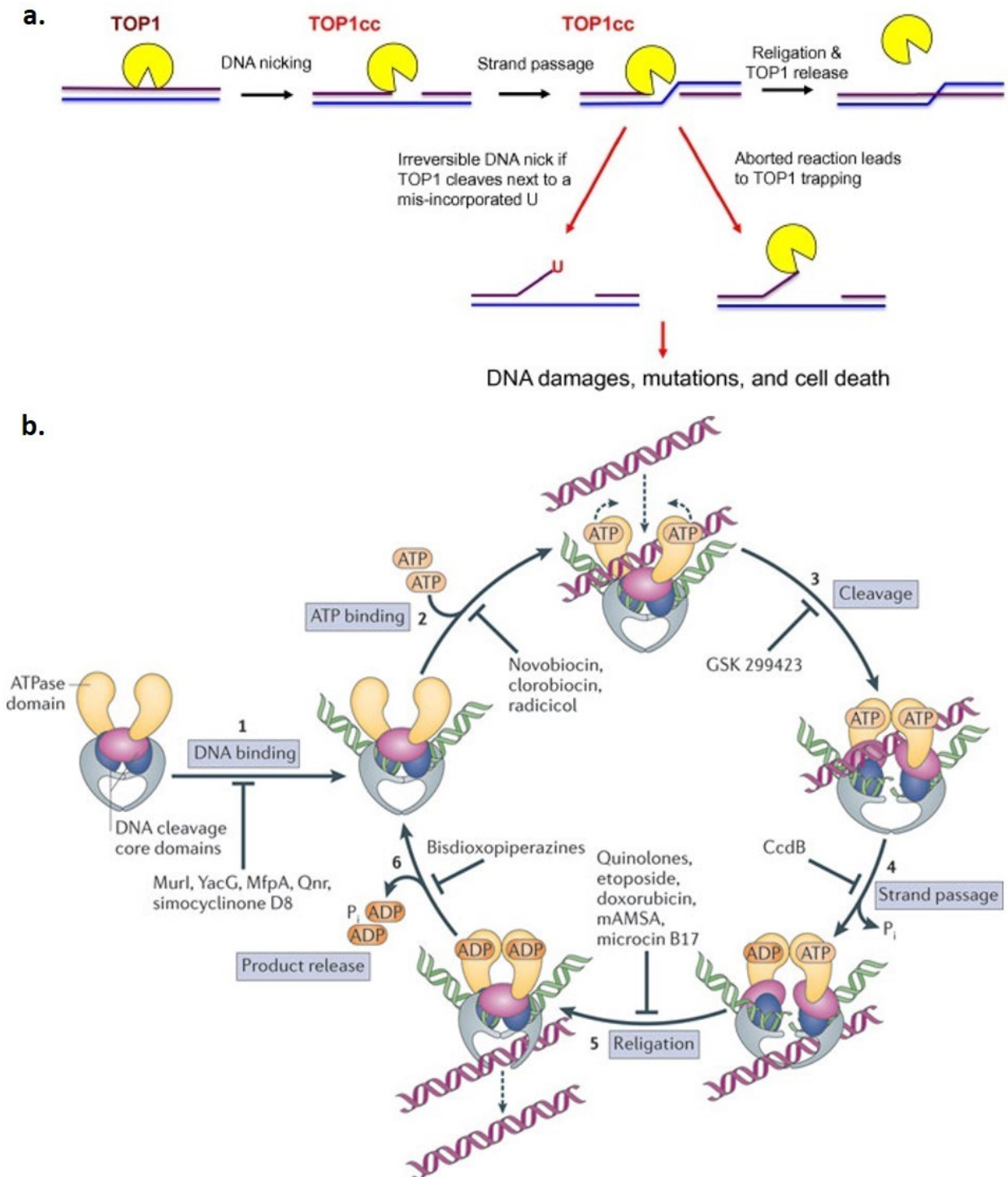


Figure 6. Catalytic cycle of type I (a) [48] and type II (b) [49] topoisomerases.

Type I DNA topoisomerases are monomeric proteins which mediate the relaxation of DNA supercoils generated during transcription and replication by introducing a transient nick in one strand of duplex DNA.^[50] They consist of 765 residues and include four domains: N-terminal domain (1-214), core domain (215-635), linker domain (636-712) and C-terminal domain (713-765). For its catalytic cycle, DNA topoisomerase I requires neither ATP hydrolysis nor the presence of bivalent cations; the cycle can be divided in four phases as shown in **Figure 6a**. In the first step, the enzyme ties the DNA and produces a break in a single strand of DNA forming a covalent complex. Then, it links interrupted strands by using the energy stored in the substrate (supercoiled form) and finally releases DNA. Topoisomerases I are further classified in two subfamilies: type IA which binds to a 5' phosphate (called type I-5'), and type IB which links to a 3' phosphate (called type I-3').^[47]

Type II DNA topoisomerases are homodimer proteins and cleave both DNA strands. These enzymes are composed of 1531 residues divided in three domains: ATPase domain (1-659), DNA binding/cleavage domain (660-1163) and C-terminal tail (1164-1531). The two subtypes of topoisomerases II (IIA and IIB) are characterized by a similar mechanism but differ in overall tertiary structure.^[47] In presence of Mg^{2+} , the tyrosine from each topoisomerase II monomer (Tyr804 in human Topo IIA or Tyr821 in human Topo IIB) binds DNA.^[51] The catalytic cycle requires the hydrolysis of two molecules of ATP and the presence of bivalent cations and, in particular, it can be divided in six phases as shown in **Figure 6b**. At the first step, topoisomerase binds a duplex DNA segment and then, thanks to two ATP molecules, it associates with a second DNA filament. ATP molecules catalyze the cleavage and opening of the first DNA strand and the movement of the second, passing through the opening. Finally, the broken strands are bonded and the product can be released.

1.4.1 DNA Topoisomerases inhibitors

Topoisomerase inhibitors (**Figure 7**) can be divided according to:

- the mechanism of inhibition in
 - compounds able to form a covalent complex between the enzyme and the DNA (such as camptothecin and etoposide);
 - inhibitors impairing the functions of topoisomerases through noncovalent interactions by hydrogen bonding, electrostatic, Van der Waals and hydrophobic forces (suppressors such as β -lapachon);
- the selectivity *versus* type I (e.g. camptothecin) or type II enzymes (e.g. etoposide), although several are not selective (e.g. saintopin).

Topoisomerase poisons are so called due to their interference with the relegation phase of cycle reaction, resulting in DNA damage, cell cycle arrest and apoptosis. Despite the high structural heterogeneity (e.g. camptothecin, indolocarbazoles and indenoisoquinolines), these molecules form the ternary complex interacting with the same residues of topoisomerase I, Arg352 and Glu356 thanks to the high mobility of their side chains.^[52]

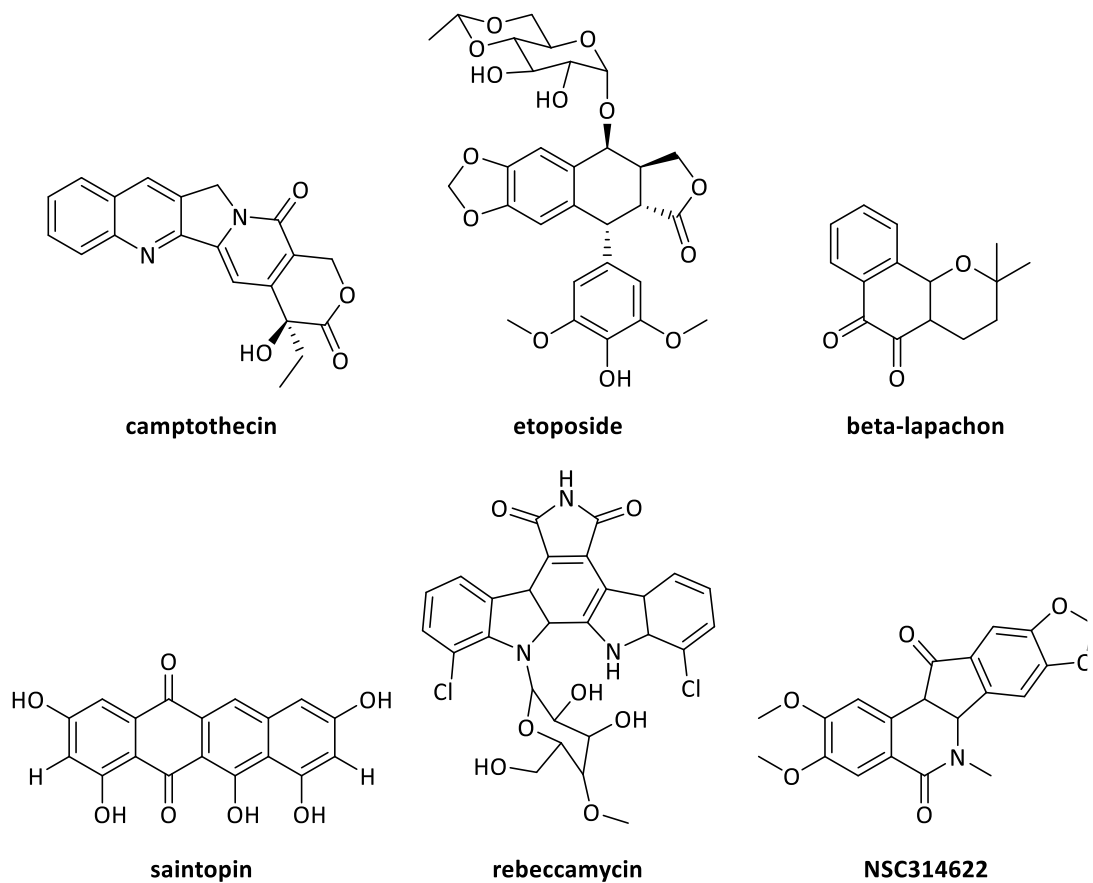


Figure 7. DNA topoisomerase inhibitors.

1.5 Hit finding

The drug discovery and development process can generally be identified with preclinical and clinical studies, respectively. This long, expensive and high-risk business starts with target identification and validation. Afterwards, *in vitro* and *in vivo* experimental models and/or computational approaches are capitalized to identify a potential hit, which has to undergo secondary assays and optimization processes to give a lead compound and then a potential drug candidate. Chemical tests for efficacy, joined with early safety and toxicity studies, are performed in preclinical phase, and are usually followed by investigations on formulation, stability and scale up synthesis. Besides, this *molecular target screening approach*, a High-Throughput Screening (HTS) can sometimes be performed even without knowing the target, which will be identified later (*phenotypic screening approach*); a third strategy could also be the *drug repurposing screen* in which a known drug, already marketed and approved for a particular indication, is used as lead for the treatment of a different disease.

Generally, the HTS could involve:

- synthetic chemical libraries, composed of molecules characterized by a high structural diversity (for instance obtained by the diversity-oriented synthesis approach);
- targeted focused libraries, which consist of compounds known to be active against a particular target (with natural or synthetic origin, small molecules or peptides or peptidomimetics, etc.);
- fragment based libraries, built up by fragments selected from active compounds.

1.5.1 Scaffold hopping

The aim of scaffold hopping is to discover structurally innovative entities starting from known active molecules, by modifying the central core structure but maintaining some essential features of the template. Therefore, scaffold hopping has been widely applied by medicinal chemists to discover equipotent compounds with novel backbones that have improved properties. For instance, the replacement of a lipophilic scaffold with a more polar one will increase the solubility of the compound, while the substitution of a metabolically labile scaffold with a more stable/less toxic one will improve the pharmacokinetic properties. Moreover, the replacement of a very flexible scaffold (such as a peptide backbone) with a rigid central one can significantly improve the binding affinity, leading to a novel structure that is patentable.^[53] In literature, there are different criteria for defining how different derivatives must be from their parent compounds in order to be classified as scaffold hopping. For instance, Boehm *et al.* classified two scaffolds as different if they were synthesized using different synthetic routines, no matter how small the change might be. On the other hand, Sun *et al.* rationalized the concept of scaffold hopping by focusing on the degree of change associated with the original parent molecule.^[54]

1.5.2 Fragment-based drug design

Fragment-based drug design (FBDD) has emerged as promising methodology to generate lead compounds active against therapeutic targets in the past decade. Compared with high-throughput screening hits, the advantage is that the identified small molecules are expected to be optimized efficiently into a drug candidate which maintains low molecular weight and possesses both a great binding affinity and a favorable pharmacokinetic profile.

This screening could be run using different experimental approaches (physical or computational methods), according to the sample range and the specific information. For instance, among physical techniques, the throughput of a biochemical approach is higher than Surface Plasmon Resonance (SPR) (>10.000 vs 1000s)

or X ray crystallography and isothermal titration calorimetry one (10s and <10, respectively). While fluorescence method can be used with a wide range of throughput (10-1000s).

On the other hand, *in silico* site-directed FBDD^[55] is a computational approach (**Figure 8**) whose fragment libraries are built from known inhibitors and are divided into binding site-specific sublibraries, according to docking poses.

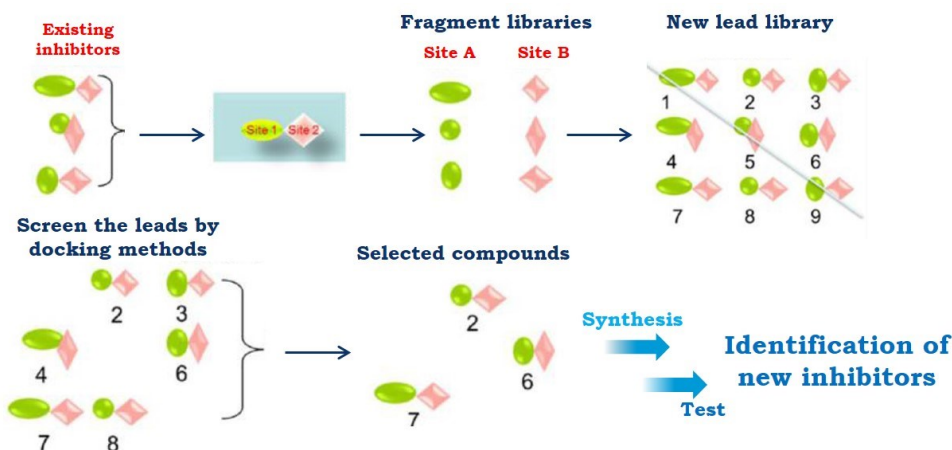


Figure 8. Site-directed FBDD strategy. The first step is to screen fragment libraries fitted to the site that might be essential for ligand-binding. The chemically merged privileged fragments may maintain their original orientation in the protein binding pocket, and thus jointly contribute to the final binding energy.

Linkers are chosen from known inhibitors or applying the concept of bioisosterism, merged potential candidates may be quickly screened via computational docking methods to further narrow the number of molecules that will be selected for synthesis and testing. **Table 1** shows a comparison between conventional and *in silico* site-directed FBDD methods.

| | Conventional FBDD | In silico site-directed FBDD |
|--------------------------------|--|---|
| Fragments library | Screened by X-ray, NMR and other methods | Built from known inhibitors and divided into binding site specific sub-libraries according to docking poses |
| Linkers | Selected from linker libraries or by chemical intuition | Original linkers or bioisosteres derived from original linkers |
| Merge methods | Fragments are randomly merged together | Fragments selected from sublibraries are merged together |
| Pre-selected candidates | According to structural variety, purchase/synthesis availability or chemical intuition | According to computational docking results |

Table 1. Comparison of conventional FBDD and *in silico* site-directed FBDD.

FBDD has proven to be a successful approach to identify potent inhibitors for specific targets, among which also STAT3.^[55,56]

Chapter 2

MD77 derivatives

2.1 Research project

1,2,5-Oxadiazoles have received considerable attention in recent years from Prof. Barlocco's research group in light of the interesting biological results supporting a potential antitumor activity. In particular, these compounds have been investigated for inhibitory effects towards STAT3 signaling pathway.^[57-60]

Starting from the oxadiazole ureido derivative **AVS-0288**, in collaboration with one of its discoverer, Prof. B-M. Kwon (Korea University of Science and Technology), the above mentioned research group investigated different compounds, structurally related to the parent molecule and able to increase STAT3 inhibition. On this respect, the antiproliferative potential of the 1,2,5-oxadiazole ring was explored by synthesizing several new compounds differently substituted at positions 3 and 4 of the heterocycle. Of note, the derivative bearing the amide function (**MD77**) emerged for its interesting biological results (**Table 2**). In order to deepen its anti-proliferative activity profile, this compound was submitted to a panel of 58 human tumor cell lines, derived from 9 cancer cell types (NCI, Bethesda, USA).

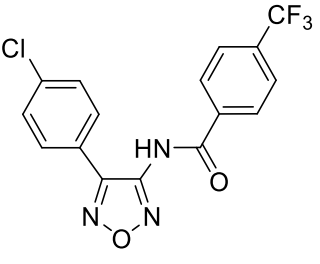
|  MD77 | Anti-proliferative activity (IC ₅₀ μM) | |
|--|---|------|
| | | H460 |
| | HCT-116 | 1.3 |
| | MCF-7 | 20.5 |
| | A549 | 1.3 |
| | HSF | N.E. |

Table 2. MD77 structure and biological activity: H460 = non-small-cell lung carcinoma; HCT-116 = colorectal cancer; MCF-7 = breast cancer; A549 = lung adenocarcinoma; HSF = human skin fibroblasts.

Besides, an *in vitro* competitive binding test, the AlphaScreen-based assay confirmed **MD77** ability to disrupt the interaction between STAT3 and a phospho-Tyr (pTyr) peptide (5-carboxyfluorescein (FITC)-GpYLPQTV), by interfering with the STAT3-SH2 domain (IC₅₀ = 17.7 μM).

In light of these data, I designed and synthesized a small group of **MD77** derivatives aimed at structure-activity relationship (SAR) studies. Although some of them are endowed with antiproliferative activity, no one displayed affinity for STAT3-SH2 domain. Since the introduced modifications did not justify the total loss of STAT3 affinity, **MD77** was retested and, differently from the data published in ref.^[59], it resulted to be inactive.

Hence, considering **MD77** antiproliferative profile and the cytotoxicity emerged for its derivatives, I focused my research efforts in the identification of the actual molecular target of this series. In order to achieve this goal, I employed a combination of synthetic and computational approaches.

In collaboration with Prof. S. Guccione's research group (University of Catania, Italy), structure-activity relationship studies were carried out through the innovative Activity Miner module as implemented in the software Cresset Forge^[61,62]. As the Activity Miner module has to be applied on a broad range of structurally and electronically heterogeneous derivatives, the starting pool of derivatives was enlarged.

A wide pool of synthesized derivatives, summed up in **Figure 9**, underwent the MTT-assay on human colon cancer cells and a structure-activity relationship analysis. This computational phase, in which the 3D shape and the electrostatic environment similarity were correlated with the change in activity, was performed by using Cresset Forge as software.

Once all the antiproliferative activity will be available, this analysis will be repeated to obtain an improved disparity matrix that could be used as query for recognizing a potential target^[63].

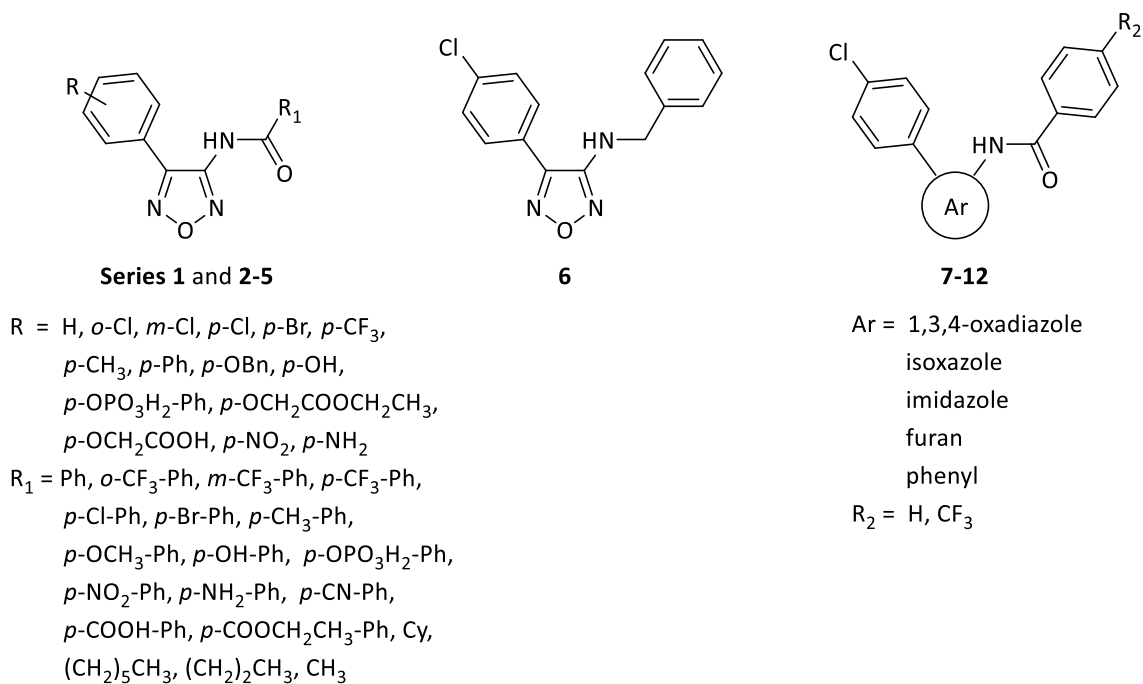
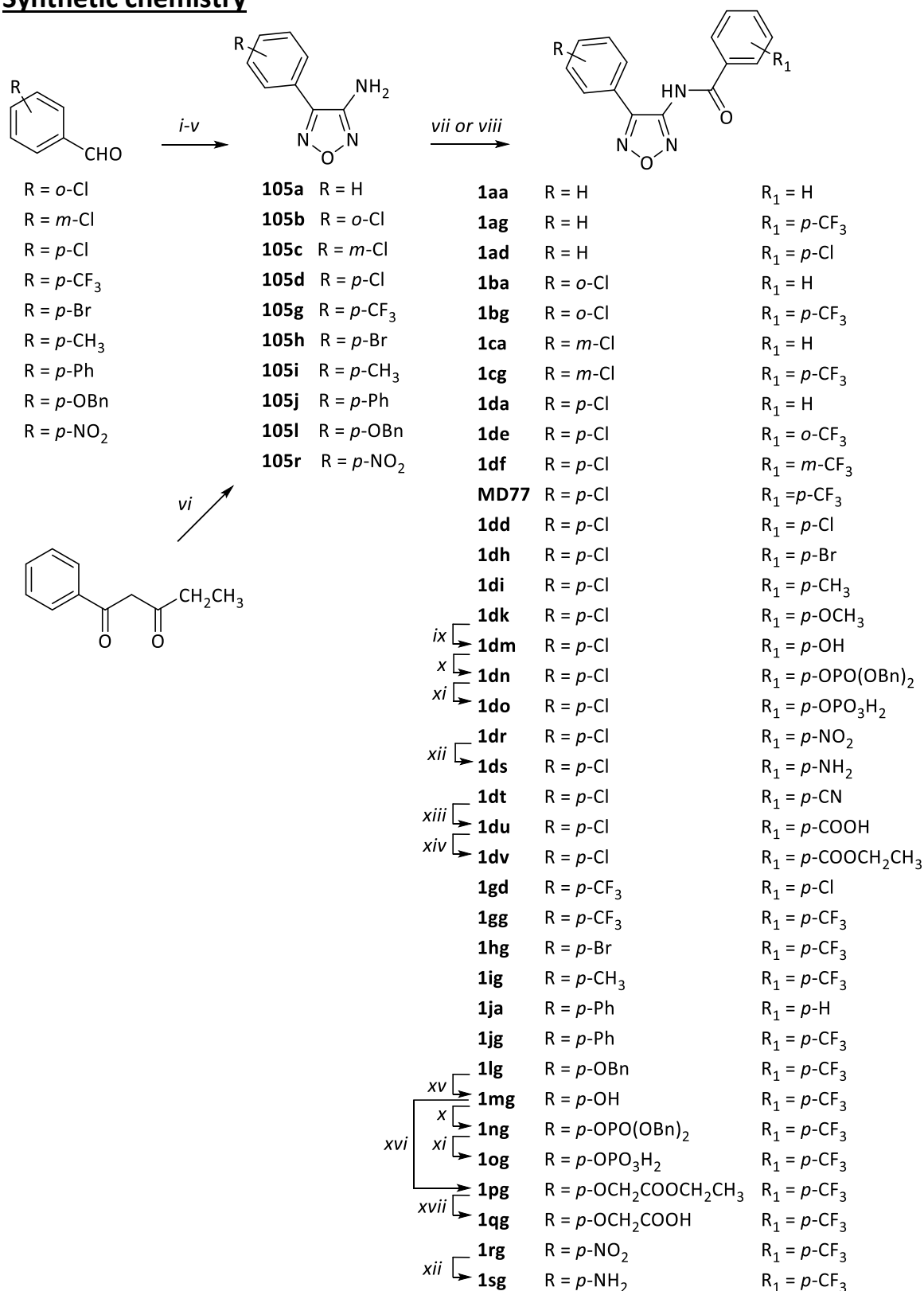


Figure 9. MD77 derivatives

Besides, considering their structural characteristics (see **Section 2.3.4** and Ref. ^[59]), **MD77** and some of its derivatives were assayed as topoisomerase inhibitors or DNA intercalators, thanks to the collaboration with Prof. L. Dalla Via (University of Padua). Screening assays are ongoing.

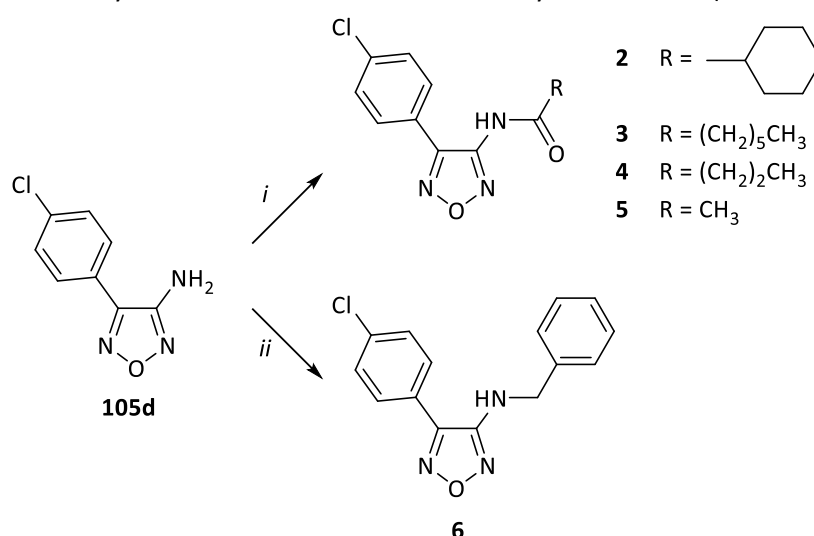
This project was supported by PRIN Research Project, grant no. 20105YY2H_007.

2.2 Synthetic chemistry



Scheme 1. Reagents and conditions: *i*) NH₂OH · HCl, NaHCO₃, MeOH, 2h, reflux; *ii*) NCS, DMF, 12h, rt; *iii*) KCN, Et₂O/H₂O, 5h, rt; *iv*) NH₂OH · HCl, NaHCO₃, MeOH, 12h, reflux; *v*) 2N NaOH, 12h, reflux; *vi*) a. NaOH, 12h, 0°C; b. NaNO₂, 20% HClO₄, 14h, rt; c. NH₂OH · HCl, NaOH, 2h, 95°C; d. urea, 3h, reflux; *vii*) R₁-PhCOCl, DMAP, dry ClCH₂CH₂Cl₂, 45 min, 120°C, mw, N₂; *viii*) a. 60% NaH, dry DMF, 30 min, 0°C, N₂, b. R₁-PhCOCl, 12h, 60°C; *ix*) BBr₃, dry CH₂Cl₂, 12h, rt, N₂; *x*) (BnO)₂PHO, CCl₄, DIPEA, DMAP, dry CH₃CN, 3h, -10°C, N₂; *xi*) H₂, Pd/C, MeOH, 3h, rt, 1 atm; *xii*) SnCl₂, AcOEt, 7h, reflux; *xiii*) NaOH, EtOH, 3h, reflux; *xiv*) (EtO)₂CO, dry MgCl, dry EtOH, 12h, 40°C, Ar; *xv*) H₂, Pd/C, AcOEt/MeOH (9:1), 24h, rt; *xvi*) ClCH₂COOCH₂CH₃, dry DMF, 24h, rt, N₂; *xvii*) 1M NaOH, THF/EtOH (1:1), 30 min, reflux.

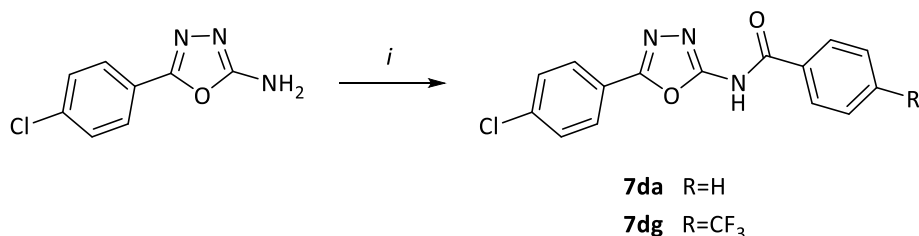
Compounds of **Series 1** were prepared following the general procedures reported in **Scheme 1**. In detail, a one-pot reaction on ethyl benzoylacetate (according to a literature method ^[64]) afforded 4-phenyl-1,2,5-oxadiazol-3-amine, intermediate **105a**, while the key intermediates **105b-d,g-j,l** and **105r** were synthesized from the appropriate benzaldehyde following the multi-step procedure previously reported in literature. ^[59] 4-phenyl-1,2,5-oxadiazol-3-yl-benzamides (**Series 1**) were obtained by coupling reactions of these 4-phenyl-1,2,5-oxadiazol-3-amines with the suitable benzoyl chlorides. The hydrolysis of **1dk,lg** and **1dt** led to compounds **1dm,mg** and **1du**, respectively. The latter underwent a Fisher esterification (**1dv**) and the nitro group of **1dr** and **1rg** was reduced (**1ds** and **1sg**). Moreover, compounds **1dm** and **1mg** were phosphorylated with dibenzylphosphite ^[65] and intermediates **1dn** and **1ng** were subsequently debenzylated by a catalytic hydrogenation over Pd/C leading to derivatives **1do** and **1og**. **1pg** was prepared by substitution reaction of phenol **1mg** with methyl chloroacetate ^[66] and hydrolyzed to **1qg** in basic conditions. Finally, coupling reactions performed with **105d** and aliphatic acyl chlorides gave compounds **2-5**, while compound **6** was obtained by reductive amination of benzaldehyde with **105d** (**Scheme 2**).



Scheme 2. Reagents and conditions: *i*) a. 60% NaH, dry DMF, 30 min, 0°C, N₂; b. RCOCl, 12h, 60°C; *ii*) a. PhCHO, AcOH, 3h, rt; b. NaBH₄, 1h, 0°C.

The other *N*-heteroaryl-benzamides herein presented (**7da,dg**, **8da,dg**, **9da,dg**, **10da,dg**, **119da,dg** and **12da,dg**) were prepared starting from the corresponding heteroarylamines (2-amino-5-(4-chlorophenyl)-1,3,4-oxadiazole, **109**, **114**, **116**, **118** and **121**) which were coupled with the suitable benzoyl chloride in presence of the proper basis (pyridine, trimethylamine or 60% sodium hydride).

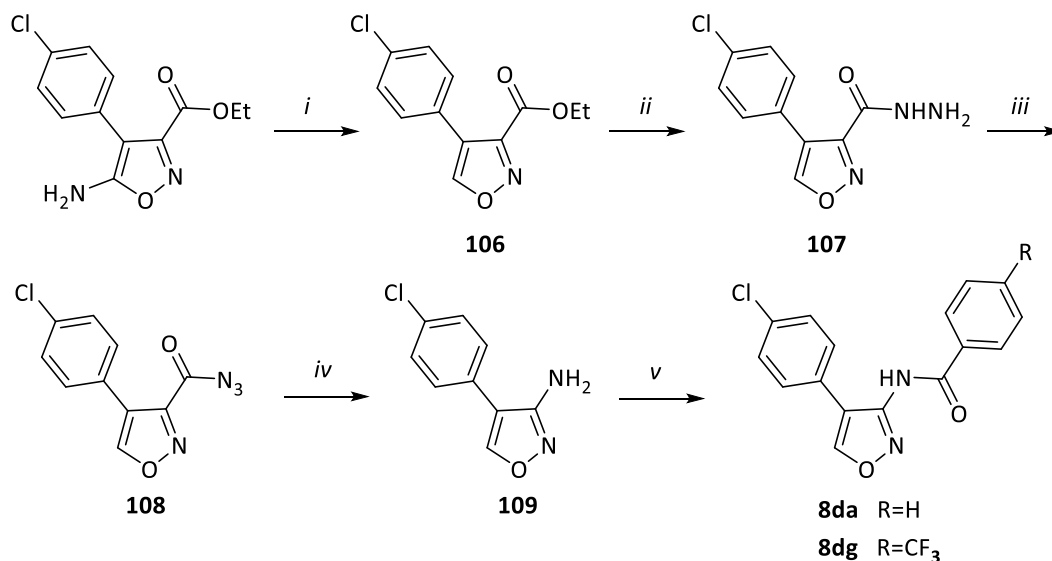
In details, compounds **7da,dg** were prepared from the commercially available 2-amino-5-(4-chlorophenyl)-1,3,4-oxadiazole by acylation in pyridine, as shown in **Scheme 3**.



Scheme 3. Reagents and conditions: *i*) a. dry Py, 10 min, 0°C, N₂; b. R-PhCOCl, 3-16h, rt.

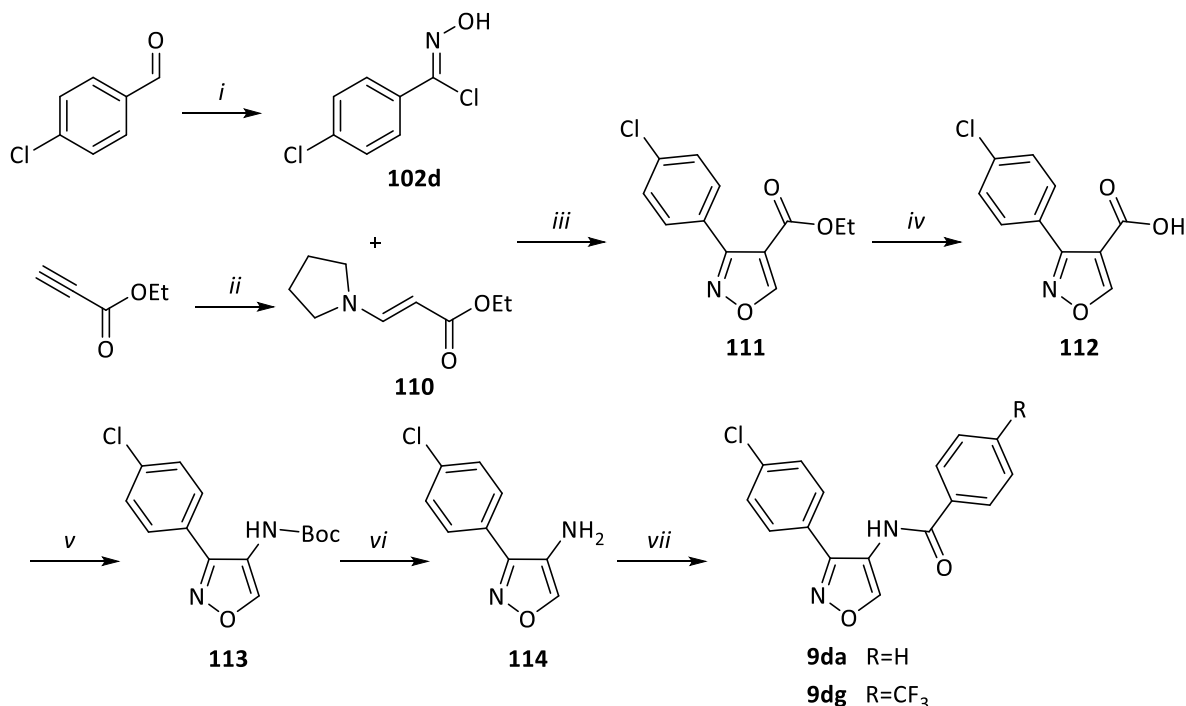
For the synthesis of the *N*-(4-(4-chlorophenyl)-isoxazol-3-yl)benzamides (**8da,dg**), the key intermediate **109** was obtained by a Sandmeyer reaction (**106**) in aqueous solution ^[67] performed on the commercially available ethyl 5-amino-4-(4-chlorophenyl)isoxazol-3-carboxylate. The treatment with hydrazine monohydrate (**107**) and subsequently with sodium nitrite in acetone and hydrochloric acid as catalyst gave the carbonyl azide

(**108**) with a Curtius rearrangement. The addition of water led to the desired 3-amino-4-(4-chlorophenyl)isoxazole (**109**)^[68] which was acylated with the proper benzoyl chloride in presence of trimethylamine, providing the final benzamide (**Scheme 4**).



Scheme 4. Reagents and conditions: *i*) NaNO₂, AcOH/H₂O (1:1), THF, 1h, rt; *ii*) NH₂NH₂ · H₂O, EtOH, 90 min, rt; *iii*) NaNO₂, CO(CH₃)₂/10% HCl (1:1), 40 min, rt; *iv*) AcOH, H₂O, 1h, reflux; *v*) a. NEt₃, dry CH₂Cl₂, 30 min, 0°C, N₂; b. R-PhCOCl, 90 min, 40°C.

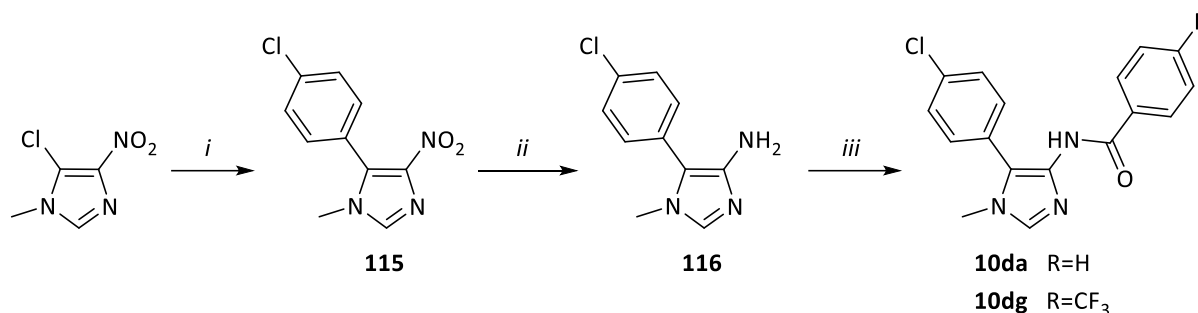
As described in **Scheme 5**, the key intermediate 4-amino-3-(4-chlorophenyl) isoxazole (**114**) was prepared starting from the commercially available 4-chlorobenzaldehyde which was firstly treated with hydroxylamine hydrochloride and then with *N*-chlorosuccinimide.^[59] The chloroxime **102d** reacted with **110**, previously synthesized following a well-described literature procedure^[69], and the resulting ethyl 3-(4-chlorophenyl)-4-isoxazolcarboxylate (**111**) was firstly hydrolyzed in acidic condition and then the acyl azide was formed by the



Scheme 5. Reagents and conditions: *i*) a. NH₂OH · HCl, NaHCO₃, MeOH/H₂O (2:1), 2h, rt; b. NCS, DMF, 16h, rt; *ii*) pyrrolidine, toluene, 16h, rt; *iii*) NEt₃, dry Et₂O, 18h, rt, N₂; *iv*) 6N HCl, AcOH, 6h, reflux; *v*) DPPA, NEt₃, dry *t*-BuOH, 16h, reflux, N₂; *vi*) a. TFA, dry CH₂Cl₂, 16h, rt, N₂; b. 1N NaOH; *vii*) a. 60% NaH, dry DMF, 30 min, 0°C, N₂; b. R-PhCOCl, 12h, 60°C.

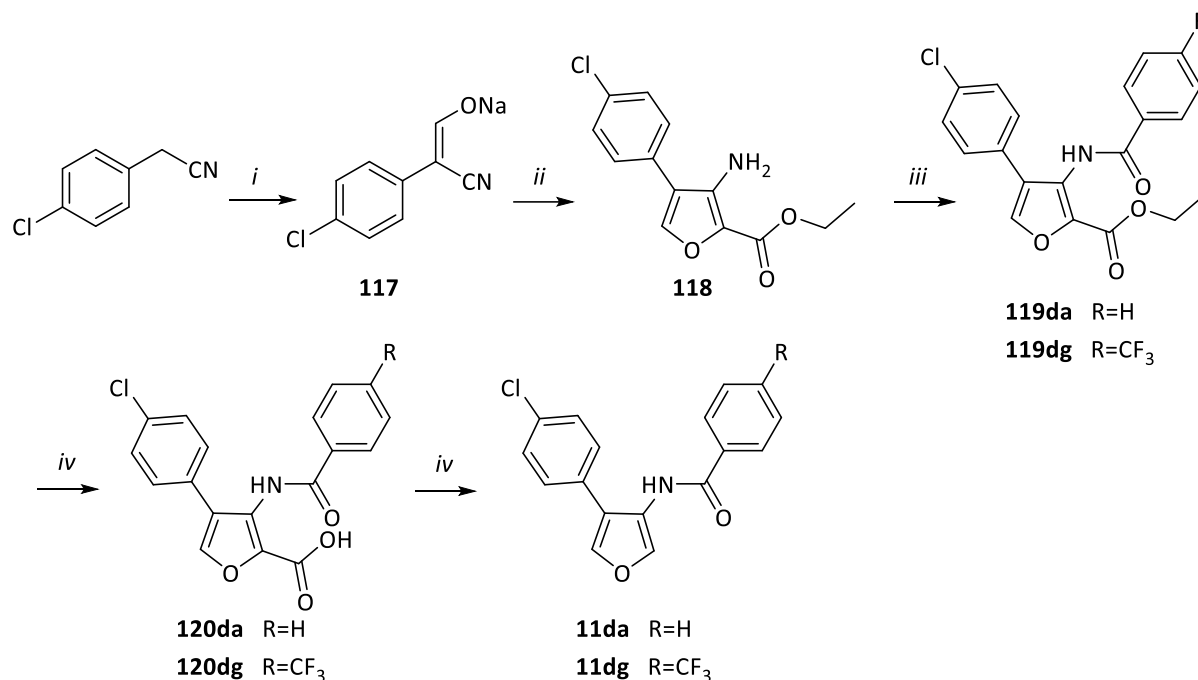
direct reaction of the carboxylic acid with diphenyl phosphoryl azide (DPPA). According to Curtius rearrangement, acyl azide group decomposed to isocyanate which underwent nucleophilic attack to yield the corresponding carbamate (**113**). *N*-Boc protecting group was successively removed with trifluoroacetic acid and the amine **114** was finally condensed with the suitable acyl chloride in presence of 60% sodium hydride leading to **9da,dg**.

The synthesis of **10da,dg** started from the commercially available 5-chloro-1-methyl-4-nitroimidazole which underwent a Suzuki coupling reaction (**115**)^[70] followed by a catalytic hydrogenation with Pd/C to afford amine **116**^[71]. This latter was condensed using triethylamine as basis leading to the final products, as shown in **Scheme 6**.



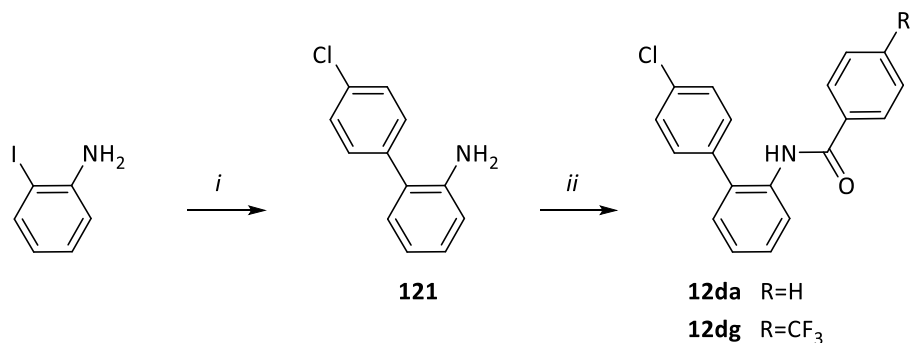
Scheme 6. Reagents and conditions: *i*) 4-ClPhB(OH)₂, K₂CO₃, TBAB, Pd(PPh₃)₂Cl₂, H₂O, 16 h, 75–85°C, N₂; *ii*) H₂ (30 atm), Pd(OH)₂, CH₂Cl₂/MeOH (9:1), 16 h, rt; *iii*) a. NEt₃, dry CH₂Cl₂, 30 min, 0°C, N₂; b. R-PhCOCl, 90 min, 0°C.

The synthetic pathway for the obtainment of furan derivatives (**Scheme 7**) started from 4-chlorophenylacetonitrile which was treated with metallic Na, ethyl formate and ethanol for 16 hours leading to the sodium salt intermediate **117**. The latter was cyclized by a one-pot reaction^[72] to intermediate **118** which was condensed with the proper acyl chloride, in presence of triethylamine by a microwave assisted reaction to obtain compounds **119da,dg**. The ester group was firstly hydrolyzed (**120da,dg**) and then the final compounds **11da,dg** were obtained by decarboxylation^[73].



Scheme 7. Reagents and conditions: *i*) HCOOCH₂CH₃, Na, dry EtOH, 16h, reflux, N₂; *ii*) a. Cl(COOCH₂CH₃)₂, dry DMF, 5h, rt, N₂; b. 1,5-diazabicyclo[4.3.0]non-5-ene, dry EtOH, 16h, reflux, N₂; *iii*) R-PhCOCl, NEt₃, dry CH₂Cl₂, 40 min, 80°C, mw, N₂; *iv*) 1N NaOH, THF/EtOH (1:1), 1h, reflux; *v*) Ag₂CO₃, AcOH, dry DMSO, 16h, 120°C, N₂.

The synthesis of *N*-(4-chloro-[1,1-biphenyl]-2-yl) benzamides (**12da,dg**) started from 2-iodoaniline which was arylated with a Suzuki reaction (**121**)^[74] and condensed in presence of triethylamine as basis with the suitable acyl chloride, as shown in **Scheme 8**.



Scheme 8. Reagents and conditions: *i*) 4-ClPhB(OH)₂, saturated Na₂CO₃, Pd(PPh₃)₄, dry toluene/EtOH (20:1), 16h, 70°C, N₂; *ii*) a. 60% NaH, dry DMF, 30 min, 0°C, N₂, b. R-PhCOCl, 12h, 60°C.

2.3 Results and discussion

Starting from **AVS-0288**^[57], a STAT3 inhibitor characterized by an oxadiazole ureido scaffold, Prof. Barlocco's research group identified **MD77**^[59] as promising candidate for lead optimization. Its antiproliferative activity was evaluated on a panel of 58 human tumor cell lines (NCI, Bethesda, USA) while its ability to disrupt STAT3 dimerization was proven by the AlphaScreen-based assay.

Therefore, in order to deeply understand the structural characteristics responsible for its STAT3 affinity, I designed and synthesized a small set of derivatives, performing iterative modifications on the scaffold.

This first group of analogues underwent biological evaluation, resulting to be cytotoxic but without affinity for the STAT3-SH2 domain. Since the structural diversity of these derivatives with respect to the parent compound did not justify this complete loss of activity in the AlphaScreen-based assay, **MD77** was retested showing no activity on STAT3 dimerization, differently from the data previously published^[59].

However, considering the interesting cytotoxic profile of this class of compounds, I looked for their real molecular target, employing a combined synthetic-computational approach. Firstly, I enlarged the pool of **MD77** derivatives obtaining a wide range of structural and electronical heterogeneity, and, in collaboration with Prof. S. Guccione's research group (University of Catania, Italy), a structure-activity relationship analysis was performed using the Activity Miner module of Cresset Forge^[61,62]. This approach should help in defining whether the electronic characteristics or the position of the substituent prevail in these derivatives, affecting on their antiproliferative activity.

Regarding the performing iterative modifications, I firstly decided to maintain the 1,2,5-oxadiazole scaffold and the amide linkage (compounds **1-5**) and changed electronic characteristics and/or the positions of the substituents. Therefore, I designed and synthesized compounds characterized by:

- different functional groups at position 4 of the heterocycle;
- various substituents on the phenyl ring of the benzamide;
- the replacement of the benzamide with aliphatic moieties.

Then, the attention was focused on the amidic function, which was reduced to the corresponding amine (**6**), and the 1,2,5-oxadiazole scaffold, which was replaced with 1,3,4-oxadiazole isomer (**7da,dg**) and other heterocycles (such as isoxazole (**8da,dg** and **9da,dg**), imidazole (**10da,dg**) and furan (**11da,dg**) rings) or the phenyl ring (**12da,dg**).

Part of the synthesized compounds was evaluated for its antiproliferative activity by MTT-assay on human colon cancer cells (HCT-116) by Dr. N. Ferri (University of Padua, Italy). Besides, in order to find where small structural differences cause a large change in activity, each pair of molecules was compared *in silico* by the Active Miner module. The field difference map generated by Cresset Forge displays the surfaces as relative values between pairs of molecules or as sum of all molecules, considering electrostatic or hydrophobic or steric fields. Once all the antiproliferative results will be available, this analysis will be repeated on the whole library and the generated disparity matrix will be used as query in search of a potential target^[63].

Moreover, considering the structural characteristics of this class of compounds, **MD77** and some of its derivatives are under evaluation (with other structurally different compounds synthesized by Prof. Barlocco's research group) for their potential activity as topoisomerase inhibitors or DNA intercalators. Indeed, even if it was traditionally thought that only molecules with fused-ring structures could be good DNA intercalators, it was shown that the presence of basic, cationic, or electrophilic functional groups was often necessary, while the fused-ring structures were not always required.^[75,76]

These assays are performed by Prof. L. Dalla Via (University of Padua) who also selected a pool of compounds to be tested on human cervical (HeLa), ovarian (A2780) and mesothelioma (MSTO-211H) cancer cell lines.

2.3.1 Antiproliferative activity

This series of compounds was evaluated for its antiproliferative activity by MTT-assay on human colon cancer cells (HCT-116) by Dr. N. Ferri (University of Padua, Italy). The available results were reported as half maximal inhibitory concentration (IC₅₀) in **Tables 3,4**.

| Cmp | R | R ₁ | IC ₅₀ μM |
|------|---|--|---------------------|
| MD77 | <i>p</i> -Cl | <i>p</i> -CF ₃ | 1.3 |
| 1aa | H | H | n.a. |
| 1ag | H | <i>p</i> -CF ₃ | n.a. |
| 1ad | H | <i>p</i> -Cl | n.t. |
| 1ba | <i>o</i> -Cl | H | 76.3 |
| 1bg | <i>o</i> -Cl | <i>p</i> -CF ₃ | 56.7 |
| 1ca | <i>m</i> -Cl | H | 73.4 |
| 1cg | <i>m</i> -Cl | <i>p</i> -CF ₃ | 15.4 |
| 1da | <i>p</i> -Cl | H | n.a. |
| 1de | <i>p</i> -Cl | <i>o</i> -CF ₃ | n.a. |
| 1df | <i>p</i> -Cl | <i>m</i> -CF ₃ | 7.4 |
| 1dd | <i>p</i> -Cl | <i>p</i> -Cl | n.a. |
| 1dh | <i>p</i> -Cl | <i>p</i> -Br | n.t. |
| 1di | <i>p</i> -Cl | <i>p</i> -CH ₃ | n.t. |
| 1dk | <i>p</i> -Cl | <i>p</i> -OCH ₃ | n.a. |
| 1dm | <i>p</i> -Cl | <i>p</i> -OH | n.a. |
| 1dn | <i>p</i> -Cl | <i>p</i> -OPO(OBn) ₂ | n.t. |
| 1do | <i>p</i> -Cl | <i>p</i> -OPO ₃ H ₂ | n.a. |
| 1dr | <i>p</i> -Cl | <i>p</i> -NO ₂ | 46.7 |
| 1ds | <i>p</i> -Cl | <i>p</i> -NH ₂ | n.a. |
| 1dt | <i>p</i> -Cl | <i>p</i> -CN | 19.4 |
| 1du | <i>p</i> -Cl | <i>p</i> -COOH | n.a. |
| 1dv | <i>p</i> -Cl | <i>p</i> -COOCH ₂ CH ₃ | n.t. |
| 1hg | <i>p</i> -Br | <i>p</i> -CF ₃ | n.t. |
| 1gg | <i>p</i> -CF ₃ | <i>p</i> -CF ₃ | 24.1 |
| 1ig | <i>p</i> -CH ₃ | <i>p</i> -CF ₃ | n.t. |
| 1gd | <i>p</i> -CF ₃ | <i>p</i> -Cl | 0.95 |
| 1ja | <i>p</i> -Ph | H | n.t. |
| 1jg | <i>p</i> -Ph | <i>p</i> -CF ₃ | n.t. |
| 1lg | <i>p</i> -OBn | <i>p</i> -CF ₃ | n.t. |
| 1mg | <i>p</i> -OH | <i>p</i> -CF ₃ | n.a. |
| 1ng | <i>p</i> -OPO(OBn) ₂ | <i>p</i> -CF ₃ | n.t. |
| 1og | <i>p</i> -OPO ₃ H ₂ | <i>p</i> -CF ₃ | n.t. |
| 1pg | <i>p</i> -OCH ₂ COOCH ₂ CH ₃ | <i>p</i> -CF ₃ | n.t. |
| 1qg | <i>p</i> -OCH ₂ COOH | <i>p</i> -CF ₃ | n.t. |
| 1rg | <i>p</i> -NO ₂ | <i>p</i> -CF ₃ | 58.2 |
| 1sg | <i>p</i> -NH ₂ | <i>p</i> -CF ₃ | n.a. |

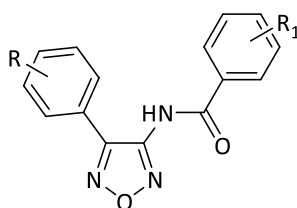


Table 3. Antiproliferative activity of **Series 1** on HCT-116: not active (n.a.) means IC₅₀ is higher than 100 μM, while not tested (n.t.) means that it is currently under evaluation.

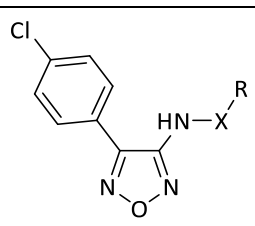
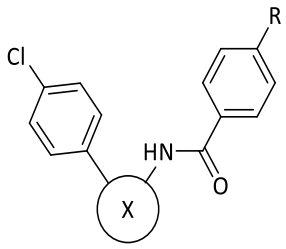
| | Cmp | X | R ₁ | IC ₅₀ μM |
|---|-------------|------------------------|---|---------------------|
|  | 2 | C=O | Cy | n.t. |
| | 3 | C=O | (CH ₂) ₅ CH ₃ | n.t. |
| | 4 | C=O | (CH ₂) ₂ CH ₃ | n.a. |
| | 5 | C=O | CH ₃ | n.t. |
| | 6 | CH ₂ | Ph | n.t. |
| | | 7da | 1,2,4-oxadiazole | H |
| | 7dg | 1,2,4-oxadiazole | CF ₃ | 45.0 |
|  | 8da | 1,2-isoxazole | H | n.a. |
| | 8dg | 1,2-isoxazole | CF ₃ | n.a. |
| | 9da | 1,5-isoxazole | H | n.a. |
| | 9dg | 1,5-isoxazole | CF ₃ | n.a. |
| | 10da | <i>N</i> -Me-Imidazole | H | n.a. |
| | 10dg | <i>N</i> -Me-Imidazole | CF ₃ | 52.3 |
| | 11da | Furan | H | n.t. |
| | 11dg | Furan | CF ₃ | n.a. |
| | 12da | Phenyl | H | n.a. |
| | 12dg | Phenyl | CF ₃ | n.a. |

Table 4. Antiproliferative activity of **Series 2-12** on HCT-116: not active (n.a.) means IC₅₀ is higher than 100 μM, while not tested (n.t.) means that it is currently under evaluation.

Preliminary results showed that isomers bearing the chlorine atom in *ortho* (**1bg**, IC₅₀ = 56.7 μM) and *meta* (**1cg**, IC₅₀ = 15.4 μM) positions, respectively, were endowed with lower antiproliferative activity than the parent compound. In particular, **1bg** showed moderate growth inhibition properties, while **1cg** exhibited a more interesting activity, although the *para* substitution remained the preferred.

Regarding the effects of moving the CF₃ group to different positions on the phenyl ring, the isomers **1de** (n.a) and **1df** (IC₅₀ = 7.4 μM) indicated the *ortho* position as detrimental, because **1de** completely lost the activity, whereas the *meta* isomer retained almost the same biological properties of the lead.

When the CF₃ group in *para* position of the benzoyl ring was substituted by NO₂ (**1dr**, IC₅₀ = 46.7 μM) or CN (**1dt**, IC₅₀ = 19.4 μM) group, a partial cytotoxic activity was retained. Analogously, **1rg**, bearing NO₂ substituent instead of the *p*-Cl atom on the 4-phenyl ring, showed modest growth inhibition properties (IC₅₀ = 58.2 μM). If the phenyl rings were both substituted with the Cl atoms (**1dd**) or with the CF₃ groups (**1gg**) a different behavior was observed: the first one was completely inactive, while the latter showed a moderate activity (IC₅₀ = 24.1 μM).

Among the bioisosteric analogues of **MD77**, only **7dg** and **10dg** presented cytotoxic activity (IC₅₀ = 45.0 and 52.3 μM, respectively). Otherwise, **1da** analogue, **7da**, characterized by the 1,3,4-oxadiazole ring displayed a significant cytotoxicity (IC₅₀ = 14.7 μM).

Compound **1gd**, bearing the same substituents of **MD77** but in inverted position, was slightly more potent with respect to the reference **MD77** (IC₅₀ = 0.95 versus 1.3 μM, respectively).

2.3.2 AlphaScreen-based assay

Considering **AVS-0288** inhibitory activity on STAT3 pathway, compounds **1-12** were evaluated by Prof. A. Asai (University of Shizuoka, Japan) for their potential inhibition of the interaction between STAT3-SH2 domain and *p*Tyr-containing peptides at 30 μ M concentration. The obtained data indicated that all the synthesized derivatives did not disrupt STAT3 dimerization.

2.3.3 Cresset Forge

In the attempt to understand the key factors that affect the activity on HCT-116 of these derivatives, a structure-activity relationship analysis was performed using Cresset Forge^[61,62] as software.

This technique allows the assessment of the structure-activity landscape for a series of aligned compounds based on the chemical similarity principle, which asserts that molecules having similar features often have comparable bioactivities.^[77] Therefore, Activity Miner module pinpointed those pairs of derivatives where small structural differences cause changes in activity.

The disparity between a pair of molecules was calculated as the difference in their activity divided by the distance between them, where the distance was obtained from their 2D or 3D similarity.

$$\text{Disparity} \propto \frac{\Delta \text{ Activity}}{1 - \text{ Similarity}}$$

Molecule pairs that had a low disparity and high similarity defined bioisosteres or flat regions in the SAR. These regions could be useful to modify the physicochemical properties of the molecules without losing activity and this overview could help to create a 'protein's eye view' of the scaffold.

The compounds alignment was performed starting from **MD77** crystallographic coordinates (for sake of clarity, the three rings were named *A*, *B* and *C* as shown in **Figure 10a**), as we found that its molecular arrangement in the solid state almost corresponds to the most stable conformation calculated *in vacuo*.^[59] To verify the reliability of this approximation, the crystal structures of two monosubstituted analogues, bearing the phenyl ring carrying either the Cl atom on system *A* (**1ad**) or the CF₃ group on ring *C* (**1ag**), were determined.

As compounds share a fair degree of structural similarity across the series, they were aligned considering on their maximum common substructure with reference **MD77**. The functional groups, which were not part of the maximum common substructure, were aligned basing on a combination of three-dimensional shape and molecular interaction fields.

Therefore, Activity Miner module on this aligned dataset (**Figure 10b**) allowed the activity cliff analysis (**Figure 10c-f**) and generated the disparity matrix (**Figure 11**) across the ligands. This technique will be repeated once all the antiproliferative activity will be available.

Cresset Forge software provided various field difference maps as sum of the electrostatic or hydrophobic or steric fields for the whole pool of molecules. In detail:

- *Average Electrostatics or Hydrophobics of Actives* (**Figure 10c,d**), calculated considering only the active molecules and pointed out the essential structural features for the activity;
- *Active Cliff Summary of Electrostatics or Hydrophobics* (**Figure 10e,f**) displayed the effects of the introduced modifications (in the different regions) on the activity considering both cytotoxic and inactive compounds.

This graphical representation could provide indications about the electrostatic, hydrophobic and shape features underlying the cytotoxic activity. These preliminary results, discussed considering **MD77** as reference, suggested that an increasing of negative electrostatic field on the core *B* of the structure could

have positive effects on the activity (in cyan in **Figure 10c**), while an enhanced π electrostatic potential on the system *C* is not suitable (in red in **Figure 10c**). Besides, electron withdrawing substituents which generate a more positive (or less negative) electrostatic field (in red in **Figure 10e**) in *meta* position on ring *A* are beneficial for activity, whereas opposite characteristics are required for *para* position.

As for the hydrophobic and steric aspects, **Figure 10d** highlighted the regions (in yellow) where active molecules could make hydrophobic interactions, while **Figure 10f** showed that steric hindrance in *para* position was well tolerated on ring *A* (green area), but not on system *B* (magenta area). Otherwise, steric bulk in *ortho* or *meta* position at phenyl *A* (magenta area) was detrimental for activity.

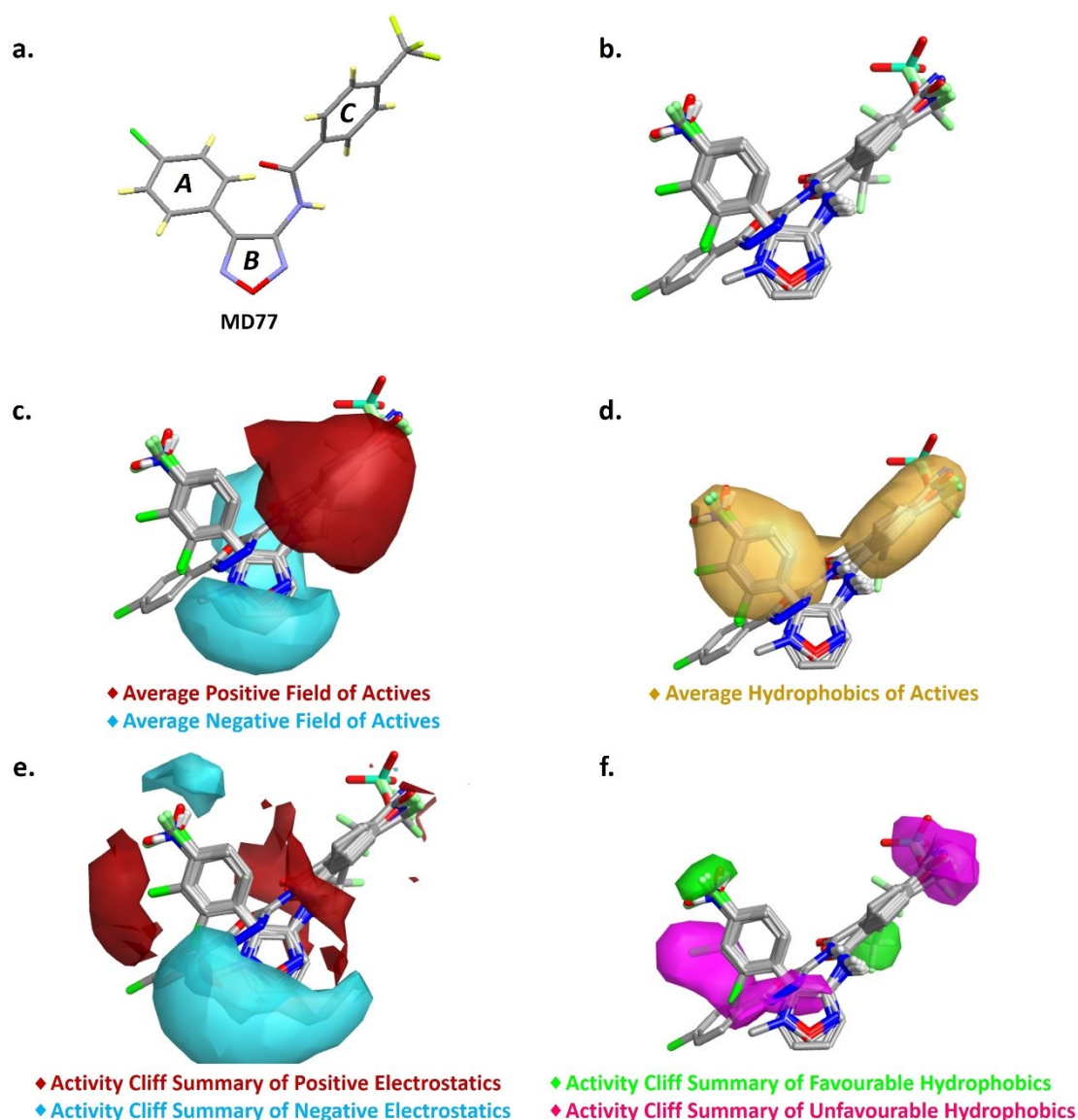


Figure 10. **a.** MD77 structure, used as reference compound in the discussion. **b.** Representative low energy conformations of the aligned compounds. **c.** Average electrostatic field of activity. **d.** Average hydrophobics of activity. **e.** Active cliff summary of electrostatic field. **f.** Active cliff summary of hydrophobics.

As previously introduced, the Activity Miner module also generated a preliminary disparity matrix (**Figure 11a**), in which the similarity value for each pair of compounds was computed as the average of their three-dimensional field and shape similarity.^[78,79] The height of each wedge corresponds to the 'distance' between them: a smaller wedge reflects very similar compounds. The color of the wedge points out the direction the activity is going: red means the activity is decreasing; green means the activity is increasing between the pair. The shading evidences the disparity, which relates to how steep the activity cliff is.

a.

| | 1gg | 1da | 7dg | 9dg | 8dg | 10dg | 12dg | 11dg | 1aa | 1dd | 1dk | 1dm | 1ds | 1dr | 1dt | 1du | 4 | 1ba | 1ca | 1cg | 1bg | 1do | 1gd | 1df | 1de | 1rg | 1mg | 1sg | MD77 | 1ag | |
|------|-------|-------|------|-------|-------|------|-------|-------|-------|-------|-------|-------|-------|-------|-------|-------|-------|-------|-------|-------|-------|-------|------|------|-------|-------|-------|-------|-------|-------|-----|
| 1gg | | -7.3 | -0.7 | -16.0 | -8.5 | -2.2 | -5.6 | -8.3 | -4.9 | -12.5 | -9.6 | -6.8 | -5.5 | -3.0 | 1.1 | -5.7 | -4.6 | -2.6 | -3.0 | 2.5 | -3.4 | -4.6 | 28.0 | 3.6 | -4.7 | -5.8 | -8.8 | -8.2 | -16.0 | -10.0 | |
| 1da | 7.3 | | 1.1 | 0.0 | 0.0 | 2.3 | 0.0 | 0.0 | 0.0 | 0.0 | 0.0 | 0.0 | 0.0 | 6.1 | 11.7 | 0.0 | 0.0 | 3.6 | 5.2 | 7.5 | 2.7 | 0.0 | 29.6 | 17.0 | 0.0 | 3.3 | 0.0 | 0.0 | 0.0 | 0.0 | |
| 7dg | 0.7 | -1.1 | | -1.3 | -1.2 | -0.2 | -1.3 | -1.3 | -1.1 | -1.3 | -1.2 | -1.1 | -1.1 | -0.0 | 0.8 | -1.1 | -0.9 | -0.5 | -0.5 | 1.2 | -0.3 | -1.0 | 3.8 | 1.6 | -1.0 | -0.3 | -1.3 | -1.3 | -1.3 | -1.4 | |
| 9dg | 16.0 | 0.0 | 1.3 | | 0.0 | 3.3 | 0.0 | 0.0 | 0.0 | 0.0 | 0.0 | 0.0 | 0.0 | 5.9 | 11.8 | 0.0 | 0.0 | 1.9 | 2.3 | 17.9 | 5.5 | 0.0 | 27.7 | 9.7 | 0.0 | 7.7 | 0.0 | 0.0 | 0.0 | 0.0 | |
| 8dg | 8.5 | 0.0 | 1.2 | 0.0 | | 4.9 | 0.0 | 0.0 | 0.0 | 0.0 | 0.0 | 0.0 | 0.0 | 3.8 | 8.0 | 0.0 | 0.0 | 1.5 | 1.6 | 9.1 | 3.4 | 0.0 | 17.2 | 7.4 | 0.0 | 4.0 | 0.0 | 0.0 | 0.0 | 0.0 | |
| 10dg | 2.2 | -2.3 | 0.2 | -3.3 | -4.9 | | -5.3 | -5.7 | -1.9 | -2.8 | -2.7 | -2.2 | -2.2 | 0.3 | 2.7 | -2.3 | -1.7 | -0.6 | -0.6 | 3.2 | -0.2 | -1.9 | 8.9 | 3.8 | -1.8 | -0.2 | -2.7 | -2.8 | -3.9 | -3.0 | |
| 12dg | 5.6 | 0.0 | 1.3 | 0.0 | 0.0 | 5.3 | | 0.0 | 0.0 | 0.0 | 0.0 | 0.0 | 0.0 | 3.0 | 5.8 | 0.0 | 0.0 | 1.2 | 1.3 | 6.9 | 2.7 | 0.0 | 12.1 | 6.1 | 0.0 | 2.9 | 0.0 | 0.0 | 0.0 | 0.0 | |
| 11dg | 8.3 | 0.0 | 1.3 | 0.0 | 0.0 | 5.7 | 0.0 | | 0.0 | 0.0 | 0.0 | 0.0 | 0.0 | 3.9 | 7.8 | 0.0 | 0.0 | 1.4 | 1.5 | 9.2 | 3.4 | 0.0 | 15.9 | 7.0 | 0.0 | 4.1 | 0.0 | 0.0 | 0.0 | 0.0 | |
| 1aa | 4.9 | 0.0 | 1.1 | 0.0 | 0.0 | 1.9 | 0.0 | 0.0 | | 0.0 | 0.0 | 0.0 | 0.0 | 4.0 | 7.4 | 0.0 | 0.0 | 6.0 | 6.2 | 8.0 | 3.6 | 0.0 | 16.8 | 10.7 | 0.0 | 2.6 | 0.0 | 0.0 | 0.0 | 0.0 | |
| 1dd | 12.5 | 0.0 | 1.3 | 0.0 | 0.0 | 2.8 | 0.0 | 0.0 | 0.0 | | 0.0 | 0.0 | 0.0 | 7.9 | 16.9 | 0.0 | 0.0 | 2.5 | 3.2 | 11.9 | 3.8 | 0.0 | 44.0 | 14.3 | 0.0 | 5.1 | 0.0 | 0.0 | 0.0 | 0.0 | 0.0 |
| 1dk | 9.6 | 0.0 | 1.2 | 0.0 | 0.0 | 2.7 | 0.0 | 0.0 | 0.0 | 0.0 | | 0.0 | 0.0 | 8.5 | 15.0 | 0.0 | 0.0 | 2.1 | 2.6 | 9.4 | 3.2 | 0.0 | 31.3 | 12.3 | 0.0 | 4.1 | 0.0 | 0.0 | 0.0 | 0.0 | 0.0 |
| 1dm | 6.8 | 0.0 | 1.1 | 0.0 | 0.0 | 2.2 | 0.0 | 0.0 | 0.0 | 0.0 | 0.0 | | 0.0 | 4.8 | 11.5 | 0.0 | 0.0 | 2.2 | 2.9 | 6.9 | 2.5 | 0.0 | 29.8 | 10.8 | 0.0 | 3.0 | 0.0 | 0.0 | 0.0 | 0.0 | 0.0 |
| 1ds | 5.5 | 0.0 | 1.1 | 0.0 | 0.0 | 2.2 | 0.0 | 0.0 | 0.0 | 0.0 | 0.0 | 0.0 | | 3.3 | 6.7 | 0.0 | 0.0 | 2.2 | 2.7 | 5.9 | 2.3 | 0.0 | 22.4 | 12.4 | 0.0 | 2.6 | 0.0 | 0.0 | 0.0 | 0.0 | 0.0 |
| 1dr | 3.0 | -6.1 | 0.0 | -5.9 | -3.8 | -0.3 | -3.0 | -3.9 | -4.0 | -7.9 | -8.5 | -4.8 | -3.3 | | 7.6 | -6.0 | -3.5 | -1.3 | -1.5 | 4.1 | -0.5 | -2.9 | 17.5 | 6.4 | -3.2 | -0.8 | -4.6 | -4.4 | -7.3 | -4.6 | |
| 1dt | -1.1 | -11.7 | -0.8 | -11.8 | -8.0 | -2.7 | -5.8 | -7.8 | -7.4 | -16.9 | -15.0 | -11.5 | -6.7 | -7.6 | | -9.3 | -5.9 | -3.9 | -4.3 | 1.0 | -3.4 | -5.8 | 15.3 | 3.4 | -5.6 | -4.7 | -9.3 | -8.9 | -15.9 | -9.4 | |
| 1du | 5.7 | 0.0 | 1.1 | 0.0 | 0.0 | 2.3 | 0.0 | 0.0 | 0.0 | 0.0 | 0.0 | 0.0 | 0.0 | 6.0 | 9.3 | | 0.0 | 1.5 | 1.8 | 6.0 | 2.3 | 0.0 | 17.9 | 7.8 | 0.0 | 2.7 | 0.0 | 0.0 | 0.0 | 0.0 | |
| 4 | 4.6 | 0.0 | 0.9 | 0.0 | 0.0 | 1.7 | 0.0 | 0.0 | 0.0 | 0.0 | 0.0 | 0.0 | 0.0 | 3.5 | 5.9 | 0.0 | | 1.7 | 2.0 | 4.8 | 1.8 | 0.0 | 14.2 | 8.5 | 0.0 | 2.1 | 0.0 | 0.0 | 0.0 | 0.0 | |
| 1ba | 2.6 | -3.6 | 0.5 | -1.9 | -1.5 | 0.6 | -1.2 | -1.4 | -6.0 | -2.5 | -2.1 | -2.2 | -2.2 | 1.3 | 3.9 | -1.5 | -1.7 | | 0.1 | 4.9 | 1.5 | -1.2 | 11.7 | 6.6 | -1.9 | 0.6 | -1.9 | -2.1 | -1.9 | -2.6 | |
| 1ca | 3.0 | -5.2 | 0.5 | -2.3 | -1.6 | 0.6 | -1.3 | -1.5 | -6.2 | -3.2 | -2.6 | -2.9 | -2.7 | 1.5 | 4.3 | -1.8 | -2.0 | -0.1 | | 9.3 | 0.9 | -1.4 | 13.5 | 7.5 | -2.2 | 0.6 | -2.6 | -2.5 | -2.4 | -2.8 | |
| 1cg | -2.5 | -7.5 | -1.2 | -17.9 | -9.1 | -3.2 | -6.9 | -9.2 | -8.0 | -11.9 | -9.4 | -6.9 | -5.9 | -4.1 | -1.0 | -6.0 | -4.8 | -4.9 | -9.3 | | -10.3 | -5.1 | 10.7 | 1.9 | -4.9 | -8.2 | -19.8 | -17.9 | -19.8 | -19.8 | |
| 1bg | 3.4 | -2.7 | 0.3 | -5.5 | -3.4 | 0.2 | -2.7 | -3.4 | -3.6 | -3.8 | -3.2 | -2.5 | -2.3 | 0.5 | 3.4 | -2.3 | -1.8 | -1.5 | -0.9 | 10.3 | | -2.0 | 11.9 | 4.5 | -1.9 | -0.1 | -5.4 | -6.4 | -5.7 | -8.6 | |
| 1do | 4.6 | 0.0 | 1.0 | 0.0 | 0.0 | 1.9 | 0.0 | 0.0 | 0.0 | 0.0 | 0.0 | 0.0 | 0.0 | 2.9 | 5.8 | 0.0 | 0.0 | 1.2 | 1.4 | 5.1 | 2.0 | | 12.3 | 6.0 | 0.0 | 2.2 | 0.0 | 0.0 | 0.0 | 0.0 | |
| 1gd | -28.0 | -29.6 | -3.8 | -27.7 | -17.2 | -8.9 | -12.1 | -15.9 | -16.8 | -44.0 | -31.3 | -29.8 | -22.4 | -17.5 | -15.3 | -17.9 | -14.2 | -11.7 | -13.5 | -10.7 | -11.9 | -12.3 | | -7.7 | -14.7 | -18.0 | -18.1 | -16.4 | -34.7 | -18.9 | |
| 1df | -3.6 | -17.0 | -1.6 | -9.7 | -7.4 | -3.8 | -6.1 | -7.0 | -10.7 | -14.3 | -12.3 | -10.8 | -12.4 | -6.4 | -3.4 | -7.8 | -8.5 | -6.6 | -7.5 | -1.9 | -4.5 | -6.0 | 7.7 | | -9.8 | -5.4 | -8.2 | -8.0 | -11.1 | -8.3 | |
| 1de | 4.7 | 0.0 | 1.0 | 0.0 | 0.0 | 1.8 | 0.0 | 0.0 | 0.0 | 0.0 | 0.0 | 0.0 | 0.0 | 3.2 | 5.6 | 0.0 | 0.0 | 1.9 | 2.2 | 4.9 | 1.9 | 0.0 | 14.7 | 9.8 | | 2.1 | 0.0 | 0.0 | 0.0 | 0.0 | |
| 1rg | 5.8 | -3.3 | 0.3 | -7.7 | -4.0 | 0.2 | -2.9 | -4.1 | -2.6 | -5.1 | -4.1 | -3.0 | -2.6 | 0.8 | 4.7 | -2.7 | -2.1 | -0.6 | -0.6 | 8.2 | 0.1 | -2.2 | 18.0 | 5.4 | -2.1 | | -4.9 | -3.5 | -8.4 | -5.0 | |
| 1mg | 8.8 | 0.0 | 1.3 | 0.0 | 0.0 | 2.7 | 0.0 | 0.0 | 0.0 | 0.0 | 0.0 | 0.0 | 0.0 | 4.6 | 9.3 | 0.0 | 0.0 | 1.9 | 2.6 | 19.8 | 5.4 | 0.0 | 18.1 | 8.2 | 0.0 | 4.9 | | 0.0 | 0.0 | 0.0 | |
| 1sg | 8.2 | 0.0 | 1.3 | 0.0 | 0.0 | 2.8 | 0.0 | 0.0 | 0.0 | 0.0 | 0.0 | 0.0 | 0.0 | 4.4 | 8.9 | 0.0 | 0.0 | 2.1 | 2.5 | 17.9 | 6.4 | 0.0 | 16.4 | 8.0 | 0.0 | 3.5 | 0.0 | | 0.0 | 0.0 | |
| MD77 | 16.0 | 0.0 | 1.3 | 0.0 | 0.0 | 3.9 | 0.0 | 0.0 | 0.0 | 0.0 | 0.0 | 0.0 | 0.0 | 7.3 | 15.9 | 0.0 | 0.0 | 1.9 | 2.4 | 19.8 | 5.7 | 0.0 | 34.7 | 11.1 | 0.0 | 8.4 | 0.0 | 0.0 | | 0.0 | |
| 1ag | 10.0 | 0.0 | 1.4 | 0.0 | 0.0 | 3.0 | 0.0 | 0.0 | 0.0 | 0.0 | 0.0 | 0.0 | 0.0 | 4.6 | 9.4 | 0.0 | 0.0 | 2.6 | 2.8 | 19.8 | 8.6 | 0.0 | 18.9 | 8.3 | 0.0 | 5.0 | 0.0 | 0.0 | 0.0 | | |

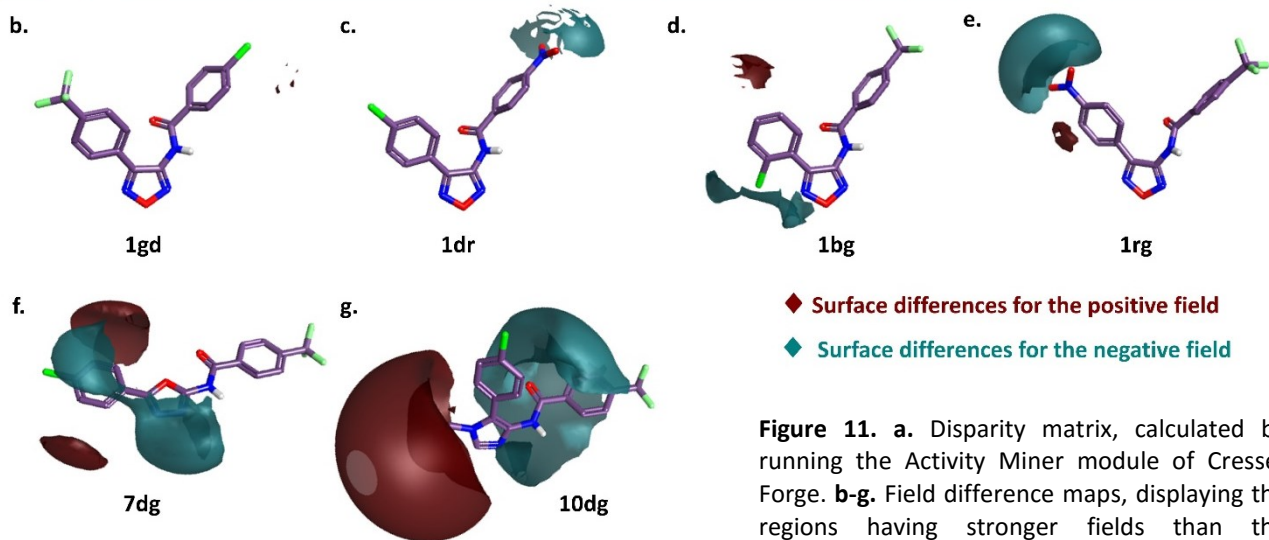


Figure 11. a. Disparity matrix, calculated by running the Activity Miner module of Cresset Forge. **b-g.** Field difference maps, displaying the regions having stronger fields than the corresponding regions in the compared molecule (MD77).

The result is a focused view of the SAR around a particular compound which can help to understand subtle molecule-to-molecule structure-activity changes and identify potential outliers.

This outcome can also be visually represented by the field difference maps (**Figure 11b-g**), displaying the regions having stronger fields than the corresponding regions in the compared molecule.

For instance, the most active derivative **1gd** has almost the same potential profile of **MD77** (**Figure 11b**), in line with their equivalent biological activity.

Small differences of positive and negative electrostatic potential are reported for isomer **1cg** which maintain cytotoxicity. Also a negative electrostatic potential localized on system C substituent (NO₂ in **1dr**, **Figure 11c**, and CN in **1dt**) seems to be well tolerated. Otherwise, compounds **1bg** (**Figure 11d**) and **1rg** (**Figure 11e**) showed an inversion of the potential distribution at level of the substituted position of ring A, possibly resulting in their lower activity.

As for the bioisosteric analogues of **MD77**, where the oxadiazole was replaced by 1,3,4-oxadiazole (**7dg**) or with *N*-methylimidazole (**10dg**), important field differences were observed (**Figure 5f,g**), which could justify the lower activity. Indeed, in **10dg** there is an inversion of electrostatic potential and **7dg** lacks the π -cloud over the 1,3,4-oxadiazole ring compared to the corresponding groups of the parent **MD77**.

2.3.3.1 Computational methodologies

A qualitative 3D model based on a molecular field technology was fine-tuned using the Activity Miner module as implemented in Cresset Forge v10.4.2 software. Through the shape and electrostatic character of molecules, qualitative and quantitative 3D models of activity were calculated using Cresset's patented ligand comparison method to align, score and compare molecules from a biological viewpoint. This technology helps you to understand how compounds interact with protein targets. Working from just a few 2D structures of known active ligands, Forge generates a series of conformations that the ligands might adopt under physiological conditions. It analyses them to find sets with a high molecular field similarity and hence with similar shape and binding properties to find the bioactive conformation. The eXtended Electron Distribution (XED) force field was used to generate molecular fields^[80]; all other settings were left as default. **MD77** crystallographic structure^[59] was used as template to align its derivatives and calculate field differences. Compounds were drawn by using ChemDraw^[81] program and VEGA ZZ suite^[82,83].

2.3.4 Crystallographic studies

The X-ray structure determination of two representative terms **1ag** and **1da** was carried out to understand in the solid state the influence of the phenyl substituents on the conformation, in order to find out the role of each molecular features for the activity (**Figure 12**).

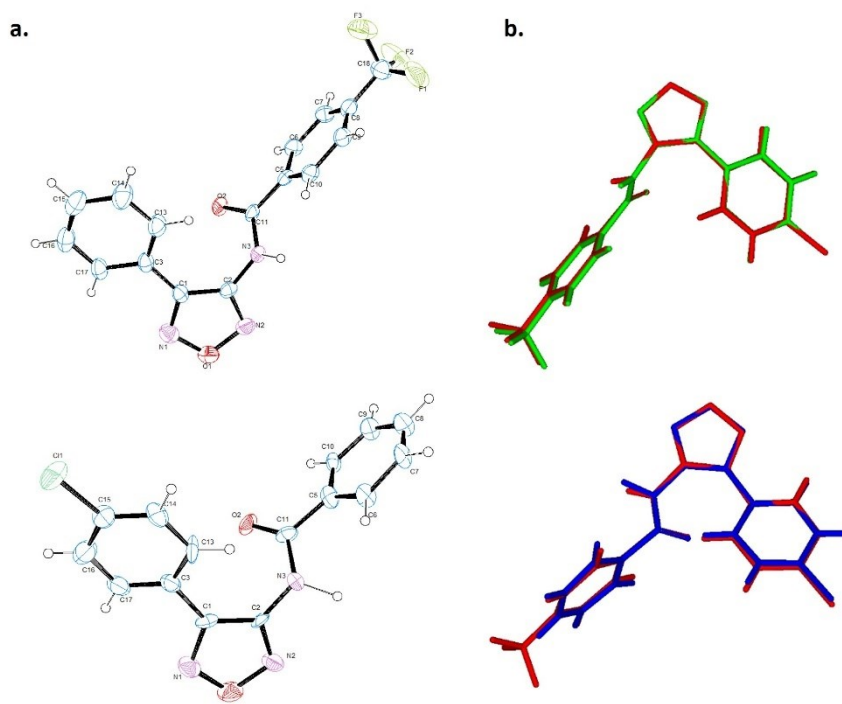


Figure 12. a. ORTEP ^[84] views of **1ag** (above) and **1da** (below), showing the arbitrary atom-labeling scheme. Atomic displacement parameters for non-H atoms are at 40% probability level. b. The overlay of the crystallographic structure of **MD77** in red onto **1ag** and **1da** in green and blue, respectively.

The comparison between the crystal structures of **1ag**, **1da** and **MD77** shows an almost perfect superimposition. This molecular arrangement corresponds to the most stable conformation calculated *in vacuo*, as evidenced in the previous results^[59]. For both derivatives, the analysis of the crystal packing shows that adjacent molecules are connected by NH \cdots O, C π H \cdots N, and C=O \cdots F (**1ag**), C π H \cdots Cl (**1da**) type contacts, also stabilized by stacking interactions. These findings pointed out that the two derivatives arrange the amidic linker and the two benzene moieties in the same way of the reference molecule **MD77**, despite the presence in this latter of substituents in both phenyl rings, which lead to an increased number of intermolecular interactions.

This result supports the hypothesis that the 3D electrostatic environment could have a greater influence on the activity over other types of geometry.

2.4 Conclusions

In my PhD project, I aimed at the identification of molecularly targeted chemotherapeutic agents and, in this section, I described the method I employed in order to search for the molecular target of antiproliferative compounds, structurally related with **AVS-0288**.

Among its 1,2,5-oxadiazole derivatives, **MD77** displayed a very interesting antiproliferative profile but, differently from the parent compound, it was not characterized by STAT3 affinity. Therefore, I focused my research efforts in the identification of its molecular target employing a combined synthetic-computational approach. A wide pool of synthesized derivatives underwent the MTT-assay on human colon cancer cells and a SAR analysis using Cresset Forge as software, whereas the remaining compounds are under evaluation.

This methodology will allow the assessment of a structure-activity landscape for a series of aligned compounds based on the principle of the 'activity cliff' and this overview could help to build up a 'protein's eye view' of the scaffold which will be used as query in search of a potential target.

Chapter 3

Platinum (II) complexes

3.1 Research project

In light of literature data reported in **Section 1.3**, this branch of my PhD project, carried out in collaboration with Dr. I. Rimoldi's research group (University of Milan) and Dr. N. Ferri (University of Padua), was focused on the design, synthesis and biological evaluation of Pt(II) complexes endowed with antiproliferative activity due to a dual mechanism of action: interference with DNA replication and inhibition of STAT3 signaling pathway.

This project was supported by PRIN Research Project, grant no. 20105YY2H_007.

3.1.1 3-aminomethyl-1,2,5-oxadiazole derivatives as ligands in Pt(II) complexes

Starting from the 1,2,5-oxadiazole derivative **AVS-0288** ^[57], known as potent STAT3 inhibitor, and taking advantage of the experience of Dr. Rimoldi's research group in platinum compounds ^[85,86], I synthesized 3-aminomethyl-1,2,5-oxadiazole derivatives as ligands in Pt(II) complexes (**Figure 13**). The scaffold (**13** and **Pt-13**) was firstly functionalized by a *para*-chlorophenyl system at position 4 of the heterocycle (**14** and **Pt-14**) and then by a substituted benzoyl group at its aminomethyl moiety (**15a-c** and **Pt-15b,c**).

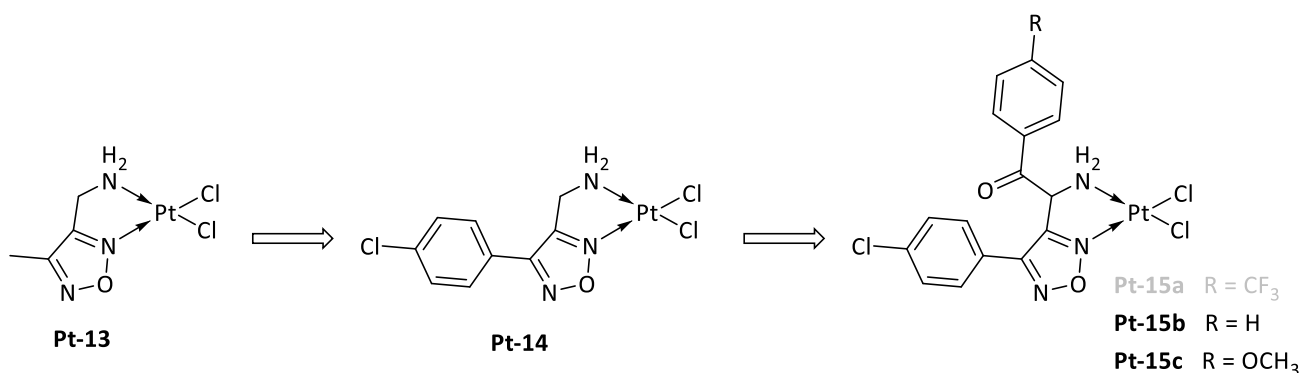


Figure 13. 3-aminomethyl-1,2,5-oxadiazole derivatives.

Due to compound **15a** instability as free amine, its biological activity was not evaluated and its Pt(II) complex was not synthesized. All the other ligands (**13**, **14**, **15b,c**) and the corresponding Pt(II) complexes were evaluated for their antiproliferative activity on colorectal cancer cells (HCT-116) and their ability to disrupt STAT3 dimerization. According to these data, **15b** and **Pt-15b** were selected for further investigation aimed at deeply understanding their molecular mechanism.

3.1.2 3-hydroxylaminomethyl-1,2,5-oxadiazole derivatives as ligands in Pt(II) complexes

Considering the characteristics of STAT3-SH2 (see **Section 5.2**) domain and how different substituents at the *para* position of the benzoyl function could modulate the keto-enol equilibrium ratio (and the stability) of ligands **15a-c**, I hypothesized that these ligands could interact with the target as enols. In order to verify this thesis, I substituted the primary amine with a hydroxylamine (**16a**), blocking the equilibrium in the keto form.

Compound **16a** was coordinated to the corresponding Pt(II) complex and in light of **Pt-16a** very interesting profile, the benzoyl (**Pt-16b**) and *para*-methoxybenzoyl (**Pt-16c**) derivatives were synthesized (**Figure 14**) and they are currently under biological evaluation.

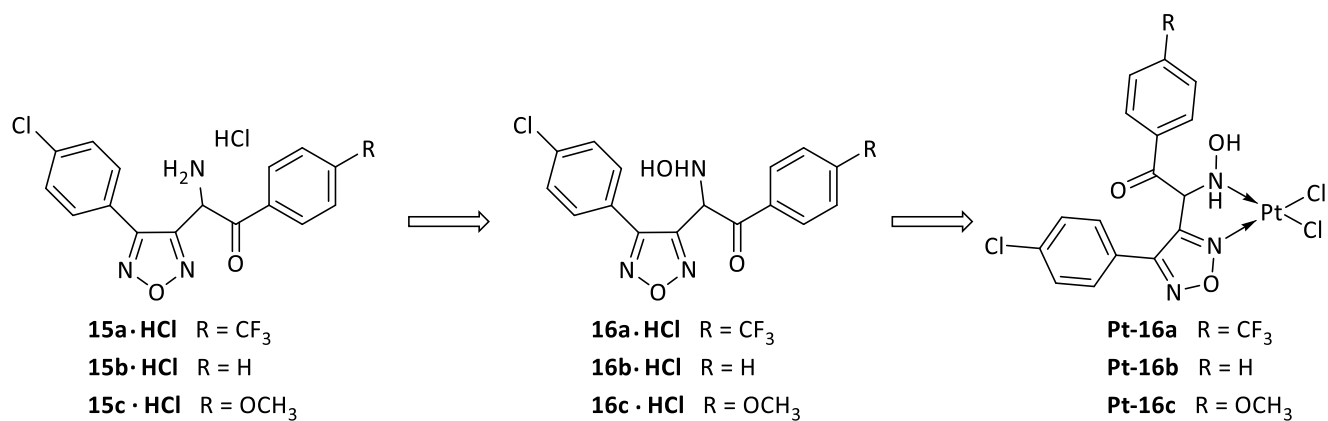


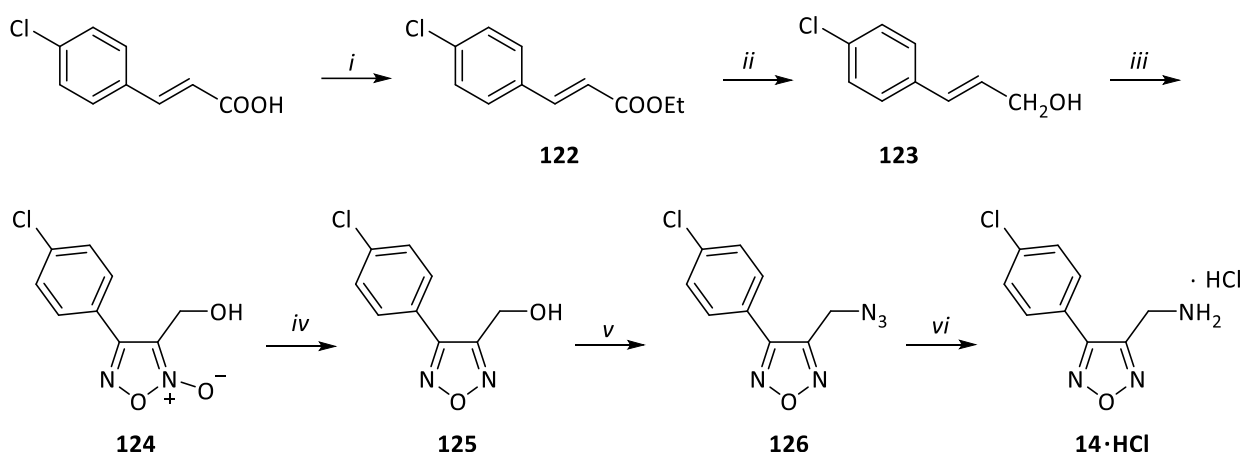
Figure 14. 3-hydroxylaminomethyl-1,2,5-oxadiazole derivatives

Meanwhile, the preliminary data led us to select **Pt-15b** and **Pt-16a** for *in vivo* studies.

3.2 Synthetic chemistry

The strategies for the synthesis of compounds **14-16**, **Pt-13-16** are shown in **Scheme 9-11**.

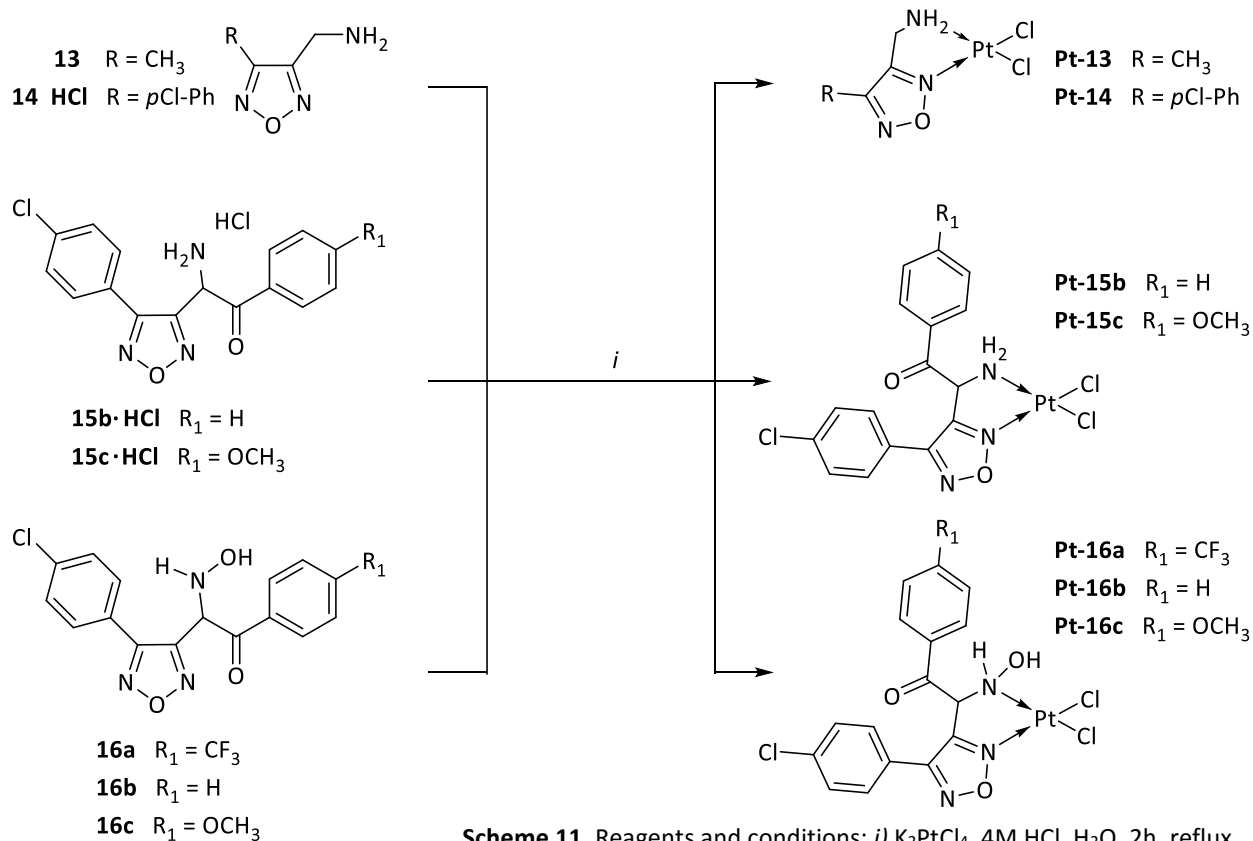
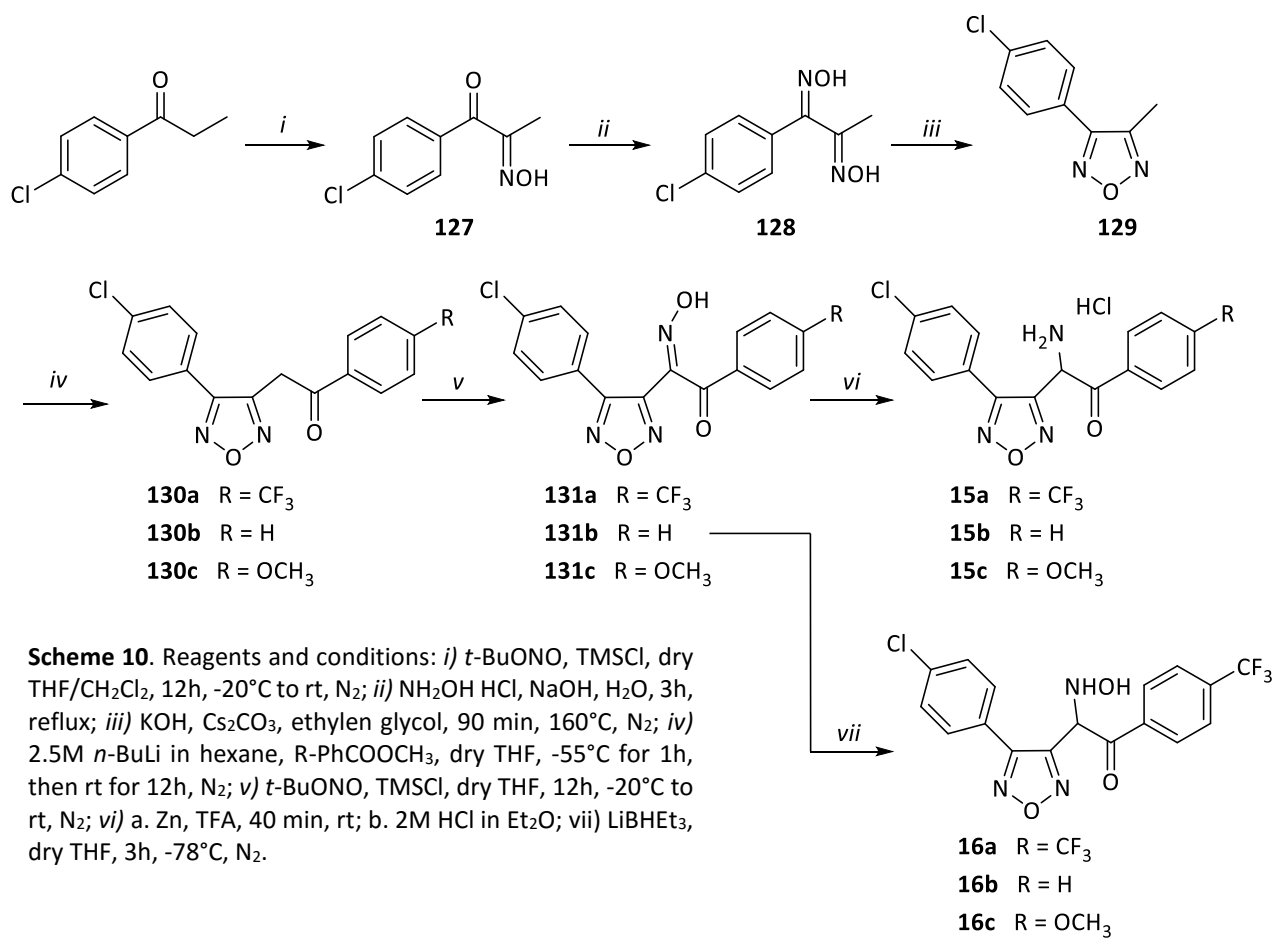
Compound **14** was synthesized starting from the commercially available 4-chlorocinnamic acid (**Scheme 9**). According to the literature procedure^[87], it was esterified (**122**) and, subsequently, reduced with DIBAL-H to give intermediate **123**. The sodium nitrate-mediated cyclization of the 4-chlorocinnamyl alcohol afforded the corresponding 4-phenyl-3-furoxanmethanol derivative (**124**) and its *N*-oxide moiety was removed upon treatment with trimethylphosphite^[88] to give intermediate **125**. Azide **126** was prepared by a one-pot reaction^[89], in presence of NaN₃ and Ph₃P in CCl₄/DMF, and converted to the amine (**14**) by catalytic hydrogenation. The final product was isolated as hydrochloride salt.



Scheme 9. Reagents and conditions: *i*) TMSCl, dry EtOH, 12h, rt, N₂; *ii*) DIBAL-H, dry toluene, 3h, -78°C to rt, N₂; *iii*) NaNO₂, AcOH, 48h, rt; *iv*) P(OCH₃)₃, 24h, reflux, N₂; *v*) NaN₃, Ph₃P, dry CCl₄/DMF (1:4), 5h, 90°C, N₂; *vi*) a. Pd/C, H₂, MeOH, 20 atm, 4h; b. 2M HCl in Et₂O.

The synthesis of compounds **15a-c** (**Scheme 10**) started from the commercially available *para*-chloropropiophenone which was treated with *tert*-butyl nitrite and chlorotrimethylsilane to obtain the correspondent α -keto oxime **127**. This latter was converted to the bis-oxime **128**, in presence of hydroxylamine hydrochloride and sodium hydroxide^[90], and then cyclized with potassium hydroxide and cesium carbonate at high temperature to give the intermediate **129**. Treatment with *n*-butyllithium and the suitable methyl benzoate gave ketones **130a-c**, which underwent α -oximation with *tert*-butyl nitrite and chlorotrimethylsilane. The reduction of compounds **131a-c** with zinc in trifluoroacetic acid or by using lithium triethylborohydride in tetrahydrofuran led to compounds **15a-c** or **16a-c**, respectively (**Scheme 10**).

The corresponding platinum(II) complexes (**Scheme 11**) were prepared according to the classical methodology^[91]: **13** (commercially available), **14** · HCl, **15b,c** · HCl and **16a-c** were treated with K₂PtCl₄ in water in presence of 4 M HCl affording the target compounds **Pt-13**, **Pt-14**, **Pt-15b,c**, **Pt-16a-c**, respectively. Ligand **15a** was not coordinated to the platinum core due to its instability as free amine, as shown in **Section 3.3.1.3**.



Ligands (**13**, **14**, **15b,c**) and their corresponding complexes were tested by MTT assay for cytotoxic activity on colorectal cancer cells (HCT-116) and by the AlphaScreen-based assay to determine the effect on STAT3 dimerization.

The MTT assay highlighted that whilst ligands generally showed a negligible (**13**, **14** · HCl and **15c** · HCl) or weak (**15b** · HCl) cytotoxic activity (IC_{50} 95.2 μ M), their coordination to the Pt center resulted in an increased cytotoxicity. In particular, **Pt-15b** displayed an IC_{50} value of 18.4 μ M, being about 5 times more effective than the uncoordinated **15b** · HCl ligand.

Regarding the AlphaScreen-based assay, if compounds **13** and **14** · HCl were inactive, compounds **15b** · HCl and **15c** · HCl not only disrupted STAT3 dimerization (IC_{50} value of 8.2 ± 0.1 μ M and 19.4 ± 0.7 , respectively) but were selective over STAT1 (IC_{50} value >30 μ M), a different STAT isoform characterized by a high degree of sequence homology with STAT3 but an opposite physiological role.^[92] Moreover, the coordination to platinum led to higher inhibitory activity but lower selectivity, partially maintained by **Pt-15b** and **Pt-15c**. On the basis of these preliminary data, I focused the attention on compound **Pt-15b** for further investigations in order to deeply understand its molecular mechanism.

The ability of **Pt-15b** to interact with DNA was confirmed by binding studies, using 9-ethylguanine as model. **Pt-15b** intracellular and nuclear accumulation was determined by ICPMS, pointing out that even if the efficiency of **Pt-15b** in reaching the DNA was significantly lower than cisplatin, its diffusion across the cell membrane was threefold higher. Besides, a significant induction of p53 was observed.

Although the AlphaScreen-based assay clearly demonstrated the capacity of **Pt-15b** to inhibit STAT3 dimerization, a possible effect on phosphorylation was excluded but an induction of the protein expression was observed. Finally, considering the resistance issue and despite the interaction of **Pt-15b** with GSH (binding studies were performed by using 1H NMR), its antiproliferative activity was evaluated on cell lines poorly sensitive to cisplatin, highlighting a significant inhibition of cell viability for DLD-1 (colorectal cancer cell line).

3.3.1.1 Analysis of the coordination environment of Pt(II) core

The identity and purity of all synthesized compounds and their Pt(II) complexes were determined by 1H NMR, ^{195}Pt NMR, ESI-MS or elemental analysis (see Chapter 6 - Experimental part: Chemistry). The observed chemical shifts (around -2070 ppm) for ^{195}Pt NMR spectra were in the range expected for a Pt(II) core with a N_2Cl_2 coordination environment^[93], as confirmed by single-crystal X-ray diffraction of **Pt-13** (performed by Dr. F. Meneghetti, University of Milan, Italy). The ORTEP^[84] diagram of **Pt-13** is shown in **Figure 17** with selected bond distances and angles.

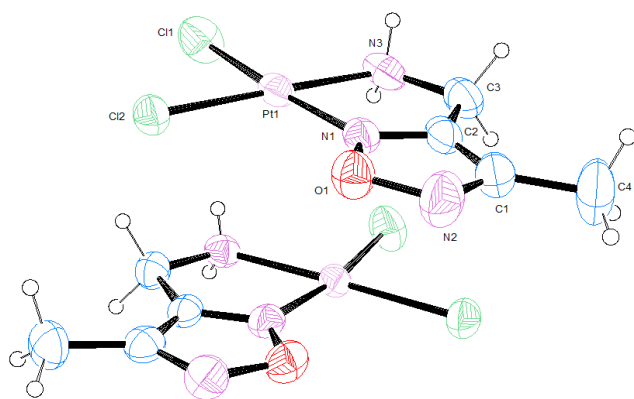


Figure 17. ORTEP view of the asymmetric unit of **Pt-13**. For the sake of clarity, only one of the two independent molecules shows the arbitrary atom labeling scheme, which is also followed by the other molecule. Ellipsoids are drawn at 40% probability and H atoms are shown as spheres of arbitrary radius. Selected averaged bond distances (Å): Pt-N1, 1.956(1)[1.967(1)]; Pt-N3, 2.046(1) [2.057(1)]; Pt-Cl1, 2.274(1)[2.276(1)]; Pt-Cl2, 2.294(1)[2.300(1)]; N1-C2, 1.291(1)[1.290(1)]; N3-C3, 1.497(1)[1.484(1)]. Angles (°): N1-Pt-N3, 80.8(1) [80.6(1)]; N3-Pt-Cl1, 90.7(1)[89.9(1)]; Cl1-Pt-Cl2, 91.6(1)[92.6(1)]; Cl2-Pt-N1, 96.8(1)[97.1(1)]; C2-N1-Pt, 119.9(1)[119.3(1)]; C3-N3-Pt, 112.2(1) [113.1(1)]; C2-C3-N3, 110.5(1)[113.1(1)]. Values in the square brackets refer to the second molecule present in the asymmetric unit.

This compound crystallized with two independent molecules in the asymmetric unit, which were almost planar and parallel-oriented. The Pt coordination was slightly distorted square planar and the chlorine atoms were *cis* to each other. The angles around the Pt atoms were close to the expected 90° and 180°. The mean deviation of the PtNClCl coordination plane was ca. 0.030(6) Å (N1) and the methyl groups lied almost in the same plane of the oxadiazole ring. The determined lengths and angles were in agreement with the literature for similar Pt(II) complexes.^[94] The crystal packing consists of molecular layers, parallel to the *ab* plane, where consecutive molecules interact through Pt···Pt contacts at 3.612 and 3.3364 Å, forming chains along the *c* axis^[95] also consolidated by N-H···Cl type interactions.

3.3.1.2 Aqueous stability and lipophilicity

The aqueous stability for Pt(II) complexes was performed using 0.9% w/v NaCl solution in DMF by monitoring UV-vis spectra at their respective λ_{max} during a period of 48 hours. Each compound was first dissolved in DMF and then diluted with physiological solution to 100 μM final concentration (1% v/v DMF).

Pt-13, **Pt-14** and **Pt-15b** demonstrated good stability in physiological solution with negligible variation of their UV peak profile after 48 hours, as shown in **Figure 18**. Aqueous stability of **Pt-15c** is still under evaluation.

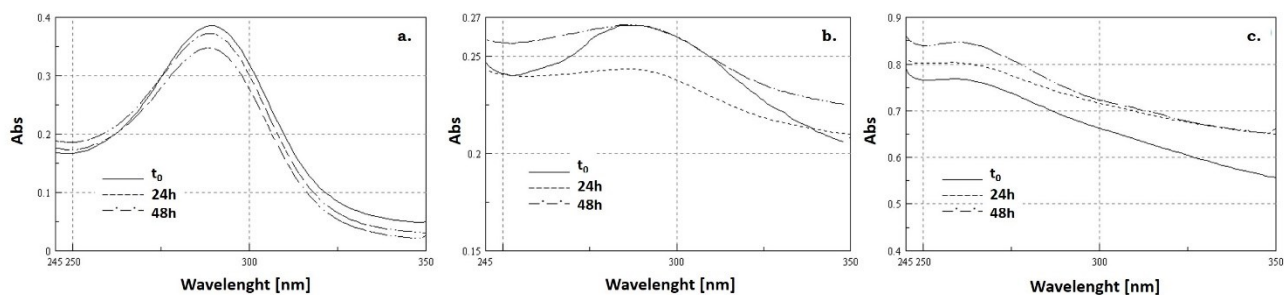


Figure 18. UV spectra profiles of **Pt-15b** (a), **Pt-14** (b) and **Pt-13** (c) for their stability evaluation under physiological conditions.

The values of $\log P_{\text{ow}}$ were determined using RP-HPLC technique.^[96-98] The lipophilicity increased along the series (-0.123 and 2.28 for **13** and **14** · HCl, respectively), reaching the maximum value of 1.09 and 3.01 with **15b** · HCl (in the keto and enolic form, respectively, as explained in **Section 3.3.1.3**). The same trend characterized the corresponding Pt(II) complexes (-0.773, 2.00 and 2.99 for **Pt-13**, **Pt-14** and **Pt-15b**, respectively) still satisfying the Lipinski's lipophilicity criterion for 'druglikeness'.

Furthermore, **15c** displayed a value of $\log P_{\text{ow}}$ higher than 5 while **Pt-15c** is under evaluation.

3.3.1.3 pH dependent enolization of ligands 15a-c

The scaffold of compounds **15a-c** is characterized by a chiral center in α position to a keto group. The amine derivatives **15a-c** showed a keto-enolic equilibrium responsible for the racemization at the chiral center.^[99,100]

The tautomerism of the free amines **15b,c** was evaluated at different pH conditions by RP-HPLC (**Figure 19a**): the peaks showed the different ratio between the ketone and the enol species. This experiment was also performed on **15a**, which unfortunately quickly degraded as free amine after treatment in basic condition.

Compound **15a** · HCl enolization was observed by using ^1H NMR. **Figure 19b** shows its time-dependent enolization ratio: the alkyl hydrogen bonded to a carbon atom in α position relative to the carbonyl group is characterized by a singlet at 6.80 ppm; however, after 36 hours this peak disappeared because of the formation of an equilibrium between the two tautomeric forms and, as a consequence, a downfield chemical shift of the aromatic system could be detected.

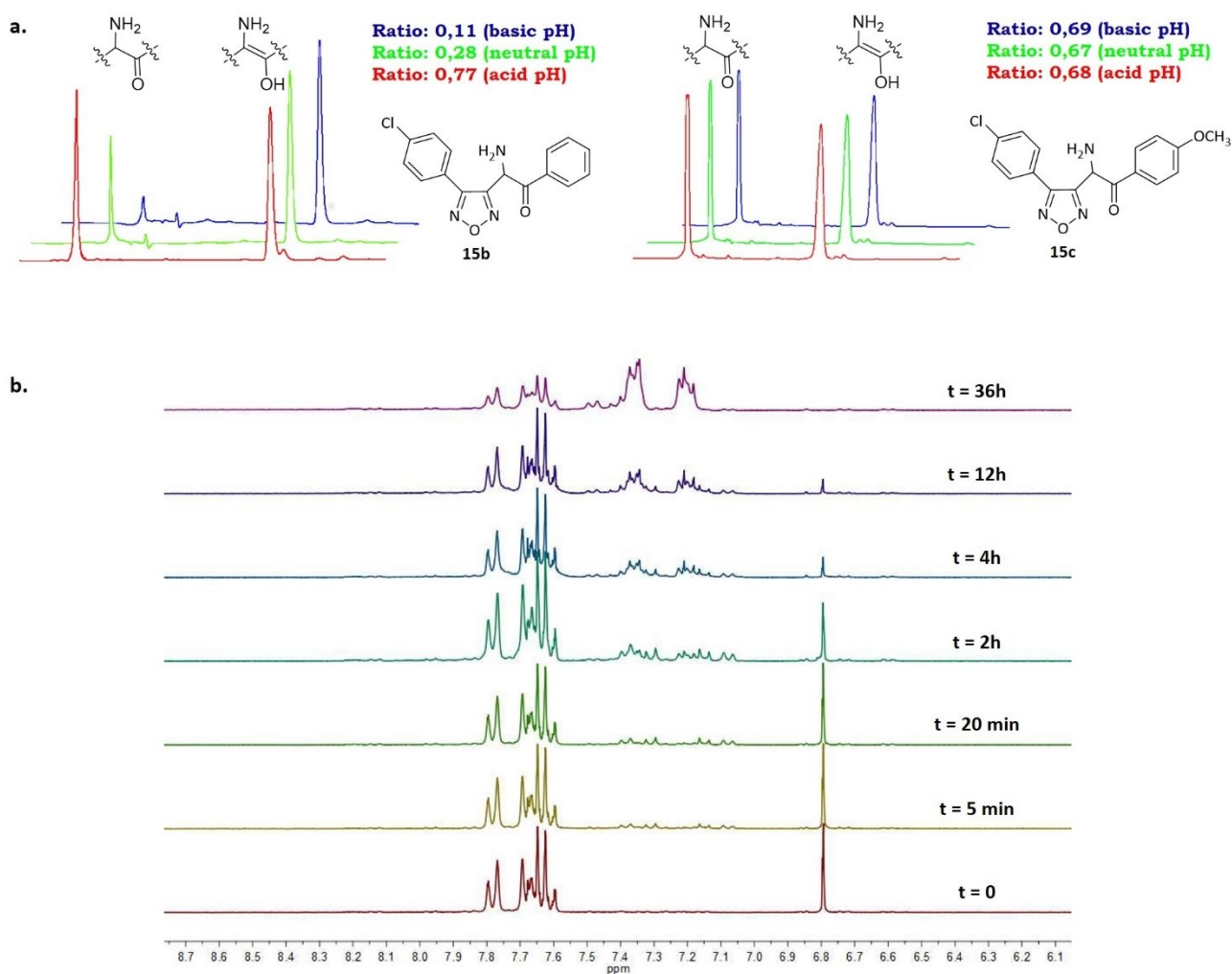


Figure 19. a. Compounds **15b** and **15c** pH-dependent enolization ratio (keto/enol). RP-HPLC was performed on a Partisil ODS at 25°C, using water/acetonitrile (50:50) and a flow rate of 1 mL/min. The UV traces were measured at 230 nm. **b.** ^1H NMR of compound **15a**·HCl in CD_3OD .

3.3.1.4 *In vitro* biological evaluation

MTT assay on HCT-116. The cytotoxic effect of the new ligands and their corresponding Pt(II) complexes was initially assessed in cultured colorectal cancer cells HCT-116 (**Table 5**). The cell viability was estimated by MTT assay after 48 hour incubation with increasing concentrations (10 ÷ 150 μM) of the compounds.

AphaScreen-based assay. This test, performed by Prof. A. Asai (University of Shizuoka, Japan), is an *in vitro* competitive binding test used to identify compounds able to inhibit the binding of SH2-containing proteins to their correspondent phosphopeptides (5-carboxyfluorescein (FITC)-GpYLPQTV for STAT3 and FITC-GpYDKPHVL for STAT1). Compounds characterized by an interesting affinity were also investigated for their selectivity *versus* STAT1, a different STAT isoform characterized by a high degree of sequence homology to STAT3 (78%) but an opposite physiological role.^[92] Data are summed up in **Table 5**.

| | MTT on HCT-116 ^a | AlphaScreen ^b (IC ₅₀ , μM) | |
|------------------|-----------------------------|--|-----------|
| | IC ₅₀ (μM) | STAT3 | STAT1 |
| 13 | n.a. | >30 | |
| Pt-13 | 122.9 | 0.4 ± 0.04 | 1.2 ± 0.1 |
| 14 · HCl | n.a. | >30 | |
| Pt-14 | 150 | 0.3 ± 0.01 | 1,9 ± 0.1 |
| 15b · HCl | 95.2 | 8.2 ± 0.1 | >30 |
| Pt-15b | 18.4 | 1.4 ± 0.1 | 5.9 ± 0.4 |
| 15c · HCl | n.a. | 19.4 ± 0.7 | >30 |
| Pt-15c | n.a. | 0.5 ± 0.1 | 4.1 ± 4.5 |

Table 5. Biological properties of 3-aminomethyl-4-methyl-1,2,5-oxadiazole derivatives. ^aIC₅₀ values measured by MTT assay on HCT-116 cell lines (n.a. means not active at 150 μM) ^bThe ability to disrupt the binding of STAT to the cognate pTyr-peptide (5-carboxyfluorescein (FITC)-GpYLPQTV for STAT3 and FITC-GpYDKPHVL for STAT1) is expressed as IC₅₀.

3.3.1.5 DNA binding study

In order to verify the ability of **Pt-15b** to interact with deoxyguanosine-rich regions of DNA, binding studies were performed with the model nucleobase 9-ethylguanine (9-EtG) by using ¹H NMR (**Figure 20**).^[101,102] The N⁷ of guanine is the putative binding position for the metal center, thus a downfield chemical shift of the H⁸ next to N⁷ in ¹H NMR should be observed after binding. The experiment was realized using 0.9 % w/v NaCl-D₂O solution in DMF-d₇ in order to mimic physiological conditions. In the free 9-EtG, the H⁸ is characterized by a singlet at 7.68 ppm; however, after 12 hours it was possible to evidence the presence of a new singlet at 8.32 ppm, thus confirming the binding between **Pt-15b** and 9-EtG.

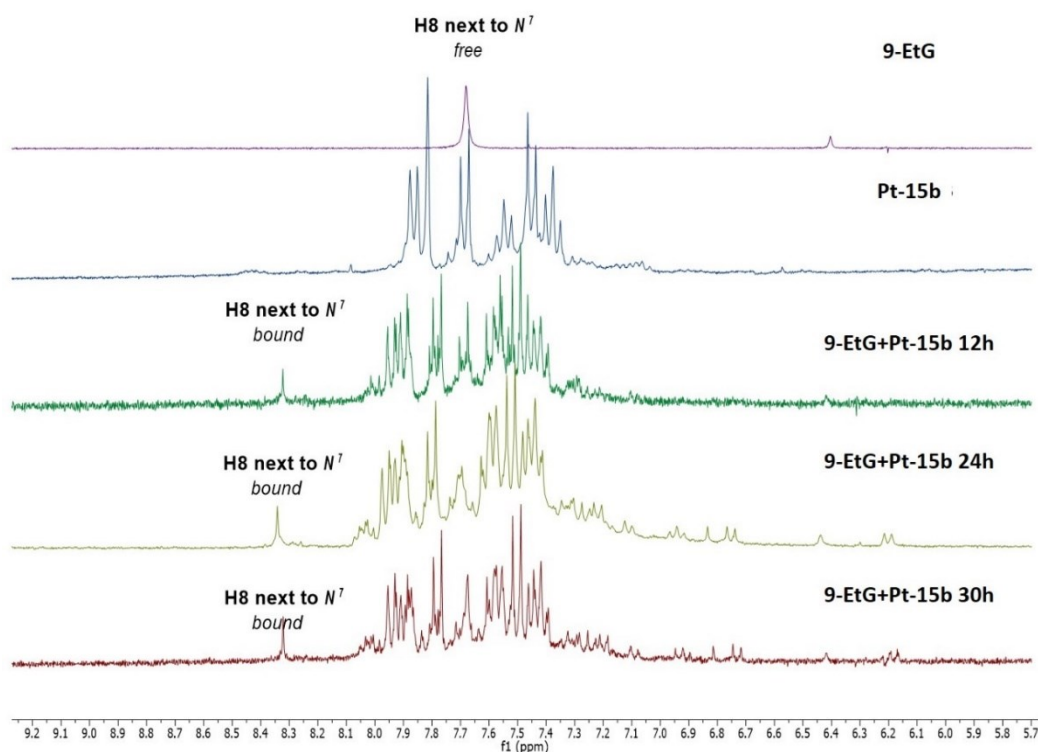


Figure 20. Binding study of 9-ethylguanine with **Pt-15b** in 20 % physiological D₂O solution-DMF-d₇: stack plot of ¹H NMR for aromatic region.

3.3.1.6 Intracellular and nuclear accumulation of Pt-15b and induction of p53

In order to explore the molecular mechanism of action of **Pt-15b**, the presence of ^{195}Pt was measured from total homogenates and nuclear DNA preparations of HCT-116 cell line incubated with the complex (25 and 50 μM) or cisplatin (10 and 25 μM). A concentration-dependent accumulation of Pt was observed in the DNA extract (**Figure 21a**). However, the efficiency of **Pt-15b** in reaching the DNA was significantly lower than cisplatin: at 25 μM the amount of Pt measured was 0.48 ± 0.30 ng Pt/ μg DNA and 9.0 ± 0.1 ng Pt/ μg DNA for **Pt-15b** and cisplatin, respectively. By contrast, **Pt-15b** diffused across the cell membrane with higher efficiency than cisplatin, reaching a threefold higher intracellular concentration after incubation with 25 μM (126.6 ng Pt/ μg protein and 42.3 ng Pt/ μg protein for **Pt-15b** and cisplatin, respectively) (**Figure 21b**).^[29]

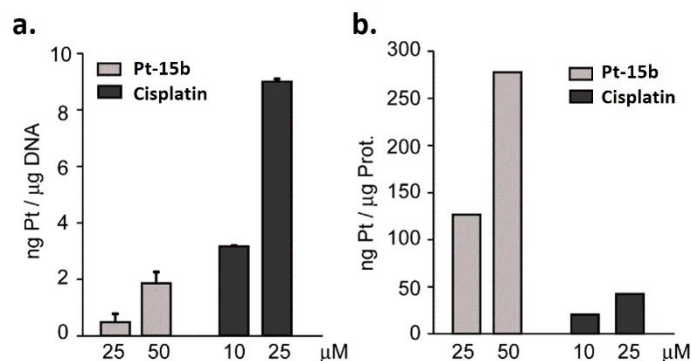


Figure 21. DNA and intracellular concentration of ^{195}Pt in HCT-116 cell line incubated with **Pt-15b** and cisplatin. Cells were seeded (250,000/35 mm petri dish) and incubated with McCoy's supplemented with 10% FCS; 24 hours later the medium was replaced with one containing 10% FCS and indicated concentrations of compound or cisplatin. After 3 hours, the nuclear DNA and total cell homogenates were prepared. ^{195}Pt concentrations were determined by ICPMS and normalized with total DNA and protein contents.

Although **Pt-15b** was incorporated less efficiently than cisplatin into the nuclear DNA, the incubation of HCT-116 cell line with increasing concentrations of Pt complex for 24 hours determined the induction of p53, as determined by Western blot analysis (**Figure 22**).

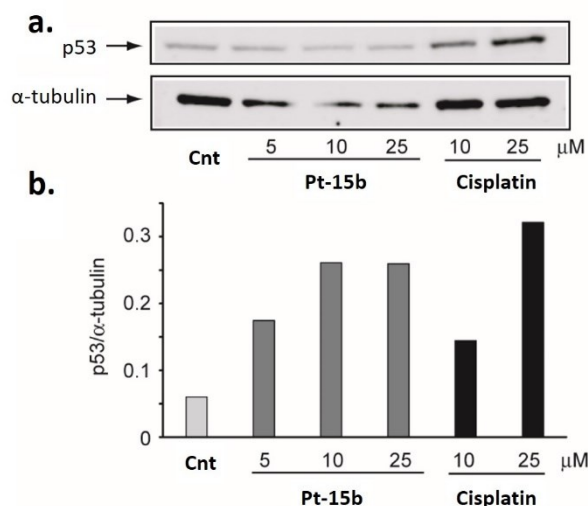


Figure 22. Effect of **Pt-15b** on p53 expression in HCT-116 cell line. Cells were seeded (250,000/35 mm petri dish) and incubated with McCoy's supplemented with 10% FCS; 24 hours later the medium was replaced with one containing 10% FCS and the reported concentrations of **Pt-15b** and cisplatin. The incubation was continued for a further 24 hours at 37°C and Western blot analysis was performed from total cell lysates. α -tubulin antibody was utilized as loading control.

These results suggested that **Pt-15b** could elicit its cytotoxic effect by interacting with nuclear DNA thus inducing the expression of p53, similarly to cisplatin.

3.3.1.7 Effect of Pt-15b on STAT3 expression and phosphorylation

The data obtained with the AlphaScreen-based assay clearly demonstrated the capacity of **15b** and **Pt-15b** to inhibit the binding between the SH2 and the phosphotyrosine of the other monomer and, therefore, the dimerization. In order to deeply explore the pharmacological activity, a series of experiments aimed at investigating the expression and the phosphorylation state of STAT3 were performed.

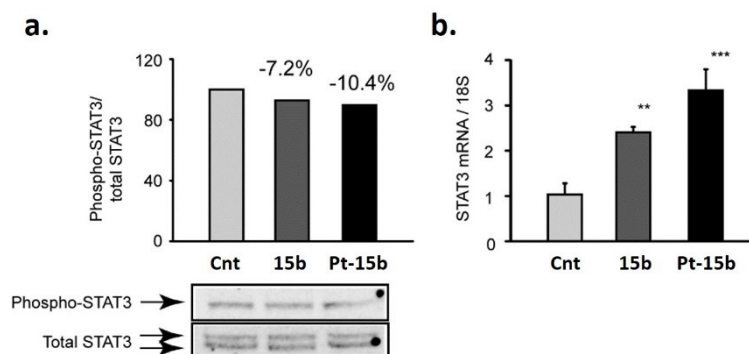


Figure 23. Effect of **15b** and **Pt-15b** on STAT3 expression and phosphorylation in HCT-116 cell line. Cells were seeded and incubated with McCoy's supplemented with 10% FCS; 24 hours later the medium was replaced with one containing 10% FCS and the reported concentrations of **15b** and **Pt-15b**. The incubation was continued for a further 24 hours at 37°C and Western blot analysis (a) and real time PCR (b) were performed from total cell lysates and total RNA, respectively. The ratio of phosphoSTAT3/STAT3 signals are shown in the histogram plot (a).

HCT-116 cells were incubated with 25 μ M concentration of **15b** and **Pt-15b** for 24 hours and both total protein extracts and RNA were prepared. As shown in **Figure 23a**, both compounds did not significantly affect the STAT3 tyrosine phosphorylation state, with a 7.2% and 10.4% inhibition after incubation with **15b** and **Pt-15b**, respectively.

Under the same experimental conditions, a significant induction of STAT3 mRNA was observed by quantitative real time PCR (**Figure 23b**). In particular, **15b** determined a 2.4 ± 0.43 fold induction of STAT3, while **Pt-15b** was more potent by upregulating the STAT3 mRNA levels by 3.3 ± 0.5 fold. These data indicate that **Pt-15b** did not inhibit the phosphorylation of STAT3 but more likely could affect its transcriptional activation, reflecting a significant induction of STAT3 mRNA expression. Unfortunately, it was not possible to directly measure the STAT3 transcriptional activity by a luciferase assay due to the interference of the Pt(II) complex with the assay.

3.3.1.8 Glutathione binding study

Glutathione (GSH), a thiol-containing tripeptide, is considered to be responsible for most of the drug resistance mechanism, especially towards Pt drugs. [38, 103, 104] The GSH-binding study with **Pt-15b** was conducted using 0.9% w/v NaCl-D₂O solution in DMSO-d₆. The ¹H NMR spectrum showed the appearance of two multiplets at 3.04-3.09 and 3.10-3.14 ppm that may be assigned to the methylene protons next to the SH group, which are set at 2.60-2.70 and 2.74-2.82 ppm in the unbound form. These signals underlined the interaction between **Pt-15b** and GSH, thus limiting the bioavailability of the metal compound (**Figure 24**).

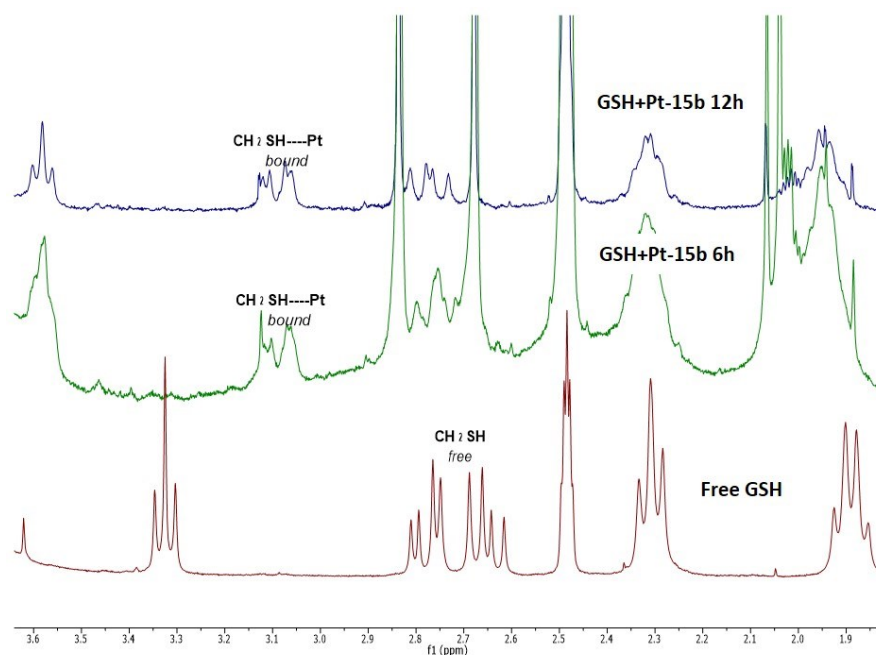


Figure 24. Binding study of GSH with **Pt-15b** in physiological D_2O solution- $DMSO-d_6$: stack plot of 1H NMR for aliphatic region.

3.3.1.9 Cytotoxic effect of **Pt-15b** and **15b** on cell lines poorly sensitive to cisplatin

The cytotoxicity of **Pt-15b** was then assessed on two additional cancer cell lines poorly sensitive to cisplatin^[85], like the breast cancer cell line MCF-7 and the colorectal cancer cell line DLD-1, in comparison with HCT-116. As shown in **Figure 25**, **Pt-15b** did not affect the cell viability of MCF-7 at the concentration range of $1\div 25\ \mu M$, while a significant inhibition was observed for DLD-1 at $25\ \mu M$ concentration. As expected, cisplatin showed a limited cytotoxic efficacy on all three cell lines with no concentration-dependent action. The MCF-7 resulted particularly resistant to both **Pt-15b** and cisplatin.

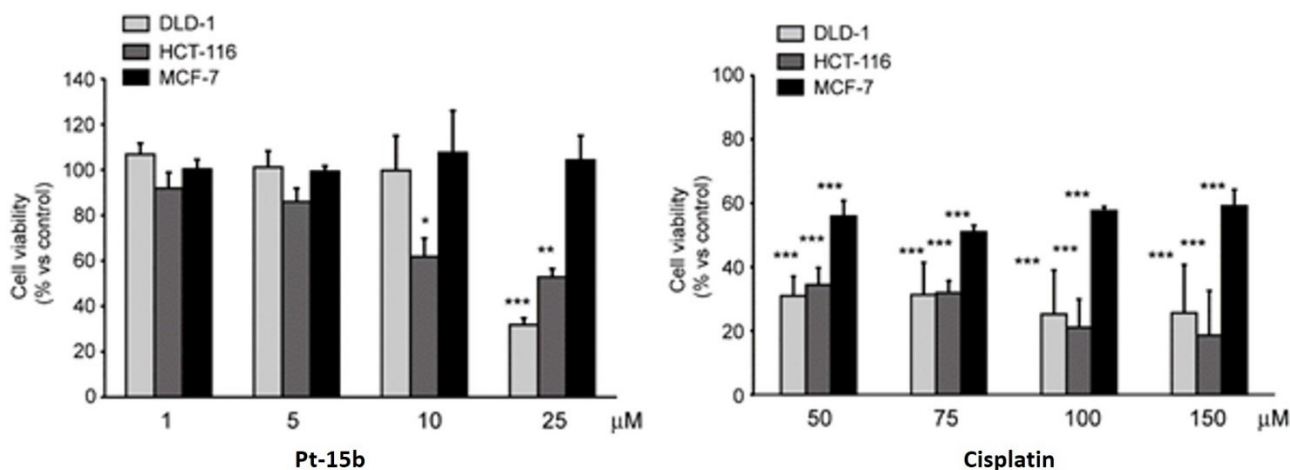


Figure 25. Cytotoxic effects of **Pt-15b** complex and cisplatin on DLD-1, HCT-116 and MCF-7 cell lines. Cells were seeded at the density of 40,000/well in a 48 well tray. The day after the medium was replaced with one containing 10% FCS and the reported concentrations of **Pt-15b** and cisplatin. After 48 hours the cell viability was estimated by MTT assay. Each bar represents the mean \pm SD of three determinations. **Pt-15b** and cisplatin *versus* control * $P < 0.05$; ** $P < 0.01$; *** $P < 0.001$.

3.3.2 3-hydroxylaminomethyl-4-methyl-1,2,5-oxadiazoles

As described in **Section 5.2**, SH2 domain is crucial for STAT3 dimerization. Among its different hot spots, subpocket A, which hosts the key pTyr705 of the other monomer, is characterized by polar and basic residues Lys591, Ser611, Ser613 and Arg609 which are engaged as hydrogen bond donors (HBD) or hydrogen bond acceptors (HBA) with the inhibitors.

Therefore, considering these characteristics of STAT3-SH2 domain and the keto-enol equilibrium ratio of the differently substituted ligands, I hypothesized that **15b** and **15c** could interact with this hot spot as enols. In the attempt to verify this theory, I substituted the primary amine of **15a** with a hydroxylamine (**16a**, **Figure 26**), blocking the equilibrium in the keto form and resulting in no affinity for the SH2 domain (IC_{50} value $>30 \mu\text{M}$ versus STAT3 and STAT1).

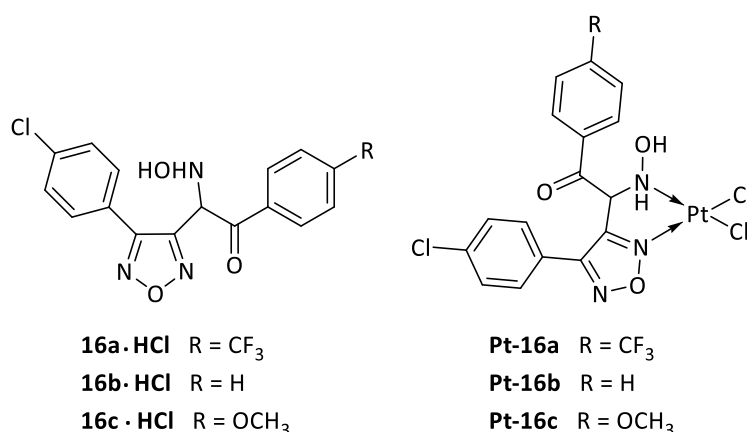


Figure 26

However, considering **16a** promising antiproliferative activity (IC_{50} 7.2 μM), it was coordinated with a platinum core (**Pt-16a**) resulting in a cytotoxic compound (IC_{50} value of 5.0 μM), able to selectively disrupt STAT3 dimerization (IC_{50} value of $3.4 \pm 0.3 \mu\text{M}$ versus STAT3 and $23.5 \pm 1.6 \mu\text{M}$ versus STAT1). In light of these results and in order to deeply characterize these last derivatives (**16a** and **Pt-16a**) and justify their particular behavior, further investigations are ongoing. Meanwhile, the benzoyl (**Pt-16b**) and *para*-methoxybenzoyl (**Pt-16c**) derivatives were synthesized and are currently under biological evaluation.

3.3.2.1 Enolization of ligand 16a

The substitution of the primary amine (**15b**) with a hydroxylamine (**16a**) resulted in the stabilization of the keto form, as confirmed by chiral column chromatography (**Figure 27**)

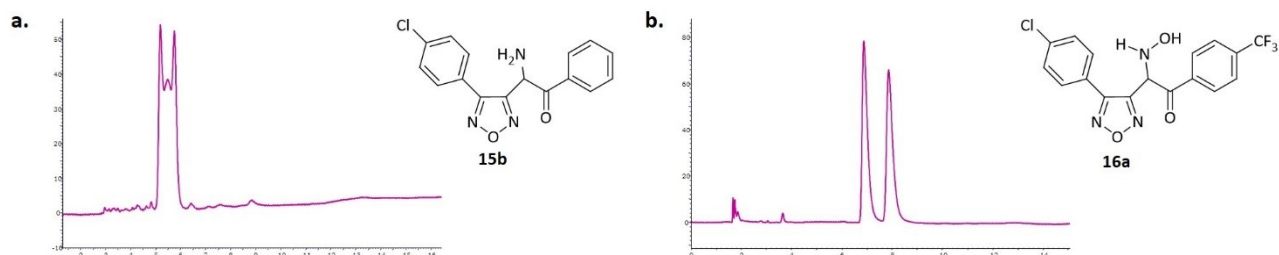


Figure 27. **a.** Compound **15b** chromatogram performed at physiological pH by normal phase HPLC on a Chiralcel OD-H column at 25°C, using hexane/ethanol (90:10) and a flow rate of 1 mL/min. The UV traces were measured at 230 nm. **b.** Compound **16a** chromatogram performed at physiological pH by normal phase HPLC on a Lux cellulose 4 column at 25°C, using hexane/isopropanol (90:10) and a flow rate of 1 mL/min. The UV traces were measured at 230 nm.

3.3.3 *In vivo* tumor growth inhibition

According to all these preliminary data, the *in vivo* antitumor activity of **Pt-15b** and **Pt-16a** was evaluated thanks to the collaboration with Prof. C. Marzano and Prof. V. Gandin (University of Padua).

Tumor growth inhibition was determined in a model of solid tumor, the syngeneic murine Lewis lung carcinoma (LLC) implanted i.m. in C57BL/6 mice. From day 7 after tumor inoculation, when tumors became visible, tumor-bearing mice received daily i.p. doses of **Pt-15b** (30 mg kg⁻¹), **Pt-16a** (30 mg kg⁻¹), or cisplatin (1.5 mg kg⁻¹). Cisplatin treatment schedule was selected according to standard protocols designed to optimize its efficacy and minimize the occurrence of adverse events.^[105]

As shown in **Table 6**, **Pt-16a** tested at 30 mg kg⁻¹ induced a significant tumor growth inhibition that was, however, lower than that promoted by cisplatin, while the chemotherapy with **Pt-15b**, tested at 30 mg kg⁻¹, reduced the tumor mass by roughly 85%, a slightly lower value compared with the one obtained by the reference metallo-drug.

| | Daily dose <i>i.p.</i> (mg kg ⁻¹) | Average tumor weight (mean ± SD, g) | Inhibition of tumor growth (%) |
|----------------------|--|--|-----------------------------------|
| Control ^a | - | 0.582±0.16 | - |
| Pt-15b | 30 | 0.086±0.06 ** | 85.2 |
| Pt-16a | 30 | 0.129±0.09 ** | 77.8 |
| Cisplatin | 1.5 | 0.073±0.03 ** | 87.5 |

Table 6. *In vivo* antitumor activity toward LLC. ^a vehicle (20% Cremophor EL (v/v), 20% PEG400 (v/v) and 60% saline solution (v/v)); ** p<0.01.

For the assessment of the side effects, changes in the body weight of tumor-bearing mice were monitored at day 1 and every two days from day 7 to day 15.

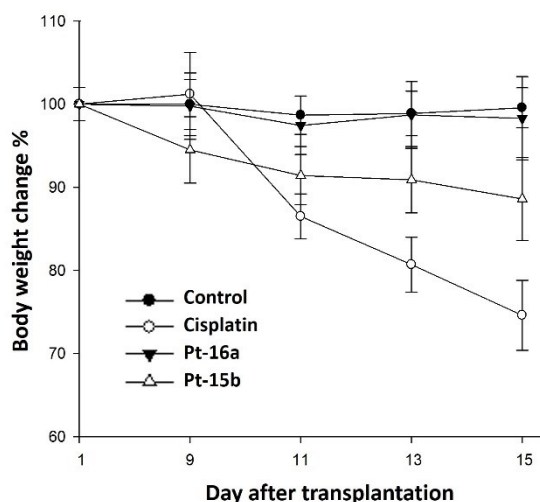


Figure 28. The body weight changes of LLC-bearing C57BL mice treated with vehicle or tested compounds. Body weight was measured at day 1 and every two days from day 7 and was taken as a parameter of systemic toxicity. The error bars indicate the SD.

The time course of body weight changes, depicted in **Figure 28**, highlights that, despite the higher dose than the reference compound, treatment with **Pt-15b** and **Pt-16a** induced very low or no body weight loss, respectively, compared with cisplatin (which caused a substantial weight loss, about 27%).

Even if these preliminary results seem to support our main goal, namely, the identification of effective antitumor metallo-agents able to interfere with DNA replication and to inhibit STAT3 signaling pathway. However, the molecular mechanism of these Pt(II) complexes (**Pt-15b** and **Pt-16a**) still needs to be clarified.

3.4 Conclusions and perspectives

This section of my research project was focused on the identification of platinum(II) complexes able to interfere with DNA replication and to inhibit STAT3 signaling cascade.

STAT3 was chosen as additional target considering its overexpression in various cancer cell lines and its involvement in oncogenesis. Therefore, the structure of a known STAT3 inhibitor, **AVS-0288**, was modified in order to obtain a ligand able to chelate platinum and characterized by antiproliferative activity due to this dual mechanism of action. The 3-aminomethyl-1,2,5-oxadiazole scaffold was functionalized by different substituents, allowing the modulation of both cytotoxicity and affinity/selectivity for STAT3 and among the synthesized derivatives, **Pt-15b** and **Pt-16a** were selected for *in vivo* studies. The chemotherapy with these compounds reduced the tumor mass similarly to cisplatin and, despite the higher dose, they seemed to be better tolerated than the reference compound.

There are several opportunities for the future. Firstly, a deep investigation of the binding mode:

- regarding platinum complexes, as reported in **Section 1.3.1**, they could target thiol-containing proteins. Therefore, Prof. Asai's research group will repeat the AlphaScreen-based assay using a Cys blocking reagent. Indeed, even if there are not cysteine residues in STAT3-SH2 domain, it was shown that their alkylation could inhibit the formation of the STAT3:STAT3 protein dimer complex^[106];
- if platinum interaction with cysteine is proven, a mass spectrometry method will be developed to investigate which cysteines are involved;
- as for ligands and the hypothesis they could interact as enol, Molecular Dynamics simulation will be performed. Furthermore, thermodynamic and kinetic studies on the keto/enol equilibrium by computational methods could justify how the different substituents affect its rate and compound stability.

From a pharmacological point of view, our results agree with literature evidences^[44,45] confirming that this dual targeting approach could be very promising. Therefore, further information could be achieved by:

- co-administration of **15b** with cisplatin;
- the use of **15b** as axial ligands in a platinum(IV) complex. Besides the advantages of this prodrug (see **Section 1.3.2**), this could confer additional cytotoxicity upon their release inhibiting STAT3 dimerization.

Chapter 4

DTT and MTTS derivatives

4.1 Research project

Dithiolethiones (DTTs) and methanethiosulfonates (MTTs) were recently reported to exert chemopreventive and anticancer activities. These electrophilic moieties could react with thiol groups, and therefore, hypothetically, with cysteines of biologically important peptides and proteins.

In light of this data, in collaboration with Prof. A. Sparatore's research group (as part of the PRIN research project, grant no. 20105YY2H_007, and, consequently, of another PhD thesis ^[107]), we designed and synthesized a new series of sulfurated compounds (**17a,b,e** and **18a-e**), characterized by having the DTT and MTT systems linked to a differently substituted 1,2,5-oxadiazole ring through an ester (**17a**, **18a** and **18c**) or an amidic bond (**17e**, **18d** and **18e**) (**Figure 29**). In addition, we synthesized the bioisosteric analogues of **17a** and **18a**, by replacing the oxadiazole with a 4,5-disubstituted *N*-methylimidazole (**17b** and **18b**, respectively).

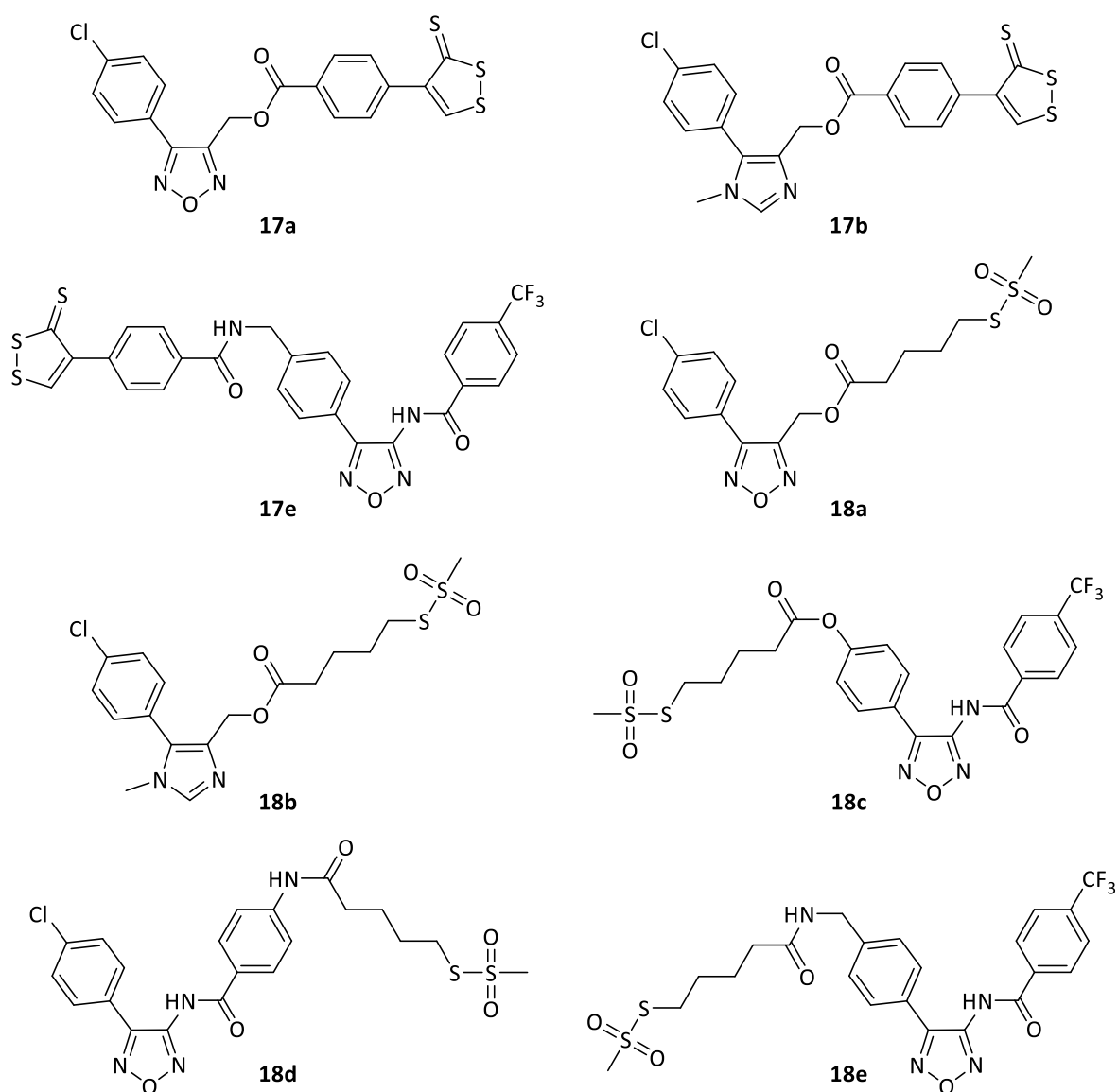
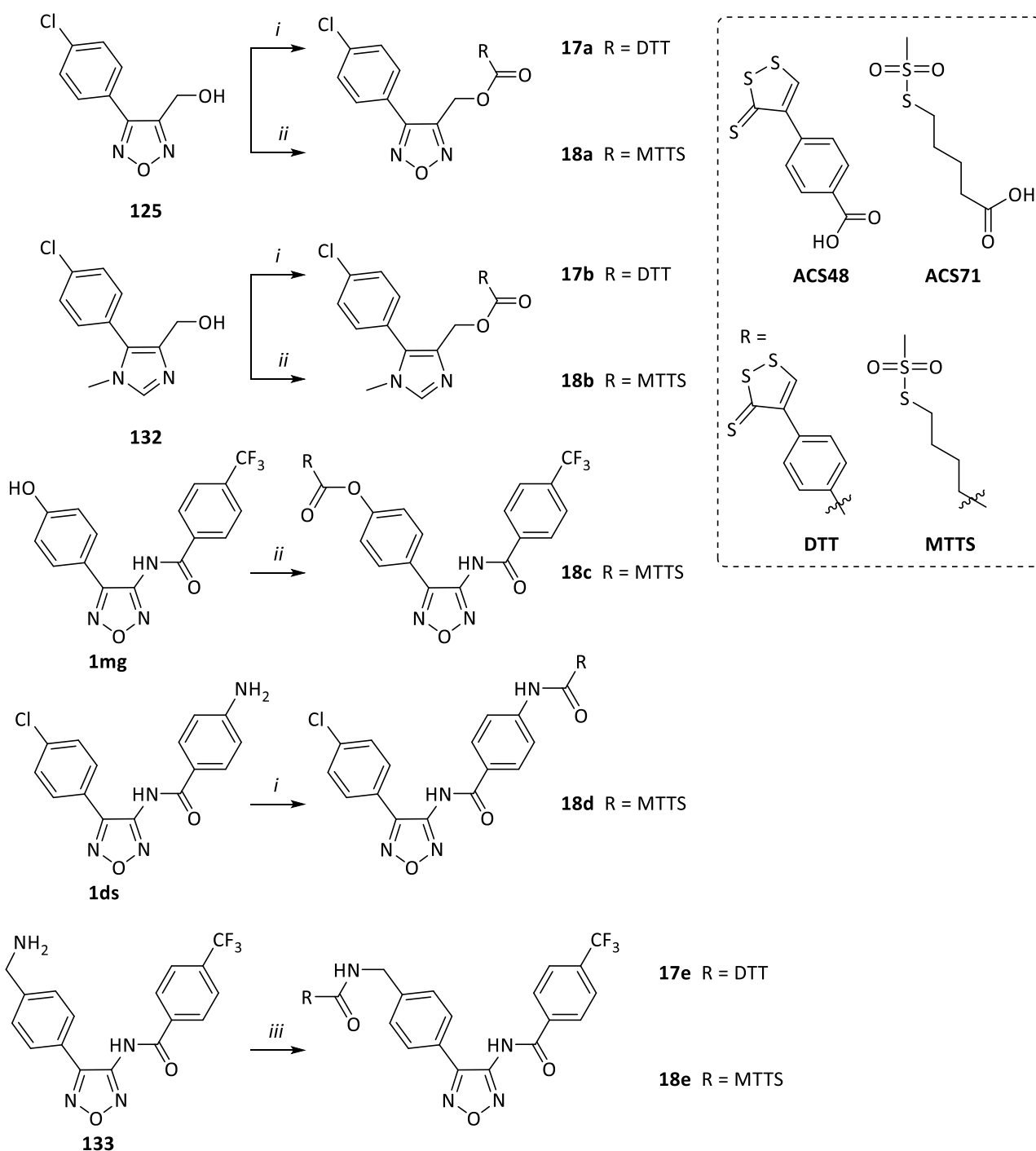


Figure 29. Structures of the newly synthesized dithiolethione and methanethiosulfonate derivatives.

4.2 Synthetic chemistry

The final products **17a,b,e** and **18a-e** were prepared^[107,108] by condensation of the suitable intermediate with **ACS48** or **ACS4871**, in presence of different coupling reagents (**Scheme 12**).



Scheme 12. Reagents and conditions: *i*) ACS48 or ACS71, EDC-HCl, DMAP, dry DMF, rt, 24h or 20h; *ii*) ACS48 or ACS71, DCC, DMAP, dry THF or dry CH₂Cl₂ or dry DMF, rt, 4h or 20h; *iii*) ACS48 or ACS71, TBTU, NMM, dry DMF, rt, 20h.

The procedure for the synthesis of **1mg** and **1ds** is reported in **Section 2.2**, while compound **125** is described in **Section 3.2**. The synthesis of intermediates **132** and **133** was performed by Dr. Rimoldi's and Prof. Romeo's research groups, respectively.

4.3 Conclusions

This part of my PhD project was performed in collaboration with Prof. A. Sparatore's research group and it aimed at the identification of potential dual inhibitors, able to covalently link cysteines of two transcription factors, STAT3 and NF- κ B. ^[108]

In order to achieve this goal, I synthesized differently substituted 1,2,5-oxadiazole derivatives which were coupled with DTT and MTTS systems by Dr. Elena Gabriele ^[107].

These compounds were evaluated for their affinity for STAT3 and NF- κ B and for the antiproliferative activity. The results showed that MTTS derivatives (**18b-e**) could strongly disrupt STAT3 dimerization, whereas the corresponding DTTs (**17a,b,e**) possessed lower affinity, independently from the nature of the linked heterocyclic scaffold. On the other hand, none of them was able to inhibit the NF- κ B transcriptional activity and the MTT assay, performed on HCT-116, highlighted that only **18a,b,e** exhibited a moderate antiproliferative activity.

The physicochemical properties of these compounds could be the discriminating factor to explain the low correspondence between cytotoxicity and STAT3 inhibition (tested in a cell-free assay). Based on these data, the MTTS moiety appears worth of further investigation, as promising ligand of STAT3-SH2 domain.

Chapter 5

Computationally Driven Drug Design

5.1 Research project

The aim of this branch of my PhD project was the identification of new chemical scaffolds endowed with antiproliferative activity by targeting STAT3-SH2 domain.

In order to achieve this goal, computationally driven drug design was performed employing a fragment-based drug design (FBDD) approach. Starting from small chemical fragments, this method allowed to find potential lead compounds, characterized by enhanced activity and suitable drug-like properties.

The STAT3:STAT3-DNA ternary complex crystal structure (PDB code 1BG1) revealed the structural composition and topology of the SH2 domain binding hot spots.^[25]

Analyzing STAT3 direct inhibitors reported in the literature, a set of privileged fragments were selected (Database A) and, on the basis of their docking score, the most interesting ones were heterogeneously merged. The linked compounds (Database B) were docked in a region of 12 Å around the Arg609 and ranked by binding energies and binding modes. Unfortunately, the docking calculations were not useful to identify new chemical scaffolds, because the selected combinations of two fragments were strictly related to some substructures already known in literature to be STAT3 binders. Although this result could appear a failure, this first study proved that the computational protocol could be used to build scaffolds with potential activity on STAT3.

Therefore, I decided to apply the same strategy on a different and larger base set of fragments, created by filtering PubChem database (Database C) with the aim to increase the chemical space. This new pool of fragments was docked and selected according to the ligand efficiency. Subsequently, the different possible poses were analyzed in order to identify two different groups of fragments depending on the region of interaction: region A (Arg609 – Ser636 – Lys 591) or B (Arg595 – Ser636 – Lys 591). The most interesting ones were heterogeneously merged (one fragment of each group) and searched in structures reported in literature or commercially available. These compounds (Database D) were docked and analyzed.

In this way, I could easily obtain a pool of chemical entities with high structural diversity which underwent *in vitro* binding assays for the purpose of evaluating their affinity for the target.

5.2 STAT3 structure

STAT proteins are monomeric structure which can be associated with other monomers to create homo or heterodimer. They consist of 750-850 amino acids and, through biochemical and mutagenic assays, a common primary structure, with highly conserved regions, was identified. In detail:

- The *N-terminal domain* (ND, ~125 residues) is a well conserved sequence. It is fundamental for the formation of the tetrameric STAT complex, involved in STAT-DNA interaction.^[109] The deletion of the *N-terminal domain* and, in particular, of a conserved residue of tryptophan, crucial for the interaction between the two dimers, prevents tetramer formation.^[110] This complex regulates the transcriptional induction, influencing receptor recognition, monomer phosphorylation, nuclear translocation and dephosphorylation.^[111]
- The *coiled-coil domain* (CCD, from ~135 to ~315 residues) is a region presenting four α -helices connected by short loops. This domain is characterized by a large hydrophilic surface which can interact with transcription factors and other regulatory proteins, while the central region of the helices is hydrophobic and includes residues of leucine, isoleucine and valine. As for the *N-terminal domain*, the coiled-coil domain acts as a protein-protein interaction site, allowing potential contacts between transcriptional factors and other regulatory proteins.^[112]
- The *DNA binding domain* (DBD, from ~320 to ~490 residues) is constituted by β -sheet structure. It is folded as the analogous sequence in the DNA-binding domains of tumor protein p53 and nuclear-factor kappaB (NF- κ B).^[111] This region is also involved in the interaction between STAT and DNA and it modulates the nuclear import and export.^[5]
- The *linker domain* (LK, from ~490 to ~580 residues) is composed of a series of α helices and guarantee the suitable conformation between the DBD and the SH2 domain. Mutations cause instability in DNA and STAT binding.^[113]
- The *Src homology 2 domain* (SH2, from ~580 to ~680 residues) is the most highly conserved domain. This sequence is also common in other signaling molecules. In STAT activation pathway, it is essential for the recruitment of STATs, their activation mediated by JAK proteins and the dimerization of two activated monomers (through reciprocal interactions between the SH2 domain and the pTyr).^[7] The SH2 domain also seems to be involved in dimer formation of unphosphorylated STAT (non-canonical pathway), interacting with the *N-terminal domain*.^[114]
- The *tyrosine activation domain* includes a conserved tyrosine, usually near residue 700, whose phosphorylation by JAKs activates STATs. Besides, its interaction with the SH2 domain of the other monomer stabilizes the association as dimer.^[113]
- The *C-terminal Transcriptional Activation Domain* (TAD) presents several crucial elements for STAT activation. For instance, this domain is involved in transcriptional activation of STAT regulated genes, because it contains a conserved residue of serine (Ser727), which can be phosphorylated to enhance transcriptional activity through the recruitment of co-activators.^[7] Deletion experiments have shown that each STAT isoform possesses a different amino acid sequence in the primary residues of the TAD domain, which is essential for its function.^[115]

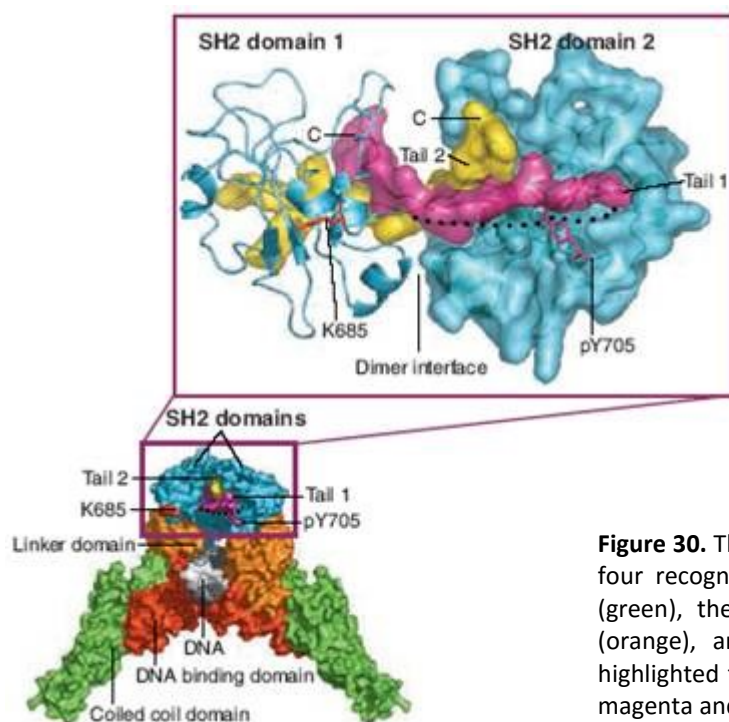


Figure 30. The active binding site of the STAT3 protein.^[103] The four recognized domains are shown: the coiled-coil domain (green), the DNA binding domain (red), the linker domain (orange), and the SH2 domain (cyan). The detailed view highlighted the dimer interface and the two tail segments are magenta and yellow

As previously mentioned, SH2 domain is crucial for the dimerization of both the phosphorylated and unphosphorylated STAT3.^[116] Using the STAT3:STAT3-DNA ternary complex crystal structure (PDB code 1BG1), Shahani and coworkers identified three subpockets in the SH2 domain, which revealed its structural composition and topology. In particular, subpocket A has a key role in the dimerization since it hosts the key pTyr705 of the other monomer and it is characterized by polar and basic residues Lys591, Ser611, Ser613 and Arg609 which are engaged as hydrogen bond donors (HBD) or hydrogen bond acceptors (HBA) with the inhibitors.^[25]

From a topological point of view, a central $\beta\beta\beta\beta\beta\beta$ anti-parallel β -sheet, flanked by adjacent α helices, characterizes the SH2 domain. The crucial arginine (Arg609) is located on the central β B strand, forming two positive charges on the pTyr-recognition site. Besides, the side chain of another arginine residue (Arg595, on the α A) determines the distinct hydrophobic side pocket on the side of pTyr705 and the Leu706 binding subpockets, which are absent in other STAT SH2 domains.^[117]

5.3 Computational methods

This section reports the main computational methods that were used in this phase of my research study. It is not supposed to be a comprehensive compendium on this matter, but only a summary on the main topics.

5.3.1 Conformational analysis and molecular mechanics

The steric and energetic features have to be well parameterized in the *score* functions. Therefore, conformational analysis has to be performed in order to study the relationship between the energy of a given molecular system and the variation of relevant torsion angles. The calculation of the total energy of the molecule can be achieved by three methods:

- *quantum* or *ab initio* methods are very accurate but also costly in terms of computation time since they allow the calculation of the electronic distribution within the molecular orbitals by the Schrödinger equation;
- *semi-empirical* methods are based on the calculation of the electronic distribution of molecular orbitals but consider only the valence electrons, leading to a significant increase in computing performance; they cannot yet be applied to biomacromolecular systems;
- *molecular mechanics* considers atoms as partially charged rigid spheres with a radius corresponding to that of Van der Waals and connected by springs (bonds) endowed with appropriate elastic constants. These approximations imply that the electrons are not explicitly considered, and therefore it is not possible to simulate charge transfer, break and formation of a covalent bond during a chemical reaction or consider the effect of a single charge on the distribution of electrons in orbital. Methods based on these assumptions have the advantage of being markedly less demanding than the previous ones. The calculated potential energy has a relative value that allows to compare only the conformers of the same molecule. Furthermore, the considerable speed of the method means that it can be applied to complex systems such as proteins and nucleic acids.

In this research work, the only viable option was the use of the molecular mechanics, in order to have acceptable calculation times.

5.3.2 Molecular docking

Molecular docking is based on computational methods that allow the study of the interactions between a generic ligand and a known three-dimensional biomacromolecule (protein or nucleic acid). The interaction between the two partners takes into account both the steric complementarity between the ligand (usually with low molecular weight) and the binding region of the target as well as the chemical and physical complementarity between the two molecules. These steric and energetic features are well parameterized in the *score* functions, used in all docking programs to assess the quality of a ligand-receptor complex (the term "receptor" is used here in a broad sense). Based on the size and/or molecular weight (MW) of the two partners of the simulated interaction, several cases may arise:

- high MW receptor-low MW ligand is the most common case, when a drug that typically have a molecular weight less than 500 D, must interact with its target (protein or nucleic acid);
- high MW receptor-high MW ligand is the typical case that occurs considering the quaternary structure of proteins, how a protein interacts with its receptor (docking protein-protein) or how a nucleic acid (RNA or DNA) interacts with an enzyme or, more generally, with a protein (docking DNA/RNA-protein);
- low MW receptor-low MW ligand such as studying the formation of host-guest complexes.

5.3.2.1 PLANTS software

In particular, in this research, it was necessary to perform calculations of molecular docking studies on “high MW receptor - low MW ligand” and the docking software chosen for this *virtual screening* study was PLANTS (Protein-Ligand ANT System).^[118-121] This software is based on a particular class of stochastic optimization algorithms called *Ant Colonization Optimization* (ACO). These are inspired by the natural ants’ behaviour, consisting in the search for the shortest path between their anthill and the food supplies. The ants use an indirect form of communication based on the pheromones traces through which every single ant marks its own path. Molecular docking exploits an artificial “ant colony” to evaluate the lowest energy conformation of the ligand in the binding site: the virtual ants mime their real behaviour marking the most favourable conformations with “artificial pheromones”.

Ligands are considered completely flexible by PLANTS, in particular they have $6+r$ degrees of freedom: 3 translational, 3 rotational and r degrees due to the torsion flexible angles whose number depends on the structure of the molecule (**Figure 31**). By contrast, the receptor is considered fixed or partially fixed.

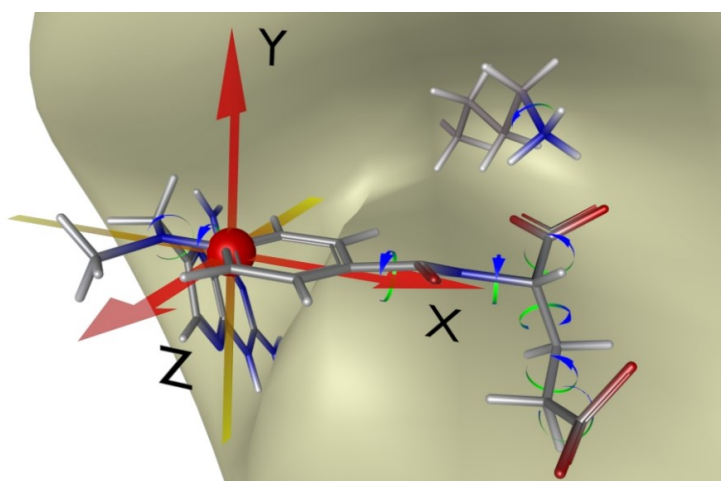


Figure 31. Degrees of freedom of the ligand. The original system coordinates are shown as a sphere and the arrows indicate where and how the ligand can be moved in the space.

The degrees of freedom, by definition, are continuous functions, but the ACO was developed to be applied to combinatorial problems and so to discrete systems. For this reason, in PLANTS the degrees of freedom have been “discretized”, considering a step of 0,1 Å for translations and of 1° for rotations. Hence, to each degree of freedom i is assigned a “pheromone vector” τ ; for example, for a torsional angle, the vector can assume discrete values between 1 and 360.

The software is based on MAX-MIN Ant System (MMAS) that allows the virtual ants to choose the most favorable poses of the ligands, exploring the potential of each conformation, which is determined by the values associated to the degrees of freedom. Through this approach, it is also possible to calculate the probability that an ant chooses the right values and to avoid the construction of high energy conformations. The software assigns a score to the sampled potential space using a scoring function, which considers different interaction parameters, then, applying the algorithm criteria, only the poses with a negative score are selected. PLANTS uses three scoring functions PLP, CHEMPLP and PLP 95 that consider and evaluate different patterns of interactions.

Once the poses have been generated, they are optimized by the application of local search algorithms designed by Nelder and Mead, and a clustering method was used to facilitate the analysis of the results: the software automatically ranks the poses according to the scoring function values, then extracts a given number of ranking structures, usually ten, which have an RMSD larger than 2 Å.

5.3.3 Preparation of the STAT-SH2 domain structure

The X-ray crystallographic structure of STAT3-SH2 domain used for the docking studies was the STAT3:STAT3-DNA ternary complex, downloaded from the Protein Data Bank (PDB code 1BG1).

PDB^[122] is a central archive including the 3D structures of biological molecules: it contains thousands of proteins, nucleic acids and complex assemblies which come from experiments in X-ray crystallography, nuclear magnetic resonance and electron microscopy. Besides, PDB includes several other additional information such as ID, author, bibliographic notes, organization of origin, data on the methods used, primary structure.

The 1BG1 structure, composed of a pTyr705-STAT3 dimer which is linked to the DNA, was dimerized applying the transformation matrix as reported in the PDB file. The model was completed by adding the hydrogens in two steps: 1) to STAT3, applying the algorithm for proteins; 2) to DNA, applying the algorithm for nucleic acids. Atom charges (Gasteiger - Marsili method^[123]) and potentials (CHARMM 22 for proteins and nucleic acids^[124]) were assigned to the obtained structure. Finally, the model was optimized through a conjugate gradients minimization (50.000 steps) in order to reduce the high-energy sterical interactions. To preserve the experimental data, atom constraints were applied to protein and DNA backbones. The model preparation and the energy minimization were carried out respectively by NAMD 2^[125] and VEGA ZZ^[82,83] programs.

Therefore, I retrieved the docking area selecting a region of 8-12 Å around the Arg609 from a pTyr705-STAT3 monomer, according to the size of the considered ligand and/or the selection of specific sub-pockets.

5.3.4 Preparation of the dataset of fragments and compounds

For the docking calculations, compounds were drawn by using ChemDraw^[81] program and VEGA ZZ suite or downloaded from PubChem^[126]. PubChem is a large database of small molecules collected according to their chemical structure and physicochemical properties including molecular weight, XLogP, and hydrogen bond donor and acceptor count, and their biological activities. The collection is managed by the National Center for Biotechnology Information (NCBI), which is a department of the United States National Institutes of Health (NIH). PubChem can be accessed for free and consists of three dynamically growing primary databases:

- *Compounds*, containing pure and characterized chemical compounds (2D and/or 3D);
- *Substances*, containing mixtures, extracts, complexes and uncharacterized substances;
- *BioAssay*, including bioactivity results from HTS programs with several million values.

The compounds, selected for the docking studies, were grouped in four databases:

- Database A is composed of fragments selected starting from known STAT3 inhibitors;
- Database B includes compounds obtained by combing two fragments from Database A;
- Database C comes from PubChem dataset, converted and filtered according to various properties, the synthesizability and the stability;
- Database D is a collection of compounds, reported in literature or commercially available, bearing at least two fragments of Database C.

All molecules included in the databases underwent the same computational protocol consisting in the attribution of atom types (SP4 force field), the calculation of the atomic charges (Gasteiger-Marsili method), the energy minimization by molecular mechanics calculation (AMMP software^[127], conjugate gradients minimizer, RMSD value of 0.01 as convergence criterion). Finally, each structure was significantly optimized by MOPAC 2016^[128] (PM7 hemiltonian method), a semi empirical quantum chemistry program.

Weak acids and bases were considered ionized at physiological pH.

5.4 Results and discussion

5.4.1 Virtual screening

The aim of this research project was the identification of new chemical scaffolds capable of disrupting STAT3-PPI (Protein-Protein Interaction) and characterized by an increased activity and suitable drug-like properties. Among the different approaches to STAT3-targeted drug design (inhibitors directly targeting the SH2 domain or the DNA-binding domain and antisense approaches using oligonucleotides to inhibit STAT3 transcription), I focused on analyzing SH2 domain direct inhibitors since it is the most feasible approach to design small molecules, especially with a structure-based computer-aided drug design strategy.^[129] In order to achieve this goal, I employed a *fragment-based drug design* (FBDD) approach.

Considering all STAT3 inhibitors reported in literature, the first problem I observed was that several compounds were presented as direct inhibitors on the basis of antiproliferative assays and computational studies but without any direct binding test.

As previously mentioned (see **Section 5.2**), the crystal structure of STAT3:STAT3-DNA ternary complex (PDB code 1BG1) allowed to describe the structural composition and topology of the SH2 domain binding hot spots. In particular, the polar and basic residues (Lys591, Ser611, Ser613 and Arg609) of a region (labeled as subpocket A) of the SH2 domain could be engaged as hydrogen bond donors (HBD) or as hydrogen bond acceptors (HBA) with the direct STAT3 inhibitors.

Using this model, two new different subpockets (**Figure 32**) were recognized:

- subpocket A, defined by Arg609, Lys591 and Ser636;
- subpocket B, lined by Arg595, Lys591 and Ser636.

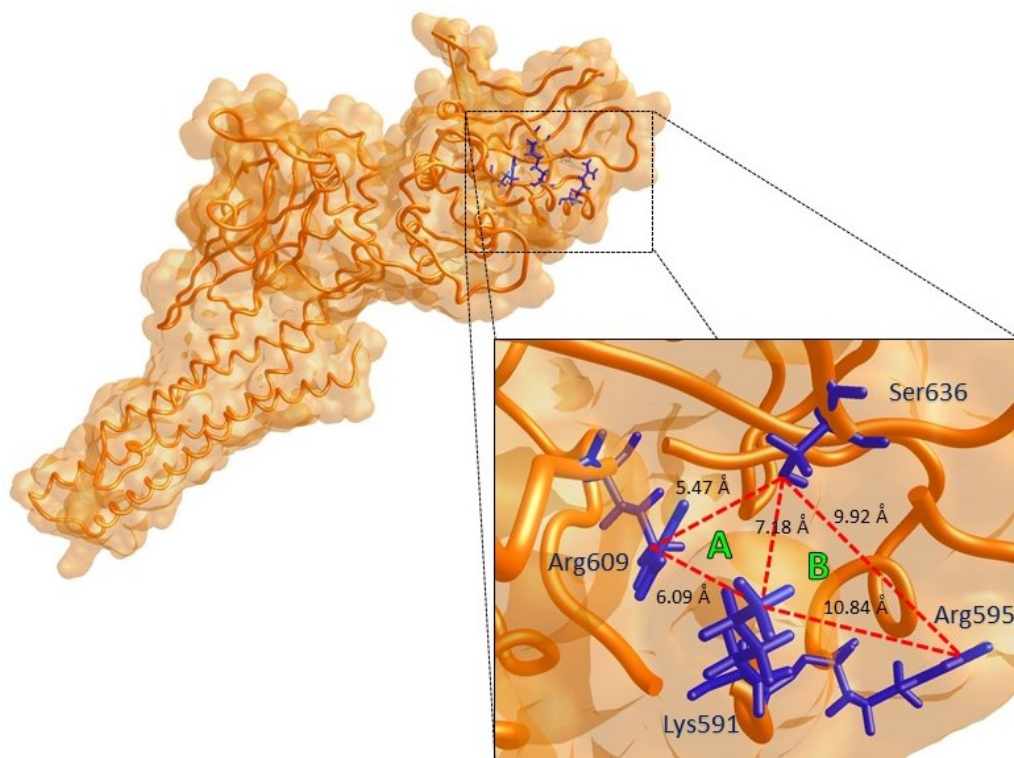


Figure 32. Subpockets A and B.

The analysis of the different scaffolds, supported by their proposed binding poses, highlighted that all the selected compounds interacted mainly with subpocket A. Therefore, I focused my attention on the pTyr-mimetic fragments, such as 4-phosphonodifluoromethyl-cinnamate^[20, 21], arylsulfonamide^[22], 4-amino and 4-hydroxyl salicylic acid^[23], the catechol structure^[24] or the purine scaffold^[25] (**Figure 33a**). Each fragment

was docked in a region of 12 Å around the Arg609, using PLANTS software (*ChemPLP* scoring function, *speed1* as exhaustiveness of docking search, 10 poses for each docked ligand).

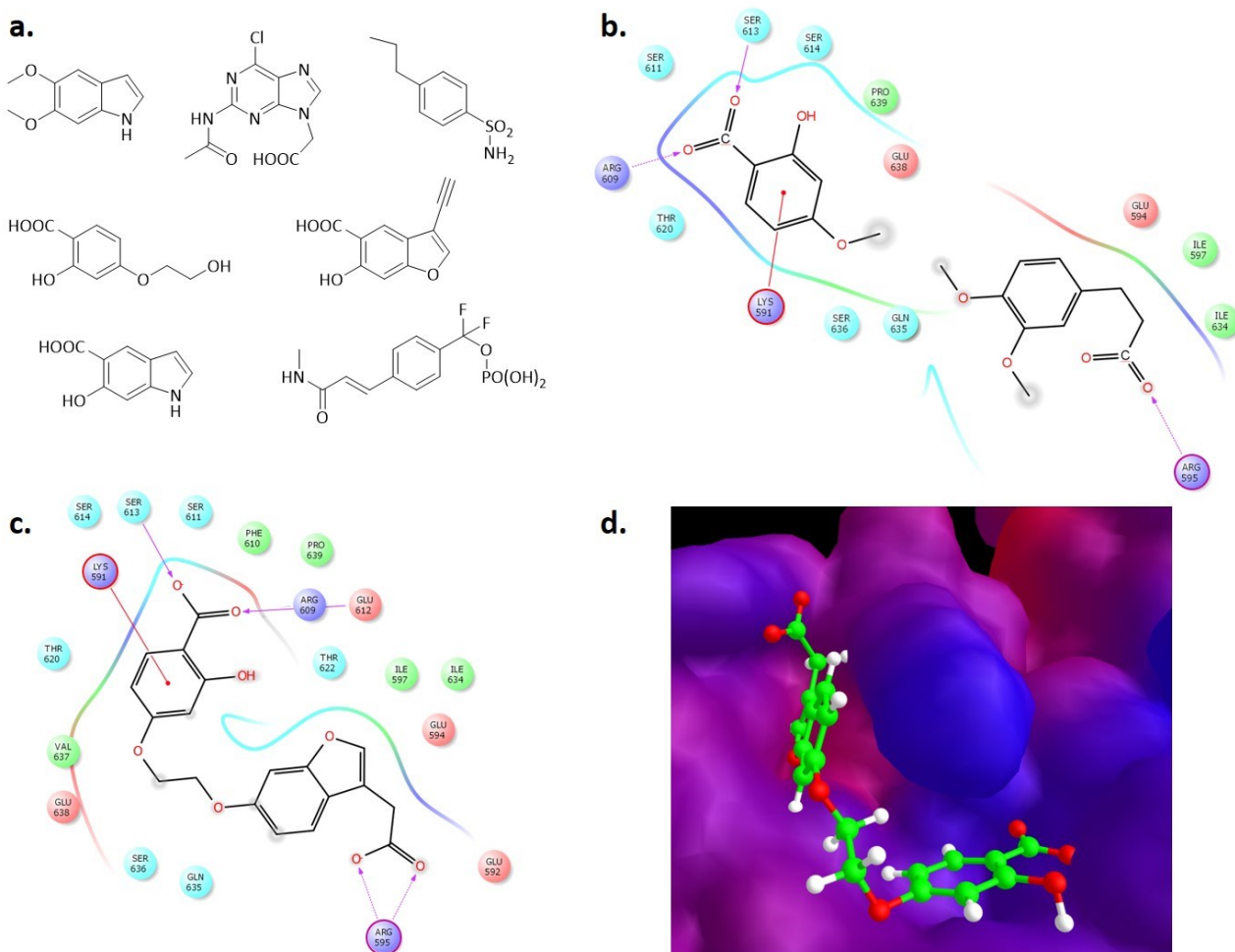


Figure 33. a. Some examples of pTyr-mimetic fragments; b. Example of multiple ligand simultaneous docking of two fragments; c. and d. Docking pose of one of the most interesting linked compounds.

I analyzed the ligand efficiency, calculated as ratio between *ChemPLP* docking score and the number of heavy atoms, and the different possible poses by visual inspection. This kind of analysis was required because in some cases different poses of the same ligand don't have significant differences in ligand efficiency values but involve pockets lined by a different set of aminoacids.

Afterwards, I considered region B with the aim to capitalize the interaction with Lys591 and Arg595, applying multiple ligand simultaneous docking of multiple fragments (**Figure 33b**) in a concerted way to A and B binding hot spots. Hence, I obtained *virtual template compounds* by linking docked fragments of these two groups using various chemical tethers such as amide, amine, ether and ester. The purpose was to investigate how various linkers could:

- influence the flexibility of the scaffold (and if fragments maintained their poses in the binding sites);
- enhance binding affinity;
- modulate biophysical features such as water solubility.

The linked compounds were finally docked (**Figure 33c,d**), ranked by binding energies and binding modes, and their drug properties were calculated.

Considering that the best *virtual template compounds* were strictly related to substructures already reported in the literature as STAT3 inhibitors, these docking calculations were not useful to identify new chemical scaffolds. However, this result was not a failure, it proved that the computational protocol could be used to build up scaffolds with potential activity on STAT3. Therefore, I decided to apply the same strategy on a different base set of fragments (**Figure 34**).

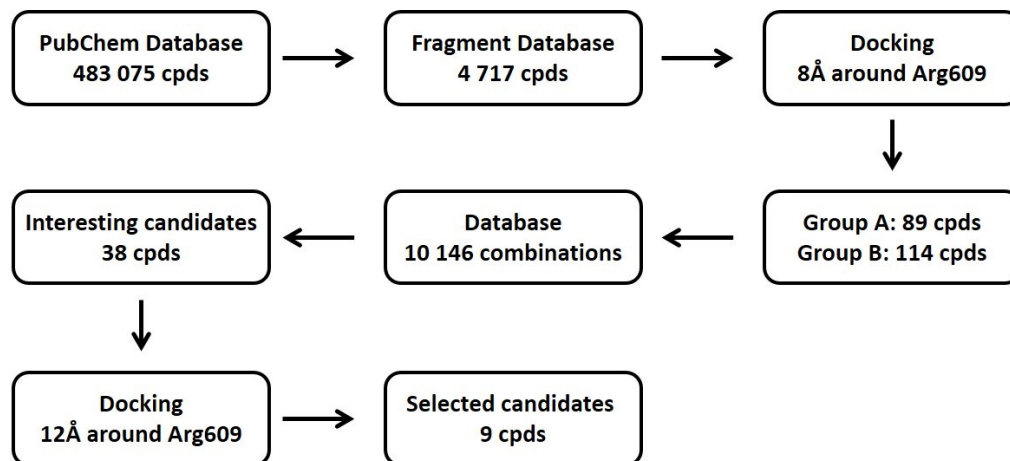


Figure 34. Flowchart showing the main steps of the docking studies involving the fragments selected from PubChem collection.

PubChem compounds were filtered considering various characteristics such as molecular weight ($80 < MW < 200$), XLogP (less than 2), number of hydrogen bond donors and hydrogen bond acceptors ($HBD + HBA > 0$). In this way, a smaller pool of fragments (4717 cpds) was identified and docked by PLANTS (CHEMPLP scoring function) in a region of 8 Å around Arg609, generating 10 poses for each one. The results were ranked according to the ligand efficiency (energy barrier -7.5 Kcal/mol) and divided into two groups, considering the region of interaction. This last division was performed considering the barycenter of each fragment:

- Group A (641 fragments): the barycenter was far from the barycenter of region A (Arg609 - Ser 636 - Lys 591) less than 6 Å;
- Group B (370 fragments): the barycenter was far from the barycenter of region B (Arg595 - Ser 636 - Lys 591) less than 9 Å but more than 6 Å from the barycenter of region A.

Therefore, 89 fragment from group A and 114 from group B were selected by visual inspection considering their structural characteristics, stability and synthesizability.

Due to the low molecular weight, each fragment weakly binds the biological target, but their combination could result in higher ligand efficiency.

Hence, I could choose two different strategies for their heterogeneous merging (at least two of these fragments, one for each region of interaction):

- linking through various chemical tethers such as amide, amine, ether and ester;
- searching through structures reported in literature or commercially available.

Following the first approach, the advantage would have been the possibility to investigate how various linkers could:

- influence the flexibility of the scaffold;
- arrange fragments in the binding sites;
- enhance binding affinity;
- modulate biophysical properties such as water solubility.

The disadvantage would have been the need to build up new synthetic strategies for each compound. For this reason, I firstly decided to perform the second approach in order to capitalize cost and time.

The interaction energy with STAT3 of all the possible combinations (10 146) of one fragment from group A and one from group B were recalculated using different scoring functions such as Van der Waals energy based on CHARMM 22 force field, distance-dependent electrostatic energy according to Coulomb's equation (ElectDD), hydrophilic/hydrophobic complementarity (MLP_{inS} = Molecular Lipophilic Potential Interaction Score), and ChemPLP ligand efficiency as implemented in PLANTS software. All these scores were also combined as consensus in order to build a new ranked list of scaffolds taking into account the scores all together. Considering the first 3 000 combinations of this list and applying <-16.9 Kcal/mol as energetic threshold, the best 734 couples were chosen. Their structures were delivered in cluster groups and the most representative fragments of each cluster underwent a literature search which pointed out 38 molecules.

They were docked in a region of 12 Å around Arg609 and the best poses were selected according to the ligand efficiency (<-3.5 Kcal/mol) and the right orientation in the SH2 domain (it had to interact with both the regions) to give 9 candidates (**Figure 35**). The synthesized compounds (**19-24**) and the commercially available ones (**25-27**) were evaluated by *in vitro* binding assay (AlphaScreen-based assay).

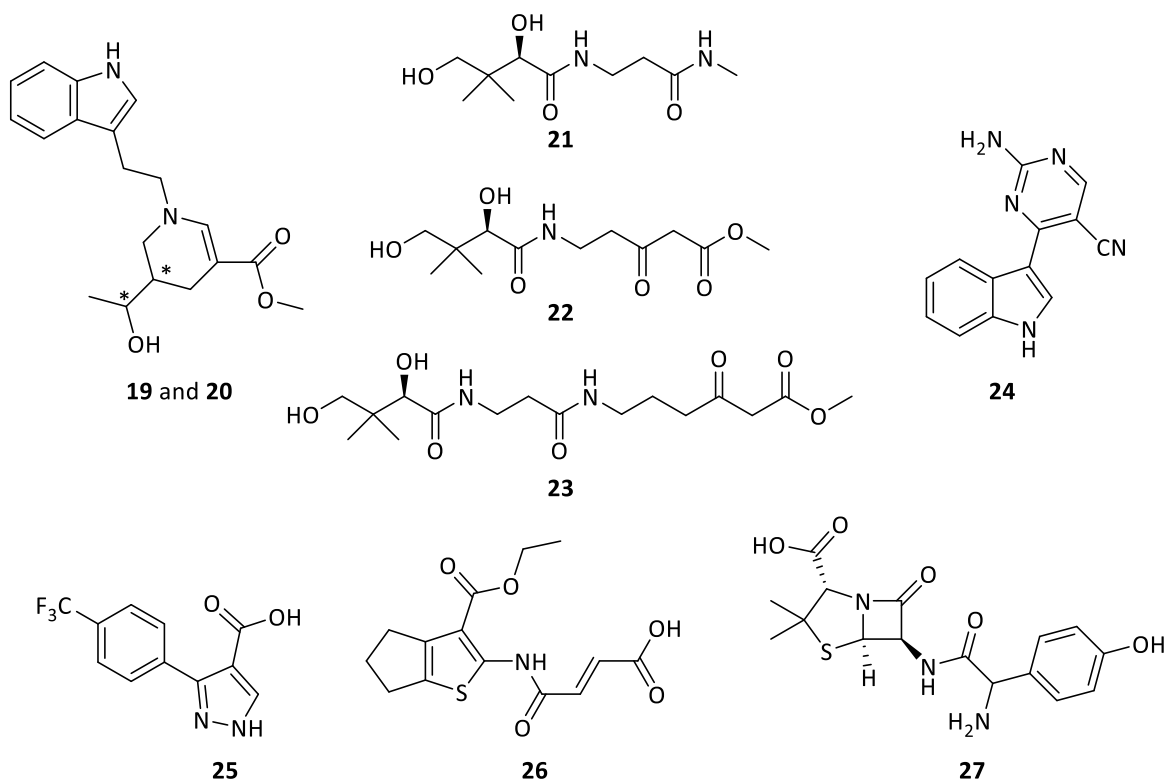
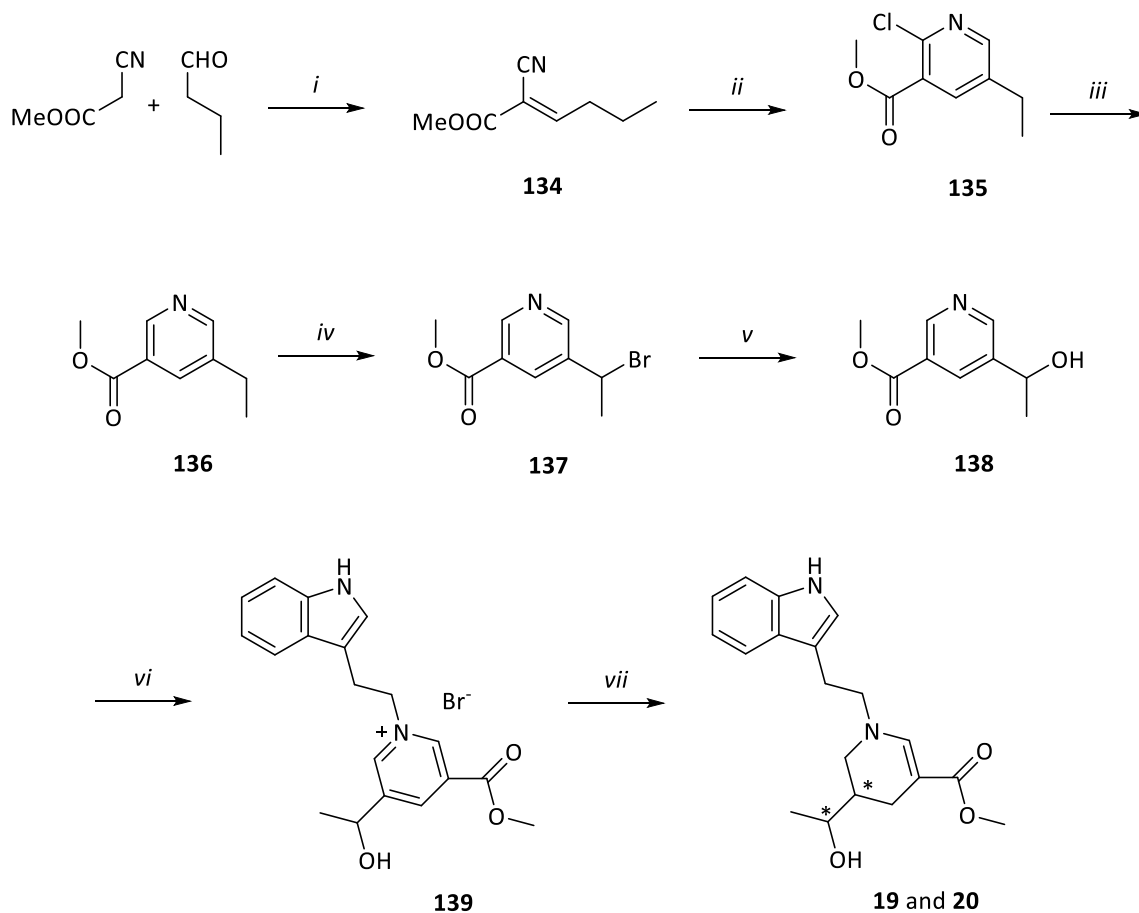


Figure 35. Synthesized (**19-24**) and commercially available (**25-27**) compounds.

5.4.2 Synthetic chemistry

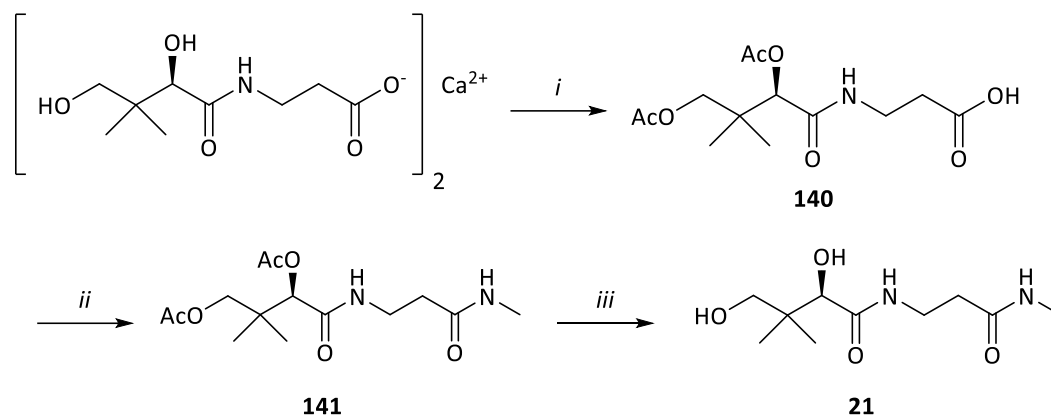
The synthesis of compounds **19** and **20** (**Scheme 13** ^[130,131]) started from a Knoevenagel condensation between methyl cyanoacetate and butanal in acetic acid and piperidine. Intermediate **134** underwent an intramolecular cyclization by treatment with phosphoryl chloride (**135**), followed by a palladium catalyzed hydrogenation in order to remove the chlorine atom leading to compound **136**. The bromination of the side chain, using *N*-bromosuccinimide in presence of benzoyl peroxide, and its nucleophilic substitution with a hydroxyl group led to intermediate **138**. Finally, its treatment with 3-(2-bromoethyl)-indole gave the corresponding quaternary ammonium salt (**139**) which underwent a palladium catalyzed hydrogenation affording the tetrahydropyridine compounds (**19** and **20**), whose pairs of diastereoisomers were separated.



Scheme 13. Reagents and conditions: *i*) piperidine, AcOH, 24h, rt; *ii*) a. POCl₃, dry DMF, 2h, 0°C to 80°C; b. H₂O, 12h, rt; *iii*) H₂, Pd/C, NaOAc, MeOH, 20h, rt; *iv*) NBS, benzoyl peroxide, CCl₄, 3h, reflux; *v*) H₂O/acetone (10:4), 20h, reflux; *vi*) 3-(2-bromoethyl)-indole, MeOH, 90 min, reflux; *vii*) H₂, Pd/C, Et₃N, MeOH, rt, 16h.

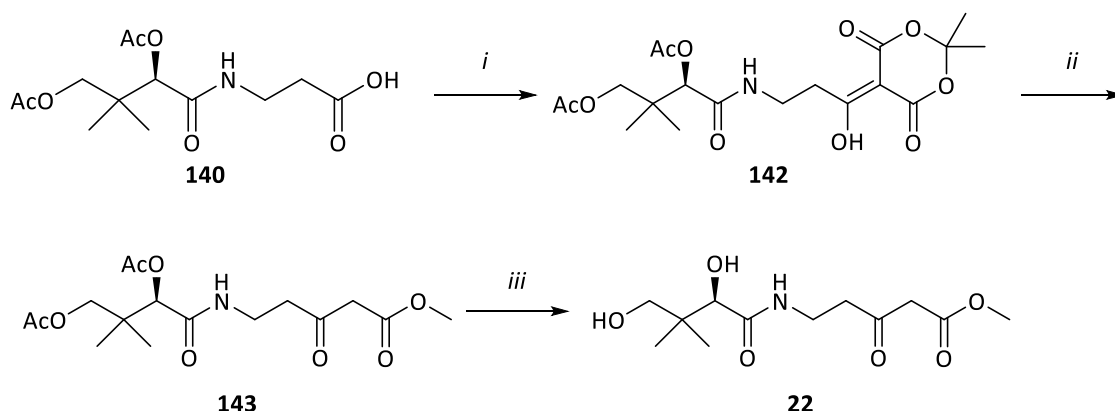
Compounds **21-23** were synthesized according to a slightly modified literature procedure ^[132] as shown in **Scheme 14-16**, respectively.

D-pantothenic acid calcium salt was firstly protected by acylation in presence of acetic anhydride and then the anhydride moiety was selectively hydrolyzed to give intermediate **140**. Its coupling with methylamine (**141**) and a subsequent cold basic treatment led to the final compound **21** (**Scheme 14**).



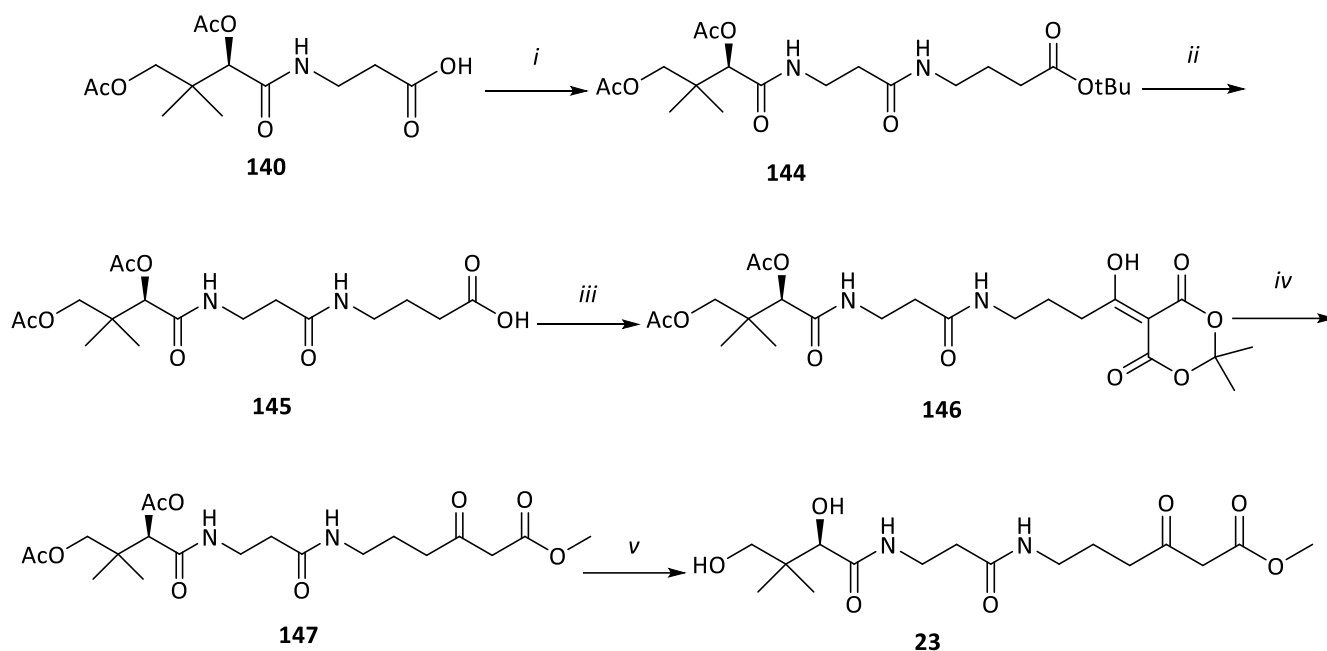
Scheme 14. Reagents and conditions: *i*) Ac_2O , I_2 , 2h at 0°C and then 18h at rt; b. $\text{H}_2\text{O}/\text{THF}$ (2:1), 16h, rt; *ii*) a. CH_3NH_2 , HOBT , Et_3N , dry CH_2Cl_2 , 10 min, 0°C , N_2 ; b. $\text{EDC}\cdot\text{HCl}$, 30 min at 0°C and then 14h at rt; *iii*) K_2CO_3 , dry MeOH , 210 min, 0°C .

For the synthesis of compound **22**, intermediate **140** reacted with Meldrum's acid (2,2-dimethyl-1,3-dioxane-4,6-dione), in presence of 4-dimethylaminopyridine and *N*-(3-dimethylaminopropyl)-*N'*-ethylcarbodiimide hydrochloride, affording the corresponding derivate **142**. The latter was refluxed in methanol (**143**) and deprotected in basic condition resulting in the final methyl β -ketoester **22** (Scheme 15).



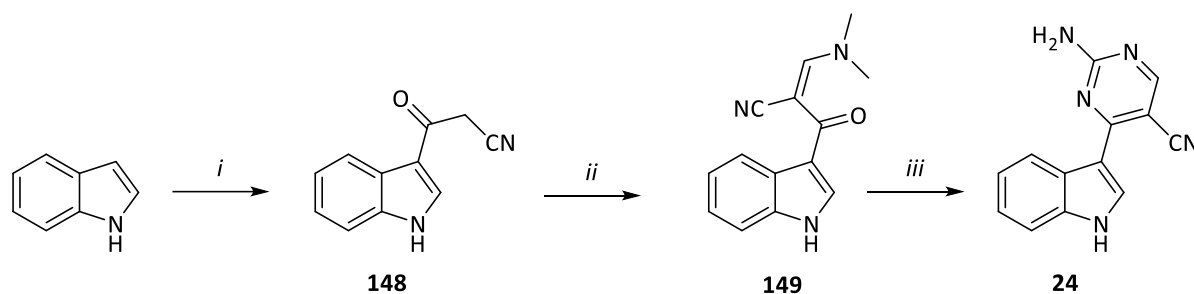
Scheme 15. Reagents and conditions. *i*) a. Meldrum's acid, DMAP , dry CH_2Cl_2 , 10 min, rt, N_2 ; b. $\text{EDC}\cdot\text{HCl}$, 4h, rt; *ii*) dry MeOH , 18h, reflux; *iii*) K_2CO_3 , dry MeOH , 210 min, 0°C .

Methyl 6-(3-(2,4-dihydroxy-3,3-dimethylbutanamido)propanamido)-3-oxohexanoate (**21**) was synthesized starting from intermediate **140** which was coupled with *tert*-butyl- γ -amino butanoate hydrochloride leading to the corresponding amide **144**. The *tert*-butyl group was removed upon treatment with trifluoroacetic acid (**145**) and the reaction with Meldrum's acid afforded the corresponding derivate **146** which was refluxed in methanol to obtain the methyl β -ketoester (**147**). Finally, the cold basic treatment led to the deprotection of the hydroxyl groups resulting in the final compound **23** (Scheme 16).



Scheme 16. Reagents and conditions: *i*) a. *tert*-butyl- γ -aminobutanoate hydrochloride, HOBT, Et₃N, dry CH₂Cl₂, 10 min, 0°C, N₂; b. EDC·HCl, 30 min at 0°C and then 14h at rt; *ii*) TFA, dry CH₂Cl₂, 4h, rt; *iii*) a. Meldrum's acid, DMAP, dry CH₂Cl₂, 10 min, rt, N₂; b. EDC·HCl, 4h, rt; *iv*) dry MeOH, 18h, reflux; *v*) K₂CO₃, dry MeOH, 210 min, 0°C.

For the synthesis of compound **24** (Scheme 17), 3-substituted acylindole **148**, obtained by refluxing cyanoacetic acid with indole in acetic anhydride solution^[133], underwent a microwave-assisted condensation with *N,N*-dimethylformamide dimethyl acetal leading to the α,β -unsaturated- α -cyanoketone (**149**) whose cyclization in presence of guanidine hydrochloride and sodium ethoxide^[134] afforded the pyrimidine nucleus formation (**24**).



Scheme 17. Reagents and conditions: *i*) cyanoacetic acid, Ac₂O, 30 min, reflux; *ii*) *N,N*-dimethylformamide dimethyl acetal, toluene, 45 min, 120°C, mw; *iii*) guanidine hydrochloride, NaOEt, EtOH, 40 min, 120°C, mw.

5.4.3 AlphaScreen-based assay

Thanks to a collaboration with Prof. A. Asai (University of Shizuoka, Japan), the effect of compounds **19-27** on STAT3 dimerization was evaluated by using the AlphaScreen-based assay (**Table 7**).

| | AlphaScreen (IC ₅₀ , μM) |
|-----------|-------------------------------------|
| | <u>STAT3</u> |
| 19 | >100 |
| 20 | >100 |
| 21 | >100 |
| 22 | >100 |
| 23 | >100 |
| 24 | >100 |
| 25 | >100 |
| 26 | 26.3 ± 4.95 |
| 27 | >100 |

Table 7. AlphaScreen-based Assay results. The ability to disrupt the binding of STAT3 to the cognate pTyr-peptide (5-carboxyfluorescein (FITC)-GpYLPQTV) is expressed as IC₅₀.

5.5 Conclusions and perspectives

In this section, I employed computationally driven drug design and investigated new chemical scaffolds able to disrupt STAT3 dimerization. The computational protocol was firstly validated and then applied on a larger base set of fragments leading to nine drug candidates. The synthesized compounds and the commercial ones were evaluated by an *in vitro* binding assay to determine their affinity for the target and compound **26** displayed an interesting activity in inhibiting STAT3-PPI (IC₅₀ value of 26.3 ± 4.95 μM).

Therefore, considering these results, the next step of this study will concern a deeper literature search on the active compound aimed at:

- evaluating known properties, both from a chemical and biological point of view;
- a further optimization of the synthetic plan;
- investigating the presence of analogues already characterized;
- considering intellectual property implication and action potential.

According to these data, SAR studies on compound **26** will be performed.

Chapter 6

Outcomes

Thanks to the available national and international collaborations network, I had the chance to develop my PhD project through a multidisciplinary approach.

Since the selectivity for cancer cells is one of the most important characteristics of anticancer agents, my efforts were mainly pointed to the discovery of molecularly targeted potential chemotherapeutic agents.

In order to achieve this goal, I employed different combined synthetic-computational methods.

On the one hand, a computationally driven drug design approach allowed me to identify nine potential STAT3 inhibitors, which were synthesized and tested. This led to the identification of a new chemical entity which could be the starting point for further optimization.

On the other hand, working on **MD77** and a wild pool of its derivatives, I started the search for their potential target using Cresset Forge as software. The preliminary data suggested the main structural-activity relationships along this series of compounds which will be useful for designing new molecules. In addition, the obtained disparity matrix might shed light on the search of the potential target.

Moreover, considering that cancer is a multifactorial disease, often caused by mutation or loss of several genes, whose treatment is highly restricted by the appearance of resistance, I followed a multitarget strategy, which could result in better therapeutic effects. In particular, I focused my attention on DNA, STAT3 and NF- κ B, considering their well-documented involvement in oncogenesis.

In light of the above, besides several STAT3 and NF- κ B inhibitors, I identified platinum(II) complexes, endowed with the 1,2,5-oxadiazole scaffold and a dual mechanism of action, e.g. inhibition of DNA replication and STAT3 signaling pathway. Preliminary *in vivo* studies showed that they possessed an activity similar to cisplatin but a better tolerance.

In conclusion, my PhD project supported the potentiality of a multitarget approach and paved the way to further investigation on structural-activity relationships and molecular mechanisms of several interesting compounds, herein described.

Chapter 7

Experimental Part: Chemistry

Materials and methods

Reagents and solvents were purchased from Sigma-Aldrich and used without further purification. Some reactions involving air-sensitive reagents were performed under nitrogen atmosphere and anhydrous solvents were used when necessary. Reactions were monitored by thin layer chromatography analysis on aluminum-backed Silica Gel 60 plates (70-230 mesh, Merck), using an ultraviolet fluorescent lamp at 254 nm and 365 nm. Visualization was aided by opportune staining reagents. Purification of intermediates and the final compounds was performed by flash chromatography using Geduran® Si 60 (40-63 µm, Merck). The Biotage Initiator microwave synthesizer was used.

Physical measurements

¹H and ¹³C NMR spectra were recorded in CDCl₃, CD₃OD, acetone-d₆, DMSO-d₆ or DMF-d₇ on Bruker DRX Avance 300 MHz or on a Varian 300 MHz Oxford equipped with a non-reverse probe at 25° C. Chemical shifts are expressed as δ (ppm). Multiplicity is reported as *s* (singlet), *br s* (broad singlet), *d* (doublet), *t* (triplet), *q* (quartet), *m* (multiplet), *dd* (doublet of doublets), *dt* (doublet of triplets). The coupling constants (J-values) are given in Hertz (Hz). All spectroscopic data match the assigned structures. Melting points were determined in open capillary tubes on a Büchi Melting Point B-540. FTIR spectra were collected by using a Perkin Elmer (MA, USA) FTIR Spectrometer "Spectrum One" in a spectral region between 4000 and 450 cm⁻¹ and analyzed by transmittance technique with 32 scans and 4 cm⁻¹ resolution. ESI-MS analyses were performed by using a Thermo Finnigan (MA, USA) LCQ Advantage system MS spectrometer with an electrospray ionization source and an 'Ion Trap' mass analyzer. The MS spectra were obtained by direct infusion of a sample solution in MeOH under ionization, ESI positive. Log *P_{ow}*'s values and purity were evaluated with Partisil C18-ODS reversed-phase HPLC column with Merck-Hitachi L-7100 equipped with Detector UV6000LP. Elemental analyses were performed using a Perkin Elmer SeriesII/CHNS/O 2400 Analyzer. ICP-MS data were recorded with BRUKER Aurora M90 ICP-MS (MA, USA).

Crystallization, data collection and structural determination

The crystals of **1ag** and **1da** were obtained by crystallization from methanol as colorless prisms, while single crystals of **Pt-13** were obtained as small yellow needles by slow evaporation of a solution 33% w/V in MeOH at room temperature. Crystals of **1ag** were mounted on an Enraf-Nonius CAD-4 diffractometer, while those of **1da** and **Pt-13** on a Bruker-Axs CCD-based three circle diffractometer, both working at ambient temperature with graphite-monochromatized using MoKa (λ=0.71073 Å) radiation.

The structures were solved by direct methods (*SIR-97*^[135]) and completed by iterative cycles of full-matrix least squares refinement on *F_o²* using the *SHELXL-97*^[136] program (*WinGX* suite).^[84] All non-H-atoms were refined anisotropically. The H-atoms positions were introduced in calculated positions in their described geometries and allowed to ride on the attached carbon atom with fixed isotropic thermal parameters.

Geometrical calculations were carried out with the program PARST.^[137] CCDC-1496339 (**1ag**), CCDC-1496338 (**1da**) and CCDC-1478539 (**Pt-13**) contains the supplementary crystallographic data. These data can be obtained free of charge via www.ccdc.cam.ac.uk/conts/retrieving.html (or from the Cambridge Crystallographic Data Centre, 12, Union Road, Cambridge CB21EZ, UK; fax: ++44 1223 336 033; or deposit@ccdc.cam.ac.uk).

Crystal data 1ag: C₁₆ H₁₀ F₃ N₃ O₂, *M_r* = 333.27 g/mol, orthorhombic, Space group *Pbc21* *a* = 4.982 (2) Å, *b* = 14.446 (3) Å, *c* = 20.630 (5) Å, *V* = 1484.6 (8) Å³, *Z* = 4, *D_{calc}* = 1.491 Mg/m³, *F*(000) = 680, *R* = 0.0985 (reflections collected = 1163), *wR2* = 0.229, *T* = 293(2) K, *GOF* = 1.219. The reflections were collected in the range 2.82° ≤ θ ≤ 25.97° (limiting indices = -1 ≤ *h* ≤ 6, -1 ≤ *k* ≤ 17, -1 ≤ *l* ≤ 25) employing a 0.65 x 0.52 x 0.42 mm³ crystal. The residual positive and negative electron densities in the final map were 0.386 and -0.244 eÅ⁻³.

Crystal data 1da: C₁₅ H₁₀ Cl N₃ O₂, $M_r = 299.71$ g/mol, orthorhombic, Space group *Pbc21* $a = 13.768$ (3) Å, $b = 5.074$ (2) Å, $c = 19.460$ (3) Å, $V = 1382.5$ (5) Å³, $Z = 4$, $D_{calc} = 1.44$ Mg/m³, $F(000) = 616$, $R = 0.028$ (reflections collected = 10460), $wR2 = 0.059$, $T = 293$ (2) K, $GOF = 0.929$. The reflections were collected in the range $2.08^\circ \leq \theta \leq 27.12^\circ$ (limiting indices = $-17 \leq h \leq 17$, $-6 \leq k \leq 6$, $-25 \leq l \leq 25$) employing a $0.55 \times 0.22 \times 0.02$ mm³ crystal. The residual positive and negative electron densities in the final map were 0.129 and -0.159 eÅ⁻³.

Crystal data Pt-13: C₄ H₇ O₁ Pt₁ Cl₂ N₃, $M_r = 379.01$ g/mol, trigonal, Space group *R-3* $a = 39.836$ (2) Å, $c = 6.724$ (3) Å, $V = 9240.8$ (5) Å³, $Z = 12$, $D_{calc} = 2.439$ Mg/m³, $F(000) = 6120$, $R = 0.026$ (reflections collected/unique = 3614/3228), $wR2 = 0.031$, $T = 293$ (2) K, $GOF = 1.057$. The reflections were collected in the range $1.02^\circ \leq \theta \leq 25.03^\circ$ (limiting indices = $-47 \leq h \leq 47$, $-47 \leq k \leq 47$, $-8 \leq l \leq 7$) employing a $0.01 \times 0.02 \times 0.01$ mm³ crystal. The residual positive and negative electron densities in the final map were 0.950 and -0.540 eÅ⁻³.

Stability test

The stability study of complexes (**Pt-13**, **Pt-14** and **Pt-15b**) was performed under physiological conditions through UV-vis spectroscopy at their respective λ_{max} . Stock solutions were diluted to a final concentration of 100 μM with 1 % DMF. The UV-vis peak profile of the sample was monitored for 48 hours at 4 hour intervals.

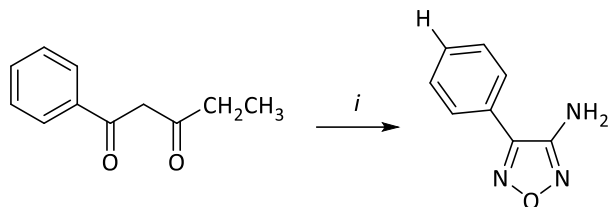
Log P_{ow} determination

RP-HPLC analysis were performed to correlate the hydrophobicity of the compounds and the platinum(II) complexes with their retention time. The chromatograms were registered using Partisil C18-ODS reversed-phase HPLC column at 25°C and water/acetonitrile (60:40) as mobile phase with KI as internal standard (flow rate: 1 mL/min; $\lambda = 230$ nm).

For platinum complexes the same column was used and water (15 mM HCOOH)/MeOH (70:30) mobile phase with KI as internal standard (flow rate of 1 mL/min, $\lambda = 210$ nm).^[96-98,138] The calibration curve was realized in comparison with reference compounds chosen in OECD guideline.^[139]

General procedures for the synthesis of 4-phenyl-1,2,5-oxadiazol-3-amines (105a-d,g-j,l,r)

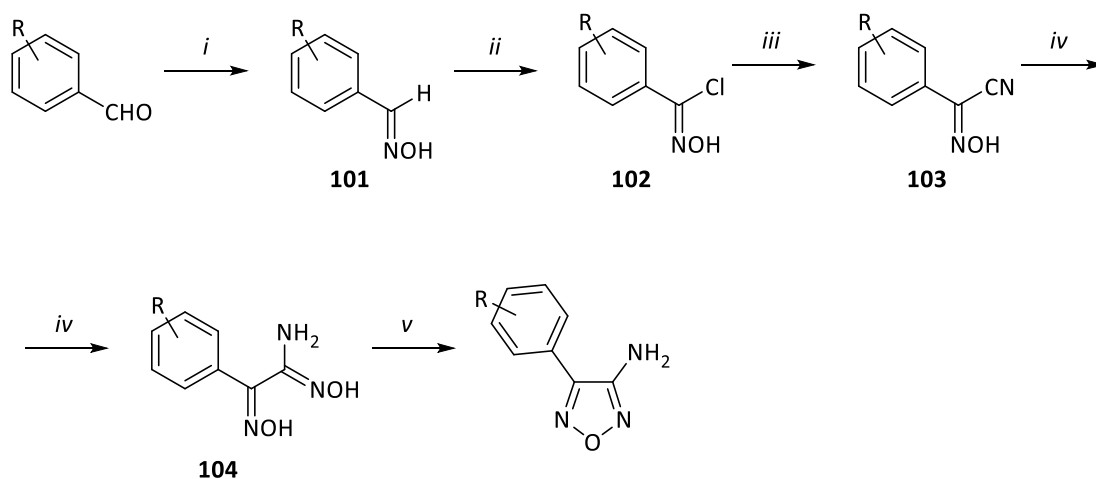
Procedure a



Reagents and conditions: *i*) a. NaOH, 12h, 0° C; b. NaNO₂, 20% HClO₄, 14h, rt; c. NH₂OH · HCl, NaOH, 2h, reflux; d. urea, 3h, reflux.

A one-pot reaction ^[63] on ethyl benzoylacetate afforded 4-phenyl-1,2,5-oxadiazol-3-amine, **105a** intermediate.

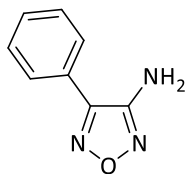
Procedure b



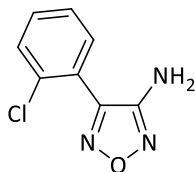
- 105b** R = *o*-Cl
- 105c** R = *m*-Cl
- 105d** R = *p*-Cl
- 105g** R = *p*-CF₃
- 105h** R = *p*-Br
- 105i** R = *p*-CH₃
- 105j** R = *p*-Ph
- 105l** R = *p*-OBn
- 105r** R = *p*-NO₂

Reagents and conditions: *i*) NH₂OH · HCl, NaHCO₃, MeOH, 2h, reflux; *ii*) NCS, DMF, 12h, rt; *iii*) KCN, Et₂O/H₂O, 5h, rt; *iv*) NH₂OH · HCl, NaHCO₃, MeOH, 12h, reflux; *v*) 2N NaOH, 12h, reflux.

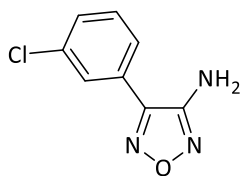
The key intermediates **105b-d,g-j,l** and **105r** were obtained according to a literature method ^[59] starting from the appropriate benzaldehyde.

4-phenyl-1,2,5-oxadiazol-3-amine (105a)

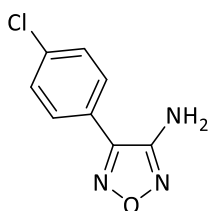
Procedure a: yield 34 % as white solid (m.p. 99.5-100.5°C). TLC: petroleum ether/ethyl acetate (7:3) - R_f : 0.45. Purified by flash chromatography (eluent: petroleum ether/ethyl acetate (7:3)). Molecular formula: $C_8H_7N_3O$. Molecular weight: 161.16 g/mol. 1H NMR (300 MHz, $CDCl_3$): δ 7.70-7.81 (m, 2H, ArH), 7.51-7.59 (m, 3H, ArH), 4.20 (br s, 2H, NH_2 exchanged with D_2O) ppm. ^{13}C NMR (75 MHz, $CDCl_3$): δ 154.30, 146.94, 130.58, 129.42, 127.57, 125.49 ppm.

4-(2-chlorophenyl)-1,2,5-oxadiazol-3-amine (105b)

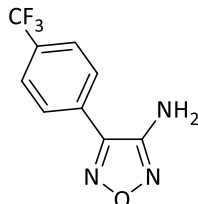
Procedure b: yield 60 % (starting from 15 mmol of 2-chlorobenzaldehyde, 9 mmol of **105b** were obtained) as light yellow solid (m.p. 59.1-59.7°C). TLC: petroleum ether/ethyl acetate (8:2) - R_f : 0.18. Molecular formula: $C_8H_6ClN_3O$. Molecular weight: 195.61 g/mol. 1H NMR (300 MHz, $CDCl_3$): δ 7.33-7.57 (m, 4H, ArH), 4.22 (br s, 2H, NH_2 exchanged with D_2O) ppm. ^{13}C NMR (75 MHz, $CDCl_3$): δ 154.99, 146.46, 133.48, 132.29, 132.22, 130.54, 127.77, 124.78 ppm.

4-(3-chlorophenyl)-1,2,5-oxadiazol-3-amine (105c)

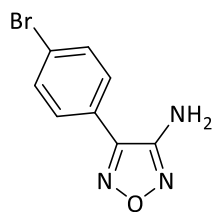
Procedure b: yield 41 % (starting from 15 mmol of 3-chlorobenzaldehyde, 6.15 mmol of **105c** were obtained) as light yellow solid (m.p. 132.6-132.9°C). TLC: petroleum ether/ethyl acetate (7:3) - R_f : 0.48. Molecular formula: $C_8H_6ClN_3O$. Molecular weight: 195.61 g/mol. 1H NMR (300 MHz, $CDCl_3$): δ 7.74 (t, J = 1.6 Hz, 1H, ArH), 7.63 (dt, J_1 = 1.6 Hz, J_2 = 6.9 Hz, 1H, ArH), 7.45-7.54 (m, 2H, ArH), 4.22 (br s, 2H, NH_2 exchanged with D_2O) ppm. ^{13}C NMR (75 MHz, acetone- d_6): δ 155.41, 146.24, 134.74, 131.12, 130.44, 128.36, 127.74, 126.55 ppm.

4-(4-chlorophenyl)-1,2,5-oxadiazol-3-amine (105d)

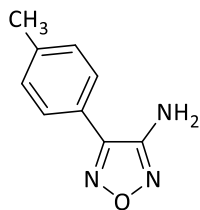
Procedure b: yield 19 % (starting from 15 mmol of 4-chlorobenzaldehyde, 2.85 mmol of **105d** were obtained) as white solid (m.p. 140.3-143.8°C). TLC: petroleum ether/ethyl acetate (7:3) - R_f : 0.59. Molecular formula: $C_8H_6ClN_3O$. Molecular weight: 195.61 g/mol. 1H NMR (300 MHz, $CDCl_3$): δ 7.69 (d, J = 8.1 Hz, 2H, ArH), 7.52 (d, J = 8.1 Hz, 2H, ArH), 4.21 (br s, 2H, NH_2 exchanged with D_2O) ppm. ^{13}C NMR (75 MHz, acetone- d_6): δ 155.10, 146.20, 135.77, 129.44, 129.31, 124.95 ppm.

4-(4-trifluoromethyl)-1,2,5-oxadiazol-3-amine (105g)

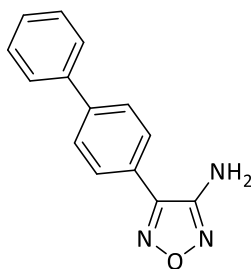
Procedure b: yield 25 % (starting from 15 mmol of 4-trifluoromethylbenzaldehyde, 3.75 mmol of **105g** were obtained) as light brown solid (m.p. 107.2-109.3°C). TLC: cyclohexane/ethyl acetate (8:2) - R_f : 0.30. Molecular formula: $C_9H_6F_3N_3O$. Molecular weight: 229.16 g/mol. 1H NMR (300 MHz, acetone- d_6): δ 8.04 (d, J = 8.7 Hz, 2H, ArH), 7.91 (d, J = 8.7 Hz, 2H, ArH), 5.74 (s, 2H, NH_2 exchanged with D_2O) ppm. ^{13}C NMR (75 MHz, acetone- d_6): δ 155.27, 146.11, 131.53, 130.18, 128.58, 125.97 (q, J = 2.9 Hz), 122.28 ppm. ^{19}F NMR (282 MHz, acetone- d_6): δ 63.47 (s, CF_3) ppm.

4-(4-bromophenyl)-1,2,5-oxadiazol-3-amine (105h)

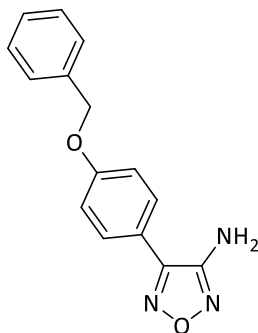
Procedure b: yield 18 % (starting from 15 mmol of 4-bromobenzaldehyde, 2.70 mmol of **105h** were obtained) as light brown solid (m.p. 143.8-144.8°C). TLC: cyclohexane/ethyl acetate (8:2) - R_f: 0.53. Molecular formula: C₈H₆BrN₃O. Molecular weight: 240.06 g/mol. ¹H NMR (300 MHz, CDCl₃): δ 7.68 (d, J = 8.3 Hz, 2H, ArH), 7.62 (d, J = 8.3 Hz, 2H, ArH), 4.20 (br s, 2H, NH₂ exchanged with D₂O) ppm. ¹³C NMR (75 MHz, CDCl₃): δ 154.56, 146.70, 135.68, 129.38, 125.89, 125.02 ppm.

4-(4-methylphenyl)-1,2,5-oxadiazol-3-amine (105i)

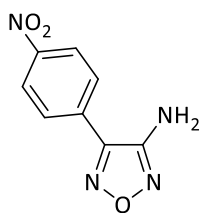
Procedure b: yield 8 % (starting from 15 mmol of 4-methylbenzaldehyde, 1.2 mmol of **105i** were obtained) as white solid (m.p. 126.7-128.5°C). TLC: cyclohexane/ethyl acetate (7:3) - R_f: 0.40. Molecular formula: C₉H₉N₃O. Molecular weight: 175.19 g/mol. ¹H NMR (300 MHz, CDCl₃): δ 7.64 (d, J = 8.2 Hz, 2H, ArH), 7.36 (d, J = 8.2 Hz, 2H, ArH), 4.26 (br s, 2H, NH₂ exchanged with D₂O), 2.38 (s, 3H, CH₃) ppm. ¹³C NMR (75 MHz, CDCl₃): δ 154.31, 146.92, 140.87, 130.09, 127.44, 122.58, 21.44 ppm.

4-(1,1'-biphenyl-4-yl)-1,2,5-oxadiazol-3-amine (105j)

Procedure b: yield 19 % (starting from 15 mmol of 1,1'-biphenyl-4-carbaldehyde, 2.85 mmol of **105j** were obtained) as light yellow solid (m.p. 161.4-161.8°C). TLC: cyclohexane/ethyl acetate (8:2) - R_f: 0.30. Molecular formula: C₁₄H₁₁N₃O. Molecular weight: 237.26 g/mol. ¹H NMR (300 MHz, CDCl₃): δ 7.74-7.84 (m, 4H, ArH), 7.62-7.66 (m, 2H, ArH), 7.38-7.52 (m, 3H, ArH), 4.24 (br s, 2H, NH₂ exchanged with D₂O) ppm. ¹³C NMR (75 MHz, DMSO-d₆): δ 156.09, 147.31, 142.55, 139.79, 129.79, 128.99, 128.77, 128.00, 127.46, 125.25 ppm.

4-(4-benzyloxyphenyl)-1,2,5-oxadiazol-3-amine (105l)

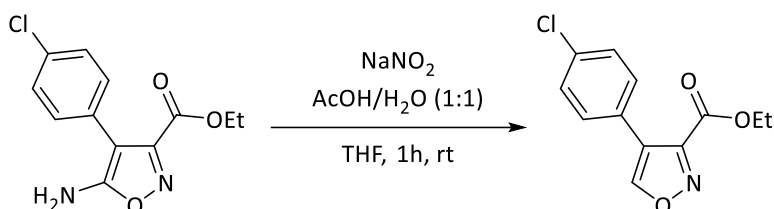
Procedure b: yield 21 % (starting from 15 mmol of 4-benzyloxybenzaldehyde, 3.15 mmol of **105l** were obtained) as white solid (m.p. 144.5-145.5°C). TLC: cyclohexane/ethyl acetate (7:3) - R_f: 0.45. Molecular formula: C₁₅H₁₃N₃O. Molecular weight: 267.29 g/mol. ¹H NMR (300 MHz, CDCl₃): δ 7.66 (d, J = 8.8 Hz, 2H, ArH), 7.32-7.48 (m, 5H, ArH), 7.11 (d, J = 8.8 Hz, 2H, ArH), 5.14 (s, 2H, CH₂), 4.19 (br s, 2H, NH₂ exchanged with D₂O) ppm. ¹³C NMR (75 MHz, CDCl₃): δ 160.67, 154.21, 146.79, 136.49, 129.31, 128.95, 128.47, 127.69, 118.24, 116.01, 70.37 ppm.

4-(4-nitrophenyl)-1,2,5-oxadiazol-3-amine (105r)

Procedure b: yield 12 % (starting from 15 mmol of 4-nitrobenzaldehyde, 1.8 mmol of **105r** were obtained) as brown-red solid (m.p. 135.4-137.6°C). TLC: cyclohexane/ethyl acetate (9:1) - R_f: 0.48. Molecular formula: C₈H₆N₄O₃. Molecular weight: 206.16 g/mol. ¹H NMR (300 MHz, CDCl₃): δ 8.40 (d, J = 8.9 Hz, 2H, ArH), 7.98 (d, J = 8.9 Hz, 2H, ArH), 4.27 (br s, 2H, NH₂ exchanged with D₂O) ppm. ¹³C NMR (75 MHz, acetone-d₆): δ 155.28, 148.87, 145.76, 132.43, 129.09, 124.09 ppm.

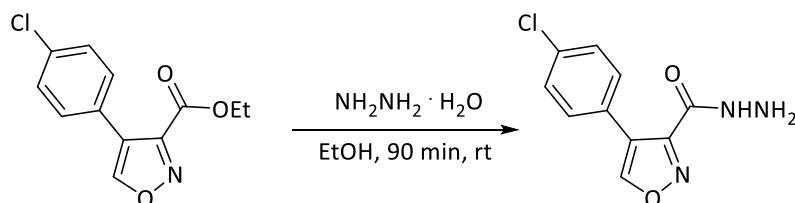
Procedures for the synthesis of 4-(4-chlorophenyl)-3-aminoisoxazole (109)

Synthesis of ethyl 4-(4-chlorophenyl)isoxazole-3-carboxylate (106)

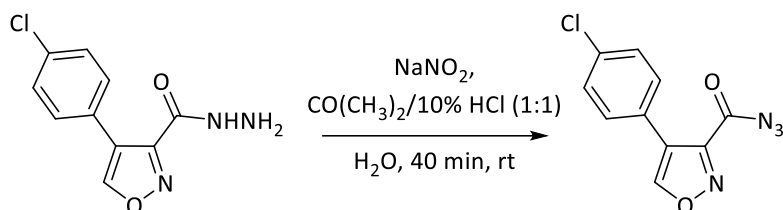


Ethyl 5-amino-4-(4-chlorophenyl)isoxazole-3-carboxylate (0.750 mmol) was dissolved in a mixture of acetic acid (1.5 mL), H₂O (1.5 mL) and THF (2 mL). NaNO₂ (7.5 mmol) was slowly added and the reaction mixture was stirred at room temperature for 1 hour (TLC: petroleum ether/ethyl acetate (95:5) - R_f: 0.26). After evaporating the solvents, the residue was diluted with water and extracted with dichloromethane. The collected organic layers were washed with a saturated aqueous solution of sodium bicarbonate and with water. The organic phase was dried over anhydrous Na₂SO₄, filtered and then concentrated under reduced pressure. The crude product was purified by flash chromatography (eluting with petroleum ether/ethyl acetate from 95:5 to 9:1) to afford compound **106**. Yield 71 % as colorless oil. Molecular formula: C₁₂H₁₀ClNO₃. Molecular weight: 251.67 g/mol. ¹H NMR (300 MHz, acetone-d₆): δ 9.12 (s, 1H, ArH), 7.57 (d, *J* = 8.6 Hz, 2H, ArH), 7.46 (d, *J* = 8.6 Hz, 2H, ArH), 4.38 (q, *J* = 7.1 Hz, 2H, CH₂), 1.30 (t, *J* = 7.1 Hz, 3H, CH₃) ppm.

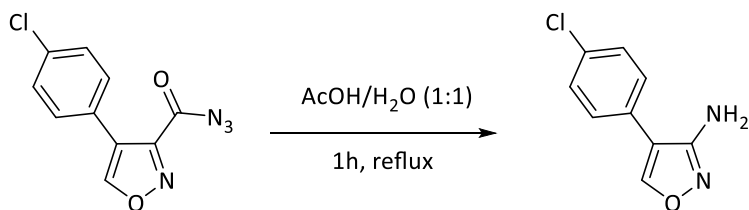
Synthesis of 4-(4-chlorophenyl)-3-hydrazinecarboxylisoxazole (107)



NH₂NH₂ · H₂O (1.596 mmol) was added portion-wise at 0°C to a stirred solution of **106** (0.397 mmol) in ethanol (1.3 mL). The reaction mixture was warmed to 40°C for 90 minutes (TLC: dichloromethane/methanol (95:5) - R_f: 0.45) and then the solvent was evaporated under reduced pressure. The residue was extracted with water and ethyl acetate and the organic layers were collected, dried over anhydrous Na₂SO₄, filtered and concentrated under reduced pressure. The intermediate **107** was used in the next step without any further purification. Yield 85 % as white solid. Molecular formula: C₁₀H₈ClN₃O₂. Molecular weight: 237.64 g/mol. ¹H NMR (300 MHz, acetone-d₆): δ 10.11 (br s, 1H, NH exchanged with D₂O), 9.17 (s, 1H, ArH), 7.65 (d, *J* = 8.6 Hz, 2H, ArH), 7.42 (d, *J* = 8.6 Hz, 2H, ArH), 3.02 (br s, 2H, NH₂ exchanged with D₂O) ppm.

Synthesis of 4-(4-chlorophenyl)-3-acylazideisoxazole (108)

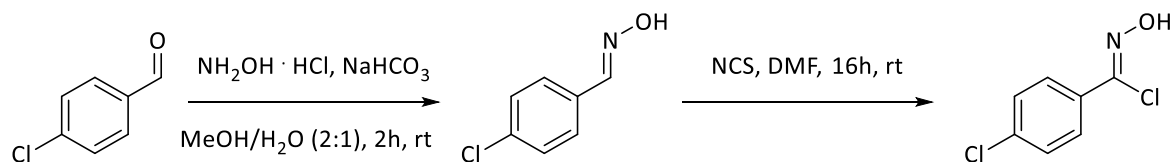
The acyl hydrazine **107** (0.420 mmol) was dissolved in a 1:1 mixture of acetone/10% HCl (1.8 mL). After cooling at 0°C, a solution of NaNO_2 (0.63 mmol) in water (1.8 mL) was added dropwise. The mixture was stirred for 40 minutes at room temperature and then quenched by slowly adding water. The resulting mixture was cooled and filtered obtaining compound **108** which was used without any further purification. Yield 86 % as white solid. Molecular formula: $\text{C}_{10}\text{H}_5\text{ClN}_4\text{O}_2$. Molecular weight: 248.63 g/mol. ^1H NMR (300 MHz, acetone- d_6): δ 9.20 (s, 1H, ArH), 7.61 (d, $J = 8.6$ Hz, 2H, ArH), 7.48 (d, $J = 8.6$ Hz, 2H, ArH) ppm.

Synthesis of 4-(4-chlorophenyl)-3-aminoisoxazole (109)

The acylazide **108** (0.403 mmol) was suspended in a mixture of water/acetic acid (1:1, 6.4 mL) and the reaction was refluxed for 1 hour (TLC: cyclohexane/ethyl acetate (7:3) - R_f : 0.25). Then the solvents were removed under *vacuum* and the residue was extracted with water and ethyl acetate, dried with anhydrous Na_2SO_4 and concentrated under reduced pressure obtaining **109**. Quantitative yield as red foam. Molecular formula: $\text{C}_9\text{H}_7\text{ClN}_2\text{O}$. Molecular weight: 194.62 g/mol. ^1H NMR (300 MHz, acetone- d_6): δ 8.58 (s, 1H, ArH), 7.57 (d, $J = 8.5$ Hz, 2H, ArH), 7.46 (d, $J = 8.5$ Hz, 2H, ArH), 5.10 (br s, 2H, NH_2 exchanged with D_2O) ppm. MS (ESI) m/z 194.9 $[\text{M} + \text{H}]^+$.

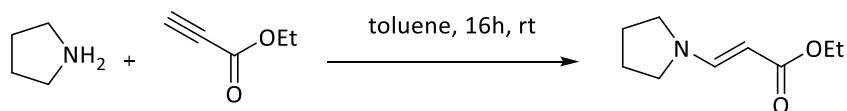
Procedures for the synthesis of 3-(4-chlorophenyl)-4-aminoisoxazole (114)

Synthesis of 4-chlorobenzoylchloride oxime (102d)



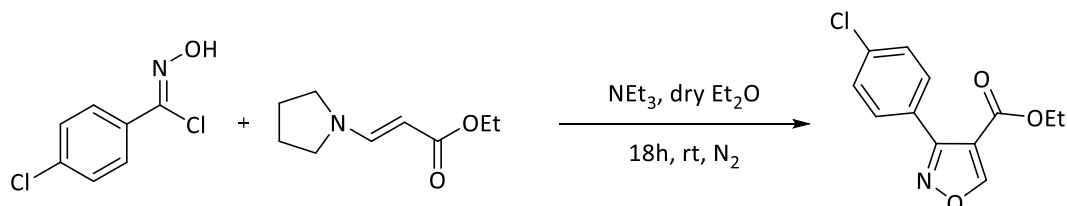
102d, an intermediate in the synthesis of **105d**, was prepared according to literature procedure^[59]: yield 87 % (starting from 10 mmol of 4-chlorobenzaldehyde, 8.7 mmol of **102d** were obtained) as light-yellow solid (m.p. 48-49°C). Molecular formula: C₇H₅Cl₂NO. Molecular weight: 190.03 g/mol. TLC: cyclohexane/ethyl acetate (8:2) - R_f: 0.60. ¹H NMR (300 MHz, CDCl₃): δ 7.74 (d, *J* = 8.7 Hz, 2H), 7.32 (d, *J* = 8.7 Hz, 2H), 2.88 (s, 1H, OH, exchanged with D₂O) ppm. ¹³C NMR (75 MHz, acetone-d₆): δ 135.80, 135.71, 131.87, 128.66, 128.31 ppm.

Synthesis of ethyl (E)-3-pyrrolidin-1-yl acrylate (110)



A solution of pyrrolidine (14.06 mmol) in toluene (2.4 mL) was added dropwise over 10 minutes to a solution of ethyl propiolate (14.06 mmol) in toluene (9.7 mL). The resulting mixture was stirred at room temperature for 16 hours (TLC: cyclohexane/ethyl acetate (9:1) - R_f: 0.11) and then the solvent was evaporated under reduced pressure. The residue was diluted with water and extracted with ethyl acetate. The collected organic layers were dried over Na₂SO₄ and concentrated in *vacuo* to give pure **110**. Quantitative yield as orange oil. Molecular formula: C₉H₁₅NO₂. Molecular weight: 169.22 g/mol. ¹H NMR (300 MHz, CDCl₃): δ 7.65 (d, *J* = 12.9 Hz, 1H, CH), 4.48 (d, *J* = 12.9 Hz, 1H, CH), 4.13 (q, *J* = 7.1 Hz, 2H, CH₂), 3.27 (br s, 4H, CH₂), 1.93 (br s, 4H, CH₂), 1.26 (t, *J* = 7.1, 3H, CH₃) ppm.

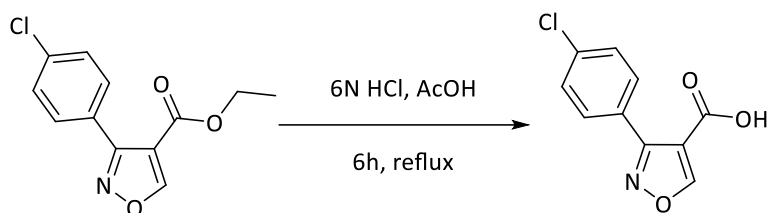
Synthesis of ethyl 3-(4-chlorophenyl)isoxazole-4-carboxylate (111)



To a stirred solution of intermediate **102d** (6.74 mmol) in anhydrous diethyl ether (13.4 mL) and trimethylamine (1.11 mL), a solution of **110** (6.74 mmol) in anhydrous diethyl ether was dripped at 0°C and

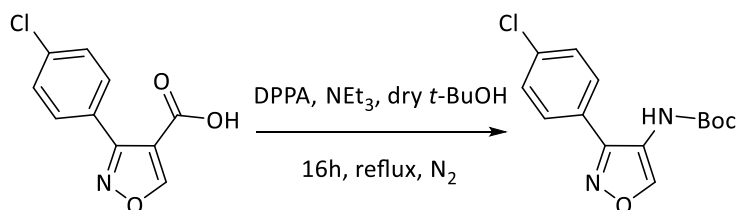
then the resulting mixture was stirred at room temperature for 18 hours under nitrogen atmosphere (TLC: cyclohexane/ethyl acetate (9:1) - R_f : 0.37). The orange suspension was partitioned between water and diethyl ether. The aqueous phase was extracted with further diethyl ether. The organic layers were combined, washed with 1M HCl, dried over anhydrous Na_2SO_4 , filtered and concentrated under reduced pressure. The crude intermediate was purified by flash chromatography on silica gel (eluent: cyclohexane/ethyl acetate 95:5) to afford **111**. Yield 74 % as colorless oil. Molecular formula: $\text{C}_{12}\text{H}_{10}\text{ClNO}_3$. Molecular weight: 251.67 g/mol. ^1H NMR (300 MHz, CDCl_3): δ 8.96 (s, 1H, ArH), 7.70 (d, $J = 8.7$ Hz, 2H, ArH), 7.36 (d, $J = 8.7$ Hz, 2H, ArH), 4.22 (q, $J = 7.5$ Hz, 2H, CH_2), 1.24 (t, $J = 7.5$ Hz, 3H, CH_3) ppm.

Synthesis of 3-(4-chlorophenyl)isoxazole-4-carboxylic acid (**112**)

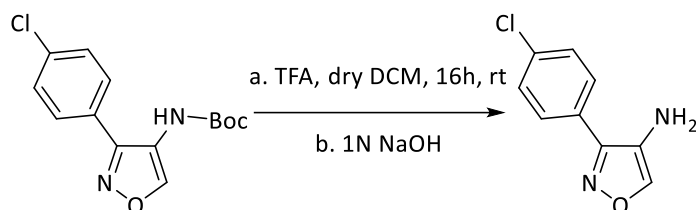


A stirred solution of **111** (5.01 mmol) in acetic acid (21 mL) was treated with 6N HCl (35 mL) at reflux for 6 hours (TLC: dichloromethane/methanol/acetic acid (98:2:0.02) - R_f : 0.25). After cooling, the reaction mixture was extracted with ethyl acetate. The concentrated organic layer was treated with sat. NaHCO_3 and the aqueous solution was separated, cooled and acidified with 6N HCl. Intermediate **112** was extracted with ethyl acetate and the combined organic phases were dried over anhydrous Na_2SO_4 , filtered and concentrated under reduced pressure. Yield 96 % as white solid. Molecular formula: $\text{C}_{10}\text{H}_6\text{ClNO}_3$. Molecular weight: 223.61 g/mol. ^1H NMR (300 MHz, CDCl_3): δ 9.12 (s, 1H, ArH), 7.69 (d, $J = 9$ Hz, 2H, ArH), 7.49 (d, $J = 9$ Hz, 2H, ArH) ppm.

Synthesis of [3-(4-chlorophenyl)isoxazol-4-yl]-carbamic acid *tert*-butyl ester (**113**)



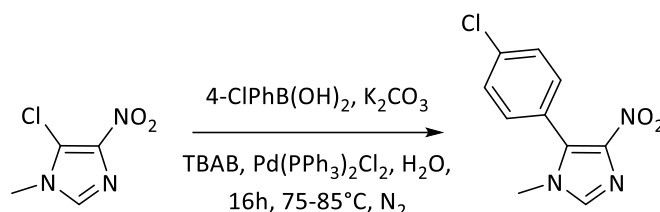
A mixture of **112** (2.94 mmol), diphenylphosphoryl azide (2.94 mmol) and trimethylamine (0.41 mL) in dry *tert*-butanol (4 mL) was refluxed for 16 hours under nitrogen atmosphere (TLC: cyclohexane/ethyl acetate (7:3) - R_f : 0.28). Compound **113** was extracted with ethyl acetate. The combined organic phases were washed with 1M HCl and brine and dried over anhydrous Na_2SO_4 . The crude was purified by flash chromatography on silica gel (eluent: cyclohexane/ethyl acetate from 8:2 to 7:3) to afford compound **113**. Yield 53 % as brown solid (m.p. 160.5-163.2°C). Molecular formula: $\text{C}_{14}\text{H}_{15}\text{ClN}_2\text{O}_3$. Molecular weight: 294.73 g/mol. ^1H NMR (300 MHz, CDCl_3): δ 8.85 (s, 1H, ArH), 7.52 (d, $J = 8.5$ Hz, 2H, ArH), 7.45 (d, $J = 8.6$ Hz, 2H, ArH), 6.26 (br s, 1H, NH exchanged with D_2O), 1.46 (s, 9H, $\text{C}(\text{CH}_3)_3$) ppm. ^{13}C NMR (75 MHz, CDCl_3): δ 152.62, 148.62, 136.27, 129.59, 129.18, 126.14, 118.21, 81.71, 28.13 ppm.

Synthesis of 3-(4-chlorophenyl)-4-aminoisoxazole (114)

To a stirred solution of **113** (1.076 mmol) in anhydrous dichloromethane (0.5 mL), trifluoroacetic acid (0.5 mL) was slowly added and the reaction mixture was stirred at room temperature for 16 hours (TLC: cyclohexane/ethyl acetate (7:3) - R_f : 0.25) and then extracted with water. The collected acidic aqueous solutions were basified with a 4N NaOH and extracted with ethyl acetate. The organic layers were combined, dried over anhydrous Na_2SO_4 , filtered and concentrated. The crude was purified by flash chromatography on silica gel (eluent: cyclohexane/ethyl acetate 7:3) to provide **114**. Yield 84 % as yellow solid. Molecular formula: $\text{C}_9\text{H}_7\text{ClN}_2\text{O}$. Molecular weight: 194.62 g/mol. ^1H NMR (300 MHz, acetone- d_6): δ 8.30 (s, 1H, ArH), 7.89 (d, J = 8.5 Hz, 2H, ArH), 7.53 (d, J = 8.5 Hz, 2H, ArH), 3.99 (s, 2H, NH_2 exchanged with D_2O) ppm.

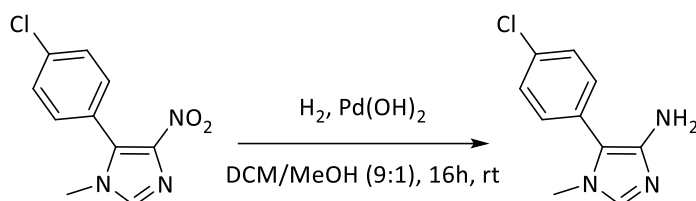
Procedures for the synthesis of 5-(4-chlorophenyl)-1-methyl-4-amino-imidazole (116)

Synthesis of 5-(4-chlorophenyl)-1-methyl-4-nitro-imidazole (115)



A mixture of 5-chloro-1-methyl-4-nitroimidazole (6.19 mmol), 4-chlorophenylboronic acid (6.19 mmol), Pd(PPh₃)₂Cl₂ (0.19 mmol), K₂CO₃ (15.48 mmol) and TBAB (6.19 mmol) in water (10 mL) was stirred at 80°C for 16 hours, under nitrogen atmosphere (TLC: dichloromethane/methanol (95:5) - R_f: 0.50). The resulting precipitate was filtered to obtain pure **115**. Yield 92 % as yellow solid. Molecular formula: C₁₀H₈ClN₃O₂. Molecular weight: 237.64 g/mol. ¹H NMR (300 MHz, CDCl₃): δ 7.48-7.55 (m, 3H, ArH), 7.34 (d, *J* = 8.5 Hz, 2H, ArH), 3.54 (s, 3H, CH₃) ppm. MS (ESI) *m/z* 238.4 [M + H]⁺.

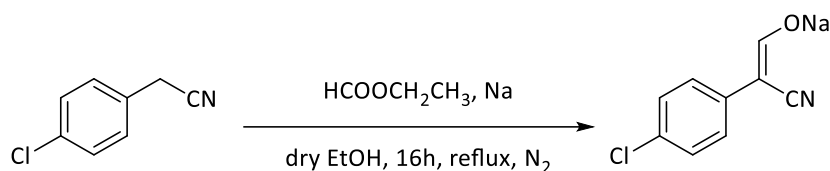
Synthesis of 5-(4-chlorophenyl)-1-methyl-4-amino-imidazole (116)



The intermediate **115** (0.42 mmol) was dissolved in dichloromethane/methanol (9:1, 3 mL) and Pd(OH)₂ (0.07 mmol) was added. The mixture was stirred under hydrogen atmosphere at room temperature overnight (TLC: dichloromethane/methanol (9:1) - R_f: 0.44) and then filtered on Celite[®]. The organic solvents were removed under *vacuum* to give the pure compound **116**. Yield 91 % as brownish oil. Molecular formula: C₁₀H₁₀ClN₃. Molecular weight: 207.66 g/mol. ¹H NMR (300 MHz, CDCl₃): δ 7.41 (d, *J* = 8.5 Hz, 2H, ArH), 7.27 (d, *J* = 8.5 Hz, 2H, ArH), 3.53 (s, 3H, CH₃), 3.41 (br s, 2H, NH₂ exchanged with D₂O) ppm. MS (ESI) *m/z* 208.8 [M + H]⁺.

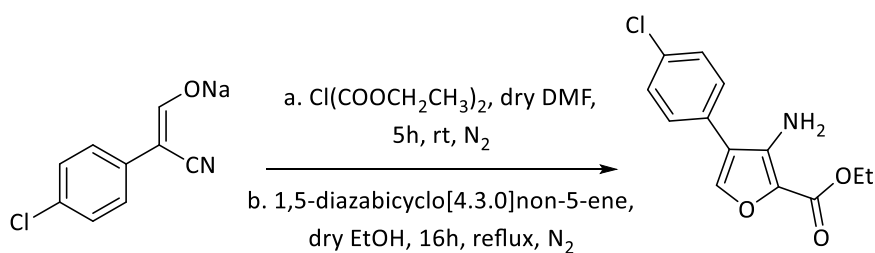
Procedures for the synthesis of ethyl 3-amino-4-(4-chlorophenyl)furan-2-carboxylate (**118**)

Synthesis of 4-chlorophenyl-acrylonitrile sodium salt (**117**)

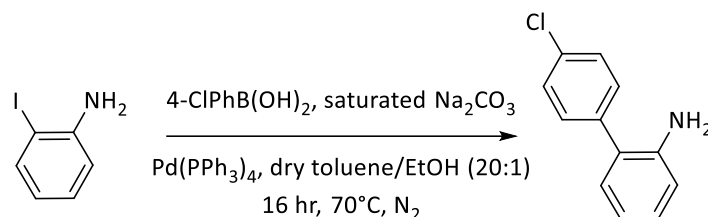


Na (6.612 mmol) was suspended in ethanol (8 mL) and refluxed under nitrogen atmosphere. A solution of 4-chlorophenylacetonitrile (3.306 mmol) and ethyl formate (4.98 mmol) in ethanol (2 mL) was added dropwise and the reaction mixture was stirred at reflux for 16 hours (TLC: dichloromethane/methanol (95:5) - R_f: 0.51). After cooling, diethyl ether was added and the resulting precipitate was collected by filtration, washed with diethyl ether and dried to give 4-chlorophenyl-acrylonitrile as sodium salt (**117**). Yield 78 % as white solid. Molecular formula: C₉H₅ClNNaO. Molecular weight: 201.58 g/mol. ¹H NMR (300 MHz, DMSO-d₆): δ 7.73 (d, *J* = 8.8 Hz, 2H, ArH), 7.06 (d, *J* = 8.8 Hz, 2H, ArH), 7.04 (s, 1H, CH) ppm.

Synthesis of ethyl 3-amino-4-(4-chlorophenyl)furan-2-carboxylate (**118**)



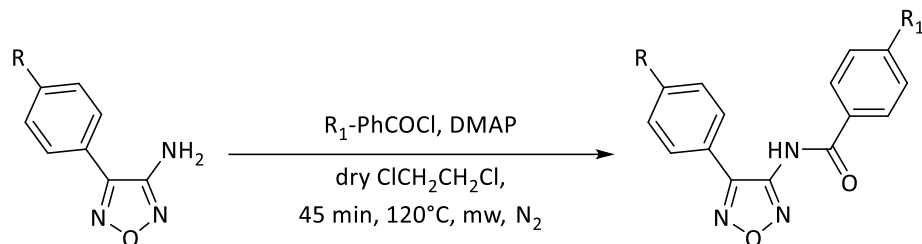
The intermediate **117** (2.48 mmol) was dissolved in dry DMF (3.97 mL) and diethyl chloromalonate (2.73 mmol) was added. The reaction mixture was stirred for 5 hours at room temperature under nitrogen atmosphere (TLC: cyclohexane/ethyl acetate (8:2) - R_f: 0.22) and then the solvent was removed under reduced pressure. The obtained orange solid was diluted with water and extracted with dichloromethane. The organic layer was dried over anhydrous Na₂SO₄, filtered and evaporated under *vacuum*. The resulting intermediate (diethyl 2-((2-(4-chlorophenyl)-2-cyanovinyl)oxy)malonate) was dissolved in dry ethanol (2.6 mL) and 1,5-diazabicyclo-[4.3.0]-non-5-ene (2.73 mmol) was added under nitrogen atmosphere. After refluxing for 16 hours (TLC: cyclohexane/ethyl acetate (8:2) - R_f: 0.51), the solution was concentrated and the residue was diluted with water and extracted with dichloromethane. The organic layers were dried over anhydrous Na₂SO₄, filtered and concentrated under reduced pressure. The crude was purified by silica gel chromatography (eluent: cyclohexane/ethyl acetate 9:1) to obtain **118**. Yield 41 % as brownish solid. Molecular formula: C₁₃H₁₂ClNO₃. Molecular weight: 265.69 g/mol. ¹H NMR (300MHz, DMSO-d₆): δ 7.87 (s, 1H, ArH), 7.41-7.56 (m, 4H, ArH), 5.54 (br s, 2H, NH₂ exchanged with D₂O), 4.22 (q, *J* = 7.1 Hz, 2H, CH₂), 1.25 (t, *J* = 7.1 Hz, 3H, CH₃) ppm. ¹³C NMR (75 MHz, CDCl₃): δ 160.35, 142.29, 141.35, 133.85, 129.42, 128.82, 128.46, 119.44, 60.13, 14.56 ppm.

Synthesis of 4'-chloro-[1,1-biphenyl]-2-amine (121)

In a two-necked flask, 2-iodoaniline (1.14 mmol) was dissolved in dry toluene/ethanol (20:1, 20 mL) under nitrogen atmosphere. Then 4-chlorophenylboronic acid (1.256 mmol), 2M Na₂CO₃ (3.43 mmol) and Pd(PPh₃)₄ (0.923 mmol) were added. The mixture was stirred at 70°C for 16 hours (TLC: cyclohexane/ethyl acetate (9:1) - R_f: 0.27). After solvent evaporation, water was added and the residue was extracted with ethyl acetate. The organic layers were collected, dried over anhydrous Na₂SO₄, filtered and concentrated under *vacuum*. The crude was purified by flash chromatography on silica gel (eluent: cyclohexane/ethyl acetate, 9:1) to afford **121**. Yield 81 % as orange oil. Molecular formula: C₁₂H₁₀ClN. Molecular weight: 203.67 g/mol. ¹H NMR (300 MHz, CDCl₃): δ 7.34-7.46 (m, 4H, ArH), 7.06-7.21 (m, 2H, ArH), 6.72-6.89 (m, 2H, ArH), 3.75 (br s, 2H, NH₂ exchanged with D₂O) ppm.

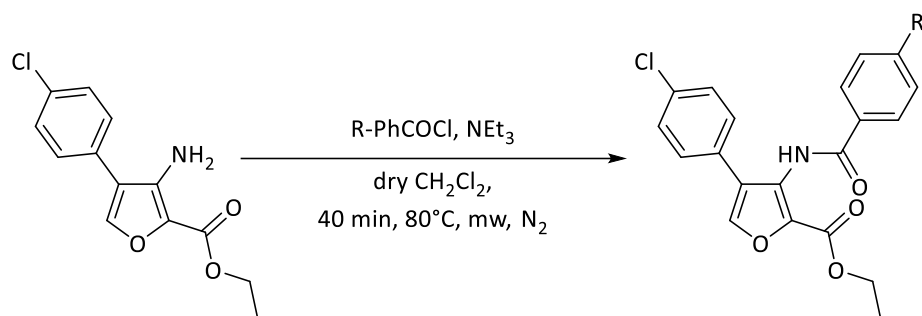
General procedures for the synthesis of *N*-aryl amides (1-5, 7-12)

Procedure a



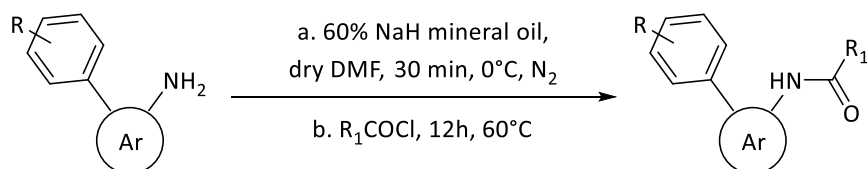
In a microwave vessel, to a solution of the suitable 4-phenyl-1,2,5-oxadiazol-3-amine (0.255 mmol) and 4-dimethylaminopyridine (0.306 mmol) in dry dichloroethane (1.5 mL), the opportune benzoyl chloride (0.306 mmol) was added at room temperature under nitrogen atmosphere. The reaction mixture was irradiated in a microwave synthesizer at 300 Watts and 120°C for 45 minutes. Upon completion, the solution was treated with water and extracted with dichloromethane and the collected organic phases were washed with 1N HCl. The organic layer was dried over Na_2SO_4 , filtered and evaporated under reduced pressure. The residue was purified by flash column chromatography.

Procedure b



In a microwave vial, the aryl amine (0.15 mmol) was dissolved in dry dichloromethane (4.29 mL) under nitrogen atmosphere. Then trimethylamine (0.378 mmol) and benzoyl chloride (0.15 mmol) were added. The reaction mixture was irradiated at 300 Watts for 40 minutes at 80°C in a microwave synthesizer. The crude was washed with 1M HCl, saturated bicarbonate solution and brine, dried over anhydrous Na_2SO_4 and concentrated under reduced pressure. The residue was purified by flash chromatography.

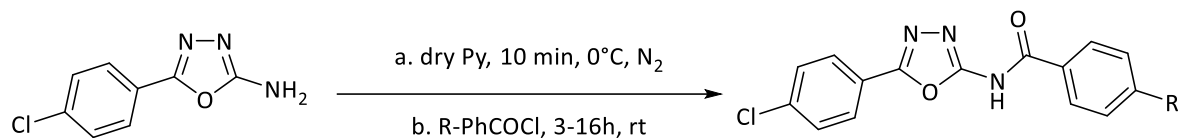
Procedure c



In a two-necked flame-dried flask under nitrogen atmosphere, the suspension of 60% NaH mineral oil (0.3 mmol) in dry DMF (3 mL) was cooled at 0°C and the appropriate aryl amine (0.25 mmol) was added. The mixture was stirred for 30 minutes at 0°C. Then, the suitable commercially available acyl chloride (0.3 mmol) was added dropwise and the mixture was stirred at 60°C for 12 hours.

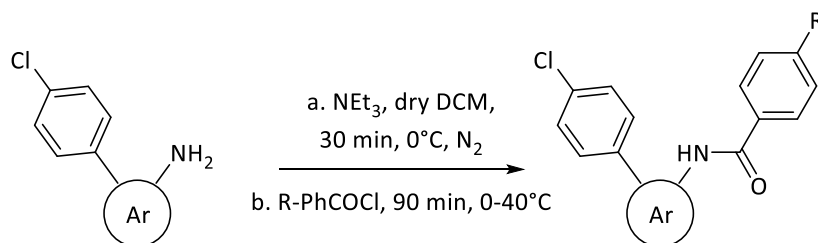
The reaction was quenched with water, and DMF was removed under *vacuum*. The residue was extracted with ethyl acetate; the collected organic layers were dried over Na_2SO_4 and evaporated. The crude product was purified by column chromatography to obtain the desired adduct.

Procedure d



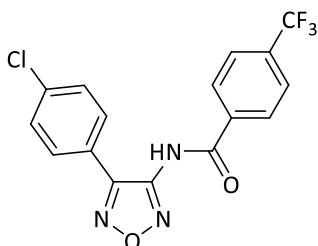
In a two-necked flame-dried flask, the proper aryl amine (0.373 mmol) was dissolved in dry pyridine (0.54 mL) under nitrogen atmosphere and cooled at 0°C. After 10 minutes, the suitable acyl chloride (0.341 mmol) was dripped and the mixture was stirred at room temperature until completion. The solvent was concentrated under reduced pressure and the residue was diluted with water and extracted with ethyl acetate. The organic layers were collected, dried over anhydrous Na_2SO_4 , filtered and concentrated in *vacuo*. The pure 1,3,4-oxadiazol-2-yl-benzamide was isolated after flash chromatography.

Procedure e



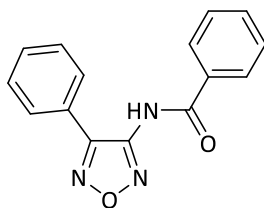
In a two-necked flame-dried flask, the opportune aryl amine (0.48 mmol) and trimethylamine (0.96 mmol) were dissolved in dry dichloromethane under nitrogen atmosphere. The solution was cooled on an ice-bath and after 30 minutes the suitable acyl chloride (0.53 mmol) was added dropwise. The reaction was stirred for 90 minutes at different temperatures for each substrate. After cooling, the reaction was quenched with water and extracted with dichloromethane. The collected organic layers were firstly washed with 1M HCl and then with brine. The resulting solution was dried over anhydrous Na_2SO_4 , filtered and concentrated in *vacuo*. The final benzamide was obtained as pure product by flash chromatography or precipitation as hydrochloride salt.

N-(4-(4-chlorophenyl)-1,2,5-oxadiazol-3-yl)-4-(trifluoromethyl)benzamide
(MD77)



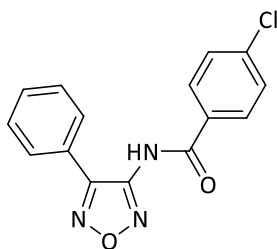
Procedure c: yield 27 % as white solid (m.p. 111-114°C). Starting compounds: **105d** and 4-(trifluoromethyl)benzoyl chloride. TLC: petroleum ether/ethyl acetate (9:1) - R_f : 0.37. Purified by flash chromatography (eluent: cyclohexane/ethyl acetate 8:2). Molecular formula: $C_{16}H_9ClF_3N_3O_2$. Molecular weight: 367.71 g/mol. 1H NMR (300 MHz, CD_3OD): δ 8.12 (d, $J = 8.6$ Hz, 2H, ArH), 7.86 (d, $J = 8.6$ Hz, 2H, ArH), 7.75 (d, $J = 8.4$ Hz, 2H, ArH), 7.50 (d, $J = 8.4$ Hz, 2H, ArH) ppm. ^{13}C NMR (75 MHz, acetone- d_6): δ 165.16, 150.73, 149.77, 136.23, 129.27, 129.22, 128.92, 125.72 (q, $J = 3.5$ Hz), 124.67 ppm. ^{19}F NMR (282 MHz, $CDCl_3$): δ -64.03 (s, CF_3) ppm.

N-(4-phenyl-1,2,5-oxadiazol-3-yl)benzamide (1aa)



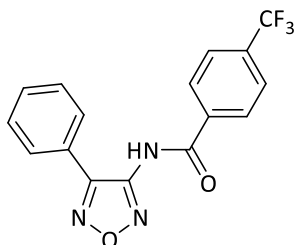
Procedure a: yield 13 % as white solid (m.p. 139-140°C). Starting compounds: **105a** and benzoyl chloride. TLC: cyclohexane/ethyl acetate (8:2) - R_f : 0.28. Purified by flash chromatography (eluent: cyclohexane/ethyl acetate from 9:1 to 6:4). Molecular formula: $C_{15}H_{11}N_3O_2$. Molecular weight: 265.27 g/mol. 1H NMR (300 MHz, $CDCl_3$): δ 8.00-8.22 (m, 4H, ArH), 7.56-7.66 (m, 2H, ArH), 7.39-7.53 (m, 4H, ArH) ppm. ^{13}C NMR (75 MHz, $CDCl_3$): δ 172.56, 133.82, 133.12, 130.76, 130.21, 129.34, 129.24, 128.97, 128.47, 127.76, 127.57 ppm.

4-(chloro)-*N*-(4-phenyl-1,2,5-oxadiazol-3-yl)benzamide (1ad)

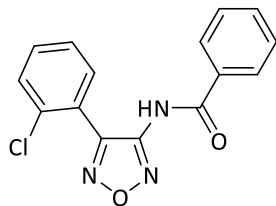


Procedure c: yield 10 % as yellow solid (m.p. 193.3-193.5°C). Starting compounds: **105a** and 4-chlorobenzoyl chloride. TLC: cyclohexane/ethyl acetate (8:2) - R_f : 0.43. Purified by flash chromatography (eluent: cyclohexane/ethyl acetate 9:1). Molecular formula: $C_{15}H_{10}ClN_3O_2$. Molecular weight: 299.71 g/mol. 1H NMR (300 MHz, acetone- d_6): δ 10.27 (br s, 1H, NH exchanged with D_2O), 7.92 (d, $J = 8.1$ Hz, 2H, ArH), 7.66-7.73 (m, 2H, ArH), 7.47 (d, $J = 8.1$ Hz, 2H, ArH), 7.33-7.41 (m, 3H, ArH) ppm. ^{13}C NMR (75 MHz, $CDCl_3$): δ 164.15, 148.55, 139.73, 130.90, 130.40, 129.39, 129.01, 127.56, 125.21, 109.99 ppm.

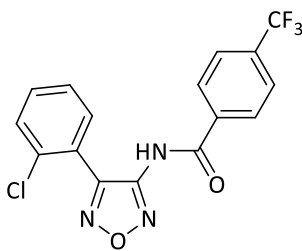
4-(trifluoromethyl)-*N*-(4-phenyl-1,2,5-oxadiazol-3-yl)benzamide (1ag)



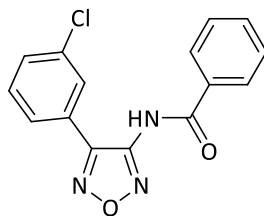
Procedure a: yield 9 %. Procedure c: yield 34 %. White solid (m.p. 198.5-199.0°C). Starting compounds: **105a** and 4-(trifluoromethyl)benzoyl chloride. TLC: cyclohexane/ethyl acetate (7:3) - R_f : 0.50. Purified by flash chromatography (eluent: cyclohexane/ethyl acetate 7:3). Molecular formula: $C_{16}H_{10}F_3N_3O_2$. Molecular weight: 333.27 g/mol. 1H NMR (300 MHz, acetone- d_6): δ 10.53 (br s, 1H, NH exchanged with D_2O), 8.26 (d, $J = 8.1$ Hz, 2H, ArH), 7.92 (d, $J = 8.1$ Hz, 2H, ArH), 7.83-7.86 (m, 2H, ArH), 7.50-7.54 (m, 3H, ArH) ppm. ^{13}C NMR (75 MHz, $CDCl_3$): δ 165.20, 151.59, 149.74, 136.25, 133.64, 133.21, 130.63, 129.04, 128.87, 127.51, 125.72 (q, $J = 3.7$ Hz), 122.11 ppm. ^{19}F NMR (282 MHz, $CDCl_3$): δ -63.58 (s, CF_3) ppm.

N-(4-(2-chlorophenyl)-1,2,5-oxadiazol-3-yl)benzamide (**1ba**)

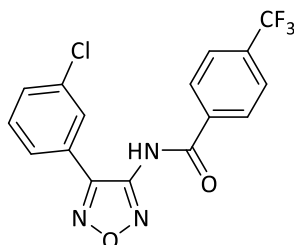
Procedure c: yield 7 % as white solid (m.p. 101.0-104°C). Starting compounds: **105b** and benzoyl chloride. TLC: cyclohexane/ethyl acetate/dichloromethane (8:1:1) - R_f : 0.28. Purified by flash chromatography (eluent: cyclohexane/ethyl acetate from 9:1 to 6:4). Molecular formula: $C_{15}H_{10}ClN_3O_2$. Molecular weight: 299.71 g/mol. 1H NMR (300 MHz, $CDCl_3$): δ 8.23 (br s, 1H, NH exchanged with D_2O), 7.78-7.84 (m, 2H, ArH), 7.55-7.63 (m, 2H, ArH), 7.41-7.53 (m, 5H, ArH) ppm. ^{13}C NMR (75 MHz, $CDCl_3$): δ 156.98, 134.46, 133.80, 130.20, 129.91, 129.85, 129.33, 128.47, 128.05, 126.00 ppm.

4-(trifluoromethyl)-*N*-(4-(2-chlorophenyl)-1,2,5-oxadiazol-3-yl)benzamide (**1bg**)

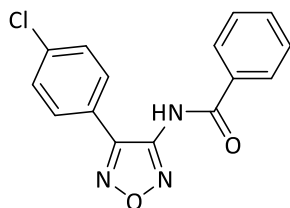
Procedure c: yield 24 % as white solid (m.p. 122.1-122.3°C). Starting compounds: **105b** and 4-(trifluoromethyl)benzoyl chloride. TLC: petroleum ether/ethyl acetate (9:1) - R_f : 0.21. Purified by flash chromatography (eluent: petroleum ether/ethyl acetate 8:2). Molecular formula: $C_{16}H_9ClF_3N_3O_2$. Molecular weight: 367.71 g/mol. 1H NMR (300 MHz, $CDCl_3$): δ 8.37 (br s, 1H, NH exchanged with D_2O), 7.94 (d, $J = 8.4$ Hz, 2H, ArH), 7.76 (d, $J = 8.1$ Hz, 2H, ArH), 7.60-7.63 (m, 1H, ArH), 7.42-7.52 (m, 3H, ArH) ppm. ^{13}C NMR (75 MHz, $CDCl_3$): δ 163.73, 149.33, 148.92, 135.60, 135.10, 134.66, 132.94, 132.42, 132.18, 130.23, 128.33, 127.90, 126.33 (q, $J = 3.7$ Hz), 125.30 ppm. ^{19}F NMR (282 MHz, $CDCl_3$): δ -63.83 (s, CF_3) ppm.

N-(4-(3-chlorophenyl)-1,2,5-oxadiazol-3-yl)benzamide (**1ca**)

Procedure c: yield 7 % as white solid (m.p. 119.0-120.7°C). Starting compounds: **105c** and benzoyl chloride. TLC: cyclohexane/ethyl acetate (8:2) - R_f : 0.20. Purified by flash chromatography (eluent: cyclohexane/ethyl acetate/dichloromethane 8:1:1 and 1% acetic acid). Molecular formula: $C_{15}H_{10}ClN_3O_2$. Molecular weight: 299.71 g/mol. 1H NMR (300 MHz, $CDCl_3$): δ 8.16 (br s, 1H, NH exchanged with D_2O), 7.88 (d, $J = 7.3$ Hz, 2H, ArH), 7.74 (t, $J = 1.6$ Hz, 1H, ArH), 7.68-7.37 (m, 6H, ArH) ppm. ^{13}C NMR (75 MHz, $CDCl_3$): δ 166.02, 149.42, 148.98, 135.16, 133.80, 133.27, 130.81, 130.41, 130.17, 128.99, 128.48, 127.73, 125.50 ppm.

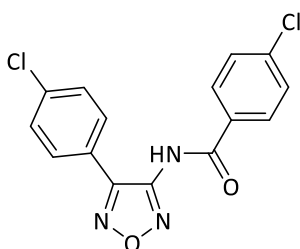
4-(trifluoromethyl)-*N*-(4-(3-chlorophenyl)-1,2,5-oxadiazol-3-yl)benzamide (**1cg**)

Procedure c: yield 32 % as white solid (m.p. 196.2-196.3°C). Starting compounds: **105c** and 4-(trifluoromethyl)benzoyl chloride. TLC: cyclohexane/ethyl acetate (8:2) - R_f : 0.35. Purified by flash chromatography (eluent: cyclohexane/ethyl acetate 75:25). Molecular formula: $C_{16}H_9ClF_3N_3O_2$. Molecular weight: 367.71 g/mol. 1H NMR (300 MHz, acetone- d_6): δ 8.25 (d, $J = 8.1$ Hz, 2H, ArH), 7.94 (d, $J = 8.4$ Hz, 2H, ArH), 7.86 (s, 1H, ArH), 7.80 (d, $J = 6.6$ Hz, 1H, ArH), 7.52-7.62 (m, 2H, ArH) ppm. ^{13}C NMR (75 MHz, acetone- d_6): δ 165.45, 150.76, 149.90, 136.41, 134.58, 133.93, 133.49, 131.06, 130.80, 129.13, 128.06, 127.63, 126.35, 125.88 (q, $J = 3.8$ Hz) ppm. ^{19}F NMR (282 MHz, acetone- d_6): δ -63.43 (s, CF_3) ppm.



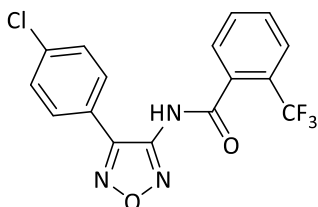
N-(4-(4-chlorophenyl)-1,2,5-oxadiazol-3-yl)benzamide (**1da**)

Procedure a: yield 12 %. Procedure c: yield 32 %. Brown solid (m.p. 177.4-178.7°C). Starting compounds: **105d** and benzoyl chloride. TLC: cyclohexane/ethyl acetate (8:2) - R_f : 0.28. Purified by flash chromatography (eluent: cyclohexane/ethyl acetate 8:2). Molecular formula: $C_{15}H_{10}ClN_3O_2$. Molecular weight: 299.71 g/mol. 1H NMR (300 MHz, $CDCl_3$): δ 8.20 (br s, 1H, NH exchanged with D_2O), 7.81 (d, $J = 7.6$ Hz, 2H, ArH), 7.62-7.52 (m, 3H, ArH), 7.42-7.50 (m, 2H, ArH), 7.39 (d, $J = 8.5$ Hz, 2H, ArH) ppm. ^{13}C NMR (75 MHz, acetone- d_6): δ 166.49, 151.07, 150.34, 136.37, 133.06, 132.74, 129.45, 129.42, 128.96, 128.27, 125.10 ppm.



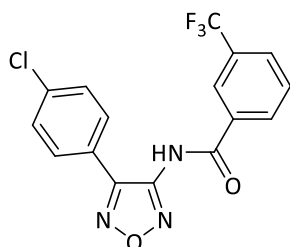
4-chloro-N-(4-(4-chlorophenyl)-1,2,5-oxadiazol-3-yl)benzamide (**1dd**)

Procedure a: yield 15 % as white solid (m.p. 155-160°C). Starting compounds: **105d** and 4-chlorobenzoyl chloride. TLC: cyclohexane/ethyl acetate (8:2) - R_f : 0.44. Purified by flash chromatography (eluent: cyclohexane/ethyl acetate 8:2). Molecular formula: $C_{15}H_9Cl_2N_3O_2$. Molecular weight: 334.16 g/mol. 1H NMR (300 MHz, $CDCl_3$): δ 8.07 (br s, 1H, NH exchanged with D_2O), 7.81 (d, $J = 8.2$ Hz, 2H, ArH), 7.64 (d, $J = 8.2$ Hz, 2H, ArH), 7.51 (d, $J = 8.7$ Hz, 2H, ArH), 7.46 (d, $J = 8.7$ Hz, 2H, ArH) ppm. ^{13}C NMR (75 MHz, $CDCl_3$): δ 166.69, 140.26, 139.97, 135.43, 130.07, 129.59, 129.49, 129.02, 128.86, 128.79, 126.27 ppm.



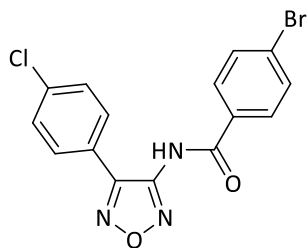
2-(trifluoromethyl)-*N*-(4-(4-chlorophenyl)-1,2,5-oxadiazol-3-yl)benzamide (**1de**)

Procedure c: yield 56 % as light gray solid (m.p. 197.1-199.8°C). Starting compounds: **105d** and 2-(trifluoromethyl)benzoyl chloride. TLC: cyclohexane/ethyl acetate (8:2) - R_f : 0.27. Purified by flash chromatography (eluent: cyclohexane/ethyl acetate 8:2). Molecular formula: $C_{16}H_9ClF_3N_3O_2$. Molecular weight: 367.71 g/mol. 1H NMR (300 MHz, CD_3OD): δ 7.85-7.67 (m, 6H, ArH), 7.55 (d, $J = 8.5$ Hz, 2H, ArH) ppm. ^{13}C NMR (75 MHz, CD_3OD): δ 149.07, 136.79, 132.38, 130.90, 129.67, 129.39, 129.14, 128.44, 127.69, 127.26, 126.65 (q, $J = 5.1$ Hz), 125.57, 124.31, 121.96 ppm. ^{19}F NMR (282 MHz, CD_3OD): δ -60.30 (s, CF_3) ppm.

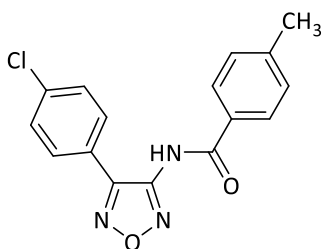


3-(trifluoromethyl)-*N*-(4-(4-chlorophenyl)-1,2,5-oxadiazol-3-yl)benzamide (**1df**)

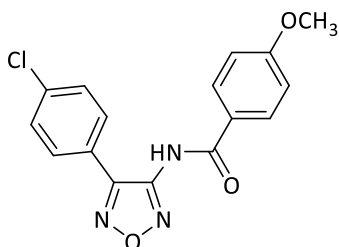
Procedure c: yield 60 % as light gray solid (m.p. 112.6-115.1°C). Starting compounds: **105d** and 3-(trifluoromethyl)benzoyl chloride. TLC: cyclohexane/ethyl acetate (8:2) - R_f : 0.36. Purified by flash chromatography (eluent: cyclohexane/ethyl acetate 8:2). Molecular formula: $C_{16}H_9ClF_3N_3O_2$. Molecular weight: 367.71 g/mol. 1H NMR (300 MHz, $CDCl_3$): δ 8.54 (br s, 1H, NH exchanged with D_2O), 8.14 (s, 1H, ArH), 8.06 (d, $J = 7.9$ Hz, 1H, ArH), 7.89 (d, $J = 7.9$ Hz, 1H, ArH), 7.71-7.60 (m, 3H, ArH), 7.49-7.40 (m, 2H, ArH) ppm. ^{13}C NMR (75 MHz, $CDCl_3$): δ 164.54, 149.88, 148.85, 137.44, 132.74, 132.25, 131.81, 131.07, 130.17, 130.08, 129.82, 129.03, 124.96 (q, $J = 3.7$ Hz), 124.03 ppm.

4-bromo-N-(4-(4-chlorophenyl)-1,2,5-oxadiazol-3-yl)benzamide (1dh)

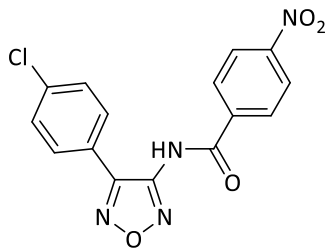
Procedure a: yield 11 % as brown solid (m.p. 195.5-197.0°C). Starting compounds: **105d** and 4-bromobenzoyl chloride (synthesized refluxing 4-bromobenzoic acid (1eq) with thionyl chloride (4eq) in dry dichloromethane for 16 hours). TLC: cyclohexane/ethyl acetate (8:2) - R_f: 0.40. Purified by flash chromatography (eluent: cyclohexane/ethyl acetate 8:2). Molecular formula: C₁₅H₉BrClN₃O₂. Molecular weight: 378.61 g/mol. ¹H NMR (300 MHz, CDCl₃): δ 8.18 (br s, 1H, NH exchanged with D₂O), 7.76 (d, *J* = 8.1 Hz, 2H, ArH), 7.68 (d, *J* = 8.7 Hz, 2H, ArH), 7.65 (d, *J* = 8.7 Hz, 2H, ArH), 7.47 (d, *J* = 8.1 Hz, 2H, ArH) ppm.

4-methyl-N-(4-(4-chlorophenyl)-1,2,5-oxadiazol-3-yl)benzamide (1di)

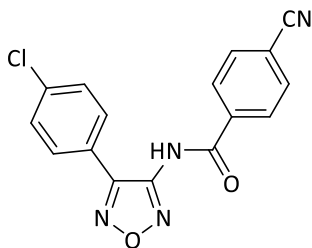
Procedure c: yield 24 % as brown solid (m.p. 163.5-164°C). Starting compounds: **105d** and 4-methylbenzoyl chloride (synthesized refluxing 4-methylbenzoic acid (1eq) with thionyl chloride (4eq) in dry dichloromethane for 3 hours). TLC: cyclohexane/ethyl acetate (8:2) - R_f: 0.30. Purified by flash chromatography (eluent: cyclohexane/ethyl acetate 8:2). Molecular formula: C₁₆H₁₂ClN₃O₂. Molecular weight: 313.74 g/mol. ¹H NMR (300 MHz, CDCl₃): δ 8.07 (br s, 1H, NH exchanged with D₂O), 7.70 (d, *J* = 8.6 Hz, 2H, ArH), 7.58 (d, *J* = 8.6 Hz, 2H, ArH), 7.38 (d, *J* = 8.4 Hz, 2H, ArH), 7.25 (d, *J* = 8.4 Hz, 2H, ArH), 2.37 (s, 3H, CH₃) ppm. ¹³C NMR (75 MHz, CDCl₃): δ 165.50, 149.75, 149.13, 144.59, 137.27 130.06, 129.79, 129.17, 129.06, 127.89, 124.31, 21.91 ppm.

4-methoxy-N-(4-(4-chlorophenyl)-1,2,5-oxadiazol-3-yl)benzamide (1dk)

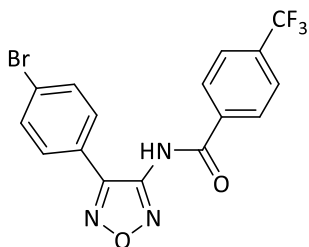
Procedure c: yield 70 % as white solid (m.p. 161-168°C). Starting compounds: **105d** and 4-methoxybenzoyl chloride. TLC: cyclohexane/ethyl acetate (8:2) - R_f: 0.20. Purified by flash chromatography (eluent: cyclohexane/dichloromethane/ethyl acetate 7:2:1). Molecular formula: C₁₆H₁₂ClN₃O₃. Molecular weight: 329.74 g/mol. ¹H NMR (300 MHz, acetone-d₆): δ 10.23 (br s, 1H, NH exchanged with D₂O), 8.02 (d, *J* = 8.7 Hz, 2H, ArH), 7.83 (d, *J* = 8.4 Hz, 2H, ArH), 7.53 (d, *J* = 8.4 Hz, 2H, ArH), 7.06 (d, *J* = 8.7 Hz, 2H, ArH), 3.89 (s, 3H, CH₃) ppm. ¹³C NMR (75 MHz, acetone-d₆): δ 165.65, 163.46, 150.84, 150.28, 136.05, 130.11, 129.15, 129.13, 124.97, 124.55, 113.91, 55.09 ppm.

4-nitro-N-(4-(4-chlorophenyl)-1,2,5-oxadiazol-3-yl)benzamide (1dr)

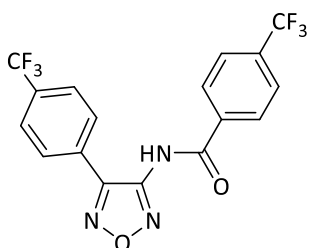
Procedure c: yield 46 % as yellow solid (m.p. 229.9-230.2°C). Starting compounds: **105d** and 4-nitrobenzoyl chloride. TLC: cyclohexane/ethyl acetate (8:2) - R_f: 0.21. Purified by flash chromatography (eluent: cyclohexane/ethyl acetate from 98:2 to 7:3). Molecular formula: C₁₅H₉ClN₄O₄. Molecular weight: 344.71 g/mol. ¹H NMR (300 MHz, acetone-d₆): δ 10.79 (br s, NH, 1H exchanged with D₂O), 8.41 (d, *J* = 8.7 Hz, 2H, ArH), 8.30 (d, *J* = 8.7 Hz, 2H, ArH), 7.88 (d, *J* = 8.4 Hz, 2H, ArH), 7.57 (d, *J* = 8.4 Hz, 2H, ArH) ppm. ¹³C NMR (75 MHz, acetone-d₆): δ 164.87, 150.85, 150.56, 149.79, 138.06, 136.37, 129.56, 129.31, 129.22, 124.74, 123.73 ppm.

4-cyano-N-(4-(4-chlorophenyl)-1,2,5-oxadiazol-3-yl)benzamide (1dt)

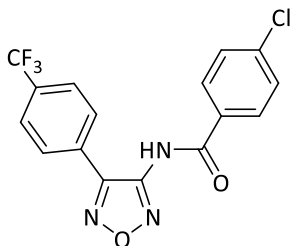
Procedure c: yield 60 % as white solid (m.p. 212.3-212.8°C). Starting compounds: **105d** and 4-cyanobenzoyl chloride. TLC: cyclohexane/ethyl acetate (8:2) - R_f : 0.27. Purified by flash chromatography (eluent: dichloromethane/cyclohexane 98:2). Molecular formula: $C_{16}H_{12}ClN_3O_3$. Molecular weight: 329.74 g/mol. 1H NMR (300 MHz, acetone- d_6): δ 10.64 (br s, NH, 1H exchanged with D_2O), 8.21 (d, $J = 9.0$ Hz, 2H, ArH), 8.00 (d, $J = 9.0$ Hz, 2H, ArH), 7.86 (d, $J = 7.8$ Hz, 2H, ArH), 7.56 (d, $J = 7.8$ Hz, 2H, ArH) ppm. ^{13}C NMR (75 MHz, acetone- d_6): δ 165.22, 150.95, 149.87, 136.58, 136.46, 132.85, 129.52, 129.47, 129.12, 124.89, 117.87, 116.32 ppm.

4-trifluoromethyl-N-(4-(4-bromophenyl)-1,2,5-oxadiazol-3-yl)benzamide (1hg)

Procedure c: yield 20 % as off-white solid (m.p. 242.5-244.8°C). Starting compounds: **105h** and 4-trifluoromethylbenzoyl chloride. TLC: cyclohexane/ethyl acetate (7:3) - R_f : 0.11. Purified by flash chromatography (eluent: from cyclohexane/ethyl acetate 9:1 to 5:5). Molecular formula: $C_{16}H_9BrF_3N_3O_2$. Molecular weight: 412.17 g/mol. 1H NMR (300 MHz, $CDCl_3$): δ 8.15 (br s, NH, 1H exchanged with D_2O), 8.00 (d, $J = 8.2$ Hz, 2H, ArH), 7.81 (d, $J = 8.2$ Hz, 2H, ArH), 7.64 (d, $J = 8.7$ Hz, 2H, ArH), 7.57 (d, $J = 8.7$ Hz, 2H, ArH) ppm. ^{13}C NMR (75 MHz, $CDCl_3$): δ 170.08, 151.41, 135.63, 135.42, 135.19, 133.18, 129.25, 129.22, 126.33 (q, $J = 3.7$ Hz), 125.12, 122.76, 121.50 ppm. ^{19}F NMR (282 MHz, $CDCl_3$): δ -63.63 (s, CF_3) ppm.

4-trifluoromethyl-N-(4-(4-trifluoromethylphenyl)-1,2,5-oxadiazol-3-yl)benzamide (1gg)

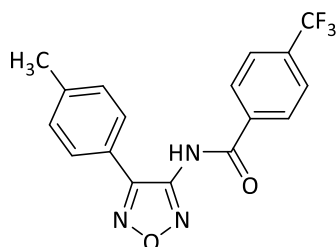
Procedure a: yield 6 % as off-white solid (m.p. 210.9-212.1°C). Starting compounds: **105g** and 4-trifluoromethylbenzoyl chloride. TLC: cyclohexane/ethyl acetate (7:3) - R_f : 0.60. Purified by flash chromatography (eluent: cyclohexane/dichloromethane 3:7). Molecular formula: $C_{17}H_9F_6N_3O_2$. Molecular weight: 401.27 g/mol. 1H NMR (300 MHz, CD_3OD): δ 8.12 (d, $J = 8.4$ Hz, 2H, ArH), 7.95 (d, $J = 8.4$ Hz, 2H, ArH), 7.86 (d, $J = 8.1$ Hz, 2H, ArH), 7.80 (d, $J = 8.1$ Hz, 2H, ArH) ppm. ^{13}C NMR (75 MHz, $CDCl_3$): δ 169.85, 149.20, 142.35, 130.75, 128.65 (q, $J = 3.6$ Hz), 128.27 (q, $J = 3.6$ Hz), 128.06, 126.32, 126.27, 126.22, 126.10, 125.91, 125.86 ppm. ^{19}F NMR (282 MHz, CD_3OD): δ -64.90 (s, CF_3), -65.43 (s, CF_3) ppm.

4-chloro-N-(4-(4-trifluoromethylphenyl)-1,2,5-oxadiazol-3-yl)benzamide (1gd)

Procedure c: yield 8 % as yellow solid (m.p. 200.0-201.0°C). Starting compounds: **105g** and 4-chlorobenzoyl chloride. TLC: cyclohexane/ethyl acetate (8:2) - R_f : 0.42. Purified by flash chromatography (eluent: cyclohexane/ethyl acetate 8:2). Molecular formula: $C_{16}H_9ClF_3N_3O_2$. Molecular weight: 367.71 g/mol. 1H NMR (300 MHz, $CDCl_3$): δ 8.11 (br s, 1H, NH exchanged with D_2O), 7.81-7.85 (m, 4H, ArH), 7.74 (d, $J = 8.4$ Hz, 2H, ArH), 7.51-7.54 (m, 2H, ArH) ppm. ^{13}C NMR (75 MHz, $CDCl_3$): δ 165.09, 149.15, 140.56, 132.69, 130.17, 129.71, 129.46, 129.17,

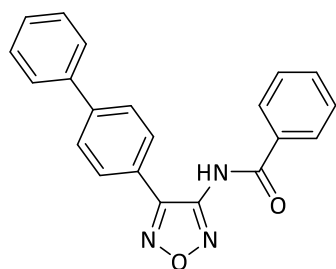
128.22, 126.27 (q, $J = 3.7$ Hz), 125.64, 121.92 ppm. ^{19}F NMR (282 MHz, CDCl_3): δ -63.08 (s, CF_3) ppm.

4-trifluoromethyl-N-(4-(*p*-tolyl)-1,2,5-oxadiazol-3-yl)benzamide (1ig)



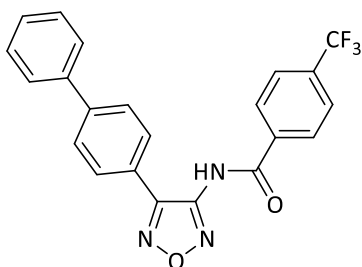
Procedure c: yield 19 % as gray solid (m.p. 118.8-121.5°C). Starting compounds: **105i** and 4-trifluoromethylbenzoyl chloride. TLC: cyclohexane/ethyl acetate (7:3) - R_f : 0.64. Purified by flash chromatography (eluent: cyclohexane/ethyl acetate 7:3). Molecular formula: $\text{C}_{17}\text{H}_{12}\text{F}_3\text{N}_3\text{O}_2$. Molecular weight: 347.30 g/mol. ^1H NMR (300 MHz, CDCl_3): δ 8.12 (br s, 1H, NH exchanged with D_2O), 7.98 (d, $J = 8.6$ Hz, 2H, ArH), 7.79 (d, $J = 8.6$ Hz, 2H, ArH), 7.57 (d, $J = 8.2$ Hz, 2H, ArH), 7.36 (d, $J = 8.2$ Hz, 2H, ArH), 2.44 (s, 3H, CH_3) ppm. ^{13}C NMR (75 MHz, CDCl_3): δ 165.78, 150.20, 148.57, 141.66, 130.45, 130.29, 128.32, 127.69, 126.45 (q, $J = 3.7$ Hz), 125.78, 125.69, 122.31, 31.15 ppm. ^{19}F NMR (282 MHz, CDCl_3): δ -63.75 (s, CF_3) ppm.

N-(4-([1,1'-biphenyl]-4-yl)-1,2,5-oxadiazol-3-yl)benzamide (1ja)



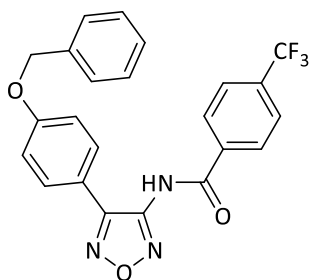
Procedure c: yield 23 % as white solid (m.p. 168.8-170.8°C). Starting compounds: **105j** and benzoyl chloride. TLC: cyclohexane/ethyl acetate (8:2) - R_f : 0.30. Purified by flash chromatography (eluent: dichloromethane/cyclohexane 8:2). Molecular formula: $\text{C}_{21}\text{H}_{15}\text{N}_3\text{O}_2$. Molecular weight: 341.37 g/mol. ^1H NMR (300 MHz, CDCl_3): δ 8.31 (br s, 1H, NH exchanged with D_2O), 7.83 (d, $J = 7.5$ Hz, 2H, ArH), 7.73 (d, $J = 8.9$ Hz, 2H, ArH), 7.66 (d, $J = 8.9$ Hz, 2H, ArH), 7.50-7.57 (m, 3H, ArH), 7.30-7.49 (m, 5H, ArH) ppm. ^{13}C NMR (75 MHz, CDCl_3): δ 165.16, 149.68, 148.67, 143.67, 139.74, 133.24, 132.03, 129.12, 128.93, 128.06, 128.00, 127.59, 127.13, 124.00 ppm.

4-(trifluoromethyl)-N-(4-([1,1'-biphenyl]-4-yl)-1,2,5-oxadiazol-3-yl)benzamide (1jg)



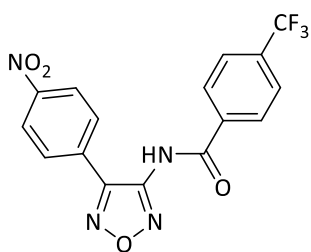
Procedure c: yield 14 % as white solid. Starting compounds: **105j** and 4-trifluoromethylbenzoyl chloride. TLC: cyclohexane/ethyl acetate (7:3) - R_f : 0.60. Purified by flash chromatography (eluent: cyclohexane/ethyl acetate 8:2). Molecular formula: $\text{C}_{22}\text{H}_{14}\text{F}_3\text{N}_3\text{O}_2$. Molecular weight: 409.37 g/mol. ^1H NMR (300 MHz, acetone- d_6): δ 10.59 (br s, 1H, NH exchanged with D_2O), 8.30 (d, $J = 8.1$ Hz, 2H, ArH), 7.90-7.97 (m, 4H, ArH), 7.82 (d, $J = 8.4$ Hz, 2H, ArH), 7.70 (d, $J = 8.7$ Hz, 2H, ArH), 7.37-7.50 (m, 3H, ArH), ppm. ^{13}C NMR (75 MHz, CDCl_3): δ 165.27, 151.31, 149.79, 143.13, 139.67, 136.29, 133.21, 128.98, 128.93, 128.24, 128.09, 128.02, 127.45, 126.90, 125.75 (q, $J = 3.45$ Hz), 124.63 ppm. ^{19}F NMR (282 MHz, CDCl_3): δ -63.58 (s, CF_3) ppm.

4-trifluoromethyl-N-(4-(4-benzyloxyphenyl)-1,2,5-oxadiazol-3-yl)benzamide
(1g)



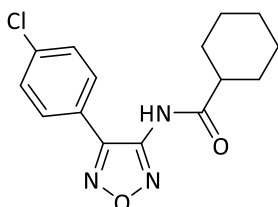
Procedure c: yield 30 % as gray solid (m.p. 217.9-220.5°C). Starting compounds: **105i** and 4-trifluoromethylbenzoyl chloride. TLC: cyclohexane/ethyl acetate (7:3) - R_f : 0.54. Purified by flash chromatography (eluent: cyclohexane/ethyl acetate 8:2). Molecular formula: $C_{23}H_{16}F_3N_3O_3$. Molecular weight: 439.39 g/mol. 1H NMR (300 MHz, $CDCl_3$): δ 8.11 (br s, 1H, NH exchanged with D_2O), 7.99 (d, $J = 8.7$ Hz, 2H, ArH), 7.79 (d, $J = 8.7$ Hz, 2H, ArH), 7.64 (d, $J = 9.0$ Hz, 2H, ArH), 7.35-7.44 (m, 5H, ArH), 7.09 (d, $J = 9.0$ Hz, 2H, ArH), 5.12 (s, 2H, CH_2) ppm. ^{13}C NMR (75 MHz, acetone- d_6): δ 165.23, 160.76, 151.23, 149.56, 136.92, 136.28, 133.60, 133.17, 129.08, 128.88, 128.43, 127.90, 127.63, 125.73 (q, $J = 3.9$ Hz), 117.90, 115.34, 69.68 ppm. ^{19}F NMR (282 MHz, $CDCl_3$): δ -63.58 (s, CF_3) ppm.

4-trifluoromethyl-N-(4-(4-nitrophenyl)-1,2,5-oxadiazol-3-yl)benzamide (1rg)



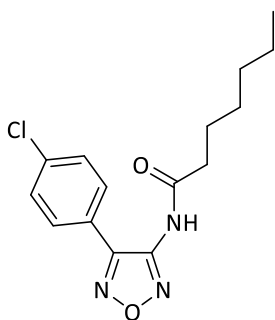
Procedure c: yield 23 % as pale yellow solid (m.p. 101.8-104.7°C). Starting compounds: **105r** and 4-trifluoromethylbenzoyl chloride. TLC: cyclohexane/ethyl acetate (8:2) - R_f : 0.37. Purified by flash chromatography (eluent: cyclohexane/ethyl acetate 8:2). Molecular formula: $C_{16}H_9F_3N_4O_4$. Molecular weight: 378.27 g/mol. 1H NMR (300 MHz, CD_3OD): δ 8.35 (d, $J = 8.9$ Hz, 2H, ArH), 8.12 (d, $J = 8.2$ Hz, 2H, ArH), 8.00 (d, $J = 8.9$ Hz, 2H, ArH), 7.86 (d, $J = 8.2$ Hz, 2H, ArH). ^{13}C NMR (75 MHz, CD_3OD): δ 180.32, 166.46, 150.20, 149.92, 149.27, 135.98, 132.45, 128.80, 128.70, 128.13, 125.70 (q, $J = 3.7$ Hz), 123.90 ppm. ^{19}F NMR (282 MHz, CD_3OD): δ -65.10 (s, CF_3) ppm.

N-(4-(4-chlorophenyl)-1,2,5-oxadiazol-3-yl)cyclohexanecarboxamide (2)

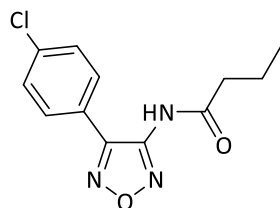


Procedure c: yield 61 % as white solid (m.p. 167.5-167.9°C). Starting compounds: **105d** and cyclohexanecarbonyl chloride. TLC: cyclohexane/ethyl acetate (8:2) - R_f : 0.46. Purified by flash chromatography (eluent: cyclohexane/ethyl acetate 9:1). Molecular formula: $C_{15}H_{16}ClN_3O_2$. Molecular weight: 305.76 g/mol. 1H NMR (300 MHz, $CDCl_3$): δ 7.51 (d, 2H, $J = 8.4$ Hz, ArH), 7.41 (d, 2H, $J = 8.4$ Hz, ArH), 7.29 (br s, 1H, NH exchanged with D_2O), 1.18-1.92 (m, 10H, CH, CH_2) ppm. ^{13}C NMR (75 MHz, $CDCl_3$): δ 174.81, 149.49, 148.79, 137.31, 129.73, 129.16, 124.07, 45.24, 29.92, 29.39, 25.58 ppm.

N-(4-(4-chlorophenyl)-1,2,5-oxadiazol-3-yl)heptanamide (3)

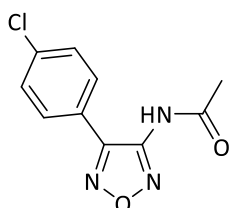


Procedure c: yield 43 % as white solid (m.p. 115.5-115.8°C). Starting compounds: **105d** and *n*-heptanoyl chloride. TLC: cyclohexane/ethyl acetate (8:2) - R_f : 0.30. Purified by flash chromatography (eluent: cyclohexane/ethyl acetate 85:15). Molecular formula: $C_{15}H_{18}ClN_3O_2$. Molecular weight: 307.78 g/mol. 1H NMR (300 MHz, $CDCl_3$): δ 7.65 (br s, 1H, NH exchanged with D_2O), 7.59 (d, 2H, $J = 8.7$ Hz, ArH), 7.47 (d, 2H, $J = 8.7$ Hz, ArH), 2.48 (t, 2H, $J = 6.9$ Hz, CH_2), 1.62-1.72 (m, 2H, CH_2), 1.25-1.39 (m, 6H, CH_2), 0.89 (t, 3H, $J = 6.9$ Hz, CH_3) ppm. ^{13}C NMR (75 MHz, $CDCl_3$): δ 172.27, 150.63, 149.94, 136.28, 129.68, 129.31, 125.00, 35.71, 31.60, 29.95, 24.94, 22.52, 13.64 ppm.



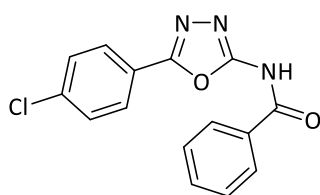
***N*-(4-(4-chlorophenyl)-1,2,5-oxadiazol-3-yl)butyramide (4)**

Procedure c: yield 98 % as white solid (m.p. 138.7-139.8°C). Starting compounds: **105d** and *n*-butyryl chloride. TLC: cyclohexane/ethyl acetate (8:2) - R_f : 0.26. Purified by flash chromatography (eluent: cyclohexane/dichloromethane/ethyl acetate 4:5:1). Molecular formula: $C_{12}H_{12}ClN_3O_2$. Molecular weight: 265.70 g/mol. 1H NMR (300 MHz, $CDCl_3$): δ 7.53 (d, 2H, $J = 8.1$ Hz, ArH), 7.42 (d, 2H, $J = 8.1$ Hz, ArH), 7.31 (br s, 1H, NH exchanged with D_2O), 2.42 (t, 2H, $J = 7.5$ Hz, CH_2), 1.61-1.73 (m, 2H, CH_2), 0.93 (t, 3H, $J = 7.4$ Hz, CH_3) ppm. ^{13}C NMR (75 MHz, $CDCl_3$): δ 172.17, 149.17, 148.68, 137.42, 129.81, 129.26, 123.81, 38.32, 18.60, 13.66 ppm.



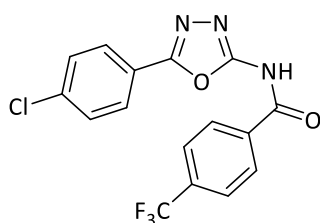
***N*-(4-(4-chlorophenyl)-1,2,5-oxadiazol-3-yl)acetamide (5)**

Procedure c: yield 32 % as white solid (m.p. 167.9-168.7°C). Starting compounds: **105d** and acetyl chloride. TLC: cyclohexane/ethyl acetate (6:4) - R_f : 0.24. Purified by flash chromatography (eluent: cyclohexane/ethyl acetate 7:3). Molecular formula: $C_{10}H_8ClN_3O_2$. Molecular weight: 237.64 g/mol. 1H NMR (300 MHz, $CDCl_3$): δ 7.51 (d, 2H, $J = 8.1$ Hz, ArH), 7.43 (d, 2H, $J = 8.1$ Hz, ArH), 7.38 (br s, 1H, NH exchanged with D_2O), 2.23 (s, 3H, CH_3) ppm. ^{13}C NMR (75 MHz, $CDCl_3$): δ 175.98, 149.10, 148.41, 137.69, 130.03, 129.30, 123.91, 22.40 ppm.



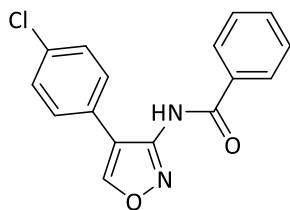
***N*-(5-(4-chlorophenyl)-1,3,4-oxadiazol-2-yl)benzamide (7da)**

Procedure d: reaction time 3 hours at room temperature, yield 24 % as pink solid (m.p. 188-189°C). Starting compounds: 2-amino-5-(4-chlorophenyl)-1,3,4-oxadiazole and benzoyl chloride. TLC: cyclohexane/ethyl acetate (7:3) - R_f : 0.14. Purified by flash chromatography (eluent: cyclohexane/ethyl acetate 7:3). Molecular formula: $C_{15}H_{10}ClN_3O_2$. Molecular weight: 299.71 g/mol. 1H NMR (300 MHz, $DMSO-d_6$): δ 12.23 (br s, 1H, NH exchange with D_2O), 8.02 (d, $J = 7.5$ Hz, 2H, ArH), 7.96 (d, $J = 8.5$ Hz, 2H, ArH), 7.51-7.72 (m, 5H, ArH) ppm.



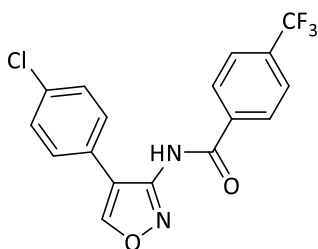
4-(trifluoromethyl)-*N*-(5-(4-chlorophenyl)-1,3,4-oxadiazol-2-yl)benzamide (7dg)

Procedure d: reaction time 16 hours at room temperature, yield 33 % as red solid (m.p. 234-235°C). Starting compounds: 2-amino-5-(4-chlorophenyl)-1,3,4-oxadiazole and 4-(trifluoromethyl)benzoyl chloride. TLC: dichloromethane/methanol/ethyl acetate (95:2.5:2.5) - R_f : 0.34. Purified by flash chromatography (eluent: dichloromethane/methanol/ethyl acetate 95:2.5:2.5 to 90:5:5). Molecular formula: $C_{16}H_9ClF_3N_3O_2$. Molecular weight: 367.71 g/mol. 1H NMR (300 MHz, $CDCl_3$): δ 11.99 (br s, 1H, NH exchange with D_2O) 8.33 (d, $J = 7.0$ Hz, 2H, ArH), 7.97 (d, $J = 8.0$ Hz, 2H, ArH), 7.73 (d, $J = 7.0$ Hz, 2H, ArH), 7.52 (d, $J = 8.0$ Hz, 2H, ArH) ppm. ^{19}F NMR (282 MHz, $CDCl_3$): δ -63.08 (s, CF_3) ppm.



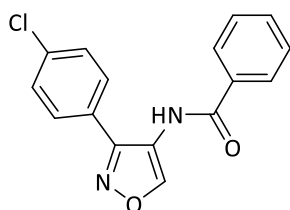
N-(4-(4-chlorophenyl)-isoxazol-3-yl)benzamide (8da)

Procedure e: at 40°C, yield 26 % as viscous brownish solid (m.p. 150.3-158.9°C). Starting compounds: **109** and benzoyl chloride. TLC: cyclohexane/ethyl acetate (75:25) - R_f : 0.37. Purified by flash chromatography (eluent: petroleum ether/ethyl acetate 85:15 to 7:3). Molecular formula: $C_{16}H_{11}ClN_2O_2$. Molecular weight: 298.05 g/mol. 1H NMR (300 MHz, $CDCl_3$): δ 8.49 (s, 1H, ArH), 8.23 (br s, 1H, NH exchanged with D_2O), 7.84 (d, $J = 7.6$ Hz, 2H, ArH), 7.59 (t, $J = 8.0$ Hz, 1H, ArH), 7.43-7.53 (m, 2H, ArH), 7.31-7.41 (m, 4H, ArH) ppm. ^{13}C NMR (75 MHz, $CDCl_3$): δ 165.14, 156.62, 134.47, 132.82, 132.63, 129.48, 129.39, 128.95, 128.84, 128.78, 127.49, 126.63 ppm.



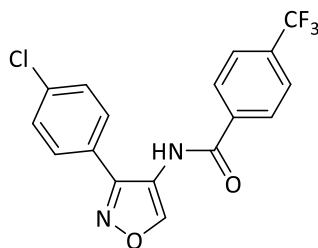
4-trifluoromethyl-N-(4-(4-chlorophenyl)-isoxazol-3-yl)benzamide (8dg)

Procedure e: at 40°C, yield 10 % as light yellow solid (m.p. 171.4-173.0°C). Starting compounds: **109** and 4-trifluoromethylbenzoyl chloride. TLC: cyclohexane/ethyl acetate (7:3) - R_f : 0.45. Purified by flash chromatography (eluent: cyclohexane/ethyl acetate 7:3). Molecular formula: $C_{17}H_{10}ClF_3N_2O_2$. Molecular weight: 366.04 g/mol. 1H NMR (300 MHz, acetone- d_6): δ 10.17 (br s, 1H, NH exchanged with D_2O), 9.08 (s, 1H, ArH), 8.22 (d, $J = 8.4$ Hz, 2H, ArH), 7.90 (d, $J = 8.4$ Hz, 2H, ArH), 7.59 (d, $J = 8.6$ Hz, 2H, ArH), 7.41 (d, $J = 8.6$ Hz, 2H, ArH) ppm. ^{13}C NMR (75 MHz, acetone- d_6): δ 165.01, 158.22, 155.66, 136.93, 133.19, 132.84, 128.85, 128.78, 128.70, 127.80, 125.59 (q, $J = 3.8$ Hz), 122.17, 117.33 ppm. ^{19}F NMR (282 MHz, acetone- d_6): δ -63.56 (s, CF_3) ppm. MS (ESI) m/z 367.0 $[M + H]^+$.



N-(3-(4-chlorophenyl)-isoxazol-4-yl)benzamide (9da)

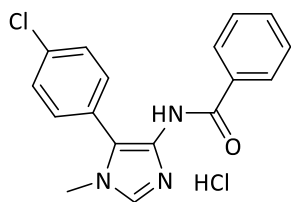
Procedure c: yield 39 % as gray solid (m.p. 162.7-165.6°C). Starting compounds: **114** and benzoyl chloride. TLC: cyclohexane/ethyl acetate (75:25) - R_f : 0.30. Purified by flash chromatography (eluent: petroleum ether/ethyl acetate 75:25). Molecular formula: $C_{16}H_{11}ClN_2O_2$. Molecular weight: 298.73 g/mol. 1H NMR (300 MHz, acetone- d_6): δ 9.28 (br s, 1H, NH exchanged with D_2O), 9.28 (s, 1H, ArH), 7.98 (d, $J = 7.2$ Hz, 2H, ArH), 7.82 (d, $J = 8.5$ Hz, 2H, ArH), 7.46-7.63 (m, 5H, ArH) ppm. ^{13}C NMR (75 MHz, acetone- d_6): δ 165.67, 155.72, 152.43, 135.38, 133.60, 131.94, 129.73, 129.18, 128.48, 127.65, 127.26, 117.95 ppm.



4-trifluoromethyl-N-(3-(4-chlorophenyl)-isoxazol-4-yl)benzamide (9dg)

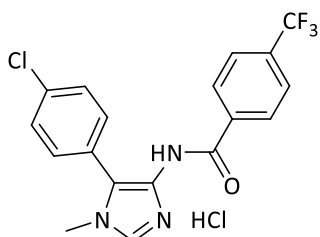
Procedure c: yield 53 % as off-white solid (m.p. 162.0-168.8°C). Starting compounds: **114** and 4-trifluoromethylbenzoyl chloride. TLC: cyclohexane/ethyl acetate (7:3) - R_f : 0.58. Purified by flash chromatography (eluent: cyclohexane/ethyl acetate 75:25). Molecular formula: $C_{17}H_{10}ClF_3N_2O_2$. Molecular weight: 366.04 g/mol. 1H NMR (300 MHz, acetone- d_6): δ 9.57 (br s, 1H, NH exchanged with D_2O), 9.31 (s, 1H, ArH), 8.19 (d, $J = 8.2$ Hz, 2H, ArH), 7.87 (d, $J = 8.2$ Hz, 2H, ArH), 7.82 (d, $J = 8.5$ Hz, 2H, ArH), 7.57 (d, $J = 8.5$ Hz, 2H, ArH) ppm. ^{13}C NMR (75 MHz, acetone- d_6): δ 164.64, 155.70, 152.68, 135.46, 132.96, 132.54, 129.78, 129.18, 128.56, 127.07, 125.46 (q, $J = 3.8$ Hz), 122.18, 117.69 ppm. ^{19}F NMR (282 MHz, acetone- d_6): δ -63.49 (s, CF_3) ppm.

N-(5-(4-chlorophenyl)-1-methyl-1H-imidazol-4-yl)benzamide hydrochloride (10da · HCl)



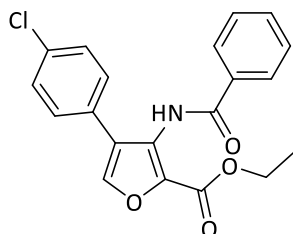
Procedure e: at 0°C, yield 32 % as brown foam. Starting compounds: **116** and benzoyl chloride. TLC: dichloromethane/methanol (9:1) - R_f: 0.52. Purified by precipitation as hydrochloride salt with 2M HCl in Et₂O. Molecular formula: C₁₇H₁₅Cl₂N₃O. Molecular weight: 348.23 g/mol. ¹H NMR (300 MHz, CD₃OD): δ 9.00 (s, 1H, ArH), 7.88 (d, *J* = 8.4 Hz, 2H, ArH), 7.46-7.65 (m, 7H, ArH), 3.84 (s, 3H, CH₃) ppm. ¹³C NMR (75 MHz, CD₃OD): δ 168.77, 136.42, 133.52, 132.62, 132.08, 131.47, 131.41, 129.23, 129.18, 128.43, 127.57, 123.07, 34.08 ppm.

N-(5-(4-chlorophenyl)-1-methyl-1H-imidazol-4-yl)-4-(trifluoromethyl)benzamide hydrochloride (10dg · HCl)



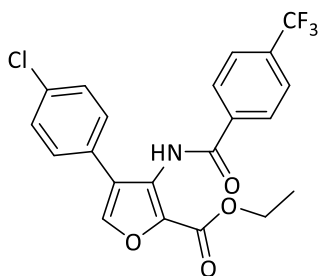
Procedure e: at 0°C, yield 25 % as brown oil. Starting compounds: **116** and 4-trifluoromethylbenzoyl chloride. TLC: dichloromethane/methanol (9:1) - R_f: 0.55. Purified by precipitation as hydrochloride salt with 2M HCl in Et₂O. Molecular formula: C₁₈H₁₄Cl₂F₃N₃O. Molecular weight: 416.23 g/mol. ¹H NMR (300 MHz, CD₃OD): δ 8.96 (s, 1H, ArH), 8.04 (d, *J* = 8.2 Hz, 2H, ArH), 7.83 (d, *J* = 8.2 Hz, 2H, ArH), 7.60 (d, *J* = 8.6 Hz, 2H, ArH), 7.55 (d, *J* = 8.6 Hz, 2H, ArH), 3.84 (s, 3H, CH₃) ppm. ¹³C NMR (75 MHz, CD₃OD): δ 167.29, 136.53, 135.79, 135.77, 133.57, 133.51, 131.55, 129.28, 128.41, 126.67, 125.39 (q, *J* = 3.7 Hz), 125.14, 122.91, 34.12 ppm. ¹⁹F NMR (282 MHz, CD₃OD): δ -64.52 (s, CF₃) ppm.

N-(5-(4-chlorophenyl)-1-methyl-1H-imidazol-4-yl)-3-ethylfuran-2-carboxylate (119da)



Procedure b: yield 42 % as off-white solid (m.p. 158.5-160.5°C). Starting compounds: **118** and benzoyl chloride. TLC: petroleum ether/ethyl acetate (9:1) - R_f: 0.14. Purified by flash chromatography (eluent: petroleum ether/ethyl acetate from 9:1 to 7:3). Molecular formula: C₂₀H₁₆ClNO₄. Molecular weight: 369.80 g/mol. ¹H NMR (300 MHz, CDCl₃): δ 9.10 (s, 1H, NH exchanged with D₂O), 7.87 (d, *J* = 7.0 Hz, 2H, ArH), 7.58 (s, 1H, ArH), 7.42-7.57 (m, 3H, ArH), 7.34 (d, *J* = 9.0 Hz, 2H, ArH), 7.30 (d, *J* = 9.0 Hz, 2H, ArH), 4.40 (q, *J* = 7.1 Hz, 2H, CH₂), 1.39 (t, *J* = 7.1 Hz, 3H, CH₃) ppm. ¹³C NMR (75 MHz, CDCl₃): δ 165.08, 159.77, 142.90, 133.87, 133.52, 133.26, 132.44, 132.33, 130.11, 128.80, 128.73, 128.19, 127.52, 124.21, 61.30, 14.31 ppm.

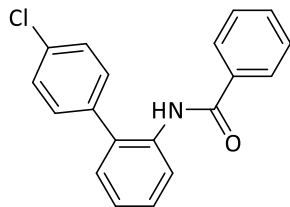
N-(5-(4-chlorophenyl)-1-methyl-1H-imidazol-4-yl)-3-ethyl-4-(4-(trifluoromethyl)phenyl)furan-2-carboxylate (119dg)



Procedure b: yield 47 % as brownish solid (m.p. 166.0-168.1°C). Starting compounds: **118** and 4-trifluoromethylbenzoyl chloride. TLC: petroleum ether/ethyl acetate (9:1) - R_f: 0.16. Purified by flash chromatography (eluent: petroleum ether/ethyl acetate 9:1). Molecular formula: C₂₁H₁₅ClF₃NO₄. Molecular weight: 437.80 g/mol. ¹H NMR (300 MHz, CDCl₃): δ 9.20 (s, 1H, NH exchanged with D₂O), 7.99 (d, *J* = 8.2 Hz, 2H, ArH), 7.74 (d, *J* = 8.2 Hz, 2H, ArH), 7.59 (s, 1H, ArH), 7.30-7.35 (m, 4H, ArH), 4.42 (q, *J* = 7.1 Hz, 2H, CH₂), 1.41 (t, *J* = 7.1 Hz, 3H, CH₃) ppm. ¹³C NMR (75 MHz, CDCl₃): δ 162.77, 158.89, 141.96,

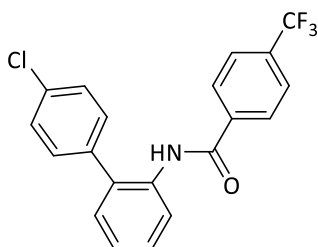
135.43, 133.31, 132.87, 132.71, 131.10, 128.95, 127.79, 127.25, 126.99, 124.89 (q, $J = 3.7$ Hz), 123.16, 120.69, 60.46, 13.31 ppm. ^{19}F NMR (282 MHz, CDCl_3): δ -63.11 (s, CF_3) ppm.

N-(4-chloro-[1,1-biphenyl]-2-yl)benzamide (12da)

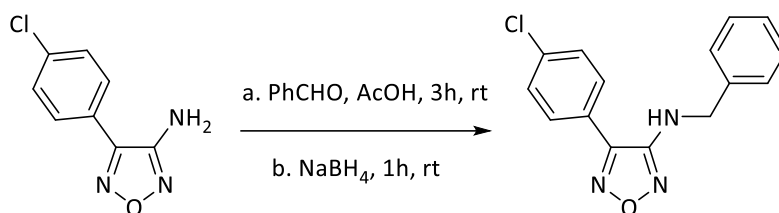


Procedure c: yield 55 % as white solid (m.p. 167-169°C). Starting compounds: **121** and benzoyl chloride. TLC: cyclohexane/ethyl acetate (8:2) - R_f : 0.44. Purified by flash chromatography (eluent: cyclohexane/ethyl acetate 9:1). Molecular formula: $\text{C}_{19}\text{H}_{14}\text{ClNO}$. Molecular weight: 307.78 g/mol. ^1H NMR (300 MHz, CDCl_3): δ 8.46 (d, $J = 7.9$ Hz, 1H, ArH), 7.83 (br s, 1H, NH exchanged with D_2O), 7.63 (d, $J = 7.0$ Hz, 2H, ArH), 7.35-7.54 (m, 8H, ArH), 7.19-7.30 (m, 2H, ArH) ppm. ^{13}C NMR (75 MHz, CDCl_3): δ 164.13, 135.57, 133.75, 133.62, 133.29, 130.86, 130.44, 129.67, 129.02, 128.39, 127.92, 127.84, 125.78, 123.68, 120.88 ppm. MS (ESI) m/z 308.0 $[\text{M} + \text{H}]^+$.

N-(4-chloro-[1,1-biphenyl]-2-yl)-4-(trifluoromethyl)benzamide (12dg)

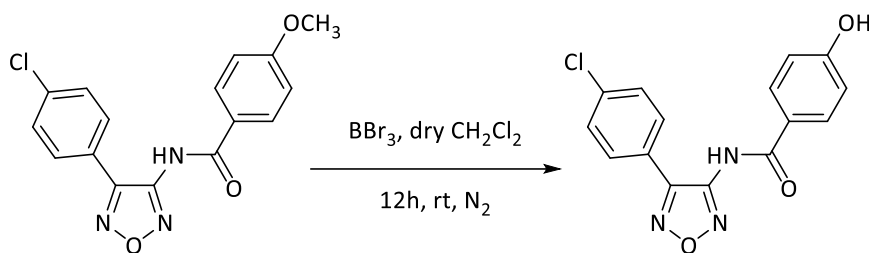


Procedure c: yield 40 % as brown solid (m.p. 169-170°C). Starting compounds: **121** and 4-trifluoromethylbenzoyl chloride. TLC (petroleum ether/ethyl acetate 9:1) - R_f : 0.28. Purified by flash chromatography (eluent: petroleum ether/ethyl acetate 9:1). Molecular formula: $\text{C}_{20}\text{H}_{13}\text{ClF}_3\text{NO}$. Molecular weight: 375.78 g/mol. ^1H NMR (300 MHz, CDCl_3): δ 8.39-8.47 (m, 1H, ArH), 7.82 (br s, 1H, NH exchanged with D_2O), 7.66-7.76 (m, 4H, ArH), 7.42-7.52 (m, 3H, ArH), 7.35-7.41 (m, 2H, ArH), 7.26-7.29 (m, 2H, ArH) ppm. ^{19}F NMR (282 MHz, CDCl_3): δ -63.09 (s, CF_3) ppm.

Synthesis of *N*-benzyl-4-(4-chlorophenyl)-1,2,5-oxadiazol-3-amine (6)

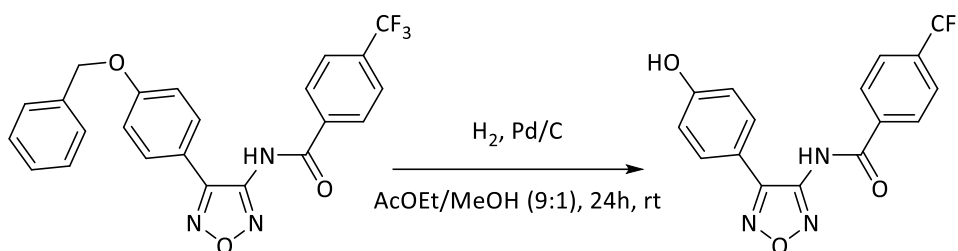
To a solution of **105d** (0.153 mmol) in acetic acid (4 mL), benzaldehyde (0.306 mmol) was added and the solution was stirred for 3 hours at room temperature. The reaction was cooled at 0°C and NaBH₄ (0.306 mmol) was added. The mixture was stirred for 1 hour. When the reaction was complete (TLC: cyclohexane/ethyl acetate (95:5) - R_f: 0.42), a solution of 2M NaOH was added, the mixture was extracted with ethyl acetate, dried over Na₂SO₄, filtered and concentrated *in vacuo*. Upon purification by flash chromatography (eluent: cyclohexane/ethyl acetate 9.5:0.5) compound **6** was obtained. Yield 67 % as brown solid (m.p. 147.5-147.7°C). Molecular formula: C₁₅H₁₂ClN₃O. Molecular weight: 285.73 g/mol. ¹H NMR (300 MHz, CDCl₃): δ 7.65 (d, *J* = 8.6 Hz, 2H, ArH), 7.38 (d, *J* = 8.6 Hz, 2H, ArH), 7.25-7.45 (m, 5H, ArH), 4.58 (s, 1H, CH₂), 4.52 (s, 1H, CH₂), 4.20 (br t, 1H, NH exchanged with D₂O) ppm. ¹³C NMR (75 MHz, acetone-d₆): δ 155.99, 146.08, 138.95, 136.06, 129.93, 129.54, 128.50, 128.02, 127.34, 125.03, 48.47 ppm.

Synthesis of 4-hydroxy-*N*-(4-(4-chlorophenyl)-1,2,5-oxadiazol-3-yl)benzamide (**1dm**)



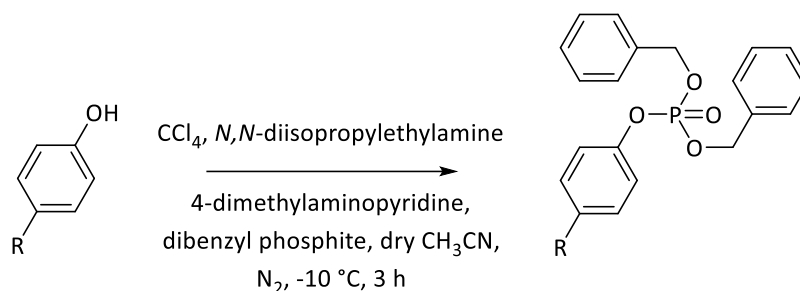
A solution of 1M BBr_3 in dry dichloromethane (2.26 mmol) was added dropwise to a solution of **1dk** (0.430 mmol) in dry dichloromethane (5 mL) at room temperature, under nitrogen atmosphere. The mixture was stirred for 12 hours and, upon completion (TLC: cyclohexane/ethyl acetate (8:2) - R_f : 0.20), the solution was treated with water and the organic layer was separated. Then the aqueous phase was extracted with ethyl acetate and the collected organic phase was washed with brine. The organic layer was dried over Na_2SO_4 , filtered and evaporated under reduced pressure giving a crude, which was purified by flash chromatography (eluent: cyclohexane/ethyl acetate 7:3) to afford **1dm**. Yield 35 % as white solid (m.p. 225-225.5°C). Molecular formula: $\text{C}_{15}\text{H}_{10}\text{ClN}_3\text{O}_3$. Molecular weight: 315.71 g/mol. ^1H NMR (300 MHz, acetone- d_6): δ 10.16 (br s, 1H, NH exchanged with D_2O), 9.23 (br s, 1H, OH exchanged with D_2O), 7.94 (d, $J = 8.7$ Hz, 2H, ArH), 7.83 (d, $J = 8.5$ Hz, 2H, ArH), 7.54 (d, $J = 8.5$ Hz, 2H, ArH), 6.96 (d, $J = 8.7$ Hz, 2H, ArH), 2.78 (br s, 1H, OH exchanged with D_2O) ppm. ^{13}C NMR (75 MHz, CD_3OD): δ 167.77, 162.38, 150.75, 150.07, 136.58, 130.30, 129.12, 128.87, 124.89, 123.05, 115.31 ppm.

Synthesis of *N*-((4-(4-hydroxyphenyl)-1,2,5-oxadiazol-3-yl)-4-trifluoromethylbenzamide (1mg)



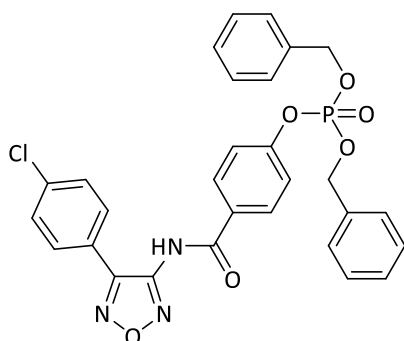
A solution of **1g** (0.54 mmol) and a catalytic amount of palladium on carbon (10 % w/w) in ethyl acetate (9 mL) and methanol (1 mL) was hydrogenated at room temperature for 24 hours (TLC: cyclohexane/ethyl acetate (8:2) - R_f: 0.13). The resulting mixture was filtered and extracted with diethyl ether. The organic layer was dried over Na₂SO₄, filtered and evaporated in *vacuo*. The crude oil was purified by flash chromatography eluting with cyclohexane/ethyl acetate (7:3) to afford **1mg**. Yield: 91.5 % as white solid. Molecular formula: C₁₆H₁₀F₃N₃O₃. Molecular weight: 349.27 g/mol. ¹H NMR (300 MHz, acetone-d₆): δ 10.43 (br s, 1H, NH exchanged with D₂O), 8.98 (br s, 1H, OH exchanged with D₂O), 8.26 (d, *J* = 8.1 Hz, 2H, ArH), 7.93 (d, *J* = 8.1 Hz, 2H, ArH), 7.71 (d, *J* = 8.7 Hz, 2H, ArH), 6.95 (d, *J* = 8.7 Hz, 2H, ArH) ppm. ¹³C NMR (75 MHz, acetone-d₆): δ 165.52, 159.90, 151.61, 149.69, 136.60, 129.44, 129.08, 125.95 (q, *J* = 3.7 Hz), 116.78, 116.20 ppm. ¹⁹F NMR (282 MHz, CDCl₃): δ -63.97 (s, CF₃) ppm.

Synthesis of dibenzyl phenylphosphates (1dn,ng)



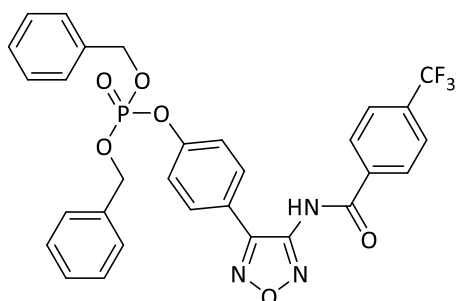
In a two-necked flask, the suitable phenol (0.143 mmol) was dissolved in dry acetonitrile (1 mL) under nitrogen atmosphere and the mixture was cooled to -10°C with an ice-acetone bath. CCl_4 (0.07 mL) was added followed by N,N -diisopropylethylamine (0.301 mmol) and N,N -dimethylaminopyridine (0.014 mmol). Dibenzylphosphite (0.208 mmol) was added dropwise and, keeping the temperature at -10°C , the mixture was stirred for 3 hours. When the reaction was complete, an aqueous solution of 0.5 M KH_2PO_4 was added and the system was allowed to warm at room temperature. The mixture was extracted with ethyl acetate and the combined organic phases were washed with water and brine, dried over Na_2SO_4 , filtered and concentrated *in vacuo*. The product was purified by flash chromatography.

dibenzyl (4-((4-(4-chlorophenyl)-1,2,5-oxadiazol-3-yl)carbamoyl)phenyl) phosphate (1dn)



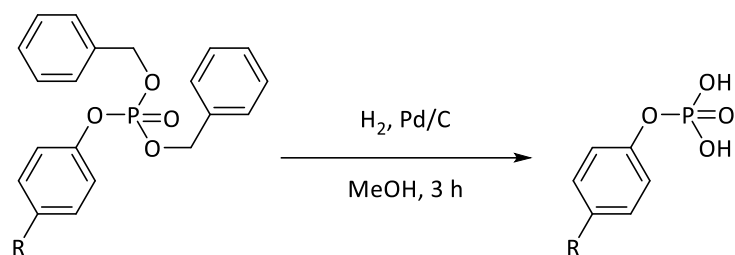
Yield 45 % as brown solid. Starting compound: **1dm**. TLC: dichloromethane/methanol (98:2) - R_f : 0.3. Eluent for flash chromatography dichloromethane/methanol 98:2. Molecular formula: $\text{C}_{29}\text{H}_{23}\text{ClN}_3\text{O}_6\text{P}$. Molecular weight: 575.94 g/mol. ^1H NMR (300 MHz, CD_3OD) δ 7.95 (d, $J = 8.8$ Hz, 2H, ArH), 7.74 (d, $J = 8.7$ Hz, 2H, ArH), 7.50 (d, $J = 8.8$ Hz, 2H, ArH), 7.34-7.39 (m, 5H, ArH), 7.27 (d, $J = 8.7$ Hz, 2H, ArH), 5.21 (s, 2H, CH_2), 5.18 (s, 2H, CH_2) ppm.

dibenzyl (4-(4-(4-(trifluoromethyl)benzamido)-1,2,5-oxadiazol-3-yl)phenyl) phosphate (1ng)



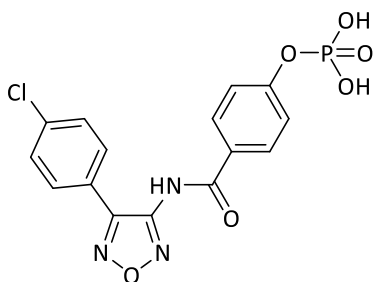
Yield 49 % as off-white solid. Starting compound: **1ng**. TLC: cyclohexane/ethyl acetate (9:1) - R_f : 0.5. Eluent for flash chromatography cyclohexane/ethyl acetate 9:1. Molecular formula: $\text{C}_{30}\text{H}_{23}\text{F}_3\text{N}_3\text{O}_6\text{P}$. Molecular weight: 609.50 g/mol. ^1H NMR (300 MHz, acetone- d_6): δ 10.59 (br s, 1H, NH exchanged with D_2O), 8.27 (d, $J = 8.1$ Hz, 2H, ArH), 7.93 (d, $J = 8.1$ Hz, 2H, ArH), 7.85 (d, $J = 8.7$ Hz, 2H, ArH), 7.30-7.45 (m, 9H, ArH), 5.22 (s, 2H, CH_2), 5.17 (s, 2H, CH_2) ppm. ^{19}F NMR (282 MHz, acetone- d_6): δ -63.80 (s, CF_3) ppm.

Synthesis of phenyl dihydrogenphosphates (**1do**,**og**)



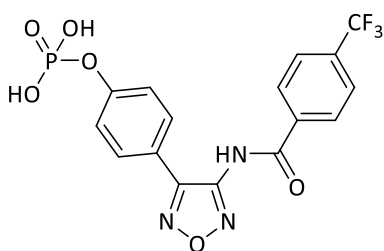
A solution of the proper dibenzyl phenylphosphate (0.044 mmol) and palladium on carbon (10 % w/w) in methanol (2.54 mg) was hydrogenated at room temperature for 3 hours. After completion of the reaction, the catalyst was filtered off on Celite® and the filtrate was concentrated under reduced pressure to afford the final compound. The product was purified on semipreparative RP-HPLC.

4-((4-(4-chlorophenyl)-1,2,5-oxadiazol-3-yl)carbamoyl)phenyl dihydrogen phosphate (**1do**)



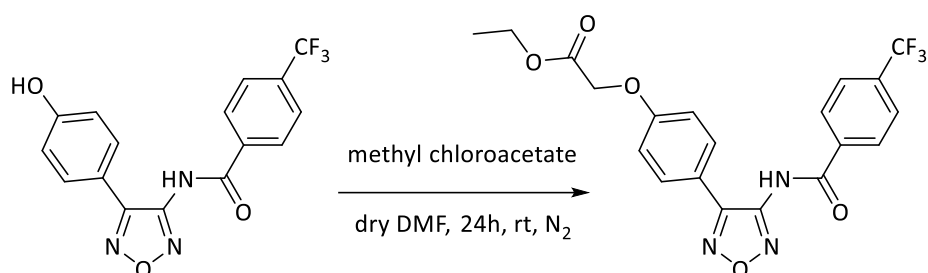
Yield 69 % as light brown solid. Starting compound: **1dn**. RP-HPLC condition: Kinetex® 2.6 μm C18 column, 100 Å, 30 x 2.1 mm, 80 % H₂O/ 20 % acetonitrile and 1/1000 of trifluoroacetic acid, flow: 0.8 mL/min flow rate and UV detector. Molecular formula: C₁₅H₁₁ClN₃O₆P. Molecular weight: 395.69 g/mol. ¹H NMR (300 MHz, CD₃OD): δ 7.84 (d, J = 10.3 Hz, 2H, ArH), 7.63 (d, J = 9.7 Hz, 2H, ArH), 7.39 (d, J = 9.7 Hz, 2H, ArH), 7.26 (d, J = 10.3 Hz, 2H, ArH) ppm. MS (ESI) m/z 396.1 [M + H]⁺.

4-((4-(4-(trifluoromethyl)benzamido)-1,2,5-oxadiazol-3-yl)phenyl dihydrogen phosphate (**1og**)



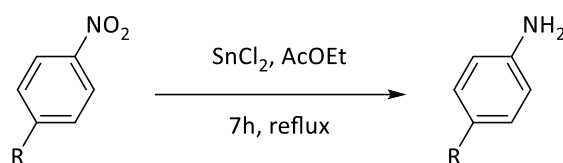
Yield 57 % as light yellow solid. Starting compound: **1ng**. RP-HPLC condition: Luna® 5 μm C8 column, 100 Å, 30 x 2 mm, 60 % H₂O/ 40 % acetonitrile and 1/1000 of trifluoroacetic acid, flow: 0.8 mL/min flow rate and UV detector. Molecular formula: C₁₆H₁₁F₃N₃O₆P. Molecular weight: 429.25 g/mol. ¹H NMR (200 MHz, CD₃OD): δ 8.12 (d, J = 8.2 Hz, 2H, ArH), 7.85 (d, J = 8.2 Hz, 2H, ArH), 7.77 (d, J = 8.7 Hz, 2H, ArH), 7.33 (d, J = 8.7 Hz, 2H, ArH) ppm. MS (ESI) m/z 430.0 [M + H]⁺. ¹⁹F NMR (282 MHz, acetone-d₆): δ -64.36 (s, CF₃) ppm.

Synthesis of ethyl 2-(4-(4-(4-(trifluoromethyl)benzamido)-1,2,5-oxadiazol-3-yl)phenoxy)acetate (1pg**)**



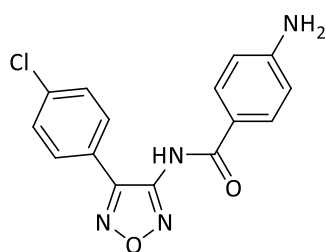
K_2CO_3 (0.177 mmol) and methyl chloroacetate (0.088 mmol) were added to a stirred solution of **1mg** (0.088 mmol) in dry DMF (0.7 mL) under nitrogen atmosphere. The reaction mixture was stirred at room temperature for 24 hours (TLC: cyclohexane/ethyl acetate (7:3) - R_f : 0.42) and filtered. The filtrate was concentrated under *vacuum* and redissolved in ethyl acetate. The organic layer was washed with 1N NaOH and brine, dried over Na_2SO_4 , filtered and evaporated under reduced pressure. The pure **1pg** was crystallized from dichloromethane. Yield: 89 % as off-white solid. Molecular formula: $C_{20}H_{16}F_3N_3O_5$. Molecular weight: 435.36 g/mol. 1H NMR (300 MHz, acetone- d_6): δ 8.38-8.49 (m, 4H, ArH), 7.71 (d, J = 8.5 Hz, 2H, ArH), 7.09 (d, J = 9.0 Hz, 2H, ArH), 4.81 (s, 2H, CH_2), 4.23 (q, J = 7.1 Hz, 2H, CH_2), 2.81 (br s, 1H, NH exchanged with D_2O), 1.26 (t, J = 7.1 Hz, 3H, CH_3) ppm. ^{19}F NMR (282 MHz, $CDCl_3$): δ -63.59 (s, CF_3) ppm.

Synthesis of 4-aminophenyl derivatives (1ds,sg)



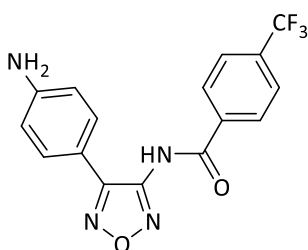
To a solution of the suitable nitrophenyl derivative (0.062 mmol) in ethyl acetate (4 mL), tin(II) chloride (0.310 mmol) was added and the mixture was refluxed for 7 hours. After quenching by addition of a saturated aqueous NaHCO_3 until pH=7-8, the precipitated tin salts were eliminated by filtration and the aqueous phase was extracted with ethyl acetate. The organic layer was dried over Na_2SO_4 , filtered and evaporated under *vacuum*. The crude residue was purified by flash chromatography to provide the final compound.

4-amino-N-(4-(4-chlorophenyl)-1,2,5-oxadiazol-3-yl)benzamide (1ds)



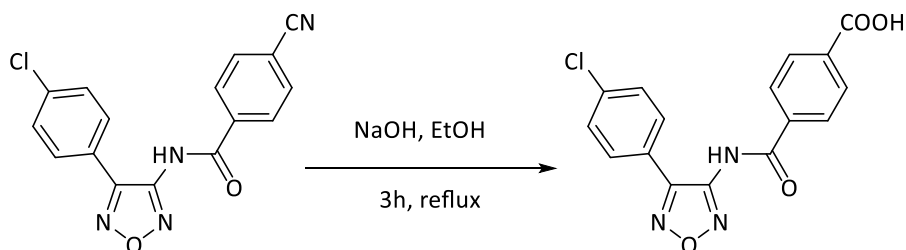
Yield 70 % as yellow solid (m.p. 153.5-154°C). Starting compound: **1dr**. TLC: cyclohexane/ethyl acetate (6:4) - R_f : 0.22. Eluent for flash chromatography cyclohexane/ethyl acetate 6:4. Molecular formula: $\text{C}_{15}\text{H}_{11}\text{ClN}_4\text{O}_2$. Molecular weight: 314.73 g/mol. ^1H NMR (300 MHz, acetone- d_6): δ 9.82 (br s, NH, 1H exchanged with D_2O), 7.64-7.70 (m, 4H, ArH), 7.40 (d, $J = 8.7$ Hz, 2H, ArH), 6.60 (d, $J = 8.4$ Hz, 2H, ArH), 5.35 (br s, 2H, NH_2 exchanged with D_2O) ppm. ^{13}C NMR (75 MHz, acetone- d_6): δ 166.09, 153.41, 151.15, 150.88, 136.17, 130.26, 129.36, 129.30, 125.46, 119.84, 113.35 ppm.

4-trifluoromethyl-N-(4-(4-aminophenyl)-1,2,5-oxadiazol-3-yl)benzamide (1sg)

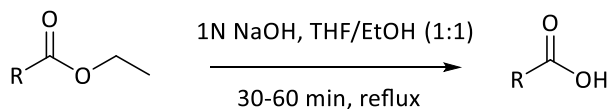


Yield: 78 % as brown solid. Starting compound: **1rg**. TLC: cyclohexane/ethyl acetate (8:2) - R_f : 0.30. Eluent for flash chromatography: from cyclohexane/ethyl acetate 8:2 to 6:4. Molecular formula: $\text{C}_{16}\text{H}_{11}\text{F}_3\text{N}_4\text{O}_2$. Molecular weight: 348.29 g/mol. ^1H NMR (300 MHz, acetone- d_6): δ 10.15 (br s, 1H, NH exchanged with D_2O), 8.14 (d, $J = 8.2$ Hz, 2H, ArH), 7.80 (d, $J = 8.2$ Hz, 2H, ArH), 7.43 (d, $J = 8.8$ Hz, 2H, ArH), 6.60 (d, $J = 8.8$ Hz, 2H, ArH), 5.03 (br s, 2H, NH_2 exchanged with D_2O) ppm. ^{13}C NMR (75 MHz, acetone- d_6): δ 165.21, 151.60, 151.02, 149.25, 136.49, 128.81, 128.64, 128.34, 125.72 (q, $J = 3.5$ Hz), 119.99, 114.09, 112.63 ppm. ^{19}F NMR (282 MHz, CDCl_3): δ -63.99 (s, CF_3) ppm.

**General procedures for the nitrile or ester hydrolysis
under basic conditions (1du,qg, 120da,dg)**

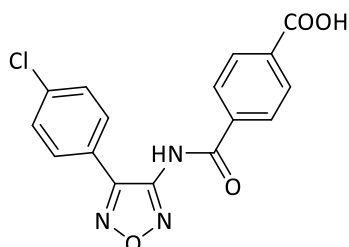
Procedure a

3N NaOH (2 mL) was added at room temperature to a solution of **1dt** (0.066 mmol) in ethanol (5 mL). The reaction mixture was heated at reflux for 3 hours. The mixture was cooled to room temperature and concentrated under *vacuum*. The residue was diluted with water and extracted with ethyl acetate. The aqueous phase, containing the sodium salt of **1du**, was acidified with a solution of 3N HCl until pH = 2 and extracted with ethyl acetate. The organic layer was dried over Na₂SO₄, filtered and evaporated under reduced pressure.

Procedure b

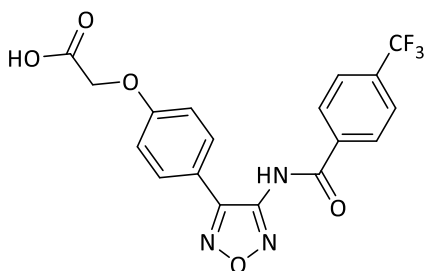
The suitable ethyl carboxylate (0.27 mmol) was dissolved in tetrahydrofuran/ethanol (1:1, 4 mL) and 1N NaOH (1 mL) was added dropwise. The reaction was refluxed until completion and the solvents were removed under reduced pressure. The residue was diluted with water and washed with dichloromethane. The aqueous layer, containing the sodium salt of the final compound, was acidified with 1N HCl and extracted with ethyl acetate. The organic layers were dried and concentrated under reduced pressure, affording the pure carboxylic acid.

4-(N-(4-(4-chlorophenyl)-1,2,5-oxadiazol-3-yl)carbamoyl)benzoic acid
(1du)



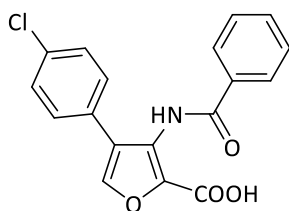
Procedure a: yield 81 % as white solid (m.p. 297-298°C). Starting compound: **1dt**. TLC: dichloromethane/methanol (9:1) - R_f: 0.21. Molecular formula: C₁₆H₁₀ClN₃O₄. Molecular weight: 343.72 g/mol. ¹H NMR (300 MHz, DMSO-d₆): δ 8.02-8.09 (m, 4H, ArH), 7.78 (d, J = 8.4 Hz, 2H, ArH), 7.59 (d, J = 8.7 Hz, 2H, ArH) ppm. ¹³C NMR (75 MHz, DMSO-d₆): δ 167.26, 166.52, 151.32, 150.66, 136.37, 136.31, 135.23, 130.20, 130.01, 129.85, 129.10, 124.78 ppm.

2-(4-(4-(4-(trifluoromethyl)benzamido)-1,2,5-oxadiazol-3-yl)phenoxy)acetic acid (1qg)



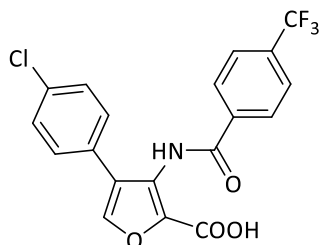
Procedure b. Reaction time: 30 minutes. Yield 93 % as light yellow foam. Starting compound: **1pg**. TLC: dichloromethane/methanol (8:2) - R_f: 0.21. Molecular formula: C₁₈H₁₂F₃N₃O₅. Molecular weight: 407.31 g/mol. ¹H NMR (300 MHz, acetone-d₆): δ 10.44 (br s, 1H, OH exchanged with D₂O), 8.26 (d, *J* = 8.1 Hz, 2H, ArH), 7.93 (d, *J* = 8.1 Hz, 2H, ArH), 7.81 (d, *J* = 9.0 Hz, 2H, ArH), 7.08 (d, *J* = 9.0 Hz, 2H, ArH), 4.80 (s, 2H, CH₂), 2.81 (br s, 1H, NH exchanged with D₂O) ppm. ¹⁹F NMR (282 MHz, CDCl₃): δ -63.61 (s, CF₃) ppm.

3-benzamido-4-(4-chlorophenyl)furan-2-carboxylic acid (120da)



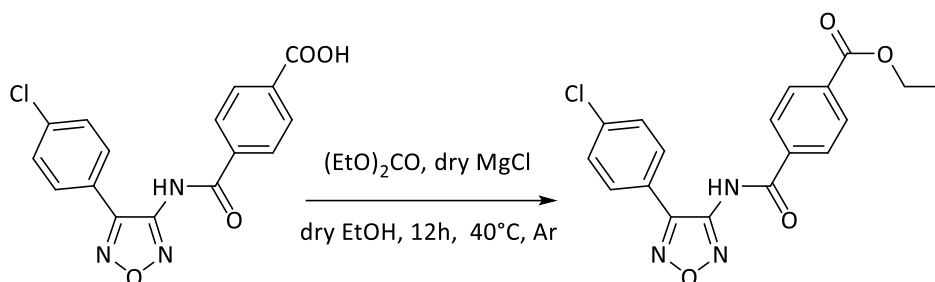
Procedure b. Reaction time: 60 minutes. Yield 86 % as white solid (m.p. 181.6-184.2°C). Starting compound: **119da**. TLC: dichloromethane/methanol (8:2) - R_f: 0.28. Molecular formula: C₁₈H₁₂ClNO₄. Molecular weight: 341.75 g/mol. ¹H NMR (300 MHz, CD₃OD): δ 7.97 (s, 1H, ArH), 7.90 (d, *J* = 7.4 Hz, 2H, ArH), 7.58 (t, *J* = 7.4 Hz, 1H, ArH), 7.42-7.53 (m, 4H, ArH), 7.34 (d, *J* = 8.7 Hz, 2H, ArH) ppm. ¹³C NMR (75 MHz, CD₃OD): δ 168.02, 159.77, 142.85, 138.89, 133.55, 133.28, 131.90, 129.32, 128.86, 128.43, 128.37, 128.29, 127.33, 125.82 ppm.

4-(4-chlorophenyl)-3-(4-(trifluoromethyl)benzamido)furan-2-carboxylic acid (120dg)



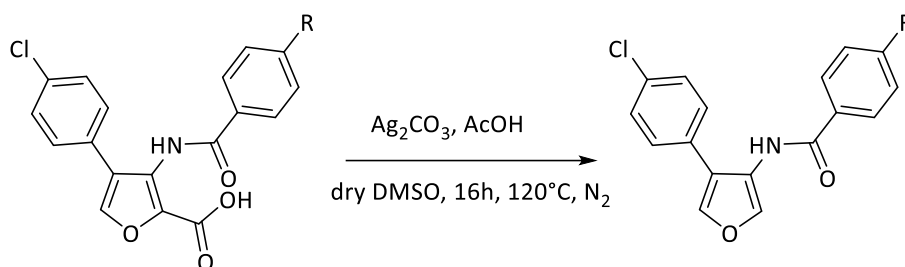
Procedure b. Reaction time: 60 minutes. Yield 71 % as yellow-brown solid (m.p. 187.9-191.1°C). Starting compound: **119dg**. TLC: dichloromethane/methanol (8:2) - R_f: 0.26. Molecular formula: C₁₉H₁₁ClF₃NO₄. Molecular weight: 409.75 g/mol. ¹H NMR (300 MHz, CD₃OD): δ 8.09 (d, *J* = 8.0 Hz, 2H, ArH), 7.79 (d, *J* = 8.0 Hz, 2H, ArH), 7.72 (s, 1H, ArH), 7.44 (d, *J* = 8.5 Hz, 2H, ArH), 7.31 (d, *J* = 8.5 Hz, 2H, ArH) ppm. ¹³C NMR (75 MHz, CD₃OD): δ 166.53, 165.74, 141.43, 140.42, 137.04, 132.62, 130.55, 128.13, 128.11, 128.09, 125.84, 125.57, 125.14 (q, *J* = 3.5 Hz), 124.17, 121.97 ppm. ¹⁹F NMR (282 MHz, CD₃OD): δ -64.49 (s, CF₃) ppm.

**Synthesis of ethyl 4-((4-(4-chlorophenyl)-1,2,5-oxadiazol-3-yl)
carbamoyl)benzoate (1dv)**



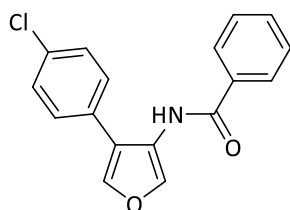
In a two-necked flask equipped with a magnetic stirring bar, dry MgCl_2 (0.0087 mmol), diethylcarbonate (0.087 mmol) and **1du** (0.087 mmol) were dissolved in ethanol (3 mL) under argon atmosphere. The mixture was stirred at 40°C for 12 hours (TLC: petroleum ether/ethyl acetate (8:2) - R_f : 0.45). The reaction mixture was diluted with H_2O , concentrated and extracted with ethyl acetate. The organic layer was dried over Na_2SO_4 , filtered and evaporated under reduced pressure. The residue was purified by flash chromatography with petroleum ether/ethyl acetate (8:2) to provide **1dv**. Yield 15 % as white solid. Molecular formula: $\text{C}_{18}\text{H}_{14}\text{ClN}_3\text{O}_4$. Molecular weight: 371.78 g/mol. ^1H NMR (300 MHz, CDCl_3): δ 8.31 (br s, 1H, NH exchanged with D_2O), 8.18 (d, $J = 8.1$ Hz, 2H, ArH), 7.94 (d, $J = 8.1$ Hz, 2H, ArH), 7.65 (d, $J = 8.1$ Hz, 2H, ArH), 7.47 (d, $J = 8.1$ Hz, 2H, ArH), 4.43 (q, $J = 7.2$ Hz, 2H, CH_2), 1.43 (t, $J = 7.2$ Hz, 3H, CH_3) ppm. ^{13}C NMR (75 MHz, CDCl_3): δ 165.56, 164.93, 149.82, 148.85, 137.44, 135.57, 135.01, 130.48, 129.85, 129.07, 127.86, 124.12, 61.93, 14.47 ppm.

Synthesis of *N*-(4-(4-chlorophenyl)-furan-3-yl)benzamides (**11da,dg**)



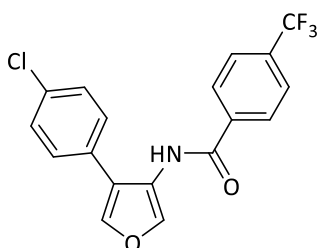
A mixture of the suitable carboxylic acid (0.293 mmol), Ag_2CO_3 (0.0293 mmol), acetic acid (0.015 mmol) in dry DMSO (0.29 mL) was stirred at 120°C under nitrogen atmosphere for 16 hours. After cooling to room temperature, ethyl acetate was added. The organic layer was washed with saturated sodium bicarbonate solution, water and brine, and dried over anhydrous Na_2SO_4 , filtered and concentrated under reduced pressure. The crude was purified by flash chromatography to give the final compound.

N-(4-(4-chlorophenyl)furan-3-yl)benzamide (**11da**)



Yield 12.6 % as pale-yellow solid (m.p. $72.3\text{--}80.8^\circ\text{C}$). Starting compound: **120da**. TLC: cyclohexane/ethyl acetate (8:2) - R_f : 0.45. Eluent for flash chromatography: cyclohexane/ethyl acetate from 95:5 to 8:2. Molecular formula: $\text{C}_{17}\text{H}_{12}\text{ClNO}_2$. Molecular weight: 297.74 g/mol. ^1H NMR (300 MHz, CDCl_3): δ 8.37 (s, 1H, ArH), 7.76 (d, $J = 7.0$ Hz, 2H, ArH), 7.67 (br s, 1H, NH exchanged with D_2O), 7.42–7.59 (m, 6H, ArH), 7.37 (d, $J = 8.4$ Hz, 2H, ArH) ppm. ^{13}C NMR (75 MHz, CDCl_3): δ 164.47, 138.48, 134.19, 134.13, 133.50, 132.05, 129.78, 129.37, 129.05, 128.92, 126.84, 122.30, 119.11 ppm.

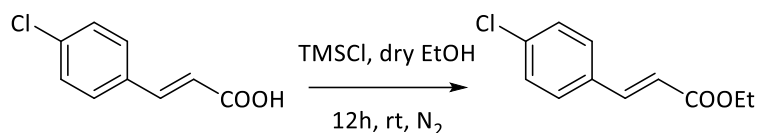
4-trifluoromethyl-*N*-(4-(4-chlorophenyl)furan-3-yl)benzamide (**11dg**)



Yield 25 % as yellow-orange solid (m.p. $115.1\text{--}116.4^\circ\text{C}$). Starting compound: **120dg**. TLC: cyclohexane/ethyl acetate (8:2) - R_f : 0.58. Eluent for flash chromatography: cyclohexane/ethyl acetate (8:2). Molecular formula: $\text{C}_{18}\text{H}_{11}\text{ClF}_3\text{NO}_2$. Molecular weight: 365.74 g/mol. ^1H NMR (300 MHz, CDCl_3): δ 8.28 (s, 1H, ArH), 7.79 (d, $J = 8.1$ Hz, 2H, ArH), 7.66 (d, $J = 8.3$ Hz, 2H, ArH), 7.62 (br s, 1H, NH exchanged with D_2O), 7.36–7.44 (m, 3H, ArH), 7.27 (d, $J = 8.3$ Hz, 2H, ArH) ppm. ^{13}C NMR (75 MHz, CDCl_3): δ 163.18, 138.63, 136.75, 134.48, 134.31, 133.54, 129.83, 129.34, 128.83, 127.86, 127.35, 125.98 (q, $J = 3.7$ Hz), 122.06, 119.01 ppm. ^{19}F NMR (282 MHz, CDCl_3): δ -63.11 (s, CF_3) ppm.

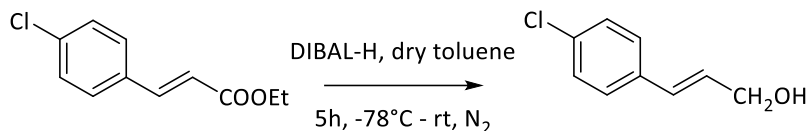
Procedure for the synthesis of 1-(4-(4-chlorophenyl)-1,2,5-oxadiazol-3-yl)methanamine hydrochloride ($14 \cdot \text{HCl}$)

Synthesis of ethyl 4-chlorocinnamate (**122**)

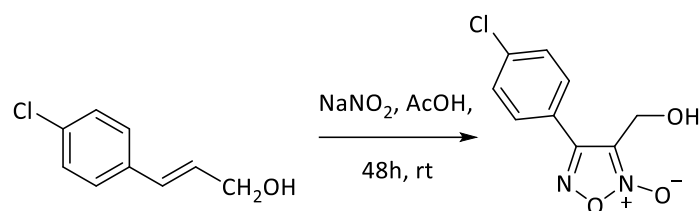


The commercially available 4-chlorocinnamic acid (1 mmol) was suspended in absolute ethanol (5 mL) under nitrogen atmosphere and chlorotrimethylsilane (2.2 mmol) was dripped. The reaction was stirred at room temperature overnight (TLC: cyclohexane/ethyl acetate (9:1) - R_f : 0.36) and then the solvent was removed under reduced pressure. The crude was dissolved in ethyl acetate, washed with saturated NaHCO_3 , water and brine. Then the organic layers were collected, dried over Na_2SO_4 and concentrated to give the pure **122** without any further purification. Yield 96 % as colorless oil. Molecular formula: $\text{C}_{11}\text{H}_{11}\text{ClO}_2$. Molecular weight: 210.66 g/mol. ^1H NMR (300 MHz, CDCl_3): δ 7.60 (d, $J = 16.0$ Hz, 1H, CH), 7.42 (d, $J = 8.3$ Hz, 2H, ArH), 7.33 (d, $J = 8.3$ Hz, 2H, ArH), 6.38 (d, $J = 16.0$ Hz, 1H, CH), 4.25 (q, $J = 7.1$ Hz, 2H, CH_2), 1.32 (t, $J = 7.1$ Hz, 3H, CH_3) ppm. ^{13}C NMR (75 MHz, CDCl_3): δ 166.64, 143.03, 136.05, 132.92, 129.14, 129.10, 118.84, 60.55, 14.26 ppm.

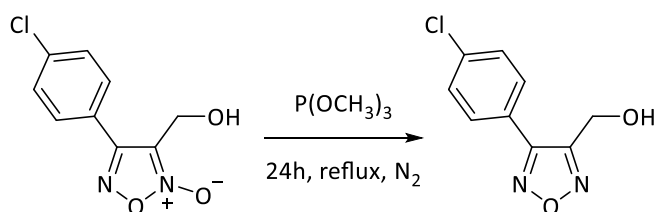
Synthesis of 4-chlorocinnamyl alcohol (**123**)



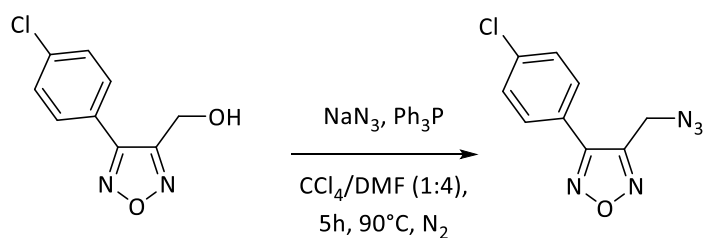
To a suspension of **122** (1 mmol) in dry toluene (2.5 mL), at -78°C under nitrogen, DIBAL-H (2.2 mmol, 1.2 M solution in toluene) was added dropwise. The reaction mixture was allowed to slowly warm to room temperature and then stirred for 5 hours (TLC: cyclohexane/ethyl acetate (7:3) - R_f : 0.16). The reaction mixture was quenched with cold 0.1N HCl and filtered. The organic layer was separated and the aqueous layer was extracted with ethyl acetate. The combined organic layer was washed with brine and water, dried over Na_2SO_4 and concentrated under *vacuum* to afford the pure intermediate **123**. Yield 94 % as white solid. Molecular formula: $\text{C}_9\text{H}_9\text{ClO}$. Molecular weight: 168.62 g/mol. ^1H NMR (300 MHz, CDCl_3): δ 7.35-7.19 (m, 4H, ArH), 6.56 (d, $J = 15.9$ Hz, 1H, CH), 6.32 (dt, $J_1 = 15.9$, $J_2 = 5.5$ Hz, 1H, CH), 4.31 (d, $J = 5.5$ Hz, 2H, CH_2) ppm. ^{13}C NMR (75 MHz, CDCl_3): δ 135.18, 133.22, 129.59, 129.19, 128.73, 127.63, 63.29 ppm.

Synthesis of 4-(4-chlorophenyl)-3-(hydroxymethyl)-1,2,5-oxadiazole 2-oxide (124)

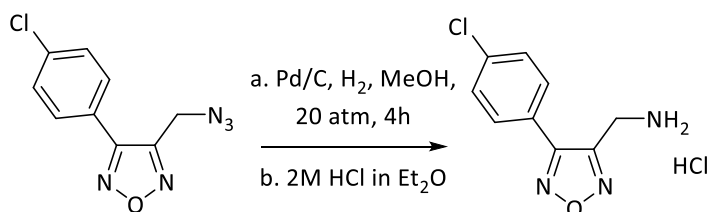
A solution of 4-chlorocinnamyl alcohol (1 mmol) in glacial acetic acid (5 mL) was cooled to 0°C and sodium nitrite (2 mmol) was added portion-wise. The reaction mixture was stirred at room temperature for 48 hours. After completion (TLC: cyclohexane/ethyl acetate (8:2) - R_f: 0.35), the reaction mixture was quenched with ice water and extracted with ethyl acetate. The organic layer was washed with saturated NaHCO₃, water, and brine. After drying over Na₂SO₄ and concentrating under reduced pressure, the residue was purified by flash chromatography (firstly with cyclohexane/ethyl acetate 7:3 and then with cyclohexane/chloroform 5:5) to obtain compound **124**. Yield 50 % as brown oil. Molecular formula: C₉H₇ClN₂O₃. Molecular weight: 226.62 g/mol. ¹H NMR (300 MHz, CDCl₃): δ 7.79 (d, *J* = 8.6 Hz, 2H, ArH), 7.53 (d, *J* = 8.6 Hz, 2H, ArH), 4.73 (s, 2H, CH₂) ppm. ¹³C NMR (75 MHz, CDCl₃): δ 155.81, 137.77, 129.74, 129.06, 124.62, 53.31 ppm. MS (ESI) *m/z* 227.01 [M+H]⁺.

Synthesis of 4-(4-chlorophenyl)-3-(hydroxymethyl)-1,2,5-oxadiazole (125)

124 (1.26 mmol) was refluxed with trimethylphosphite (2.62 mL) for 24 hours (TLC: cyclohexane/dichloromethane/ethyl acetate (50:45:5) - R_f: 0.26) in a flame-dried flask under nitrogen. After cooling, 1N HCl (26.2 mL) was added to the reaction mixture which was extracted with diethyl ether. The combined organic layers were washed with saturated NaHCO₃, and then with brine, dried and evaporated under *vacuum*. Flash chromatography (cyclohexane/ethyl acetate 8:2) was performed to afford **125**. Yield: 15 % as yellow solid (m.p. 74.8-76.5°C). Molecular formula: C₉H₇ClN₂O₂. Molecular weight: 210.62 g/mol. ¹H NMR (300 MHz, CDCl₃): δ 7.86 (d, *J* = 8.4 Hz, 2H, ArH), 7.51 (d, *J* = 8.4 Hz, 2H, ArH), 4.98 (s, 2H, CH₂) ppm. ¹³C NMR (75 MHz, acetone-d₆): δ 153.42, 153.21, 136.29, 130.19, 129.28, 124.73, 52.89 ppm. IR ν = 3369, 2963, 2929, 1692, 1453, 1415, 1260, 1095, 799 cm⁻¹. MS (ESI) *m/z* 233.6 [M+Na]⁺.

Synthesis of 4-(4-chlorophenyl)-3-(azidomethyl)-1,2,5-oxadiazole (126)

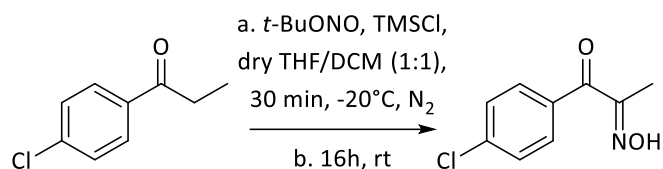
A solution of **125** (1 mmol) in $\text{CCl}_4/\text{DMF (1:4, 5 mL)}$, with sodium azide (1.2 mmol) and PPh_3 (1 mmol), was heated at 90°C for 5 hours (TLC: cyclohexane/ethyl acetate (8:2) - R_f : 0.59). After cooling, the reaction mixture was quenched with water and extracted with diethyl ether. The organic layer was dried over Na_2SO_4 and concentrated under reduced pressure. The crude was purified by flash chromatography (cyclohexane/ethyl acetate 8:2) to afford **126**. Yield: 36 % as orange foamy solid. Molecular formula: $\text{C}_9\text{H}_6\text{ClN}_5\text{O}$. Molecular weight: 235.63 g/mol. $^1\text{H NMR}$ (200 MHz, CDCl_3): δ 7.73 (d, $J = 8.5$ Hz, 2H, ArH), 7.51 (d, $J = 8.5$ Hz, 2H, ArH), 4.63 (s, 2H, CH_2) ppm. $^{13}\text{C NMR}$ (50 MHz, CDCl_3): δ 153.14, 148.91, 137.66, 129.94, 129.82, 123.65, 43.26 ppm. IR $\nu = 3435, 2961, 2921, 2110, 1449, 1412, 1350, 1096, 800$ cm^{-1} . MS (ESI) m/z 258.6 $[\text{M}+\text{Na}]^+$.

Synthesis of 1-(4-(4-chlorophenyl)-1,2,5-oxadiazol-3-yl)-methanamine hydrochloride (14 · HCl)

Intermediate **126** (0.4 mmol) was dissolved in methanol (3 mL) and the solution was degassed by bubbling argon for 10 minutes. Pd/C (10 % w/w) was then added and the mixture was stirred at room temperature under hydrogen atmosphere (20 atm) for 4 hours. After completion, the reaction mixture was filtered through Celite® and the organic layer was evaporated under *vacuum*. The crude was cooled by an ice bath and suspended in 2 M HCl in Et_2O (2 mL). The mixture was stirred for 10 minutes and then the precipitated brown solid **14 · HCl** was filtered and washed with Et_2O . Yield: 24 % as brown solid. Molecular formula: $\text{C}_9\text{H}_6\text{Cl}_2\text{N}_3\text{O}$. Molecular weight: 246.09 g/mol. $^1\text{H NMR}$ (300 MHz, acetone- d_6): δ 8.01 (d, $J = 8.8$ Hz, 2H, ArH), 7.63 (d, $J = 8.8$ Hz, 2H, ArH), 5.29 (s, 2H, CH_2) ppm. $^{13}\text{C NMR}$ (50 MHz, acetone- d_6): δ 153.57, 149.16, 136.74, 130.93, 129.64, 124.08, 40.47 ppm. IR $\nu = 3436, 2874, 2711, 2019, 1603, 1557, 1497, 1465, 1261, 1095, 830, 684$ cm^{-1} . MS (ESI) m/z 209.9 $[\text{M}]^+$.

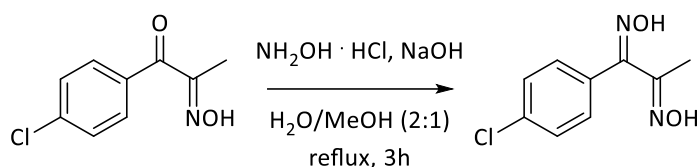
Procedure for the synthesis of 2-amino-2-(4-(4-chlorophenyl)-1,2,5-oxadiazol-3-yl)-1-phenylethan-1-one hydrochlorides (15a-c · HCl)

Synthesis of 1-(4-chlorophenyl)-2-(hydroxyimino)propan-1-one (127)



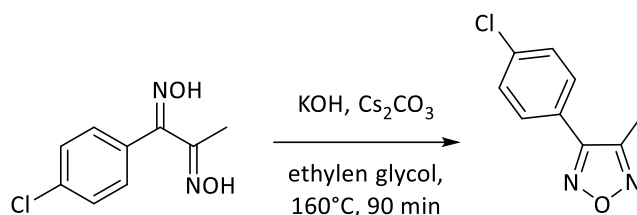
In a flame-dried flask under argon atmosphere, a solution of 4-chloropropiophenone (15 mmol) in a mixture of dry tetrahydrofuran (3 mL) and dry dichloromethane (3 mL) was cooled to -20°C. Chlorotrimethylsilane (15 mmol) and *tert*-butyl nitrite (19.5 mmol) were added dropwise. The solution was stirred at -20°C for 30 minutes and then at room temperature for 16 hours (TLC: cyclohexane/ethyl acetate (9:1) - R_f: 0.37). The solvent was evaporated under reduced pressure and the crude was firstly purified by flash chromatography with cyclohexane/ethyl acetate (95:5). Finally, intermediate **127** was recrystallized in chloroform/cyclohexane (1:5). Yield: 81 % as white solid (m.p. 118.5-119°C). Molecular formula: C₉H₈ClNO₂. Molecular weight: 197.62 g/mol. ¹H NMR (300 MHz, CDCl₃): δ 8.89 (br s, 1H, NOH exchanged with D₂O), 7.82 (dd, J₁ = 8.7 Hz, J₂ = 2.5 Hz, 2H, ArH), 7.38 (dd, J₁ = 8.7 Hz, J₂ = 2.5 Hz, 2H, ArH), 2.15 (s, 3H, CH₃) ppm. ¹³C NMR (75 MHz, CDCl₃): δ 190.80, 157.08, 139.63, 134.74, 131.97, 128.71, 10.40 ppm. IR ν = 3292, 3242, 2917, 1664, 1586, 1090, 997, 900, 840, 751 cm⁻¹. MS (ESI) *m/z* 195.9 [M-H]⁻.

Synthesis of 1-(4-chlorophenyl)propane-1,2-dione dioxime (128)



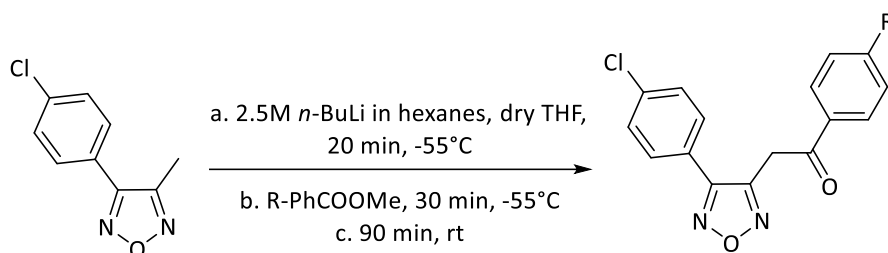
To a solution of hydroxylamine hydrochloride (150 mmol) and sodium hydroxide (150 mmol) in water (30 mL), a methanolic solution of **127** (11.6 mmol in 15 mL) was added and the mixture was heated to reflux for 3 hours (TLC: cyclohexane/ethyl acetate (8:2) - R_f: 0.28). After evaporation under reduced pressure of methanol, the remaining water layer was cooled with an ice-bath. The precipitated solid was collected by filtration and then washed with water and chloroform to give **128**. Yield: 55 % as white solid (m.p. 103.5-104°C). Molecular formula: C₉H₉ClN₂O₂. Molecular weight: 212.63 g/mol. ¹H NMR (300 MHz, CD₃OD) δ 7.89 (d, J = 8 Hz, 2H, ArH), 7.43 (d, J₁ = 8 Hz, 2H, ArH), 2.09 (s, 3H, CH₃) ppm. ¹³C NMR (75 MHz, CD₃OD): δ 154.36, 133.30, 130.66, 128.07, 127.81, 127.11, 8.62 ppm. IR ν = 3234, 3103, 2917, 1665, 1596, 1427, 1093, 982, 898, 741 cm⁻¹. MS (ESI) *m/z* 212.9 [M+H]⁺.

Synthesis of 3-(4-chlorophenyl)-4-methyl-1,2,5-oxadiazole (129)



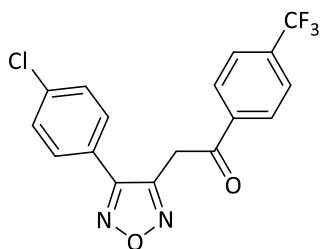
In a flame-dried flask, compound **128** (10 mmol) was added to a mixture of KOH (0.4 mmol) and Cs₂CO₃ (0.1 mmol) in ethylene glycol (4 mL) under argon atmosphere and the reaction was heated to 160°C for 90 minutes (TLC: cyclohexane/ethyl acetate (7:3) - R_f: 0.75). The mixture was dry-loaded on silica eluting with cyclohexane to remove the ethylene glycol. Afterwards, a purification of the crude by flash chromatography (cyclohexane/ethyl acetate 9:1) was performed to obtain **129**. Yield: 64 % as pale solid (m.p. 82-83°C). Molecular formula: C₉H₇ClN₂O. Molecular weight: 194.62 g/mol. ¹H NMR (300 MHz, CDCl₃): δ 7.61 (d, *J* = 8.4 Hz, 2H, ArH), 7.42 (d, *J* = 8.4 Hz, 2H, ArH), 2.50 (s, 3H, CH₃) ppm. ¹³C NMR (75 MHz, CDCl₃): δ 153.12, 149.71, 136.84, 129.62, 129.48, 124.75, 9.92 ppm. IR ν = 3436, 3100, 2917, 1920, 1603, 1445, 1386, 1096, 892, 729 cm⁻¹. MS (ESI) *m/z* 179.0 [M-CH₃]⁻.

General procedure for the synthesis of 2-(4-(4-chlorophenyl)-1,2,5-oxadiazol-3-yl)-1-phenylethan-1-ones (130a-c)



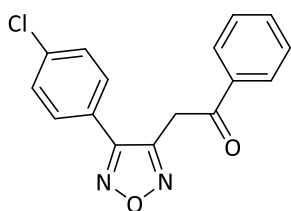
A solution of **129** (5 mmol) in dry tetrahydrofuran (3 mL) was placed in a flame-dried flask under argon atmosphere and, after cooling to -55°C, a solution of *n*-BuLi 2.7 M in heptane (5 mmol) was added dropwise. The reaction mixture was stirred for 20 minutes at -55°C and then the suitable methyl benzoate (5 mmol) was rapidly added. After 30 minutes the solution was allowed to warm to room temperature and stirred for 90 minutes. After completion, a saturated solution of NH₄Cl was added and then the solvent was evaporated under reduced pressure. The residue was diluted with water and extracted with dichloromethane. The organic phase was dried over Na₂SO₄, filtered and evaporated under *vacuum*. Purification of the crude residue by flash chromatography was performed to give the final product.

2-(4-(4-chlorophenyl)-1,2,5-oxadiazol-3-yl)-1-(4-trifluoromethyl)phenylethan-1-one (130a)



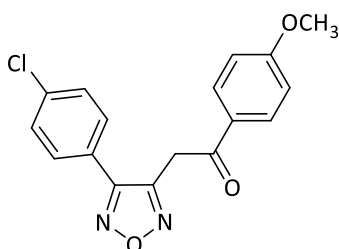
Yield: 68 % as yellow solid. Starting compounds: **129** and methyl 4-trifluoromethylbenzoate. TLC: cyclohexane/ethyl acetate (8:2) - R_f : 0.57. Purified by flash chromatography (eluent: cyclohexane/ethyl acetate 9:1). Molecular formula: $C_{17}H_{10}ClF_3N_2O_2$. Molecular weight: 366.72 g/mol. 1H NMR (300 MHz, $CDCl_3$): δ 8.10 (d, $J = 8.2$ Hz, 2H, ArH), 7.79 (d, $J = 8.2$ Hz, 2H, ArH), 7.56 (d, $J = 8.7$ Hz, 2H, ArH), 7.44 (d, $J = 8.7$ Hz, 2H, ArH), 4.64 (s, 2H, CH_2) ppm. ^{13}C NMR (75 MHz, $CDCl_3$): δ 192.42, 153.89, 147.73, 137.89, 137.00, 129.56, 129.33, 128.80, 126.09 (q, $J = 3.6$ Hz), 124.04, 34.16 ppm. ^{19}F NMR (282 MHz, $CDCl_3$): δ -63.32 (s, CF_3) ppm.

2-(4-(4-chlorophenyl)-1,2,5-oxadiazol-3-yl)-1-phenylethan-1-one (130b)

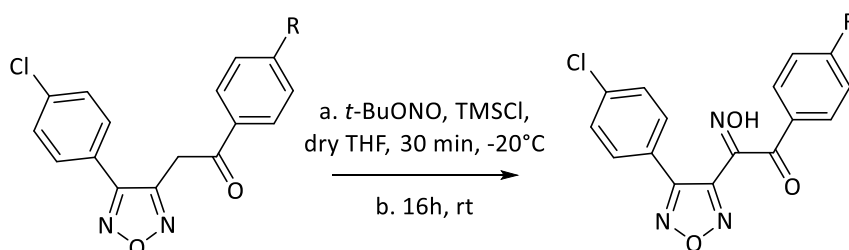


Yield: 89 % as light brown solid (m.p. 101.5-102°C). Starting compounds: **129** and methyl benzoate. TLC: cyclohexane/ethyl acetate (8:2) - R_f : 0.61. Purified by flash chromatography (eluent: cyclohexane/ethyl acetate 9:1). Molecular formula: $C_{16}H_{11}ClN_2O_2$. Molecular weight: 298.73 g/mol. 1H NMR (300 MHz, $CDCl_3$): δ 8.00 (d, $J = 7.3$ Hz, 2H), 7.66 (t, $J = 7.5$ Hz, 1H), 7.48-7.60 (m, 4H), 7.43 (d, $J = 8.4$ Hz, 2H), 4.64 (s, 2H) ppm. ^{13}C NMR (75 MHz, $CDCl_3$): δ 193.30, 153.95, 148.22, 136.83, 135.36, 134.29, 129.49, 129.39, 129.01, 128.40, 124.25, 33.89 ppm. IR $\nu = 3436, 3349, 2929, 1683, 1451, 1093, 992, 845, 689$ cm^{-1} . MS (ESI) m/z 320.9 $[M+Na]^+$.

2-(4-(4-chlorophenyl)-1,2,5-oxadiazol-3-yl)-1-(4-methoxy)phenylethan-1-one (130c)

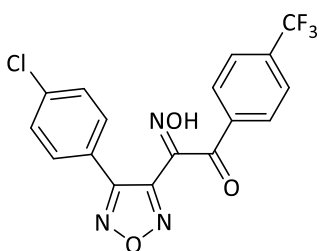


Yield: 40 % as orange solid. Starting compounds: **129** and methyl 4-methoxybenzoate. TLC: cyclohexane/ethyl acetate (8:2) - R_f : 0.29. Purified by flash chromatography (eluent: cyclohexane/ethyl acetate 8:2). Molecular formula: $C_{17}H_{13}ClN_2O_3$. Molecular weight: 328.06 g/mol. 1H NMR (300 MHz, $CDCl_3$): δ 7.95 (d, $J = 9.0$ Hz, 2H, ArH), 7.56 (d, $J = 8.7$ Hz, 2H, ArH), 7.38 (d, $J = 8.7$ Hz, 2H, ArH), 6.95 (d, $J = 9.0$ Hz, 2H, ArH), 4.57 (s, 2H, CH_2), 3.87 (s, 3H, OCH_3) ppm. ^{13}C NMR (50 MHz, $CDCl_3$): δ 191.94, 164.63, 154.18, 148.75, 136.99, 131.03, 129.66, 128.67, 124.58, 114.40, 55.82, 33.73 ppm.

Synthesis of 2-(4-(4-chlorophenyl)-1,2,5-oxadiazol-3-yl)-2-(hydroxyimino)-1-phenylethan-1-ones (131a-c)


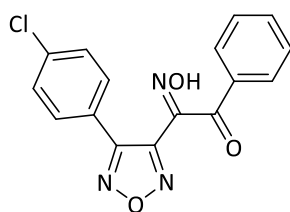
In a flame-dried flask under argon atmosphere, a solution of the starting compound (1 mmol) in dry tetrahydrofuran (3 mL) was cooled at -20°C and chlorotrimethylsilane (1 mmol) was added. After dripping *tert*-butyl nitrite (1.3 mmol), the solution was stirred at -20°C for 30 minutes and then at room temperature for 16 hours. The solvent was evaporated under reduced pressure and the purification of the crude was performed by flash chromatography to obtain the final product.

2-(4-(4-chlorophenyl)-1,2,5-oxadiazol-3-yl)-2-(hydroxyimino)-1-(4-trifluoromethyl)phenylethan-1-one (131a)



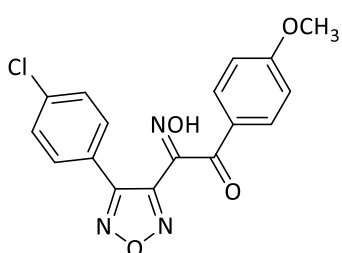
Yield: 68 % as white solid. Starting compound: **130a**. TLC: cyclohexane/ethyl acetate (8:2) - R_f : 0.36. Purified by flash chromatography (eluent: cyclohexane/ethyl acetate 8:2). Molecular formula: $\text{C}_{17}\text{H}_9\text{ClF}_3\text{N}_3\text{O}_3$. Molecular weight: 395.72 g/mol. ^1H NMR (300 MHz, CDCl_3): δ 8.90 (br s, 1H, NOH exchanged with D_2O), 8.16 (d, $J = 8.2$ Hz, 2H, ArH), 7.76 (d, $J = 8.2$ Hz, 2H, ArH), 7.58 (d, $J = 8.6$ Hz, 2H, ArH), 7.42 (d, $J = 8.6$ Hz, 2H, ArH) ppm. ^{13}C NMR (75 MHz, CDCl_3): δ 187.45, 153.42, 146.37, 144.44, 137.91, 137.63, 131.20, 130.07, 129.82, 129.22, 129.00, 125.60 (q, $J = 4.1$ Hz), 123.82 ppm. ^{19}F NMR (282 MHz, CDCl_3): δ -63.82 (s, CF_3) ppm.

2-(4-(4-chlorophenyl)-1,2,5-oxadiazol-3-yl)-2-(hydroxyimino)-1-phenylethan-1-one (131b)



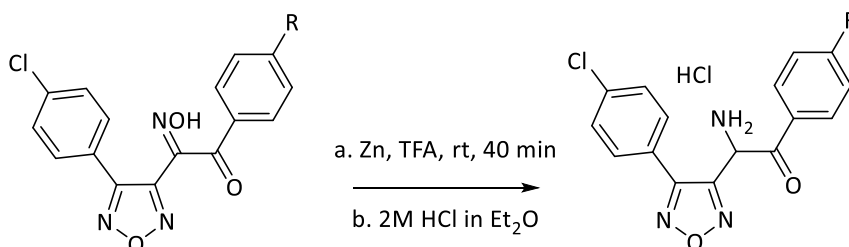
Yield: 76 % as white solid (m.p. 126.0 - 126.5°C). Starting compound: **130b**. TLC: cyclohexane/ethyl acetate (8:2) - R_f : 0.20. Purified by flash chromatography (gradient elution, from 10% to 20% ethyl acetate/cyclohexane). Molecular formula: $\text{C}_{16}\text{H}_{10}\text{ClN}_3\text{O}_3$. Molecular weight: 327.72 g/mol. ^1H NMR (300 MHz, CDCl_3): δ 8.49 (br s, 1H, NOH exchanged with D_2O), 8.09 (dd, $J_1 = 7.4$ Hz, $J_2 = 1.0$ Hz, 2H, ArH), 7.58-7.70 (m, 3H, ArH), 7.47-7.54 (m, 2H, ArH), 7.42 (dd, $J_1 = 8.6$ Hz, $J_2 = 0.9$ Hz, 2H, ArH) ppm. ^{13}C NMR (75 MHz, CDCl_3): δ 188.52, 153.22, 145.85, 144.69, 137.24, 134.73, 134.27, 130.75, 129.50, 128.81, 128.53, 123.62 ppm. IR $\nu = 3324, 3077, 2918, 1664, 1599, 1450, 1092, 878, 694$ cm^{-1} . MS (ESI) m/z 326.8 [M-H] $^-$.

2-(4-(4-chlorophenyl)-1,2,5-oxadiazol-3-yl)-2-(hydroxyimino)-1-(4-trifluoromethyl)phenylethan-1-one (131c)



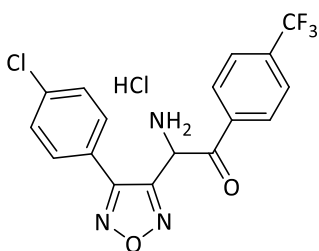
Yield: 84 % as yellow solid. Starting compounds: **130c**. TLC: cyclohexane/ethyl acetate (8:2) - R_f : 0.13. Purified by flash chromatography (eluent: cyclohexane/ethyl acetate 8:2). Molecular formula: $C_{17}H_{12}ClN_3O_4$. Molecular weight: 357.75 g/mol. 1H NMR (300 MHz, acetone- d_6): δ 12.65 (br s, 1H, NOH exchanged with D_2O), 8.16 (d, $J = 9.0$ Hz, 2H, ArH), 7.77 (d, $J = 8.8$ Hz, 2H, ArH), 7.59 (d, $J = 8.7$ Hz, 2H, ArH), 7.10 (d, $J = 9.0$ Hz, 2H, ArH), 3.94 (s, 3H, OCH_3) ppm. ^{13}C NMR (50 MHz, acetone- d_6): δ 186.54, 164.78, 153.65, 146.26, 145.40, 136.94, 133.30, 129.75, 129.37, 128.20, 124.58, 114.40, 55.46 ppm.

Synthesis of 2-amino-2-(4-(4-chlorophenyl)-1,2,5-oxadiazol-3-yl)-1-phenylethan-1-one hydrochlorides (15a-c · HCl)



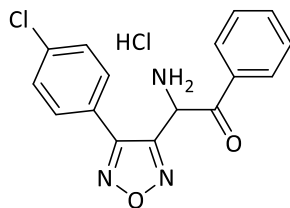
To a solution of the suitable 2-(hydroxyimino)-1-phenylethan-1-one (0.15 mmol) in trifluoroacetic acid (1.5 mL), zinc dust (0.81 mmol) was slowly added on an ice bath. The mixture was stirred at room temperature for 20-40 minutes.

2-amino-2-(4-(4-chlorophenyl)-1,2,5-oxadiazol-3-yl)-1-(4-trifluoromethyl)phenylethan-1-one hydrochloride (15a · HCl)



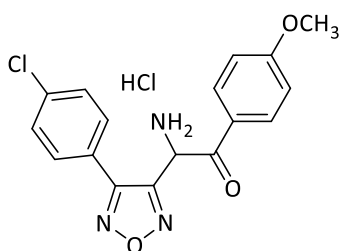
Reaction time: 20 minutes. Work up: The reaction was cooled with an ice bath and a solution of 2 M HCl in Et_2O was added. After 20 minutes, hexane was used for the precipitation of the hydrochloride salt. The solid was filtered and washed with Et_2O (3 mL). Yield: 43 % as orange solid. Starting compound: **131a**. Molecular formula: $C_{17}H_{12}Cl_2F_3N_3O_2$. Molecular weight: 418.20 g/mol. 1H NMR (300 MHz, CD_3OD): δ 7.78 (d, $J = 8.2$ Hz, 2H, ArH), 7.57-7.70 (m, 6H, ArH), 6.79 (s, 1H, CH) ppm. ^{13}C NMR (75 MHz, CD_3OD): δ 187.07, 153.07, 147.86, 136.55, 130.18, 129.64, 129.49, 129.36, 128.92, 128.11, 125.08 (q, $J = 3.9$ Hz), 122.64, 49.30 ppm. ^{19}F NMR (282 MHz, CD_3OD): δ -64.88 (s, CF_3) ppm. MS (ESI) m/z 382.5 $[M+H]^+$.

2-amino-2-(4-(4-chlorophenyl)-1,2,5-oxadiazol-3-yl)-1-phenylethan-1-one hydrochloride (15b · HCl)



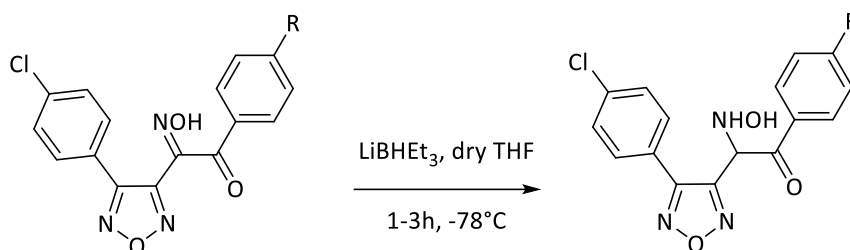
Reaction time: 40 minutes. Work up: the reaction was cooled with an ice bath and a solution of 2 M NaOH was added until pH=7-8. The insoluble material was removed by filtration and washed with dichloromethane (2 mL). The organic phase was separated, dried over dry Na₂SO₄, filtered and evaporated under reduced pressure. The obtained yellow oil was cooled and treated with 2 M HCl in Et₂O (2 mL) and the mixture was stirred for 10 minutes. The precipitated solid was filtered and washed with Et₂O (3 mL) affording **15b** as hydrochloride salt. Yield: 85 % as white solid. Starting compound: **131b**. Molecular formula: C₁₆H₁₃Cl₂N₃O₂. Molecular weight: 350.20 g/mol. ¹H NMR (300 MHz, CD₃OD): δ 7.55-7.70 (m, 7H, ArH), 7.32-7.38 (m, 2H, ArH), 6.69 (s, 1H, CH) ppm. ¹³C NMR (75 MHz, CD₃OD): δ 188.94, 153.08, 147.99, 137.60, 134.83, 132.45, 130.20, 129.6, 128.85, 128.28, 122.35, 49.30 ppm. IR ν = 3411, 3208, 2850, 1702, 1689, 1599, 1449, 1093, 995, 688 cm⁻¹. MS (ESI) *m/z* 314.1 [M + H]⁺.

2-amino-2-(4-(4-chlorophenyl)-1,2,5-oxadiazol-3-yl)-1-(4-methoxy)phenylethan-1-one hydrochloride (15c · HCl)



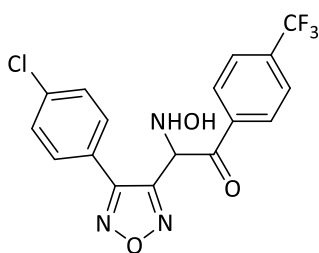
Work up: The reaction was cooled with an ice bath and a solution of 2 M HCl in Et₂O was added. The resulting precipitated solid was filtered and washed with Et₂O (3 mL) affording **15c** as hydrochloride salt. Yield: 79 % as light yellow solid. Starting compound: **131c**. Molecular formula: C₁₇H₁₅Cl₂N₃O₃. Molecular weight: 380.23 g/mol. ¹H NMR (200 MHz, CD₃OD): δ 7.58-7.67 (m, 4H, ArH), 7.57 (d, *J* = 9.1 Hz, 2H, ArH), 6.86 (d, *J* = 9.0 Hz, 2H, ArH), 6.60 (s, 1H, CH), 3.84 (s, 3H, OCH₃) ppm. ¹³C NMR (50 MHz, CD₃OD): δ 187.20, 165.61, 153.21, 148.50, 137.74, 132.97, 130.45, 129.76, 125.26, 122.67, 114.35, 55.17, 48.83 ppm. IR ν = 3413, 3193, 2931, 1692, 1670, 1601, 1428, 1259, 1094, 994, 827 cm⁻¹. MS (ESI) *m/z* 344.1 [M+H]⁺.

Synthesis of 2-(4-(4-chlorophenyl)-1,2,5-oxadiazol-3-yl)-2-(hydroxyamino)-1-phenylethan-1-ones (16a-c)



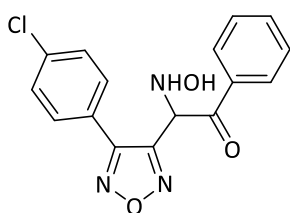
In a flame-dried flask under nitrogen atmosphere, a solution of **131a-c** (0.05 mmol) in dry tetrahydrofuran (1 mL) was cooled at -78°C and lithium triethylborohydride in tetrahydrofuran (1.7 M, 0.08 mL) was added. The solution was stirred at -78°C for 1-3 hours (TLC: cyclohexane/ethyl acetate (7:3) - R_f : 0.26). A saturated solution of NH_4Cl was added and the resulting mixture was filtered, dried over Na_2SO_4 and concentrated under reduced pressure. The crude was purified by flash chromatography (cyclohexane/ethyl acetate 7:3) affording the finale product.

2-(4-(4-chlorophenyl)-1,2,5-oxadiazol-3-yl)-2-(hydroxyamino)-1-(4-(trifluoromethyl)phenyl)ethan-1-one (16a)



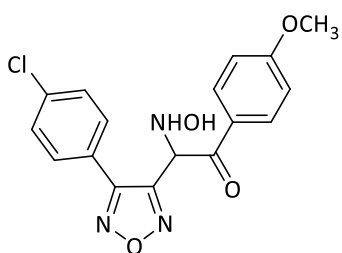
Reaction time: 3 hours. Yield: 97 % as white solid. Starting compound: **131a**. Molecular formula: $\text{C}_{17}\text{H}_{11}\text{ClF}_3\text{N}_3\text{O}_3$. Molecular weight: 397.74 g/mol. ^1H NMR (300 MHz, CD_3OD): δ 7.41-7.49 (m, 4H, ArH), 7.32-7.41 (m, 4H, ArH), 5.79 (s, 1H, CH) ppm. ^{13}C NMR (75 MHz, CD_3OD): δ 153.35, 147.75, 145.75, 143.92, 136.55, 130.00, 129.58, 129.20, 128.83, 126.86, 124.80 (d, $J = 3.7$ Hz), 124.36, 73.43 ppm. ^{19}F NMR (282 MHz, CD_3OD): δ -64.44 (s, CF_3) ppm. IR $\nu = 3469, 2963, 2461, 1714, 1621, 1605, 1452, 1418, 1328, 1262, 1166, 1066, 802$ cm^{-1} . MS (ESI) m/z 395.9 [M - H] $^-$.

2-(4-(4-chlorophenyl)-1,2,5-oxadiazol-3-yl)-2-(hydroxyamino)-1-phenylethan-1-one (16b)



Reaction time: 1 hour. Yield: 96 % as off-white solid. Starting compound: **131b**. Molecular formula: $\text{C}_{16}\text{H}_{12}\text{ClN}_3\text{O}_3$. Molecular weight: 329.74 g/mol. ^1H NMR (300 MHz, CD_3OD): δ 7.40 (d, $J = 8.7$ Hz, 2H, ArH), 7.33 (d, $J = 8.7$ Hz, 2H, ArH), 7.08-7.26 (m, 5H, ArH), 5.71 (s, 1H, CH) ppm. ^{13}C NMR (75 MHz, CD_3OD): δ 153.16, 147.94, 145.71, 139.18, 136.11, 128.94, 128.44, 127.80, 127.61, 126.05, 124.30, 73.93 ppm.

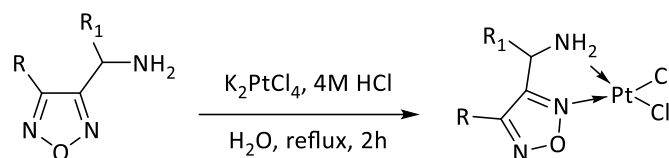
2-(4-(4-chlorophenyl)-1,2,5-oxadiazol-3-yl)-2-(hydroxyamino)-1-(4-methoxyphenyl)ethan-1-one (16c)



Reaction time: 2 hours. Yield: 74 % as grey solid. Starting compound: **131c**.

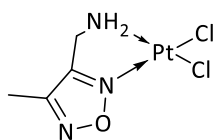
Molecular formula: C₁₇H₁₄ClN₃O₄. Molecular weight: 359.77 g/mol. ¹H NMR (300 MHz, CD₃OD): δ 7.36 (d, *J* = 8.6 Hz, 2H, ArH), 7.32 (d, *J* = 8.8 Hz, 1H, ArH), 7.02 (d, *J* = 8.8 Hz, 1H, ArH), 6.64 (d, *J* = 8.6 Hz, 1H, ArH), 5.63 (s, 1H, CH), 3.70 (s, 3H, OCH₃) ppm. ¹³C NMR (75 MHz, CD₃OD): δ 159.48, 153.15, 148.25, 145.70, 136.05, 130.76, 129.04, 128.40, 127.21, 124.17, 113.12, 73.56, 54.19 ppm.

General procedure for the synthesis of platinum complexes



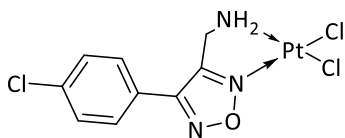
K_2PtCl_4 (1 mmol) was dissolved in 10 mL of distilled water. The ligand (1.1 mmol), when available in dihydrochloride form, was preventively neutralized with $NaHCO_3$ aqueous solution and then dripped into the platinate solution. 4 M HCl (10 mmol) was added and the mixture was refluxed under nitrogen atmosphere for 12 hours. After cooling to room temperature, the product was filtered as a solid and washed extensively with water. The precipitate was then dissolved in diethyl ether and crystallized for slow diffusion of hexane.

Pt-13



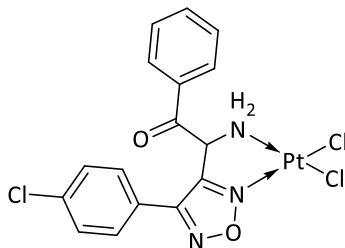
Yield: 62 % as pale-yellow solid. Starting compound: **13**. Molecular formula: $C_4H_7Cl_2N_3OPt$. Molecular weight: 377.96 g/mol. 1H NMR (300 MHz, $DMF-d_7$) δ 6.72 (br, 2H), 4.34 (t, $J = 6.3$ Hz, 2H), 2.61 (s, 3H). ^{13}C NMR (75 MHz, $DMF-d_7$) 163.18, 153.94, 42.79, 8.64. ^{195}Pt NMR (300 MHz, $DMF-d_7$) δ -2065. Elemental analysis for $C_4H_7Cl_2N_3OPt$: calculated C, 12.67; H, 1.86; N, 11.09; found C, 12.72; H, 1.78; N, 10.98. MS (ESI) m/z 365.9 $[M-Cl+Na]^+$.

Pt-14

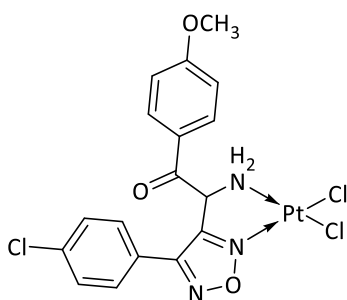


Yield: 45 % as brown solid. Starting compound: **14** · HCl. Molecular formula: $C_9H_8Cl_3N_3OPt$. Molecular weight: 473.94 g/mol. 1H NMR (300 MHz, $DMF-d_7$) δ 7.98 (d, $J = 8.8$ Hz, 2H), 7.76 (d, $J = 8.8$ Hz, 2H), 6.94 (br, 2H), 4.61 (t, $J = 6.0$ Hz, 2H). ^{13}C NMR (75 MHz, $DMF-d_7$) 137.78, 130.49, 130.19, 125.25, 123.31, 116.47, 44.35. ^{195}Pt NMR (300 MHz, $DMF-d_7$) δ -2075. Elemental analysis for $C_9H_8Cl_3N_3OPt$: calculated C, 22.73; H, 1.70; N, 8.84; found C, 23.01; H, 1.75; N, 8.89. MS (ESI) m/z 461.9 $[M-Cl+Na]^+$.

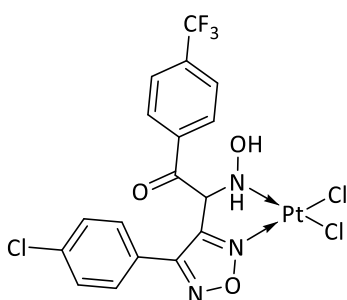
Pt-15b



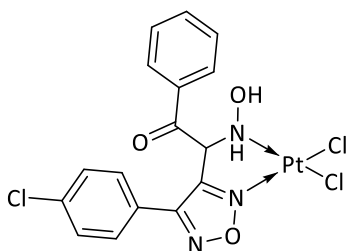
Yield: 61 % as olive-green solid. Starting compound: **15b** · HCl. Molecular formula: $C_{16}H_{12}Cl_3N_3O_2Pt$. Molecular weight: 577.96 g/mol. 1H NMR (300 MHz, $CDCl_3$) δ 7.77 (d, $J = 8.5$ Hz, 2H), 7.50-7.44 (m, 5H), 7.25-7.21 (m, 2H), 6.20 (t, $J = 5.8$ Hz, 1H), 5.46-5.41 (m, 1H), 4.88-4.85 (m, 1H). ^{13}C NMR (75 MHz, $CDCl_3$) 191.27, 152.84, 149.45, 138.06, 135.09, 132.73, 130.44, 130.35, 130.23, 130.19, 129.60, 129.51, 129.47, 129.32, 129.23, 128.93, 55.15. ^{195}Pt NMR (300 MHz, $CDCl_3$) δ -2068. Elemental analysis for $C_{16}H_{12}Cl_3N_3O_2Pt$: calculated C, 33.15; H, 2.09; N, 7.25; found C, 33.58; H, 2.18; N, 7.54. MS (ESI) m/z 578.5 $[M+H]^+$.

Pt-15c

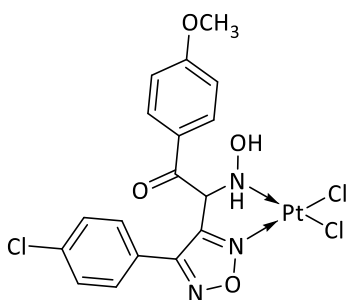
Yield: 44 % as brown solid. Starting compound: **15c** · HCl. Molecular formula: $C_{17}H_{14}Cl_3N_3O_3Pt$. Molecular weight: 609.75 g/mol. Elemental analysis for $C_{17}H_{14}Cl_3N_3O_3Pt$: calculated C, 33.49; H, 2.81; N, 6.89; found C, 33.78; H, 2.84; N, 6.67. MS (ESI) m/z 509.2 $[M-2Cl-OCH_3]^+$.

Pt-16a

Yield: 37 % as brown solid. Starting compound: **16a**. Molecular formula: $C_{17}H_{11}Cl_3F_3N_3O_3Pt$. Molecular weight: 663.72 g/mol. Elemental analysis for $C_{17}H_{11}Cl_3F_3N_3O_3Pt$: calculated C, 30.76; H, 1.67; N, 6.33; found C, 30.93; H, 1.97; N, 6.54. MS (ESI) m/z 701.4 $[M+K]^+$.

Pt-16b

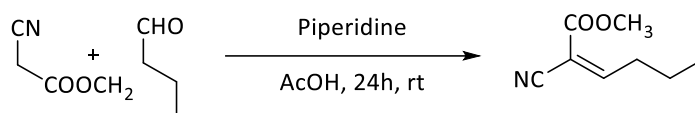
Yield: 51 % as brick-red solid. Starting compound: **16b**. Molecular formula: $C_{16}H_{12}Cl_3N_3O_3Pt$. Molecular weight: 595.72 g/mol. Elemental analysis for $C_{16}H_{12}Cl_3N_3O_3Pt$: calculated C, 32.26; H, 2.03; N, 7.05; found C, 32.98; H, 2.66; N, 7.54. MS (ESI) m/z 596.5 $[M+H]^+$.

Pt-16c

Starting compound: **16c**. Molecular formula: $C_{17}H_{14}Cl_3N_3O_4Pt$. Molecular Weight: 625.75 g/mol. Its characterization is ongoing.

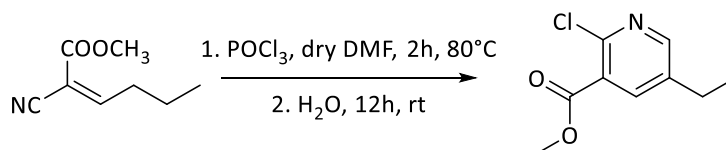
Procedures for the synthesis of methyl 1-(2-(1H-indol-3-yl)ethyl)-5-(1-hydroxyethyl)-1,4,5,6-tetrahydropyridine-3-carboxylates (19,20)

Synthesis of methyl 2-cyano-2-hexenoate (134)

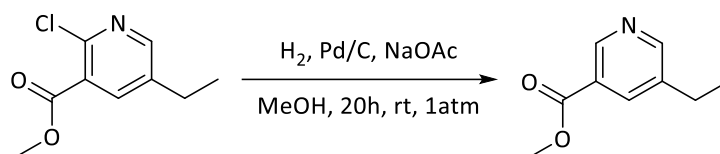


In a flame-dried flask, butyraldehyde (4.12 mmol), methyl cyanoacetate (4.04 mmol), acetic acid (9.52 mmol) and piperidine (0.162 mmol) were added under nitrogen atmosphere and stirred for 24 hours (TLC: cyclohexane/ethyl acetate (65:35) - R_f : 0.73). After water addition, the mixture was extracted with dichloromethane and the collected organic layers were dried over Na_2SO_4 and concentrated under reduced pressure to give **134**. Yield 95 % as colorless oil. Molecular formula: $\text{C}_8\text{H}_{11}\text{NO}_2$. Molecular weight: 153.18 g/mol. ^1H NMR (300 MHz, CDCl_3): δ 7.62 (t, $J = 7.9$ Hz, 1H, CH), 3.82 (s, 3H, OCH_3), 2.50 (q, $J = 7.5$ Hz, 2H, CH_2), 1.56 (dq, $J_1 = 14.7$, $J_2 = 7.3$ Hz, 2H, CH_2), 0.96 (t, $J = 7.4$ Hz, 3H, CH_3) ppm. ^{13}C NMR (75 MHz, CDCl_3): δ 163.85, 161.71, 113.55, 109.51, 53.01, 33.73, 21.14, 13.60 ppm.

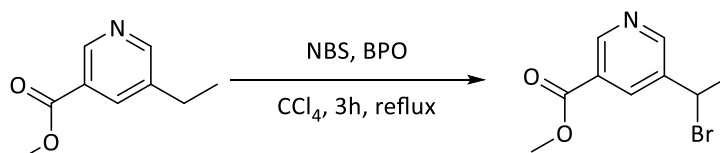
Synthesis of methyl 2-chloro-5-ethylnicotinate (135)



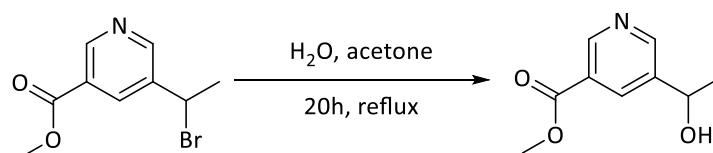
A solution of compound **134** (3.56 mmol) in dry *N,N*-dimethylformamide (2.28 mL) was cooled at 0°C and POCl_3 (7.13 mmol) was dripped. The reaction mixture was heated at 80°C for 2 hours and then ice-water was added to the cooled solution which was stirred overnight at room temperature (TLC: cyclohexane/ethyl acetate (8:2) - R_f : 0.50). The mixture was extracted with ethyl acetate and concentrated *in vacuo* to give a black oil. The residue was purified by flash chromatography (eluting with cyclohexane/ethyl acetate 9:1) to obtain compound **135**. Yield 16 % as light-brown oil. Molecular formula: $\text{C}_9\text{H}_{10}\text{ClNO}_2$. Molecular weight: 199.63 g/mol. ^1H NMR (300 MHz, CDCl_3): δ 8.35 (d, $J = 2.5$ Hz, 1H, ArH), 7.99 (d, $J = 2.5$ Hz, 1H, ArH), 3.95 (s, 3H, OCH_3), 2.69 (q, $J = 7.6$ Hz, 2H, CH_2), 1.27 (t, $J = 7.6$ Hz, 3H, CH_3) ppm. ^{13}C NMR (75 MHz, CDCl_3): δ 164.9, 151.2, 146.7, 139.4, 138.1, 125.9, 52.6, 24.9, 14.7 ppm.

Synthesis of methyl 5-ethylnicotinate (136)

The suspension of intermediate **135** (8.31 mmol), palladium on carbon (10%) and sodium acetate (10.39 mmol) in methanol (55 mL) was hydrogenated for 20 hours (TLC: cyclohexane/ethyl acetate (8:2) - R_f : 0.18) at room temperature. The mixture was filtered on Celite® and concentrated under reduced pressure to give a white solid residue which was purified by flash chromatography (eluting with cyclohexane/ethyl acetate 8:2) to give the product **136**. Yield 87 % as light-yellow oil. Molecular formula: $\text{C}_9\text{H}_{11}\text{NO}_2$. Molecular weight: 165.19 g/mol. ^1H NMR (300 MHz, CDCl_3): δ 9.00 (d, $J = 1.7$ Hz, 1H, ArH), 8.57 (d, $J = 1.7$ Hz, 1H, ArH), 8.08 (t, $J = 1.7$ Hz, 1H, ArH), 3.90 (s, 3H, OCH_3), 2.67 (q, $J = 7.6$ Hz, 2H, CH_2), 1.24 (t, $J = 7.6$ Hz, 3H, CH_3) ppm. ^{13}C NMR (75 MHz, CDCl_3): δ 165.97, 153.23, 148.27, 139.03, 136.12, 125.62, 52.27, 25.78, 15.03 ppm.

Synthesis of methyl 5-(1'-bromoethyl)nicotinate (137)

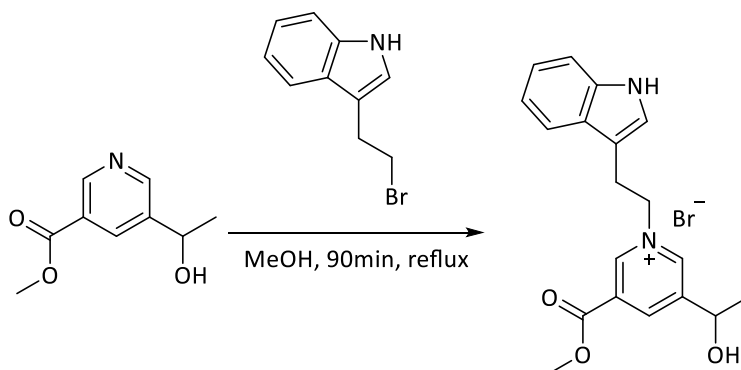
The solution of compound **136** (7.20 mmol), *N*-bromosuccinimide (9.58 mmol) and benzoyl peroxide (0.072 mmol) in CCl_4 (36 mL) was refluxed for 3 hours (TLC: cyclohexane/ethyl acetate (7:3) - R_f : 0.30). The precipitate was filtered and the solution was evaporated under *vacuum*. The residue was extracted with NaHCO_3 and dichloromethane, and the organic layer was dried over Na_2SO_4 and concentrated under reduced pressure to give the product **137**. Yield 65 % as orange oil. Molecular formula: $\text{C}_9\text{H}_{10}\text{BrNO}_2$. Molecular weight: 244.09 g/mol. ^1H NMR (300 MHz, CDCl_3): δ 9.11 (d, $J = 1.7$ Hz, 1H, ArH), 8.81 (d, $J = 1.7$ Hz, 1H, ArH), 8.36 (t, $J = 1.7$ Hz, 1H, ArH), 5.21 (q, $J = 7.0$ Hz, 1H, CH), 3.96 (s, 3H, CH_3), 2.07 (d, $J = 7.0$ Hz, 3H, CH_3) ppm. ^{13}C NMR (75 MHz, CDCl_3): δ 165.2, 151.7, 150.2, 138.8, 135.2, 125.9, 52.4, 44.2, 26.2 ppm.

Synthesis of methyl 5-(1'-hydroxyethyl)nicotinate (138)

Intermediate **137** (4.72 mmol) was refluxed in a solution of water (157 mL) and acetone (63 mL) for 20 hours (TLC: cyclohexane/ethyl acetate (7:3) - R_f : 0.06). After cooling the mixture was extracted with dichloromethane and the collected layers concentrated under *vacuum*. The product was purified by flash chromatography (eluting with cyclohexane/ethyl acetate 7:3) to give the compound **138**. Yield 74 % as colorless solid (m.p. 52-53°C). Molecular formula: $\text{C}_9\text{H}_{11}\text{NO}_3$. Molecular weight: 181.19 g/mol. ^1H NMR (300

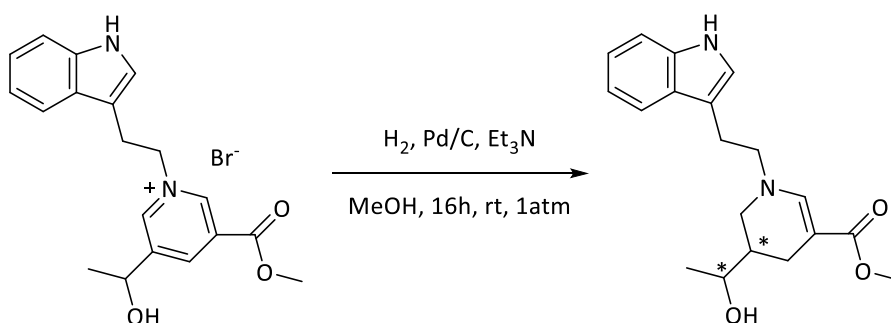
MHz, CDCl₃): δ 9.09 (d, J = 1.7 Hz, 1H, ArH), 8.76 (d, J = 1.7 Hz, 1H, ArH), 8.33 (t, J = 1.7 Hz, 1H, ArH), 5.02 (q, J = 6.5 Hz, 1H, CH), 3.95 (s, 3H, OCH₃), 1.55 (d, J = 6.5 Hz, 3H, CH₃) ppm.

Synthesis of 1-(2-(1H-indol-3-yl)ethyl)-3-(1-hydroxyethyl)-5-(methoxycarbonyl)pyridin-1-ium bromide (139)



The solution of compound **138** (1.28 mmol) and 3-(2-bromoethyl)-indole (1.38 mmol) in methanol (25 mL) was refluxed for 90 minutes. The solution was concentrated under reduced pressure and diethyl ether was added. The resulting yellow precipitate was filtered and recrystallized from methanol to give the pure salt **139**. Yield 95 % as yellow solid (m.p. 222-224°C). Molecular formula: C₁₉H₂₁BrN₂O₃. Molecular weight: 405.29 g/mol. ¹H NMR (300 MHz, CD₃OD): δ 9.02 (s, 1H, ArH), 8.85 (s, 1H, ArH), 8.60 (s, 1H, ArH), 7.35 (dd, J_1 = 8.1, J_2 = 1 Hz, 1H, ArH), 7.22 (dd, J_1 = 8.1, J_2 = 1 Hz, 1H, ArH), 7.10 (dt, J_1 = 8.1, J_2 = 1 Hz, 1H, ArH), 6.99 (s, 1H, ArH), 6.94 (dt, J_1 = 8.1, J_2 = 1.0 Hz, 1H, ArH), 4.97 (t, J = 6.3 Hz, 2H, CH₂), 4.88 (q, J = 6.7 Hz, 1H, CH), 3.96 (s, 3H, OCH₃), 3.47 (t, J = 6.3 Hz, 2H, CH₂), 1.21 (d, J = 6.7 Hz, 3H, CH₃) ppm. ¹³C NMR (75 MHz, CD₃OD): δ 147.88, 144.58, 143.59, 141.57, 136.63, 129.90, 126.66, 123.87, 121.63, 119.06, 116.71, 111.38, 107.64, 65.47, 63.08, 26.73, 23.51 ppm.

Synthesis of methyl 1-(2-(1H-indol-3-yl)ethyl)-5-(1-hydroxyethyl)-1,4,5,6-tetrahydropyridine-3-carboxylates (19,20)



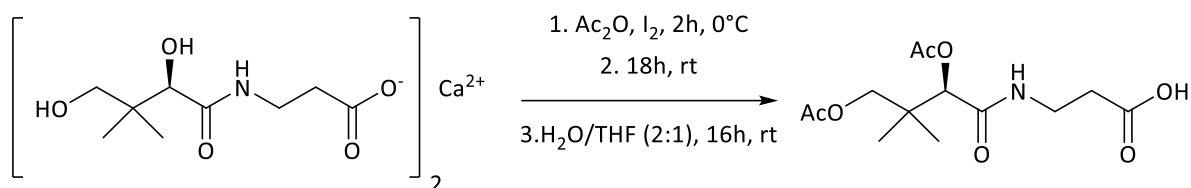
The suspension of compound **139** (1.48 mmol), palladium on carbon (10 % w/w) and triethylamine (0.25 mL) in methanol (50 mL) was hydrogenated for 16 hours. The mixture was filtered on Celite® and concentrated *in vacuo*. The residue was purified by flash chromatography (eluting with dichloromethane/methanol 98:2) to give the couple of diastereoisomers (**19** and **20**). Yield 80 % (**19/20**: 1:1) as light-yellow solids. Molecular formula: C₁₉H₂₄N₂O₃. Molecular weight: 328.41 g/mol.

19 - TLC: dichloromethane/methanol (95:5) - R_f : 0.11. ^1H NMR (300 MHz, CDCl_3): δ 8.14 (br s, 1H, NH exchanged with D_2O), 7.57 (d, $J = 7.7$ Hz, 1H, ArH), 7.35-7.38 (m, 2H, ArH), 7.21 (t, $J = 7.3$ Hz, 1H, ArH), 7.13 (t, $J = 7.3$ Hz, 1H, ArH), 6.98 (d, $J = 2.1$ Hz, 1H, ArH), 3.70-3.80 (m, 1H; CH), 3.65 (s, 3H, OCH_3), 3.44 (t, $J = 7.3$ Hz, 2H, CH_2), 2.90-3.09 (m, 4H, CH_2 and NCH_2), 2.49 (dd, $J_1 = 15.5$, $J_2 = 3.6$ Hz, 1H, CH_2), 2.01 (dd, $J_1 = 15.6$, $J_2 = 10.3$ Hz, 1H, CH_2), 1.68-1.80 (m, 1H, CH), 1.65 (br s, 1H, OH exchanged with D_2O), 1.17 (d, $J = 6.4$ Hz, 3H, CH_3) ppm. ^{13}C NMR (75 MHz, CDCl_3): δ 169.01, 145.99, 136.21, 127.13, 122.20, 122.01, 119.49, 118.54, 112.56, 111.24, 70.00, 56.45, 50.52, 48.11, 39.68, 24.94, 23.40, 21.91 ppm.

20 - TLC: dichloromethane/methanol (95:5) - R_f : 0.08. ^1H NMR (300 MHz, CDCl_3): δ 8.22 (br s, 1H, NH exchanged with D_2O), 7.58 (d, $J = 7.7$ Hz, 1H, ArH), 7.34-7.37 (m, 2H, ArH), 7.20 (t, $J = 7.4$ Hz, 1H, ArH), 7.13 (t, $J = 7.4$ Hz, 1H, ArH), 6.96 (d, $J = 2.1$ Hz, 1H, ArH), 3.65 (s, 3H, OCH_3), 3.48-3.58 (m, 1H, CH), 3.44 (t, $J = 7.0$ Hz, 2H, CH_2), 3.32-3.38 (m, 1H, CH_2), 2.92-3.09 (m, 4H, CH_2 and OH exchanged with D_2O), 2.38 (dd, $J_1 = 15.6$, $J_2 = 4.9$ Hz, 1H, CH_2), 1.88 (dd, $J_1 = 15.5$, $J_2 = 10.0$ Hz, 1H, CH_2), 1.62-1.72 (m, 1H, CH), 1.25 (d, $J = 6.4$ Hz, 3H, CH_3) ppm. ^{13}C NMR (75 MHz, CDCl_3): δ 169.13, 147.01, 136.20, 127.02, 122.19, 122.00, 119.40, 118.49, 112.40, 111.20, 69.05, 56.28, 50.41, 47.86, 38.40, 23.19, 23.14, 21.86 ppm.

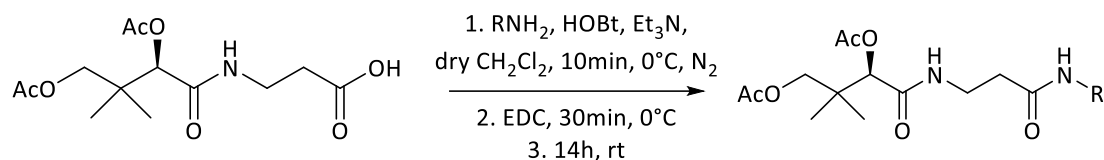
General procedures for the synthesis of 21-23

Synthesis of *O,O'*-diacetyl-D-pantothenic acid (**140**)

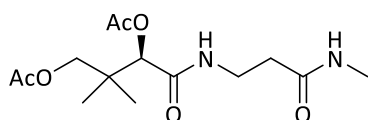


A mixture of D-pantothenic acid calcium salt (1.10 mmol) and a catalytic amount of I_2 (0.15 mmol) suspended in acetic anhydride (10 mL) was stirred at 0°C for 2 hours and then left at room temperature for 18 hours. The cooled solution was concentrated under reduced pressure by azeotrope with toluene. The obtained red oil was dissolved in dichloromethane (15 mL) and washed with sodium thiosulfate (5 mL). The organic layer was dried over Na_2SO_4 and concentrated under *vacuum* to give a yellow oil. The latter was dissolved in a solution of THF and water (2:1, 5 mL) and stirred at room temperature for 16 hours. The product was concentrated under reduced pressure to obtain **140**. Yield 85 % as light-yellow oil. Molecular formula: $\text{C}_{13}\text{H}_{21}\text{NO}_7$. Molecular weight: 303.31 g/mol. ^1H NMR (300 MHz, CDCl_3): δ 7.80 (br s, 1H, COOH exchanged with D_2O), 6.77 (br t, $J = 5.7$ Hz, 1H, NH exchanged with D_2O), 4.91 (s, 1H, CH), 3.99 (d, $J = 11.1$ Hz, 1H, CH_2), 3.81 (d, $J = 11.1$ Hz, 1H, CH_2), 3.33-3.62 (m, 2H, CH_2), 2.57 (t, $J = 5.5$ Hz, 2H, CH_2), 2.11 (s, 3H, CH_3CO), 2.06 (s, 3H, CH_3CO), 1.04 (s, 3H, $\text{C}(\text{CH}_3)_2$), 1.00 (s, 3H, $\text{C}(\text{CH}_3)_2$) ppm. ^{13}C NMR (75 MHz, CDCl_3): δ 176.28, 171.17, 170.00, 168.37, 76.84, 69.28, 37.16, 34.59, 33.57, 21.28, 20.80, 20.75, 20.64 ppm.

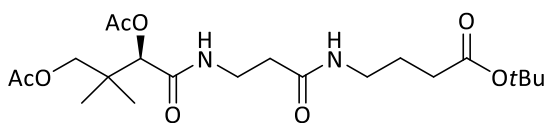
Synthesis of *O,O'*-diacetyl-D-pantothenamides (**141,144**)



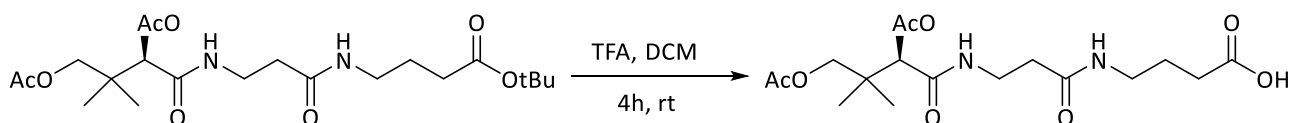
The solution of compound **138** (1.60 mmol), the proper amine (1.92 mmol) and 1-hydroxybenzotriazole hydrate (1.92 mmol) in dry dichloromethane (9.31 mL) was stirred under nitrogen atmosphere in presence of triethylamine (3.21 mmol). The solution was cooled to 0°C and *N*-(3-dimethylaminopropyl)-*N'*-ethylcarbodiimide hydrochloride (1.60 mmol) was added. The reaction mixture was stirred at 0°C for 30 minutes and then warmed to room temperature for 14 hours. The mixture was diluted with dichloromethane and washed firstly with 0.1 M HCl and then saturated NaHCO_3 . The organic phase was dried over Na_2SO_4 and concentrated under reduced pressure to obtain an oil.

*methyl O,O'-diacetyl-D-pantothenamide (141)*

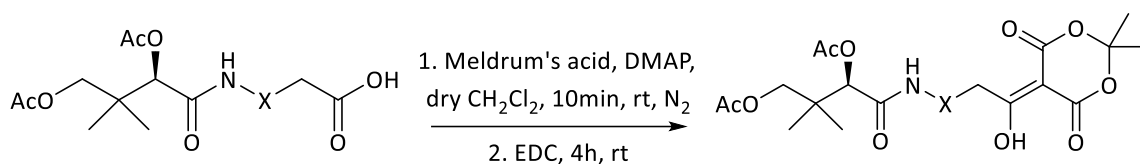
Yield: 79 % as off-white foamy solid. Starting compounds: **140** and methylamine (2.0 M in THF). Molecular formula: $C_{14}H_{24}N_2O_6$. Molecular weight: 316.35 g/mol. 1H NMR (300 MHz, $CDCl_3$): δ 6.90 (br s, 1H, NH exchanged with D_2O), 5.77 (br s, 1H, NH exchanged with D_2O), 4.92 (s, 1H, CH), 4.02 (d, $J = 11.0$ Hz, 1H, CH_2), 3.83 (d, $J = 11.0$ Hz, 1H, CH_2), 3.34-3.64 (m, 2H, CH_2), 2.79 (d, $J = 4.5$ Hz, 3H, $NHCH_3$), 2.37 (t, $J = 5.2$ Hz, 2H, CH_2), 2.15 (s, 3H, CH_3CO), 2.06 (s, 3H, CH_3CO), 1.06 (s, 3H, $C(CH_3)_2$), 1.02 (s, 3H, $C(CH_3)_2$).

tert-butyl N-(O,O'-diacetyl-D-pantothenoyl)- γ -aminobutanoate (144)

Yield 89 % as grey oil. Starting compounds: **138** and *tert*-butyl- γ -aminobutanoate hydrochloride. Molecular formula: $C_{21}H_{36}N_2O_8$. Molecular weight: 444.53 g/mol. 1H NMR (300 MHz, $CDCl_3$): δ 7.08 (br t, $J = 5.7$ Hz, 1H, NH), 6.56 (br t, $J = 5.4$ Hz, 1H, NH), 4.80 (s, 1H, CH), 3.92 (d, $J = 11.0$ Hz, 1H, $AcOCH_2$), 3.73 (d, $J = 11.0$ Hz, 1H, $AcOCH_2$), 3.26-3.47 (m, 2H, CH_2), 3.05-3.19 (m, 2H, CH_2), 2.27 (t, $J = 5.8$ Hz, 2H, CH_2), 2.16 (t, $J = 7.3$ Hz, 2H, CH_2), 2.04 (s, 3H, CH_3CO), 1.95 (s, 3H, CH_3CO), 1.62-1.71 (m, 2H, CH_2), 1.33 (s, 9H, $C(CH_3)_3$), 0.96 (s, 3H, $(CH_3)_2$), 0.91 (s, 3H, $(CH_3)_2$) ppm. ^{13}C NMR (75 MHz, $CDCl_3$): δ 172.57, 171.59, 170.79, 169.82, 168.05, 76.87, 69.22, 38.81, 36.96, 35.22, 34.85, 32.88, 27.95, 24.59, 21.29, 20.72, 20.64, 20.58 ppm.

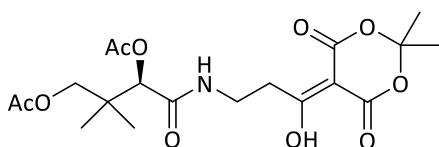
Synthesis of *N*-(*O,O'*-diacetyl-*D*-pantothenoyl)- γ -aminobutyric acid (145)

To a solution of **144** (1.42 mmol) in dry dichloromethane (6.59 mL), trifluoroacetic acid (2.75 mL) was added and the reaction mixture was stirred for 4 hours at room temperature. The resulting mixture was concentrated under reduced pressure by azeotrope with toluene to remove TFA, checked by ^{19}F NMR (282 MHz, $CDCl_3$) - absence of peak at -76.00 ppm) to obtain **145**. Yield 98 % as amber oil. Molecular formula: $C_{17}H_{28}N_2O_8$. Molecular weight: 388.42 g/mol. 1H NMR (300 MHz, $CDCl_3$): δ 7.42 (br t, $J = 5.5$ Hz, 1H, NH), 7.22 (br t, $J = 5.1$ Hz, 1H, NH), 4.85 (s, 1H, CH), 4.00 (d, $J = 11.1$ Hz, 1H, CH_2), 3.83 (d, $J = 11.1$ Hz, 1H, CH_2), 3.49-3.53 (m, 2H, CH_2), 3.20-3.34 (m, 2H, CH_2), 2.54 (t, $J = 5.7$ Hz, 2H, CH_2), 2.40 (t, $J = 7.0$ Hz, 2H, CH_2), 2.11 (s, 3H, CH_3CO), 2.05 (s, 3H, CH_3CO), 1.79-1.88 (m, 2H, CH_2), 1.02 (s, 3H, $(CH_3)_2$), 1.01 (s, 3H, $(CH_3)_2$) ppm. ^{13}C NMR (75 MHz, $CDCl_3$): δ 176.35, 172.44, 171.12, 170.25, 168.90, 77.07, 69.25, 38.93, 37.03, 35.58, 35.03, 31.33, 24.26, 21.26, 20.76, 20.62 ppm.

Synthesis of Meldrum's acid derivatives (**142**,**146**)

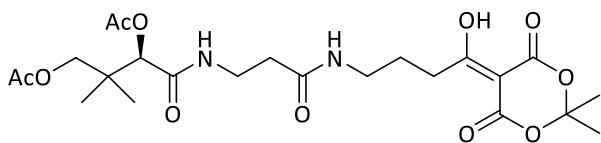
A solution of carboxylic acid (0.136 mmol), 2,2-dimethyl-1,3-dioxane-4,6-dione (Meldrum's acid, 0.136 mmol) and 4-dimethylaminopyridine (0.161 mmol) in dry dichloromethane (0.94 mL) was stirred for 15 minutes at room temperature. *N*-(3-dimethylaminopropyl)-*N'*-ethylcarbodiimide hydrochloride (0.152 mmol) was added and the solution was left stirring for other 4 hours. After dilution with dichloromethane, the organic phase was washed with 0.1 M HCl, dried over sodium sulfate and concentrated *in vacuo* to give **142** and **146**.

(*R*)-4-((3-(2,2-dimethyl-4,6-dioxo-1,3-dioxan-5-ylidene)-3-hydroxypropyl)amino)-2,2-dimethyl-4-oxobutane-1,3-diyl diacetate (**142**)

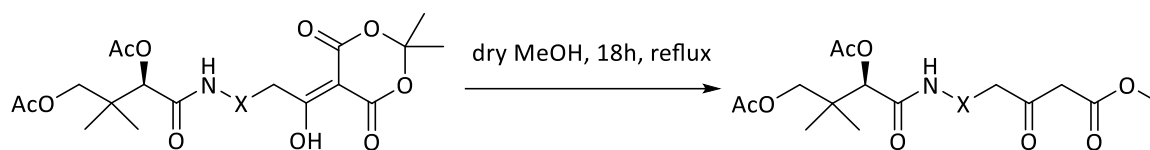


Yield: 81 % as colorless oil. Starting compound: **140**. Molecular formula: C₁₉H₂₇NO₁₀. Molecular weight: 429.42 g/mol. ¹H NMR (300 MHz, CDCl₃): δ 6.43 (br s, 1H, NH exchanged with D₂O), 4.89 (s, 1H, CH), 3.97 (d, *J* = 11.0 Hz, 1H, CH₂), 3.75 (d, *J* = 11.0 Hz, 1H, CH₂), 3.52-3.72 (m, 2H, CH₂), 3.16-3.25 (m, 2H, CH₂), 2.08 (s, 3H, CH₃CO), 1.99 (s, 3H, CH₃CO), 1.68 (s, 6H, C(CH₃)₂), 0.99 (s, 3H, C(CH₃)₂), 0.93 (s, 3H, C(CH₃)₂) ppm. ¹³C NMR (75 MHz, CDCl₃): δ 194.51, 170.81, 169.57, 168.21, 160.58, 105.35, 92.50, 76.62, 69.12, 37.26, 35.96, 35.22, 26.73, 21.33, 20.74, 20.63, 20.60 ppm.

N-[4-(2,2-dimethyl-4,6-dioxo-1,3-dioxan-5-ylidene)-4-hydroxybutyl]-*O,O'*-diacetyl-*D*-pantothenamide (**146**)

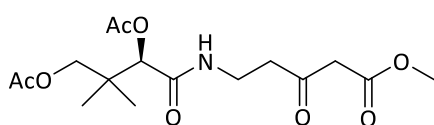


Yield: 84 % as light-brown oil. Starting compound: **145**. Molecular formula: C₂₃H₃₄N₂O₁₁. Molecular weight: 514.53 g/mol. ¹H NMR (300 MHz, CDCl₃): δ 7.09 (br t, *J* = 5.4 Hz, 1H, NH), 6.53 (br t, *J* = 5.2 Hz, 1H, NH), 4.81 (s, 1H, CH), 3.95 (d, *J* = 11.0 Hz, 1H, CH₂), 3.78 (d, *J* = 11.0 Hz, 1H, CH₂), 3.38-3.52 (m, 2H, CH₂), 3.10-3.38 (m, 2H, CH₂), 2.88-3.10 (m, 2H, CH₂), 2.27-2.37 (m, 2H, CH₂), 2.07 (s, 3H, CH₃CO), 1.99 (s, 3H, CH₃CO), 1.85 (m, 2H, CH₂), 1.68 (s, 3H, CO(CH₃)₂), 1.67 (s, 3H, CO(CH₃)₂), 0.99 (s, 3H, (CH₃)₂), 0.96 (s, 3H, (CH₃)₂) ppm. ¹³C NMR (75 MHz, CDCl₃): δ 196.98, 171.87, 170.77, 169.93, 168.09, 161.00, 104.78, 91.44, 76.97, 69.21, 38.46, 36.96, 35.37, 35.06, 26.99, 26.70, 26.64, 25.80, 21.26, 20.71, 20.65, 20.58 ppm.

Synthesis of methyl β -ketoesters (**143,147**)

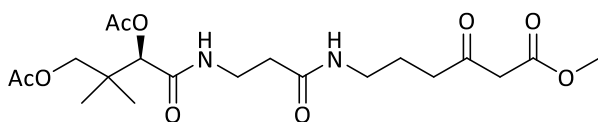
Dry methanol (14.2 mL) was used to dissolve the starting compound (0.69 mmol) and this solution was refluxed for 18 hours. The solvent was removed by evaporation under reduced pressure and the methyl β -ketoester was obtained.

(R)-4-((5-methoxy-3,5-dioxopentyl)amino)-2,2-dimethyl-4-oxobutane-1,3-diyl diacetate (**143**)

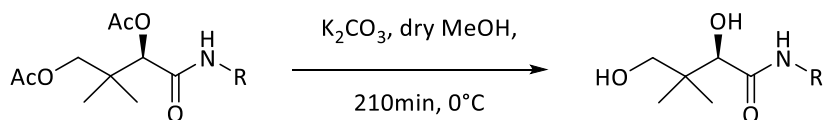


Yield: 87 % as light yellow oil. Starting compound: **142**. Molecular formula: C₁₆H₂₅NO₈. Molecular weight: 359.38 g/mol. ¹H NMR (300 MHz, CDCl₃): δ 6.51 (t, J = 5.6 Hz, 1H, NH exchanged with D₂O), 4.86 (s, 1H, CH), 3.97 (d, J = 11.0 Hz, 1H, CH₂), 3.77 (d, J = 11.0 Hz, 1H, CH₂), 3.69 (s, 3H, OCH₃), 3.32-3.58 (m, 2H, CH₂), 3.42 (s, 2H, CH₂), 2.70-2.77 (m, 2H, CH₂), 2.09 (s, 3H, CH₃CO), 2.02 (s, 3H, CH₃CO), 1.01 (s, 3H, C(CH₃)₂), 0.97 (s, 3H, C(CH₃)₂) ppm. ¹³C NMR (75 MHz, CDCl₃): δ 202.73, 170.84, 169.80, 168.02, 167.27, 76.97, 69.19, 52.39, 48.87, 42.06, 37.04, 33.54, 21.28, 20.77, 20.70, 20.61 ppm.

O,O'-diacetylmalonylcarba(dethia)pantetheine methylester (**147**)

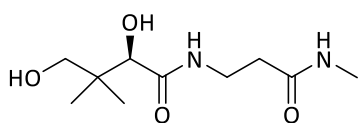


Yield: 94 % as light yellow oil. Starting compound: **146**. Molecular formula: C₂₀H₃₂N₂O₉. Molecular weight: 444.48 g/mol. ¹H NMR (300 MHz, CDCl₃): δ 6.87 (br t, J = 5.4 Hz, 1H, NH), 5.89 (br t, J = 5.2 Hz, 1H, NH), 4.89 (s, 1H, CH), 4.02 (d, J = 11.0 Hz, 1H, CH₂), 3.83 (d, J = 11.0 Hz, 1H, CH₂), 3.73 (s, 3H, OCH₃), 3.44-3.58 (m, 2H, CH₂), 3.48 (s, 2H, CH₂), 3.21-3.33 (m, 2H, CH₂), 2.62 (t, J = 6.8 Hz, 1H, CH₂), 2.35 (t, J = 5.8 Hz, 2H, CH₂), 2.15 (s, 3H, CH₃CO), 2.06 (s, 3H, CH₃CO), 1.78-1.85 (m, 2H, CH₂), 1.07 (s, 3H, CO(CH₃)₂), 1.03 (s, 3H, CO(CH₃)₂) ppm. ¹³C NMR (75 MHz, CDCl₃): δ 202.5, 171.8, 170.9, 170.0, 168.1, 167.7, 77.0, 69.3, 52.3, 48.8, 40.2, 38.7, 37.0, 35.2, 35.1, 23.0, 20.8, 20.7, 20.6 ppm.

Deprotection of *O,O'*-diacetyl groups (**21-23**)

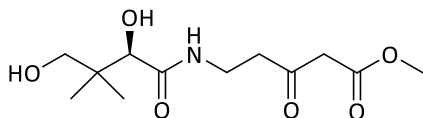
Potassium carbonate (2.25 mmol) was added to a solution of the proper *O,O'*-diacetyl pantoic derivative (0.69 mmol) in dry methanol (23 mL) at 0°C. After 210 minutes, the solvent was concentrated under *vacuum*. Upon filtration, the supernatant was dried under reduced pressure.

(R)-2,4-dihydroxy-3,3-dimethyl-N-(3-(methylamino)-3-oxopropyl)butanamide (21)



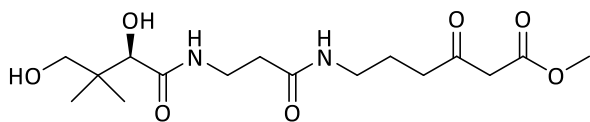
Yield: 78% as colorless oil. Starting compound: **141**.
Molecular formula: C₁₀H₂₀N₂O₄. Molecular weight: 232.28 g/mol. ¹H NMR (300 MHz, CD₃OD): δ 3.88 (s, 1H, CH), 3.35-3.48 (m, 4H, CH₂), 2.70 (s, 3H, NCH₃), 2.40 (t, *J* = 6.7 Hz, 2H, CH₂), 0.90 (s, 6H, C(CH₃)₂) ppm.

methyl (R)-5-(2,4-dihydroxy-3,3-dimethylbutanamido)-3-oxopentanoate (22)



Yield: 64% as colorless oil. Starting compound: **143**.
Molecular formula: C₁₂H₂₁NO₆. Molecular weight: 275.30 g/mol. ¹H NMR (300 MHz, D₂O): δ 4.04 (s, 1H, CH), 3.74 (s, 3H, OCH₃), 3.42-3.58 (m, 4H, CH₂), 3.41 (s, 2H, CH₂), 2.73 (t, *J* = 5.9 Hz, 2H, CH₂), 0.93 (s, 6H, C(CH₃)₂) ppm. ¹³C NMR (75 MHz, D₂O): δ 204.5, 174.7, 169.8, 76.3, 69.2, 52.4, 46.9, 40.8, 39.6, 36.3, 20.4 ppm.

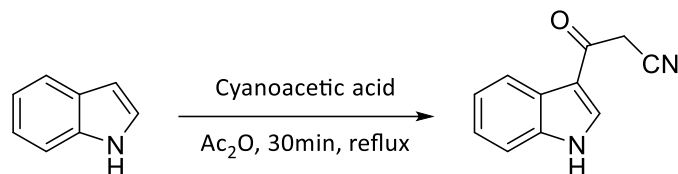
malonyl carba(dethia)-pantetheine methylester (23)



Yield: 70% as colorless oil. Starting compound: **143**.
Molecular formula: C₁₆H₂₈N₂O₇. Molecular weight: 360.41 g/mol. ¹H NMR (300 MHz, D₂O): δ 3.98 (s, 1H, CH), 3.75 (s, 3H, OCH₃), 3.43-3.56 (m, 2H, CH₂), 3.51 (d, *J* = 11.0 Hz, 1H, CH₂), 3.39 (d, *J* = 11.0 Hz, 1H, CH₂), 3.34 (s, 2H, CH₂), 3.17 (t, *J* = 7.0 Hz, 2H, CH₂), 2.68 (t, *J* = 7.0 Hz, 2H, CH₂), 2.48 (t, *J* = 6.0 Hz, 2H, CH₂), 1.72-1.80 (m, 2H, CH₂), 0.92 (s, 3H, C(CH₃)₂), 0.88 (s, 3H, C(CH₃)₂) ppm. ¹³C NMR (75 MHz, D₂O): δ 207.6, 175.0, 173.8, 170.1, 75.7, 68.2, 52.7, 40.0, 38.5, 38.4, 35.4, 35.2, 22.3, 20.4, 18.9 ppm.

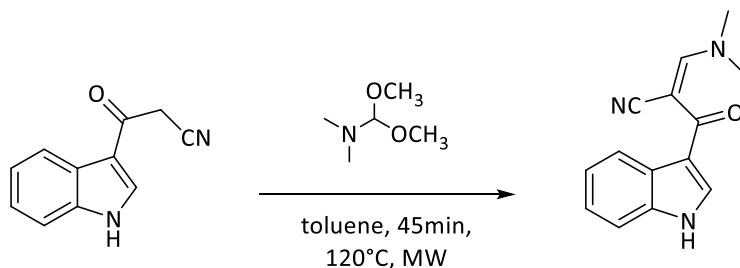
Procedures for the synthesis of 2-amino-4-(1H-indol-3-yl) pyrimidine-5-carbonitrile (24)

Synthesis of 3-(1H-Indol-3-yl)-3-oxo-propionitrile (148)

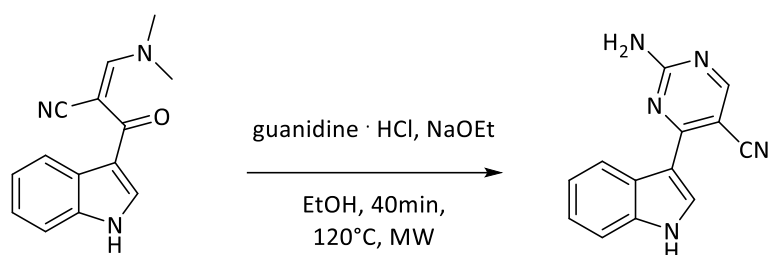


Cyanoacetic acid (20 mmol) and acetic anhydride (20 mL) were heated at 85°C for 10 minutes. Then indole (20 mmol) was added and the reaction mixture was refluxed for 30 minutes. After cooling, the precipitate was filtered and washed with ice-water. The crude product was recrystallized several times from acetic acid to give compound **148**. Yield 22 % as brown solid (m.p. 240-241°C). Molecular formula: C₁₁H₈N₂O. Molecular weight: 184.20 g/mol. ¹H NMR (300 MHz, DMSO-*d*₆): δ 12.16 (br s, 1H, NH exchanged with D₂O), 8.35 (d, *J* = 3.3 Hz, 1H, ArH), 8.07-8.19 (m, 1H, ArH), 7.37-7.59 (m, 1H, ArH), 7.11-7.31 (m, 2H, ArH), 4.48 (s, 2H, CH₂) ppm. ¹³C NMR (75 MHz, DMSO-*d*₆): δ 183.33, 137.06, 135.93, 125.59, 123.74, 122.76, 121.44, 116.87, 114.87, 112.86, 29.86 ppm.

Synthesis of (2Z)-3-(dimethylamino)-2-(1H-indole-3-carbonyl)acrylonitrile (149)



Intermediate **148** (6.4 mmol) and *N,N*-dimethylformamide dimethyl acetal (10 mmol) were dissolved in dry toluene (15 mL). The mixture was irradiated by a microwave synthesizer at 300 Watts at 120°C for 45 minutes (TLC: dichlorometane /ethyl acetate (8:2) - R_f: 0.51). After cooling, the obtained yellow solid was filtered and recrystallized from ethanol to give pure **149**. Yield 85 % as yellow prisms (m.p. 160-163°C). Molecular formula: C₁₄H₁₃N₃O. Molecular weight: 239.28 g/mol. ¹H NMR (300 MHz, DMSO-*d*₆): δ 11.73 (br s, 1H, NH exchanged with D₂O), 8.26 (s, 1H, ArH), 8.12 (d, *J* = 7.2 Hz, 1H, ArH), 7.98 (s, 1H, CH), 7.45 (d, *J* = 7.5 Hz, 1H, ArH), 7.05-7.22 (m, 2H, ArH), 3.35 (s, 3H, CH₃), 3.25 (s, 3H, CH₃) ppm. ¹³C NMR (75 MHz, DMSO-*d*₆): δ 182.18, 159.12, 136.26, 131.59, 127.20, 122.93, 122.24, 122.19, 121.57, 115.12, 112.34, 78.04, 47.85 ppm.

Synthesis of 2-amino-4-(1H-indol-3-yl)pyrimidine-5-carbonitrile (24)

A solution of compound **149** (1.11 mmol), guanidine hydrochloride (2.22 mmol) and sodium ethoxide (1.11 mmol) in ethanol (6 mL) was irradiated by a microwave synthesizer at 300 Watts, at 120°C for 40 minutes. After cooling to room temperature, the precipitate was filtered and washed with ice-cold ethanol. The obtained yellow solid was recrystallized in ethanol to give pure compound **24**. Yield 83 % as light-yellow solid (m.p. 258-259°C). Molecular formula: C₁₃H₉N₅. Molecular weight: 235.25 g/mol. ¹H NMR (300 MHz, DMSO-*d*₆): δ 11.95 (br s, 1H, NH exchanged with D₂O), 8.66 (d, *J* = 8.0 Hz, 1H, ArH), 8.56 (s, 1H, ArH), 8.46 (s, 1H, ArH), 7.64 (br s, 1H, NH₂ exchanged with D₂O), 7.54 (br s, 1H, NH₂ exchanged with D₂O), 7.50 (d, *J* = 8.1 Hz, 1H, ArH), 7.08-7.29 (m, 2H, ArH) ppm. ¹³C NMR (75 MHz, DMSO-*d*₆) δ 163.77, 163.60, 163.56, 136.81, 130.44, 126.17, 123.70, 123.19, 121.49, 120.26, 112.48, 111.95, 89.64 ppm.

Chapter 8

Experimental Part: Biology

8.1 Materials and methods

8.1.1 MTT-assay

The MTT assay was performed according to literature data.^[85,86]

HCT-116 cell line (colorectal cancer) were cultured in McCoy's media, whereas the DLD-1 (colorectal cancer) and MCF-7 were cultured in Dulbecco's modified eagle's medium (DMEM) with glutamine. All the media were supplemented with penicillin (10,000 U/mL), streptomycin (10 mg/mL), nonessential amino acids and 10% Fetal Calf Serum (FCS). The same media was utilized for the experiments where cells were incubated with newly synthesized compounds dissolved in DMSO. The same volume of solvent was added to control conditions and did not exceed 0.5% v/v.

8.1.2 AlphaScreen-based assay

It is a bead-based nonradioactive assay system for detecting biomolecular interactions in a microtiter plate format. The binding of biological partners brings donor and acceptor beads into close proximity and as a result, a fluorescent signal between 520 and 620 nm is produced. The AlphaScreen-based assays^[140-141] were performed in a final reaction volume of 25 μ L of the assay buffer containing 10 mM HEPES–NaOH (pH 7.4), 50 mM NaCl, 1 mM EDTA (pH 8.0), 0.1% NP-40, and 10 ng/ μ L BSA in a 96-well microtiter plate at 25°C. the phospho-Tyr (pTyr) peptide probes used in this study were 5-carboxyfluorescein (FITC)-GpYLPQTV for STAT3 and (FITC)-GpYDKPHVL for STAT1. Firstly, 75 nM of each SH2-containing protein was incubated with the test compound for 15 min. Each protein sample was then incubated for 90 minutes with 50 nM of its corresponding FITC-pTyr peptide, and mixed with streptavidin coated donor beads and anti-FITC acceptor beads simultaneously before detection at 570 nm using EnVision Xcite (PerkinElmer).

8.1.3 In vivo antitumor activity in Lewis Lung Carcinoma

All experiments were performed according to D.L.G.S. 26/2014 which warrants care of experimental animals in Italy. The research project was approved by the Italian Health Department according to the art. 7 of the above mentioned D.L. The LLC cell line was purchased from ECACC, United Kingdom. The LLC cell line was maintained in DMEM (Euroclone) supplemented with 10% heat-inactivated fetal bovine serum (FBS; Euroclone), 10 mM L-glutamine, 100 U mL⁻¹ penicillin, and 100 μ g mL⁻¹ streptomycin in a 5% CO₂ air incubator at 37°C. The LLC was implanted intramuscularly (im) as a 2×10^6 cell inoculum into the right hind leg of 8 week old male and female C57BL mice (24 ± 3 g body weight). After 24 hours from tumor implantation, mice were randomly divided into five groups (8 animals per group, 10 controls). From day 7 after tumor inoculation (visible tumor) animals were treated daily with a single dose of **Pt-15b** and of **Pt-16a** complex (30 mg kg⁻¹ dissolved in a vehicle solution composed of 20% Cremophor EL (v/v), 20% PEG400 (v/v) and 60% saline solution (v/v)) or with a daily ip dose of cisplatin (1.5 mg kg⁻¹ in 0.9% NaCl solution). At day 15, animals were sacrificed, the legs were amputated at the proximal end of the femur, and the inhibition of tumor growth was determined according to the difference in weight of the tumor-bearing leg and the healthy leg of the animals expressed as a percentage referred to the control animals. Body weight was measured at day 1 and every two days from day 7, and was taken as a parameter for systemic toxicity. All the values are the means \pm SD of not less than three measurements.

8.1.4 Determination of intracellular and DNA-bound Pt concentrations

For the determination of total intracellular ¹⁹⁵Pt concentrations, cells were homogenated with a lysis buffer containing 0.5% NP-40, 150 mM NaCl and 50 mM Tris-HCl at pH 7.5. The cell monolayer was treated three

times with PBS before the incubation with the lysis buffer for 30 minutes at 4°C. Cell lysates were then cleared by centrifugation at 14,000g for 10 min, and the ¹⁹⁵Pt concentration was determined by ICP-MS. The data were normalized with the protein concentrations determined using the BCA protein assay (Thermo scientific, Rockford, IL USA). The ¹⁹⁵Pt concentration bound to DNA was estimated from nuclear DNA, extracted as previously described. [86] The data were normalized with DNA concentrations determined by spectrophotometer determination with NanoDrop system.

8.1.5 Binding study with 9-ethylguanine and GSH

The binding studies were directly conducted in NMR tube preparing 1 eq. of **Pt-15b** in 20 % of 0.9 % w/v NaCl-D₂O solution in DMSO-*d*₆. 1eq. of 9-ethylguanine or GSH was added to the solution. The samples were evaluated at different times by ¹H NMR analysis.

8.1.6 Western blot analysis

Cells were washed twice with PBS and lysed by incubation with a solution of 50 mM Tris pH 7.5, 150 mM NaCl, 0.5% Nonidet-P40, containing a protease inhibitor cocktail (Sigma Aldrich, Milan, Italy) for 30 minutes on ice. Cell lysates were then cleared by centrifugation at 14,000 g for 10 minutes. [142] Protein samples were separated by SDS-PAGE under reducing conditions, transferred to nitrocellulose membrane (GE Healthcare Little Chalfont, Buckinghamshire, UK) and subsequently immunoblotted with primary antibody, following the appropriate secondary fluorescently labeled antibody, and acquired with the Odyssey FC system (LI-COR). Quantitative densitometric analyses were performed by Image Studio software (LI-COR). The following antibodies were utilized: monoclonal antibody anti p53 and β-tubulin (SIGMA), anti-pSTAT3 (Abcam) and anti-STAT3 (Santa-Cruz Biotechnology).

8.1.7 RNA Preparation and Quantitative Real Time PCR

Total RNA was extracted with the iScript Sample Preparation Buffer according to manufacturer's instructions. Reverse transcription-polymerase first-strand cDNA synthesis was realized by using the iScript cDNA synthesis Kit (Bio-Rad). qPCR was then performed by using the Kit Thermo SYBR Green/ROX qPCR Master Mix (Carlo Erba Reagents) and specific primers for STAT3 and 18S. The analyses were carried out with the ABI Prism® 7000 Sequence Detection System (Applied Biosystems; Life Technologies Europe BV). PCR cycling conditions were as follows: 94°C for 10 minute, 40 cycles at 94°C for 15 seconds, and 60°C for 1 minute. Data were expressed as Ct values and used for the relative quantification of targets by Ct calculation. [143]

Abbreviations

Abbreviations

9-EtG, 9-ethylguanine

11 β -HSD1, 11 β -hydroxysteroid dehydrogenase type 1

A2780, human ovarian cancer cell line

A549, lung carcinoma cell line

Ac₂O, acetic anhydride

ACO, Ant Colonization Optimization

AcOEt, ethyl acetate

AcOH, acetic acid

AMMP, Automated Molecular Mechanics Optimization

ATP7B, copper-transporting P-type ATPase

Bcl-2, B-cell lymphoma 2

Boc₂O, di-*tert*-butyl dicarbonate

CDDD, computational driven drug design

CDK, cyclin dependent kinase

Cnt, control

Cpd, compound

Crm1, chromosome region maintenance 1

c-Src, proto-oncogene tyr-protein kinase Src

Ctr-1, copper transporter 1

DCC, *N,N*-dicyclohexylcarbodiimide

DCU, *N,N*-dicyclohexylurea

DIBAL-H, diisobutylaluminium hydride

DIPEA, *N,N*-diisopropylethylamine

DLD-1, colorectal cancer cell line

DMAP, 4-dimethylaminopyridine

DMF, *N,N*-dimethylformamide

DMSO-d₆, dimethyl sulfoxide-d₆

DPPA, diphenylphosphoryl azide

DTT, dithiolethione

EDC·HCl = *N*-(3-dimethylaminopropyl)-*N'*-ethylcarbodiimide hydrochloride

EGF, epidermal growth factor

ElectDD, distance-dependent electrostatic energy according to Coulomb's equation

ESI, electrospray ionization

Et₂O, diethyl ether

Et₃N, triethylamine

(EtO)₂CO, ethyl carbonate

EtOH, ethanol

FBDD, fragment-based drug design

FCS, fetal calf serum

FDA, Food and Drug Administration

GSH, glutathione

H460, non-small-cell lung carcinoma

HBA, hydrogen bond acceptor

HBD, hydrogen bond donor

HCT-116, colorectal cancer cell line

HeLa, cervical cancer cell line

HOBt, hydroxybenzotriazole

HSF, human skin fibroblast

HTS, High-throughput screening

IFN, interferon

JAB, JAK-binding protein

JAK, Janus kinase

LiBHET₃, lithium triethylborohydride

LLC, Lewis lung carcinoma

MCF-7, breast cancer cell line

MeOH, methanol

MHC, major histocompatibility complex

MLP_{ins}, Molecular Lipophilic Potential Interaction Score

MMAS, MAX-MIN Ant System

MSTO-211H, mesothelioma

MT, metallothionein

MTT, 3-(4,5-dimethylthiazol-2-yl)-2,5-diphenyltetrazolium bromide

MTTS, methanethiosulfonate

mw, microwave

MW, molecular weight

n-BuLi, *n*-butyllithium

NaOAc, sodium acetate

NBS, *N*-bromosuccinimide

NCBI, National Center for Biotechnology Information

NCI, National Cancer Institute

NCS, *N*-chlorosuccinimide

NER, nucleotide excision repair

NES, nuclear export signals

NF- κ B, nuclear factor kappa-light-chain-enhancer of activated B cells

NIH, National Institutes of Health

NLS, nuclear lesions signals

NMM, *N*-methylmorpholine

NPC, nuclear pore complex

NSCLC, non-small cell lung cancer

Abbreviations

OCT, organic cation transporters

Pd/C, palladium on carbon

PDB, Protein Data Bank

PDGF, platelet-derived growth factor

Ph₃P, triphenylphosphine

PIAS, proteins that inhibit activated STAT proteins family

PLANTS, Protein-Ligand ANT System

Py, pyridine

RMSD, root-mean-square deviation

rt, room temperature

SAR, structure-activity relationship

sFRP-1, secreted frizzled related protein-1

SH2, Src homology 2

SOCS, suppressors of cytokine signaling family

SPR, surface plasmon resonance

STAT, Signal Transducer and Activator of Transcription

t-BuONO, *tert*-butyl nitrite

t-BuOH, *tert*-butanol

TBAB, tetra-*N*-butylammonium bromide

TBTU, *N,N,N',N'*-tetramethyl-*O*-(benzotriazol-1-yl)uronium tetrafluoroborate

TFA, trifluoroacetic acid

THF, tetrahydrofuran

TK, tyrosine kinase

TLC, thin layer chromatography

TMS, tetramethylsilane

TMSCl, chlorotrimethylsilane

uSTAT3, unphosphorylated STAT3

VEGF-A: vascular endothelial growth factor

References

- [1] World Health Organisation. *International Agency for Research on Cancer, World cancer report 2014*, Bernard W. Stewart and Christopher P. Wild, **2014**.
- [2] T. L. Lemke, D. A. Williams, V. F. Roche, S. W. Zito, *Foye's Principles of Medicinal Chemistry: 7th edition*, Wolters Kluwer Health Adis, **2012**.
- [3] S. Hoelder, P. A. Clarke, P. Workman, *Molecular Oncology*, **2012**, 6(2), 155-176.
- [4] K. T. Flaherty, J. R. Infante, A. Daud, R. Gonzalez, R. F. Kefford, J. Sosman, O. Hamid, L. Schuchter, J. Cebon, N. Ibrahim, R. Kudchadkar, H. A. Burris, G. Falchook, A. Algazi, K. Lewis, G. V. Long, I. Puzanov, P. Lebowitz, A. Singh, S. Little, P. Sun, A. Allred, D. Ouellet, K. B. Kim, K. Patel, J. Weber, *The New England journal of medicine*, **2012**, 367(18), 1694-1703.
- [5] J. Bromberg, J. E. Darnell Jr, *Oncogene*, **2000**, 19(21), 2468-2473.
- [6] H. Yu, R. Jove, *Nature Reviews Cancer*, **2004**, 4(2), 97-105.
- [7] T. Bowman, R. Garcia, J. Turkson, R. Jove, *Oncogene*, **2000**, 19(21), 2474-2488.
- [8] R. Buettner, L. B. Mora, R. Jove, *Clinical Cancer Research*, **2002**, 8(4), 945-954.
- [9] G. Niu, R. Heller, R. Catlett-Falcone, D. Coppola, M. Jaroszeski, W. Dalton, R. Jove and H. Yu, *Cancer Research*, **1999**, 59(20), 5059-5063.
- [10] H. Yu, D. Pardoll, R. Jove, *Nature Reviews Cancer*, **2009**, 9(11), 798-809.
- [11] D. Wei, X. Le, L. Zheng, L. Wang, J. A. Frey, A. C. Gao, Z. Peng, S. Huang, H. Q. Xiong, J. L. Abbruzzese, K. Xie, *Oncogene*, **2003**, 22(3), 319-329.
- [12] D. Masciocchi, A. Gelain, S. Villa, F. Meneghetti, D. Barlocco, *Future Medicinal Chemistry*, **2011**, 3(5), 567-597.
- [13] A. Nishimoto, N. Kugimiya, T. Hosoyama, T. Enoki, T.-S. Li, K. Hamano, *Biochemical and Biophysical Research Communications*, **2013**, 438(3), 513-518.
- [14] D. S. Goldfarb, A. H. Corbett, D. A. Mason, M. T. Harreman, S. A. Adam, *Trends in Cell Biology*, **2004**, 14(9), 505-514.
- [15] M. Vogt, T. Domszlai, D. Kleshchanok, S. Lehmann, A. Schmitt, V. Poli, W. Richtering, G. Mueller-Newen, *Journal of Cell Science*, **2011**, 124(6), 900-909.
- [16] C.-L. Yu, D. J. Meyer, G. S. Campbell, A. C. Lerner, C. Carter-Su, J. Schwartz and R. Jove, *Science*, **1995**, 269(5220), 81-83.
- [17] E. Nkansah, R. Shah, G. W. Collie, G. N. Parkinson, J. Palmer, K. M. Rahman, T. T. Bui, A. F. Drake, J. Husby, S. Neidle, G. Zinzalla, D. E. Thurston, A. F. Wilderspin, *FEBS Letters*, **2013**, 587(7), 833-839.
- [18] D. Barlocco, L. Costantino, *Current Medicinal Chemistry*, **2008**, 15(9), 834-843.
- [19] G. Zinzalla, D. E. Thurston, *Future Medicinal Chemistry*, **2009**, 1(1), 65-93.
- [20] P. K. Mandal, W. S. Liao, J. S. McMurray, *Organic Letters*, 2009, 11(15), 3394-3397.
- [21] P. K. Mandal, F. Gao, Z. Lu, Z. Ren, R. Ramesh, J. S. Birtwistle, K. K. Kaluarachchi, X. Chen, R. C. Bast Jr., W. S. Liao, J. S. McMurray, *Journal of Medicinal Chemistry*, **2011**, 54(10), 3549-3563.
- [22] D. Bhasin, J. P. Etter, S. N. Chettiar, M. Mok, P.-K. Li, *Bioorganic and Medicinal Chemistry Letters*, **2013**, 23(24), 6864-6867.
- [23] B. D. G. Page, D. C. Croucher, Z. H. Li, S. Haftchenary, V. H. Jimenez-Zepeda, J. Atkinson, P. A. Spagnuolo, Y. L. Wong, R. Colaguori, A. M. Lewis, A. D. Schimm, S. Trudel, P. T. Gunning, *Journal of Medicinal Chemistry*, **2013**, 56(18), 7190-7200.

- [24] W. Hao, Y. Hu, C. Niu, X. Huang, C.-P. B. Chang, J. Gibbons, J. Xu, *Bioorganic and Medicinal Chemistry Letters*, **2008**, 18(18), 4988-4992.
- [25] V. M. Shahani, P. Yue, S. Haftchenary, W. Zhao, J. L. Lukkarila, X. Zhang, D. Ball, C. Nona, P. T. Gunning, J. Turkson, *ACS Medicinal Chemistry Letters*, **2011**, 2(1), 79-84.
- [26] B. Rosenberg, L. Vancamp, J. E. Trosko, V. H. Mansour, *Nature*, **1969**, 222, 385-386.
- [27] M. Frezza, S. Hindo, D. Chen, A. Davenport, S. Schmitt, D. Tomco, Q. P. Dou, *Current Pharmaceutical Design*, **2010**, 16(16), 1813-1825.
- [28] A. J. Di Pasqua, J. Goodisman, J. C. Dabrowiak, *Inorganica Chimica Acta*, **2012**, 389, 29-35.
- [29] E. Raymond, S. Faivre, S. Chaney, J. Woynarowski, E. Cvitkovic, *Molecular Cancer Therapeutics*, **2002**, 1(3), 227-235.
- [30] C. A. Rabik, M. E. Dolan, *Cancer Treatment Reviews*, **2007**, 33(1), 9-23.
- [31] R. A. Alderden, M. D. Hall, T. W. Hambley, *Journal of Chemical Education*, **2006**, 83(5) 728-734.
- [32] F. Arnesano, G. Natile, *Coordination Chemistry Reviews*, **2009**, 253(15-16), 2070-2081.
- [33] F. Tadini-Buoninsegni, G. Bartolommei, M. R. Moncelli, G. Inesi, A. Galliani, M. Sinisi, M. Losacco, G. Natile and F. Arnesano, *Angewandte Chemie (International ed. in English)*, **2014**, 53(5), 1297-1301.
- [34] S. Zhang, K. S. Lovejoy, J. E. Shima, L. L. Lagpacan, Y. Shu, A. Lapuk, Y. Chen, T. Komori, J. W. Gray, X. Chen, S. J. Lippard, K. M. Giacomini, *Cancer Research*, **2006**, 66(17), 8847-8857.
- [35] J. Reedijk, *Proceedings of the National Academy of Sciences*, **2003**, 100(7), 3611-3616.
- [36] V. M. Gonzalez, M. A. Fuertes, C. Alonso, J. M. Pérez, *Molecular Pharmacology*, **2001**, 59(4), 657-663.
- [37] J. Reedijk, *Chemical Reviews*, **1999**, 99(9), 2499-2510.
- [38] M. A. Fuertes, C. Alonso, J. M. Pérez, *Chemical Reviews*, **2003**, 103(3), 645-662.
- [39] T. W. Hambley, *Coordination Chemistry Reviews*, **1997**, 166, 181-223.
- [40] M. D. Hall, H. R. Mellor, R. Callaghan, T. W. Hambley, *Journal of Medicinal Chemistry*, **2007**, 50(15), 3403-3411.
- [41] T. W. Hambley, *Dalton Transactions*, **2007**, 4929-4937.
- [42] S. Fletcher, J. Turkson, P. T. Gunning, *ChemMedChem*, **2008**, 3(8) 1159-1168.
- [43] C.-M. Che and F.-M. Siu, *Current Opinion in Chemical Biology*, **2010**, 14(2), 255-261.
- [44] J. Schust, B. Sperl, A. Hollis, T. U. Mayer, T. Berg, *Chemistry & Biology*, **2006**, 13(11), 1235-1242.
- [45] Y. Pan, F. Zhou, R. Zhang, F. X. Claret, *PLoS ONE*, **2013**, 8(1), e54565.
- [46] N. P. E. Barry, P. J. Sadler, *Chemical Communications*, **2013**, 49, 5106-5131.
- [47] J. J. Champoux, *Annual Review Biochemistry*, **2001**, 70, 369-413.
- [48] M. Li, Y. Liu, *Genomics, Proteomics & Bioinformatics*, **2016**, 14(3), 166-71.
- [49] G. M. Karimi, R.-N. Alizadeh, S. Rasouli, *International Journal of Advanced Biological and Biomedical Research*, **2014**, 2(8), 2431-2436
- [50] L. G. Beretta, P. Perego, N. Zaffaroni, *Current Medicinal Chemistry*, **2013**, 20(12), 1541-1565.
- [51] Y. Pommire, E. Leo, H. Zhang, C. Marchand, *Chemistry & Biology*, **2010**, 17(5), 421-433.
- [52] L. G. Dezhenkova, G. V. Tsvetkov, A. A. Shtil, *Russian Chemical reviews*, **2011**, 83(1), 82-94.
- [53] H.-J. Boehm, A. Flohr, M. Stahl, *Drug Discovery Today: Technologies*, **2004**, 1(3), 217-224.
- [54] H. Sun, G. Tawa, A. Wallqvist, *Drug Discovery Today*, **2012**, 17(7-8), 310-324.

- [55] W. Yu, H. Xiao, J. Lin, C. Li, *Journal of Medicinal Chemistry*, **2013**, 56(11), 4402-4412.
- [56] H. Chen, Z. Yang, C. Ding, L. Chu, Y. Zhang, K. Terry, H. Liu, Q. Shen, J. Zhou, *European Journal of Medicinal Chemistry*, **2013**, 62, 498-507.
- [57] D. S. Shin, D. Masciocchi, A. Gelain, S. Villa, D. Barlocco, F. Meneghetti, A. Pedretti, Y. M. Han, D. C. Han, B. M. Kwon, L. Legnani, L. Toma, *MedChemComm*, **2010**, 1(2), 156-164.
- [58] S. Villa, D. Masciocchi, A. Gelain, F. Meneghetti, *Chemistry & Biodiversity*, **2012**, 9(7), 1240-1253.
- [59] D. Masciocchi, S. Villa, F. Meneghetti, A. Pedretti, D. Barlocco, L. Legnani, L. Toma, B. M. Kwon, S. Nakano, A. Asai, A. Gelain, *MedChemComm*, **2012**, 3(5), 592-599.
- [60] F. Meneghetti, S. Villa, D. Masciocchi, D. Barlocco, L. Toma, D.-C. Han, B.-M. Kwon, N. Ogo, A. Asai, L. Legnani, A. Gelain, *European Journal of Organic Chemistry*, **2015**, 2015(22), 4907-4912.
- [61] <http://www.cresset-group.com/?s=activity+miner>.
- [62] T. Cheeseright, M. Mackey, S. Rose, A. Vinter, *Journal of Chemical Information and Modeling*, **2006**, 46, 665-676.
- [63] Y.-C. Lo, S. Senese, R. Damoiseaux, J. Z. Torres, *ACS Chemical Biology*, **2016**, 11(8), 2244-2253.
- [64] A. B. Sheremetev, *Russian Chemical Bulletin, International Edition*, **2005**, 54(4), 1057-1059.
- [65] L. J. Silverberg, J. L. Dillon, P. Vemishetti, *Tetrahedron Letters*, **1996**, 37(6), 771-774.
- [66] X. Wang, T. Zhao, B. Yang, Z. Li, J. Cui, Y. Dai, Q. Qiu, H. Qiang, W. Huang, H. Qian, *Bioorganic & Medicinal Chemistry*, **2015**, 23(1), 132-140.
- [67] E. M. Beccalli, A. Manfredi, A. Marchesini, *Journal of Organic Chemistry*, **1985**, 50(13), 2372-2375.
- [68] P. Conti, L. Tamborini, A. Pinto, L. Sola, R. Ettari, C. Mercurio, C. De Micheli, *European Journal of Medicinal Chemistry*, **2010**, 45(9), 4331-4338.
- [69] E. J. Hanan, A. Van Abbema, K. Barrett, W. S. Blair, J. Blaney, C. Chang, C. Eigenbrot, S. Flynn, P. Gibbons, C. A. Hurley, J. R. Kenny, J. Kulagowski, L. Lee, S. R. Magnuson, C. Morris, J. Murray, R. M. Pastor, T. Rawson, M. Siu, M. Ultsch, A. Zhou, D. Sampath, J. P. Lyssikatos, *Journal of Medicinal Chemistry*, **2012**, 55(22), 10090-10107.
- [70] H. A. Saadeh, I. M. Mosleh, M. M. El-Abadelah, *Molecules*, **2009**, 14(8), 2758-2767.
- [71] Q. Su, S. Ioannidis, C. Chuaqui, L. Almeida, M. Alimzhanov, G. Bebernitz, K. Bell, M. Block, T. Howard, S. Huang, D. Huszar, J. A. Read, C. Riverd Costa, J. Shi, M. Su, M. Ye, M. Zinda, *Journal of Medicinal Chemistry*, 2014, 57(1), 144-158.
- [72] V. Lisowski, D. Nghia Vu, X. Feng, S. Rault, *Synthesis*, **2002**, 6, 753-756.
- [73] P. Lu, C. Sanchez, J. Cornella, I. Larrosa, *Organic Letters*, **2009**, 11(24), 5710-5713.
- [74] J. Xi, Q. L. Dong, G. S. Liu, S. Wang, L. Chen, Z. J. Yao, *Synlett*, **2010**, 11, 1674-1678.
- [75] R. D. Snyder, *Mutation Research, Fundamental and Molecular Mechanisms of Mutagenesis*, **2007**, 623(1-2), 72-82.
- [76] R. D. Snyder, J. McNulty, G. Zairov, D. E. Ewing, L. B. Hendry, *Mutation Research, Fundamental and Molecular Mechanisms of Mutagenesis*, **2005**, 578(1-2), 88-99.
- [77] G. Maggiora, M. Vogt, D. Stumpfe, J. Bajorath, *Journal of Medicinal chemistry*, **2014**, 57, 31863-204.
- [78] M. Tuyishime, R. Lawrence, S. Cocklin, *Bioorganic & Medicinal Chemistry Letters*, **2016**, 26, 228-234.
- [79] S. Merlo, L. Basile, M. L. Giuffrida, M. A. Sortino, S. Guccione, A. Copani, *Journal of Natural Products*, **2015**, 78(11), 2704-2711.

- [80] S. Rose, J.G. Vinter, *Innovations in Pharmaceutical Technology*, **2007**, 14-18.
- [81] <https://www.cambridgesoft.com/>
- [82] A. Pedretti, L. Villa, G. Vistoli, *Journal of Molecular Graphics and Modelling*, **2002**, 21(1), 47-49.
- [83] <http://nova.disfarm.unimi.it/manual/pages/cite.htm>
- [84] L. J. Farrugia, *Journal of Applied Crystallography*, **1999**, 32(4), 837-838.
- [85] N. Ferri, S. Cazzaniga, L. Mazzarella, G. Curigliano, G. Lucchini, D. Zerla, R. Gandolfi, G. Facchetti, M. Pellizzoni, I. Rimoldi, *Bioorganic and Medicinal Chemistry*, **2013**, 21(8), 2379-2386.
- [86] N. Ferri, G. Facchetti, S. Pellegrino, C. Ricci, G. Curigliano, E. Pini, I. Rimoldi, *Bioorganic and Medicinal Chemistry*, **2015**, 23(10), 2538-2547.
- [87] G. Rai, C. J. Thomas, W. Leister and D. J. Maloney, *Tetrahedron Letters*, **2009**, 50(15), 1710-1713.
- [88] P. Tosco, M. Bertinaria, A. Di Stilo, C. Cena, G. Sorba, R. Fruttero, A. Gasco, *Bioorganic & Medicinal Chemistry*, **2005**, 13, 4750-4759.
- [89] G. V. Sagar Reddy, G. V. Rao, R. V. Subramanyam, D. S. Iyengar, *Synthetic Communications*, **2000**, 30(12), 2233-2237.
- [90] R. Dreos, P. Siega, S. Scagliola, L. Randaccio, G. Nardinù, C. Tavagnacco, M. Bevilacqua, *European Journal of Inorganic Chemistry*, **2005**, 2005(19), 3936-3944.
- [91] T. J. Egan, K. R. Koch, P. L. Swan, C. Clackson, D. A. Van Schalkwyk, P. J. Smith, *Journal of Medicinal Chemistry*, **2004**, 47(11), 2926-2934.
- [92] S. Pensa, G. Regis, D. Boselli, F. Novelli, V. Poli, *STAT1 and STAT3 in Tumorigenesis: Two Sides of the Same Coin?*, Madame Curie Bioscience Database.
- [93] S. J. Berners-Price, L. Ronconi, P. J. Sadler, *Progress in Nuclear Magnetic Resonance Spectroscopy*, **2006**, 49(1), 65-98.
- [94] J. Llorca, E. Molins, E. Espinosa, I. Mata, C. Miravittles, G. Cervantes, A. Caubet, V. Moreno, *Acta Crystallographica. Section C*, **2001**, 57(7), 804-806.
- [95] W. Lu, M. C. Chan, N. Zhu, C.-M. Che, C. Li, Z. Hui, *Journal of American Chemical Society*, **2004**, 126(24), 7639-7651.
- [96] J. A. Platts, D. E. Hibbs, T. W. Hambley, M. D. Hall, *Journal of Medicinal Chemistry*, **2001**, 44(3), 472-474.
- [97] S. P. Oldfield, M. D. Hall, J. A. Platts, *Journal of Medicinal Chemistry*, **2007**, 50(21), 5227-5237.
- [98] I. V. Tetko, I. Jaroszewicz, J. A. Platts, J. Kuduk-Jaworska, *Journal of Inorganic Biochemistry*, **2008**, 102(7), 1424-1437.
- [99] M. Reist, L. H. Christiansen, P. Christoffersen, P.-A. Carrupt, B. Testa, *Chirality*, **1995**, 7(6), 469-473.
- [100] S. Mohr, J. A. Weiß, J. Spreitz, M. G. Schmid, *Journal of Chromatography A*, **2012**, 1269, 352-359.
- [101] T. C. Johnstone, S. J. Lippard, *Journal of the American Chemistry Society*, **2014**, 136(5), 2126-2134.
- [102] D. Lemaire, M.-H. Fouchet, J. Kozelka, *Journal of inorganic biochemistry*, **1994**, 53(4), 261-271.
- [103] Y. Min, C.-Q. Mao, S. Chen, G. Ma, J. Wang, Y. Liu, *Angewandte Chemie (International ed. in English)*, **2012**, 51(27), 6742-6747
- [104] B. A. Jansena, J. Brouwerb, J. Reedijk, *Journal of Inorganic Biochemistry*, **2002**, 89(3-4), 197-202.
- [105] V. Gandin, A. Trenti, M. Porchia, F. Tisato, M. Giorgetti, I. Zanusso, L. Trevisi, C. Marzano, *Metallomics*, **2015**, 7(11), 1497-1507.

- [106] S. Heidelberger, G. Zinzalla, D. Antonow, S. Essex, B. Piku Basu, J. Palmer, J. Husby, P. J. M. Jackson, K. M. Rahman, A. F. Wilderspin, M. Zloha, D. E. Thurston, *Bioorganic & Medicinal Chemistry Letters*, **2013**, 23(16), 4719-4722.
- [107] E. Gabriele, PhD Thesis: *Synthesis of New Sulfurated Derivatives of Natural and Synthetic Systems as Multitarget Anticancer Agents and Development of New Drug Discovery Methodologies*, **2016**.
- [108] E. Gabriele, F. Porta, G. Facchetti, C. Galli, A. Gelain, F. Meneghetti, I. Rimoldi, S. Romeo, S. Villa, C. Ricci, N. Ferri, A. Asai, D. Barlocco, A. Sparatore, *Arkivoc*, **2017**, II, 235-250.
- [109] X. Zhang, J. E. Darnell Jr, *Journal of Biological Chemistry*, **2001**, 276, 33576-33581.
- [110] K. Imada, W. J. Leonard, *Molecular Immunology*, **2000**, 37(1-2), 1-11.
- [111] D. E. Levy, J. E. Darnell Jr, *Nature Reviews Molecular Cell Biology*, **2002**, 3(9), 651-62.
- [112] J. N. Ihle, *Current Opinion in Cell Biology*, **2001**, 13(2), 211-217.
- [113] C. Schindler, D. E. Levy, T. Decker, *Journal of biological chemistry*, **2007**, 282, 20059-20063.
- [114] O. A. Timofeeva, N. I. Tarasova, *JAK-STAT*, **2012**, 1(4), 274-284.
- [115] J. F. Bromberg, C. M. Horvath, Z. Wen, R. D. Schreiber, J. E. Darnell Jr., *Proceedings of the National Academy of Sciences of the United States of America*, **1996**, 93 (15), 7673-7678.
- [116] A. K. Kretschmar, M. C. Dinger, C. Henze, K. Brocke-Heidrich, F. Horn, *Biochemical Journal*, **2006**, 377, 289-297.
- [117] <http://chemistry.berea.edu/~biochemistry/2011/cj/>
- [118] O. Korb, T. Stutzle, T. Exner, *Lecture Notes in Computer Science*, **2006**, 4150, 247-258.
- [119] O. Korb, T. Stutzle, T. Exner, *Swarm Intelligence*, **2007**, 1(2) 115-134.
- [120] <http://www.tcd.uni-konstanz.de/research/plants.php>
- [121] O. Korb, T. Stutzle, T. Exner, *Journal of Chemical Information and Modeling*, **2009**, 49, 84-96.
- [122] <http://www.rcsb.org/>
- [123] J. Gasteiger, M. Marsili, *Tetrahedron*, **1980**, 36(22), 3219-3228.
- [124] N. Foloppe, A. D. MacKerell Jr., *Journal of Computational Chemistry*, **2000**, 21(2), 86-104.
- [125] J. C. Phillips, R. Braun, W. Wang, J. Gumbart, E. Tajkhorshid, E. Villa, C. Chipot, R. D. Skeel, L. Kale, K. Schulten, *Journal of Computational Chemistry*, **2005**, 26(16), 1781-1802.
- [126] <https://pubchem.ncbi.nlm.nih.gov/>
- [127] R. W. Harrison, *Journal of Computational Chemistry*, **1993**, 14(9), 1112-1122.
- [128] MOPAC2016, James J. P. Stewart, Stewart Computational Chemistry, Colorado Springs, CO, USA, <http://OpenMOPAC.net>.
- [129] I.-H. Park, C. Li, *Journal of Molecular Recognition*, **2011**, 24, 254-265.
- [130] M. Lounasmaa, K. Karinen, D. Din Belle, A. Tolvanen, *Tetrahedron Letters*, **1996**, 37(9), 1513-16.
- [131] D. Din Belle, A. Tolvanen, M. Lounasma, *Tetrahedron*, **1996**, 52(34), 11361-11378.
- [132] M. Tosin, D. Spiteller, J. Spencer, *ChemBioChem*, **2009**, 10(10), 1714-1723.
- [133] R. M. Abdel-Motaleb, A-M. A-S. Makhloof, H. M. Ibrahim, M. H. Elnagdi, *Journal of Heterocyclic Chemistry*, **2007**, 44(1), 109-114.
- [134] L. Anderson, M. Zhou, V. Sharma, J. M. McLaughlin, D. N. Santiago, F. R. Fronczek, W. C. Guida, M. L. McLaughlin, *Journal of Organic Chemistry*, **2010**, 75(12), 4288-4291.

-
- [135] A. Altomare, M. C. Burla, M. Camalli, G. L. Cascarano, C. Giacovazzo, A. Guagliardi, A. G. Moliterni, G. Polidori, R. Spagna, *Journal of Applied Crystallography*, **1999**, 32 (1), 115-119.
- [136] G. M. Sheldrick, SHELX97, Programs for Crystal Structure Analysis (Release 97-2); University of Göttingen, Germany, **1998**.
- [137] M. Nardelli, *Journal of Applied Crystallography*, **1995**, 28 (5), 659.
- [138] J. A. Platts, S. P. Oldfield, M. M. Reif, A. Palmucci, E. Gabano, D. Osella, *Journal of Inorganic Biochemistry*, **2006**, 100(7), 1199-1207.
- [139] OECD Guideline for Testing of Chemicals-Partition Coefficient (*n*-octanol/water), High Performance Liquid Chromatography (HPLC) Method. Adopted: 30.03.89 ed.; Vol. 117.
- [140] Y. Uehara, M. Mochizuki, K. Matsuno, T. Haino, A. Asai, *Biochemical and Biophysical Research Communications*, **2009**, 380, 627-631.
- [141] K.B. Matsuno, Y. Masuda, Y. Uehara, H. Sato, A. Muroya, O. Takahashi, T. Yokotagawa, T. Furuya, T. Okawara, M. Otsuka, N. Ogo, T. Ashizawa, C. Oshita, S. Tai, H. Ishii, Y. Akiyama, A. Asai, *ACS Medicinal Chemistry Letters*, **2010**, 1(8), 371-375.
- [142] C. M. Greco, M. Camera, L. Facchinetti, M. Brambilla, S. Pellegrino, M. L. Gelmi, E. Tremoli, A. Corsini, N. Ferri, *Cardiovascular Research*, **2012**, 95(3), 366-374.
- [143] M. Ruscica, C. Ricci, C. Macchi, P. Magni, R. Cristofani, J. Liu, A. Corsini, N. Ferri, *Journal of Biological Chemistry*, **2016**, 291(7), 3508-3519.